Cranfield University

School of Applied Sciences

Engineering Doctorate Thesis

Academic Year 2006/2007

Eric T F Chau

A Comparative study of Joining Methods for a SMART Aerospace Application

Academic Supervisors: Prof. Clifford Friend

Prof. David Allen

Industrial Supervisors: Dr. John Webster

Mr. Daniel Clark

Management Supervisor: Prof. Keith Goffin

16 April 2007

Abstract

The adaptive serrated nozzle (ASN) is one of the most promising concepts to help reduce the noise level generated by aero-engines. Shear between a hot air stream and ambient air at the nozzle exit creates noise. The serrated nozzle is designed to protrude into the air stream causing mixing between the two air streams reducing the noise level. Adaptive control system using shape memory alloy (SMA) actuators deploy the protrusion only when required in order to maximise fuel efficiency.

The successful joining of NiTi shape memory alloy (SMA) to the titanium parent structure is critical to the development of the adaptive serrated nozzle. However, joining of SMAs to dissimilar metals is widely known as extremely difficult if not impossible. This research provides a preliminary study into the potential of using SMAs in large engineering applications such as the ASN and the development of viable joining methods for joining SMA to titanium based alloy. Five most favourable conventional joining methods were selected for experimental investigation. Results proved that the successful joining of SMA to dissimilar alloys was extremely difficult, joint failures were mainly due to the formation of brittle intermetallics at joint interfaces. The formation of these intermetallics occurs irrespective of the type of joining method and level of heat input employed. However, it has been shown that the formation of these intermetallics can be suppressed by the manipulation of the joint composition. A marked improvement in joint performance has been achieved for joints that contained no more than 25 at% nickel. Joint improvement has also been achieved through the addition of titanium at the joint, although further research is necessary to investigate the effect of titanium addition to joint performance.

Acknowledgement

Although all the work reported in this thesis is entirely my own responsibility, I would like to thank many people who acted as a source of help and inspiration during this endeavour. In particular, I gratefully acknowledge the constant and invaluable academic and personal support received from my supervisors throughout this research. First of all, my two main academic supervisors: Prof. Clifford Friend and Prof. David Allen of Cranfield University: for helping me to find my elusive grounding to the research problem, without whose dedicated supervision it would have been very difficult to complete this thesis. Secondly, my industrial supervisors, Dr. John Webster and Mr. Daniel Clark of Rolls Royce Plc, for their valuable guidance. Thank you all for making constructive comments, criticisms and suggestions for improving the various drafts of this thesis. Above all, thank you for teaching me how to become a researcher!

I also humbly acknowledge the support received from Prof. Stewart Williams and Dr Heather Almond of Cranfield University for taking a special interest in my work, for reviewing and commenting on various parts of this thesis, and, also for creating stimulating intellectual discussions throughout this research. They have been substantial sources of inspiration and profound insight during this research.

I am also deeply indebted to the many others who provided help, support and encouragement in various ways. Here I include Mr. Andrew Dyer (Laboratory Technician) of Cranfield University for providing technical support in my technical work; Dr. William Kyffin of TWI Ltd for providing specialist equipment and advice for the friction stir welding work; Dr.

Alistair Smith of Rolls Royce Plc for providing his expertise in electron beam welding; Mr. Tim Pryor of Cranfield University for his support in brazing experiments. Last but not least, to the many others in Cranfield University for friendship and calming social conversations during those stressful times when the going got tough. My apologies to those that I have inadvertently overlooked or forgot to mention in my acknowledgements but who equally deserve.

Table of Contents

1 Introduction

1.1 Aircraft Noise

Noise pollution has always been a concern for the aerospace industry. The generation and radiation of noise from aero-engines poses a problem of immense complexity. Over recent years, there has been increasing pressure from environmental groups and governmental institutions on reducing noise pollution in aircraft propulsion systems. Noise reduction has since become a key requirement in the specification for next-generation propulsion systems. Engine manufacturers are constantly investigating ways to enhance the reduction of noise created by gas turbine engines.

1.2 Noise Abatement Technology

The increasing emphasis on the environmental performance of the aerospace industry has led to a surge in the research and development of environmental technology for aircraft. In this project, a number of the best-known development projects are discussed. In particular, the serrated nozzle concept is analysed. Its technical and economical attributes are assessed to determine its adaptability in the current and future aerospace market.

1.3 Serrated Nozzle

The serrated nozzle is one of the most promising short-term concepts in reducing aircraft noise. In conventional gas turbine engines (aero-engines), the air stream exiting the engine carries a much higher speed than the surrounding ambient air. The shear between the two air streams generates noise. The serrated nozzle is designed to protrude into the jet stream which creates turbulence and forces better mixing between the two air streams thus reducing noise. Boeing has already undertaken both static and in-flight engine tests on a Boeing B-777 aircraft with Trent 800 engine fitted with the serrated nozzle [**1**]. **Figure 1-1** shows a Rolls Royce engine fitted with the serrated nozzle for in-flight testing.

Figure 1-1, Engine tests for assessing the noise performance of serrated nozzle [2]

The serrated nozzle concept has one major drawback. By protruding into the exhaust airflow, the serrations generate drag and reduce the efficiency of the engine. On the

original design, the serrations are fixed which means that the performance penalty is present under all flight conditions whereas noise reduction is only required for take-off and climb conditions where noise is a concern. An actuated serrated nozzle system where the serration only protrudes into the airflow when necessary is therefore a more desirable option [**1**].

1.4 Adaptive Serrated Nozzle (ASN)

To remove the performance penalty from the fixed serrations, an adaptive concept is being developed. The adaptive design, shown in **Figure 1-2** uses actuators to deploy serrations only when noise abatement is required. The serrations would return to the original position at cruise to maximise engine performance. This adaptive design would produce considerable fuel saving compared to the fixed design, especially for long haul, transatlantic aircrafts that spend the majority of their flight time at cruise condition.

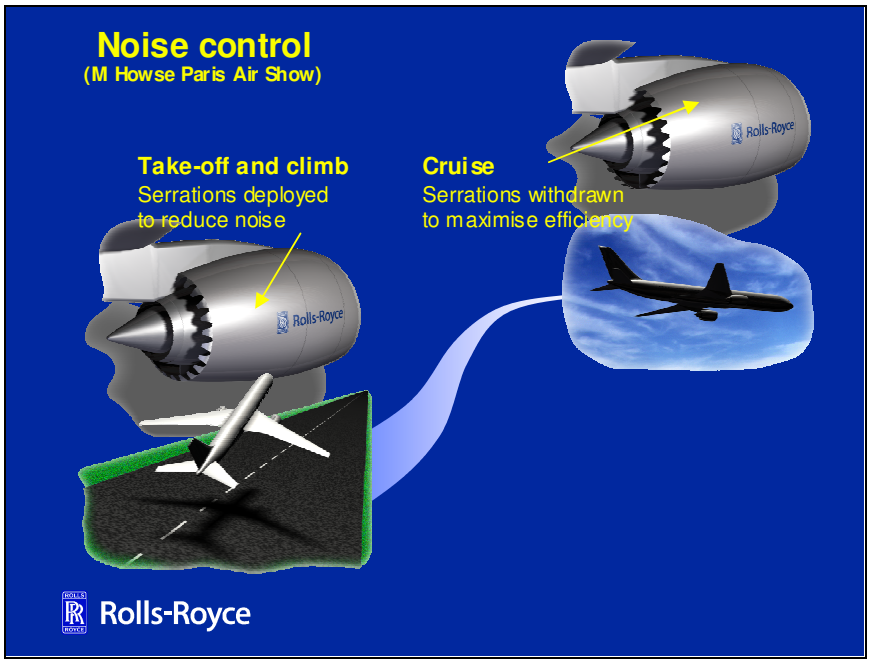

Figure 1-2, Adaptive serrated nozzle concept [3]

Several actuation mechanisms have been considered including mechanical-, electrical- and metallurgical-based systems. Like many other engineering applications, the use of conventional mechanical and hydraulic actuators or control systems is unattractive due to their cost, weight, size, complex design and reliability considerations. Shape memory alloy actuators have been proposed as a method of overcoming some of these restrictions.

1.5 Shape Memory Technology

Shape memory alloys (SMAs) possess the unique properties of shape changes controlled by their alloy temperature. SMAs have already been used in many engineering applications from thermostatic valves and fire sprinklers to spectacle

frames and medical implants. Recently, there are considerable interests and research activities from airframe and aero-engine manufacturers in the development of relatively large, high temperature SMA actuators [**4**]. The use of SMAs as actuators has numerous advantages over the conventional mechanical systems. The actuation is caused by a metallurgical change within the alloy at temperature, thus there are no moving parts involved. This translates to much simpler, lighter and more reliable actuation systems.

1.5.1 SMA Adaptive Serrated Nozzle

The adaptive serrated nozzle is designed to fully integrate SMA actuators into the structural design of the component such that the serration shape will change between two pre-determined positions at either side of the transition temperature [**4**]. A schematic representation of the serration design is shown in **Figure 1-3**.

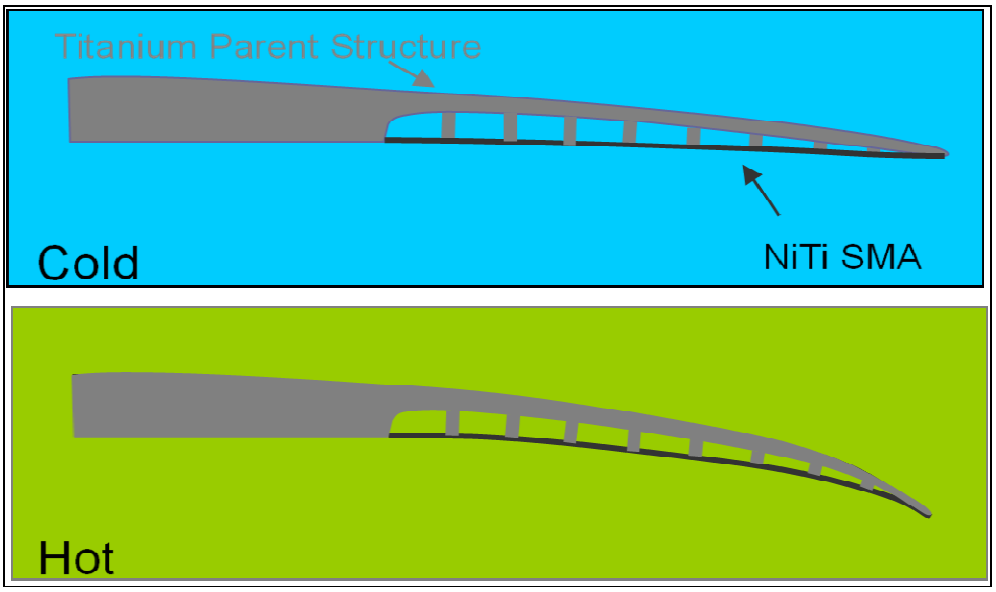

Figure 1-3, Schematic of an adaptive serration design [5]

Each serration consists of two sub-components, a parent structure made from Ti-6Al-4V alloy and a shape memory alloy actuator. The titanium parent structure has a pedestal construction designed to produce maximum tip deflection with a thin sheet of SMA actuator attached to the bottom surface of the structure. The parent structure is pre-stressed prior to joining to the SMA actuator. During operation, the pre-stressed parent structure acts as a bias-spring, inducing a constant upward force on the component. The engine temperature rises at take-off and activates the SMA actuators. The actuators undergo a phase transformation, causing the elastic modulus of the alloy to rise thus forcing the component to bend downwards thereby creating the protrusion, as illustrated in **Figure 1-3.** As the aircraft cruises at altitude, the nozzle temperature falls. The temperature drop reverses the actuation and causes the structure to return to its original position.

The use of SMA actuators does have its drawbacks. SMA technology, although rapidly developing, is still a relative new technology. Many aspects of the material are still not fully understood. In particular, the affect of mechanical and thermal treatments to the transformation temperature and hysteresis of the alloy is still not fully understood. This creates an enormous problem in securing the supply of SMA actuators with consistent properties. Also, the alloys' high sensitivity to shifts in composition has limited the manufacturing of SMA to small size and volume. These problems have seriously limited the manufacturing capability of SMA suppliers. Indeed this has caused considerably delay in this project when acquiring the SMA in the product form and volume suitable to produce downsized prototypes. It would be

impossible to implement SMA applications in the aero-engines without considerable advancement in the development of shape memory technology. In this project, the aforementioned problems have been critically analysed using a range of mechanical and metallurgical analyses and recommendations have been made in an attempt to resolve some of these problems.

1.5.2 Welding of SMAs for Aerospace Applications

Joining of NiTi SMA to itself and more importantly to dissimilar metals has been well documented to be very difficult, if not impossible [**6**]. An internal risk assessment at Rolls Royce has revealed that the development of joining methods is the task that carries the most significant risk in the development of ASN [**7**]. Further, this is also likely to be one of the most expensive tasks to mitigate.

There are two main aspects that make the joining such a difficult task. Firstly, commercial NiTi SMAs have a maximum operating temperature of around 150°C. Above this temperature, the shape memory effect (SME) of the alloy rapidly deteriorates. However, most conventional joining techniques for titanium alloys such as fusion welding and diffusion bonding processes operate at temperatures well above the limit permitted for NiTi SMAs. Secondly, there is the problem with the compositional dependency of the NiTi SMAs. The shape memory performance of NiTi SMAs is very sensitive to variations in the alloy composition. Any joining process that causes even the slightest shift in the composition of the SMA could

considerably affect the shape memory effect (SME) of the SMA. Therefore high temperature joining techniques cannot be applied without major modifications.

This project investigates whether any of the conventional joining process would be able to successfully join the NiTi SMA to Ti-6Al-4V alloy for the production of the ASN, with a view that any joining technology developed should be able to carry forward for future SMA applications in other parts of the engine.

In this project, conventional joining methods used for joining metal alloys have been extensively studied. A selection process has been carried out to determine the suitability of each joining method in producing joints desired for the ASN. Five of the most-suited joining methods have been selected for detailed experimental investigation. For each of the selected joining methods, a simple process optimisation has been carried out to produce the best possible joints. The joints have been extensively examined using a combination of mechanical and metallographic analytical techniques to determine the quality and suitability of these joints.

1.6 Economic Value of the Adaptive Serrated Nozzle

There is no doubt that the Adaptive Serrated Nozzle offers an attractive proposition to noise reduction while minimising the adverse effects on the engine performance. However, it is very difficult for the end-users to understand and envisage the added-value that the adaptive serrated nozzle or indeed any noise abatement technology provides. The cost of aircraft noise was critically assessed in this project. A number

of methods have been suggested to determine the cost of noise from an end-users point of view to enable one to clearly visualise the financial incentives that noise abatement technologies such as the adaptive serrated nozzle could provide to its stakeholders.

1.7 Objectives

The aim of this project is to develop joining techniques that effectively join NiTi SMAs to dissimilar metals for the development of adaptive serrated nozzles. However, any joining methods developed should not only be economical and technically viable but also: 1) be able to adapt by future SMA applications in gas turbine engines with minimal alteration and 2) be strategically in line with Rolls-Royce's manufacturing capability.

2 The Role of Aircraft Noise in the Civil Aviation Industry

The civil aviation business is remarkably complex and intensely competitive. What really sets the commercial aviation business apart is the enormity of the risks as well as the huge research and development costs and capital investments that must be put in place up front. The cost base of the firms operating in this market is constantly affected by volatile fuel prices, increasing airport charges and other regulatory restrictions, which all contribute to the creation of enormous barriers to the organisations who are considering competing in this market. The demands in the market are very sensitive to factors such as safety and security issues, which further add to the already huge risks that operators in this market have to endure. The huge risks, volatile operating costs base and unforeseeable changes in demands meant that organisations struggle to survive in this market and only few are successful. On the other hand, the civil aviation business is one of the most lucrative markets there is. In 1998, the direct contribution of civil aviation was valued at US $370 billion and employed no less than 6 million people worldwide. The total economic contribution from the industry, taking into consideration the 'multiplier effects' was valued at US$1360 billion and generated 27.7 million jobs worldwide [**8**]. Aviation has even out-performed the growth of world GDP since the 1960s and is expected to continue to do so, with traffic expected to double over the next 10-15 years and quadruple by 2050 [**9**].

2.1 The Growth and Outlook of the Civil Aviation Industry

According to the International Civil Aviation Organisation (ICAO), civil aviation is one of the fastest growing industries. Since the early 1960s, the industry has multiplied by a factor of 32 with an average growth rate of about 8% per annum. This industry has even outgrown the world's economy [**Figure 2-1**] [**10**]. Although the growth in air transport has been much greater than the world's economic growth, the two are closely related. The demand for air travel is primary driven by economic development as it dictates the level of disposable income available for the non-essential luxuries including air travel. However, it can also be affected by other factors such as fares, regulatory development and the quality of tourism service. In addition, the recent SARS (Severe Acute Respiratory Syndrome) outbreak, the tsunamis in South-East Asia, hurricanes such as Katrina that destroyed New Orleans and the recent terrorist attacks all created detrimental impacts on the industry, which shows that the demand for air travel is also highly sensitive to safety and security.

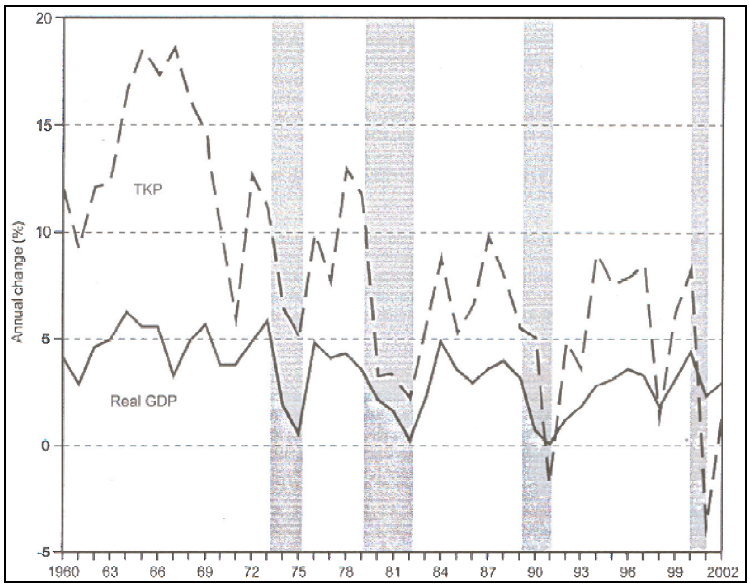

Figure 2-1, Relationship between growth of the civil aviation industry and the world economic performance [10]

Note: KTP=Thousand Kilometre Passenger miles

The latest figures from the ICAO showed that as the economy starts to recover from these aforementioned events, so does the aviation industry. Currently airlines are starting to come back into profit after some major restructuring through a series of mergers and acquisitions. The ICAO has predicted that the industry would continue to grow strongly in the near future fuelled primarily by the expansion of short-haul "no-frills" air travel.

In the UK, a similar trend applies. In spite of the poor performance in the long-haul segment, mainly due to SARS and terrorist events, the overall market performance has been strong. The drop in international air travel has been offset by the strong performance in the short haul "no-frills" carriers [**Figure 2-2**]. Overall, the number of passengers passing through UK airports has risen sharply over the last 30 years from 30 million in the 1970s to 180 million in 2000 [**11**]. This number is expected to

continue to rise to over 500 million in 2030 on the basis that the cost of air travel would continue to reduce by an average rate of 1-2% per year [**12**].

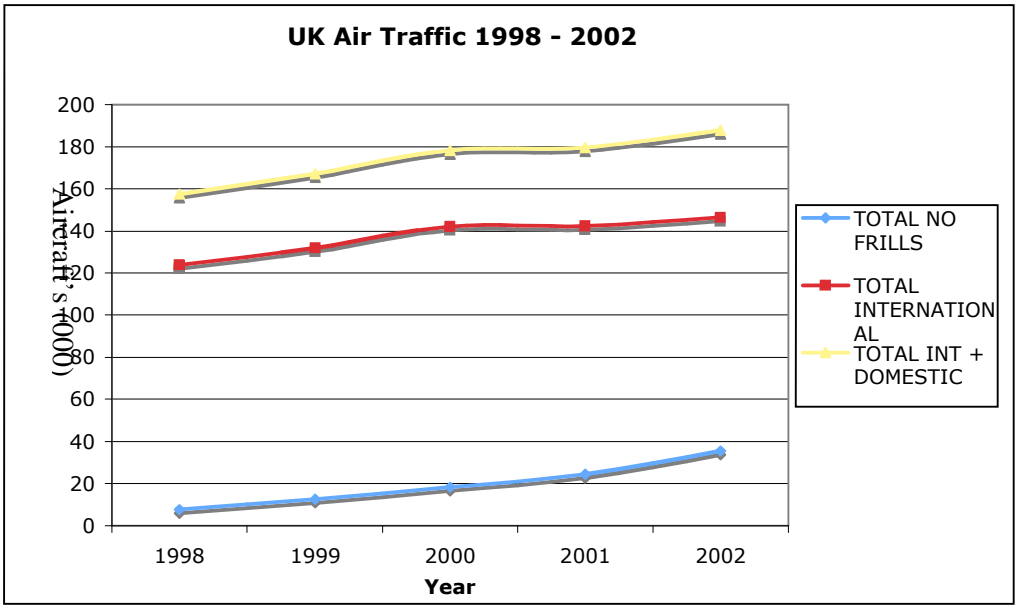

Figure 2-2, Numbers of passengers passing through UK airports 1998-2002 [13]

The strong growth in aviation has no doubt generated huge economic benefits worldwide, not to mention the spill-over effects. But this also exacerbates the problems associated with the industry such as noise nuisance, air pollution and congestion. Airport and airspace congestion has long been a problem since the 1980s, when the growth in air traffic first started to approach the capacity limit of many airports. Airspace congestion has been gradually addressed by the increase in aircraft size and load factor. To meet the ever-growing demands of air travel with limited airspace, aircraft manufacturers simply build larger aircraft. This is reflected in the reduction in annual growth rate of aircrafts since 1982 [**Table 2-1**].

	1982	1992	2002	2015 (Forecast)	Average annual growth rate		
					1982-1992	1992-2002	2002-2015 (estimated)
Passenger - kilometres (billions)	910	1,782	2,881	5,038	6.3	4.9	4.4
Aircraft - Kilometres (millions)	9,140	15,420	23,878	40,750	5.4	4.5	4.2
Aircraft Departures (thousands)	10,379	14,728	20,013	20,010	3.6	3.1	3.2

Table 2-1, Increase in aircraft capacity relieves air congestion [10]

In comparison with airspace congestion, the problem with airport congestion is much more difficult to address. The capacity of airports can only be increased by introducing new runways and terminals but plans to introduce both of these measures have been fiercely opposed by local residents and environmental groups. The general economic slowdown and the terrorist events in the early 2000 has temporary halted the increasing demand for air travel and thus temporary relieved such problem. However, as the world economy starts to recover from these events, the growth in air traffic returns and the problems with airport congestion have resurfaced again.

2.2 The Emergence of Environmental Issues

Currently, one of the main obstacles inhibiting the expansion of the aviation industry is the issue surrounding the environmental impact of air travel. Of these problems, noise nuisance is amongst one of the most significant. When aircraft were first developed, they used to fly in and out of the airport whenever and at whatever heights the airlines and the air authorities decided without any consideration of the population living in the vicinity of the airports and under the flight paths. Authorities first started to be concerned with the noise produced by aircraft when the tip rotation velocity of propellers approached the speed of sound [**14**]. However, when the large, noisy turbo-jet engines began to replace the relatively smooth and quiet turbo-prop engines in the 1950s, noise immediately became a serious problem. Since then, concern over the environmental impact from air travel accelerated as the industry grew. The problem of aircraft noise was no longer confined to aircraft in flight but extended to noise at taxiing, auxiliary power units and engine testing. In addition, the airport road network also contributes to significant noise pollution around airports.

Today, sustainability has become one of the main drivers in the sale of aircraft and aero-engine and control of noise levels has become one of the prime requirements when designing aircraft and aero-engines. As a result, modern aircraft are far quieter than those operating in previous decades [**Figure 2-3**]. The environmental impact from noise produced by modern aircraft is 75% less than that produced over half a century ago whilst increasing the level power output by a factor of 50 [**15**]. Over the past 40 years, the civil aviation industry has reduced aircraft noise by 50%, equivalent

of over 25dB. With noise reduced by 10 dB being perceived as half as loud, the 25 dB reduction achieved since the introduction of jet aircraft means that the noise of a modern aircraft has shrunk to well below a fourth of that of the first generation [**16**]. Much of the improvement is due to the technological advances in jet engines which allow engines to maximise operating efficiency by operating at ultra-high temperatures, pressures and bypass ratios. However, the increasing demands for air travel have created bigger aircraft with more powerful engines. As a result, even though the noise abatement technologies for aircrafts have continued to develop, the reduction in aircraft noise level has became somewhat stagnant since 1970s [**Figure 2-3**]. Furthermore, the reduction in noise from individual aircraft has, in many cases, been offset not only by the introduction of larger aircrafts but also by more frequent flight movements and growing expectations from community and environmental groups. Indeed, the growing pressure and expectations from environmental groups and other authorities have certainly been and will continue to be a major obstacle in the growth of the civil aviation industry worldwide.

Air traffic congestion already exists in airports where the capacity limits of runway and terminal have been reached. For those with spare capacity to expand, environmental issues will be a serious barrier to the provision of extra runway and terminal capacity. Plans to satisfy the ever-growing demand in air travel through airport expansions in the UK, such as the extra runways at Luton and Stansted and the new Terminal at Heathrow are being fiercely opposed by a diverse set of affected stakeholders and have been successfully delayed or rejected [**17**]. To sustain the continual expansion of the aviation industry, engine and airframe manufacturers

started to invest heavily on noise technologies recently, to produce quieter aircrafts so that more aircrafts can be operated within the same noise limit.

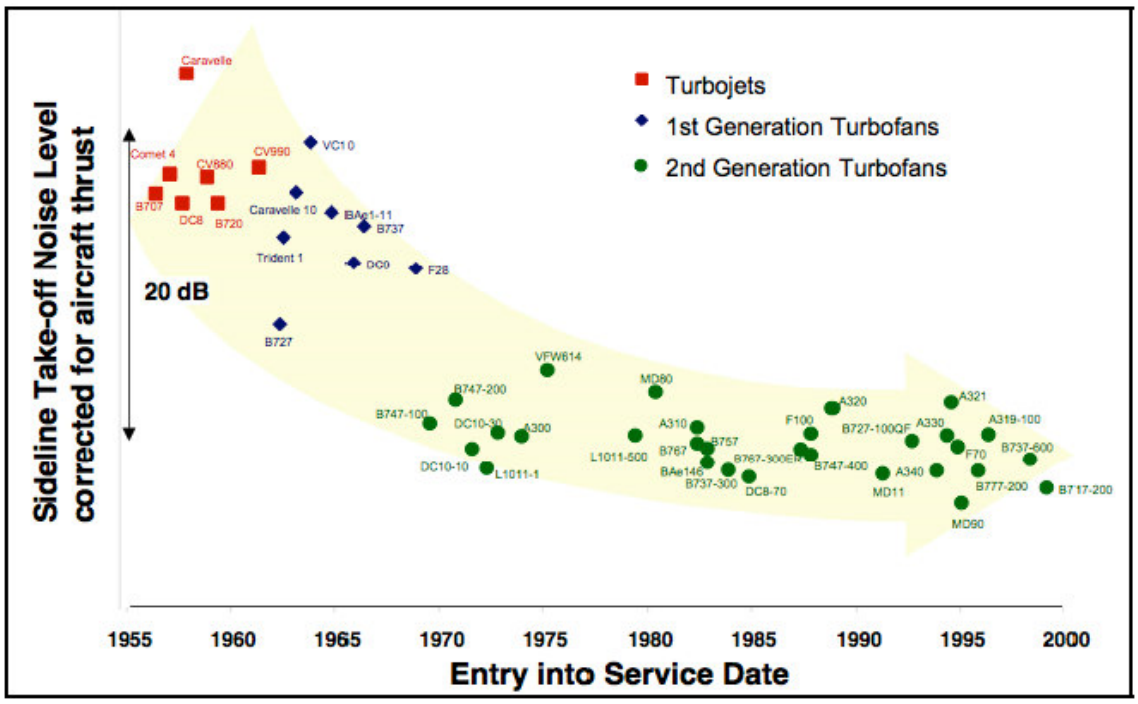

Figure 2-3, Progress in noise reduction in aircraft [18]

2.3 Aircraft Noise

Although the impact of aircraft noise on the environment is not a lasting one, it has significant detrimental effects to the people living under the flight path and around airport. Noise from aircraft is not just annoying; it can have a significant impact upon the health and the quality of life for those people living close to airports or under flight paths. Evidence from research points to clear areas of health damage in noisy environments, including sleep disturbance, reading deficiencies, hearing loss, learning acquisition problems with cognitive development among infants and cardiovascular

and psycho-physiological effects [**19**]. Children are especially vulnerable to high levels of noise. Research has shown that children living around airports and under flight paths perform significantly worse and have a lower level of memory than the ones living in quieter areas [**20**, **21**].

2.4 Noise Exposure Measurements

Noise is a measurement of sound pressure level (SPL) and is measured in units of decibels (dB). The measurement of noise is a complex subject as the concept of noise is perceptive. Different methods for measuring noise have been developed for different purposes. The Equivalent Continuous Noise Level ($L_{Aeq,T}$) for example is a method used exclusively in noise impact measurements and is defined as the "equivalent" continuous sound level. It is a measure of the equivalent continuous sound level averaged over a period, T. Noise measurements are normally weighted to reflect the sensitivity of human ear to different frequencies or pitch. The A in L_{Aeq} denotes to noise measurements weighted with A-weighting, hence the unit of L_{Aeq} is in dBA. The A-weighting is a filter commonly used to emphasise the frequencies around 3–6 kHz where the human ear is most sensitive, while attenuating the very high and very low frequencies to which human ear is less sensitive to. The aim is to ensure that the measured loudness corresponds well with subjectively perceived loudness. Various related derivatives of this metric are used around the world, and in the UK the 'average' daytime noise is expressed by the 16 hour Leq_A ($Leq_{A.16h}$) is most commonly used. Single aircraft noise events are generally governed by their effect such as interference or annoyance where the acceptance level is governed by

the maximum noise level each aircraft produces. A number of noise metrics are used for these measurements, amongst the most common ones are Maximum "Equivalent" Level (L_{Max}), Sound Event Level (SEL) and Effective Perceived Noise Level (EPNdB). These noise metrics are only used for short-term measurements and are often used as a supplement for setting penalties and monitoring noise levels. EPNdB incorporates different frequencies and duration of noise patterns, resulting from various speeds and modes of operation of aircraft. ICAO uses EPNdB in setting noise certification standards [**22**].

For setting environmental policies, a more comprehensive noise metric which measures the SPL of noise events over a longer period is required. The day-evening-night noise indicator (L_{den}) is one of the most widely used standards in measuring aircraft noise events when setting noise related policies and regulations. L_{den} is defined in terms of the average levels of noise during daytime, evening, and night-time, and applies a 5 dBA penalty to noise in the evening and a 10 dBA at night. The definition of L_{den} is as follows:

$$L_{den} = 10 \log [(12/24).10_{(LD/10)} + (4/24).10(LE+5)/10 + (8/24).10(LN+10)/10]$$

where LD, LE, and LN are the A-weighted long term $L_{Aeq,T}$ as defined in ISO 1996-2 (1987) for the day (7-19h), evening (19-23h), and night (23-7h) determined over the year at the most exposed façade [**23**].

2.5 Environmental Regulations

Under increasing pressure, governments around the world have developed a range of environmental taxes and policies in an attempt to improve the sustainability of the aviation industry. Environmental economists advocate incentive-based (IB) environmental regulations such as environmental taxes and charges where airframe and engine manufacturers are encouraged to voluntarily reduce noise pollution as a way to minimise their cost base. These regulations are in theory more effective than the so-called command and control (CAC) regulations such as night flight restrictions, engine standards and airport curfews where airliners are forced to adhere to these CAC regulations that often harm their revenue as a result [**24**]. Further, the ICAO recommended that IB regulations should be in the form of charges instead of taxes, since taxes often become fiscal resource for governments. In reality, the noise at airports is controlled through a combination of IB taxes and charges such as airport charges and penalties, as well as a number of international and local CAC regulations and restrictions such as the ICAO noise regulation and the recently introduced Civil Aviation Bill [**25**]. All of which aim to set out a tax-neutral balanced approach and provide a strategic framework for the development of sustainable air travel.

2.5.1 International Regulations

The International Civil Aviation Organisation (ICAO) was established in 1974, under the Convention on International Civil Aviation, also known as the *Chicago Convention*. The ICAO, now a division of the United Nations is responsible for

establishing rules of airspace, airplane registration and safety, and details the rights of the signatories in relation to air travel. The rules and regulations governing international air travel are set out in the Convention on International Civil Aviation and Annex 16 deals with environmental impact from civil aviation. It consists of two volumes; Volume I deals with aircraft noise and volume II deals with aircraft emissions. Within the Volume I, Chapter 1 regulates the noise performance of the earliest jet engines while Chapter 2 covers the second generation, low bypass engines. In 1977 ICAO adopted a new, more stringent Chapter 3 standard for aircraft noise, setting the requirements for noise certification that could only be met by the medium and high bypass engines. In 1990, ICAO ordered the noisy Chapter 2 aircrafts to be withdrawn from service by 2002. Some of the Chapter 2 aircraft have been fitted with 'hush-kit', a device for reducing noise of Chapter 2 engines to satisfy the Chapter 3 requirements for re-certification [**26**]. The ICAO Annex 16 was revised again in March 2002 and the new Chapter 4 standard was added. The new Chapter 4 standard applies to all new aircraft after January 1, 2006. These 4 Chapters set out the criteria for noise certification for different classes of aircrafts manufactured in various periods [**27**]

As the level of air traffic increases, the noise benefit of modern quieter aircraft diminishes. It is increasingly difficult to continue to reduce aircraft noise effectively through the advancement of individual noise abatement technology. The ICAO recognised this problem and in the ICAO Assembly in 2001, it endorsed the concept of a "balanced approach" to aircraft noise management. This consists of identifying the sources of noise at an airport and then analysing all the possible solutions through the exploration of four key areas [**28**]:

1. **Reduction at source**

Engine noise is by far the most dominant source of aircraft noise, thus the majority of the noise abatement technologies are developed for the engine. However, as the engine noise continues to decrease, airframe noise such as those generated by the deployment of flaps and landing gear during landing becomes a significant contributor to the total aircraft noise and needs to be addressed.

2. **Land-use planning and management**

Inappropriate development is discouraged or prohibited around airports through land-use planning and management schemes to ensure population affected by aircraft noise are kept at a minimum. Schemes such as home-relocation and buy-out offer homeowners in the high-noise areas assistance in relocating away from these areas. While the establishment of noise zones around airports in which residential property development are restricted ensure that the gains achieved by the reduced aircraft noise are not offset by further residential development around airports.

3. **Noise abatement operational procedures**

This area investigates the steps that can be taken by pilots and air traffic controllers to minimise the noise nuisance, such as the use of Noise Preferential Routes (NPR), Continuous Descend Approach (CDA) procedure and the Low Power/Low Drag Approach (LPLD) procedure.

a. Noise Preferential Route (NPR)

NPRs direct aircrafts over less densely populated areas to minimise the number of population affected by aircraft noise. Noise Track-keeping systems (NTK) are put in place by airports and fines aircraft operate outside the designated NPRs.

b. Continuous Descent Approach (CDA)

Originally developed as a procedure for reducing fuel consumption, the CDA procedure also reduces the noise of approaching aircraft close to airports by operating a continuous steady descent from 6,000ft, or higher, rather than following a number of short descents. The CDA procedure has 2 main noise advantages: 1) as illustrated in **Figure 2-5**, the CDA flight path is higher and further away from the ground at all times, compared to that of the conventional approach procedure, this causes less noise at ground level; 2) by keeping the aircraft on a continuous descent, the overall engine power levels are kept lower, generating comparatively less noise. In addition, the aircraft operating CDA procedure uses a more constant power level than on a conventional approach, resulting in a more uniform noise levels which is perceived to be less intrusive [**28**]. A similar procedure for take-off known as the *Continue Climb* procedure has also been proposed which has been used with similar effect [**29**].

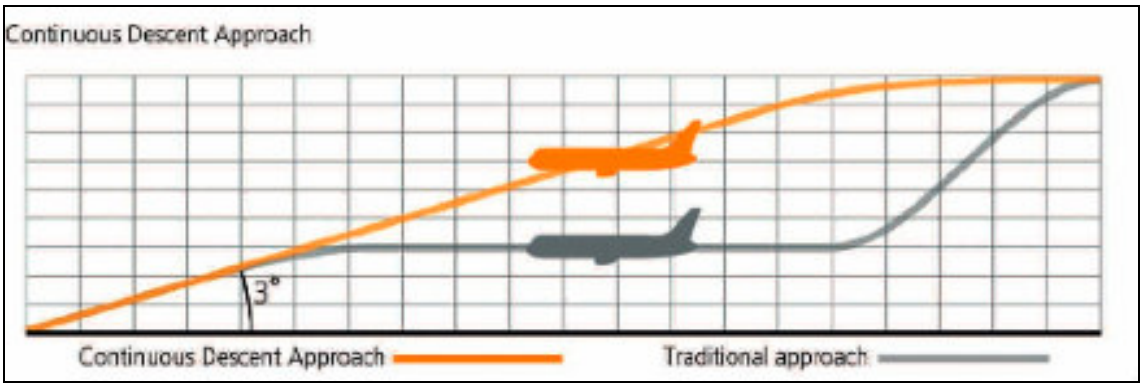

Figure 2-4, Graphical Representation of the Continuous Descent Approach [28]

c. Low Power/ Low Drag (LPLD)

In a LPLD approach, aircraft are refrained from deploying flaps and landing gear for as long as possible, within the limit of safety requirements, to reduce the level of airframe noise at approach as much as possible. Such a procedure can be used in conjunction with the CAD procedure to achieve additional noise reduction.

4. Operating restrictions

Airport restrictions such as annual movement and noise quota which restrict the number of aircraft movements operate over a specific period. The phase out of the noisiest aircraft types, such as the ICAO Chapter 2 aircraft, help to limit the exposure to noise for people living near airports.

ICAO reckons that further significant reduction in aircraft noise can only be achieved by combining efforts in these four areas [**29**].

The evolution of ICAO noise policies were originally set out to lead the aviation industry and encourage them to utilise the "best available" noise technology and continue to reduce aircraft noise through research and development. On the contrary, the current ICAO noise policy is actually tracing the industry's progress. Over 90% of the latest aircraft already meet the latest Chapter 4 requirement. This is hardly an encouragement for the industry to acquire and develop quieter aircrafts. This also explains why the improvement of noise performance of aircrafts has become somewhat stagnant since 1970s [**Figure 2-3**]. This problem arises because members of ICAO consist of primarily representatives of governments and industries of the states that are signatories to the Chicago Convention (i.e. most of the industrialised countries). ICAO regulations are binding on the member states. When considering proposal of new environmental regulations, members not only take into account the environmental concerns but also the economic interests of their domestic airline and manufacturing industries. This often leads to members opposing regulations that are beneficial to the environment but could potentially harm their domestic economy [**30**]. The most contentious debate has been in the issue of 'hush-kit' and the phasing out of the Chapter 2 aircrafts. In April 1999, the European Council adopted a regulation that would ban hush-kitted Chapter 2 aircraft from operating in European airports, even though these aircraft have been re-certified under the Chapter 3 standards. This has sparked furious complaints from the US State Department where large numbers of US business and commercial aircraft are affected, claiming that the regulation is discriminating the US carriers, hush-kit and engine manufacturers. As a retaliatory precaution, the US have threatened to impose economic sanctions, including a ban on Concorde, which at the time was considered to be the noisiest aircraft ever certified, from operating in US airports. The problem ended up with the European Commission

agreeing to withdraw the implementation of the regulation and to adopt a noise policy under the new ICAO regulation which would deal with the issue on an airport-by-airport basis [**31, 32**].

2.5.2 Local and National Restrictions

Without the influence of other member states, local governments that are in favour of strict noise controls have been far more effective in setting noise policy for their domestic aviation industry. Local governments, especially the ones in Europe, have been given huge powers to the aviation and airport authorities in setting noise regulations and airport charges in an attempt to contain any further increases in airport and aircraft noise despite the continual growth in demands for air travel. In the UK, the Department of Transport has overall responsibility for aircraft noise. The 'Future of Air Transport' White Paper published in 1998 sought views on strengthening and clarifying the powers given to local authorities for controlling noise at airports [**33**]. Following the recommendations from the 'Future of Air Transport' White Paper, the Civil Aviation Bill was introduced in the House of Commons on 9 June 2005 [**25**]. The Bill is designed to implement important commitments set out in the White Paper to sustainable aviation and protection of passenger interests and would clarify and strengthen the measures available to airports for dealing with aircraft noise. This includes a greater ability to introduce and enforce noise control measures beyond airport boundaries and to impose financial penalties if aircraft strayed from NPRs.

2.5.3 Local Airport Charges

Airport noise charge is an example of an effective and economic way to offset the costs of eliminating the effect of noise in the vicinity of airports. It also encourages airlines to voluntarily eliminate pollution by acquiring greener, modern aircraft, thus minimising operating costs. Most airports charge penalties for noisy aircraft and offer discounts to the quieter ones. These restrictions vary depending on the rules and regulations set by the local government. Heathrow airport, for example, offer up to 50% discount in landing charges for the quietest aircrafts while charging 50% over its base landing charge rate for the noisy Chapter 2 aircrafts. In addition Heathrow has several Noise Preference Routes (NPRs) which all aircraft departing from the airport must follow until they reach 4000ft when flying into Heathrow. The NPRs were designed by the British government over 30 years ago to minimise the population under flight paths, taking into account the manoeuvrability of aircrafts.

Nationally, the UK government sets noise limits for aircrafts and specifies the location of the noise monitors following ICAO guidelines. From 07:00 to 23:00 the current limit is 94 dBA, from 23:30 to 06:00 it is 87 dBA and for the periods 23:00 to 23:30 and 06:00 to 07:00 the limit is 89 dBA. Heathrow airport use its noise track-keeping system to constantly monitor the adherence to these levels and fines operators in breach of these conditions £500 for the first three decibels above the limit and £1,000 above that. Heathrow receives over £100,000 a year in noise infringement and the money raised from these fines is reinvested into community noise mitigation projects [**Table 2-2**] [**34**].

	2003/04	2004/05	2005/06
Day Infringements	82	15	42
Night Infringements	113	117	168
Total Infringements	195	135	210
Total Fines	£112,500	£73,500	£121,500

Table 2-2, Penalties for noise infringement at Heathrow airport

Aircraft arriving at Heathrow have to adhere to a strict landing procedure given by the Air Traffic Control (ATC). There are also landing charge in place which follows the ICAO aircraft noise certification and maximum take-off weights of aircraft. **Table 2-3** lists a detail description of Heathrow's landing charge system.

	Peak	Shoulder	Off-Peak
Chapter 3 Minus			
Fixed Wing Aircraft over 16 Metric Tonnes not exceeding 50 Metric Tonnes (fixed charge)	GBP 548.10	315.00	232.20
Fixed Wing Aircraft over 50 Metric Tonnes (fixed charge)	GBP 548.10	531.00	394.20
Chapter 3 - Base			
Fixed Wing Aircraft over 16 Metric Tonnes not exceeding 50 Metric Tonnes (fixed charge)	GBP 609.00	351.00	258.00
Fixed Wing Aircraft over 50 Metric Tonnes (fixed charge)	GBP 609.00	590.00	438.00
Chapter 3 - High			
Fixed Wing Aircraft over 16 Metric Tonnes not exceeding 50 Metric Tonnes (fixed charge)	GBP 913.50	526.50	387.00
Fixed Wing Aircraft over 50 Metric Tonnes (fixed charge)	GBP 913.50	885.00	657.00
Chapter 2 and Non-Cert			
Fixed Wing Aircraft over 16 Metric Tonnes not exceeding 50 Metric Tonnes (fixed charge)	GBP 1827.00	1053.00	774.00
Fixed Wing Aircraft over 50 Metric Tonnes (fixed charge)	GBP 1827.00	1770.00	1314.00
Note: Peak Period: 0700 – 0959 (GMT), and 1700 – 1859 (GMT), 1April to 31 October Night Period: 2300 – 0459 (GMT) 1 April to 31 October and 0000 – 0559 (GMT) 1 November to 31 March. Between 0000 – 0329 (GMT) 1 April to 31 October and 0100 – 0429 (GMT) 1 November to 31 March the charge will be peak x1.5			

Shoulder Period: 0500 – 0659 (GMT), 1 April to 31 October Off Peak: All other times. Chapter 2 aircrafts and aircrafts not meeting the ICAO Chapter 2 noise certification standard will be subjected to a landing charge equivalent to 200% of the Chapter 3 base charge. 'Chapter 3 base' charge applies to aircraft meeting the ICAO Chapter 3 noise certification standard. 'Chapter 3 minus' charge applies to aircraft with Quota Count (QC) values on both arrivals and departure of 0.5 or 1.0 or exempt as described under Section 3 of the London/Heathrow Noise Restriction Notice. 'Chapter 3 High' charge applies to aircraft whose noise performance lies within 5 EPNdB of the ICAO Chapter 3 limits. These aircrafts will be subjected to a landing charge equivalent to 150% of the 'Chapter 3 Base' landing charge.

Table 2-3, Landing charges at Heathrow airport [35]

For using the airport at night, Heathrow impose a Night Noise Quota Scheme. The noise quota restricts the total aircraft noise generated over a specific time and is measured on a Quota Count (QC) classification system. The QC system was developed in 1993 by the UK Government to help manage the noise generated by aircraft night operations at the three designated London airports - Gatwick, Heathrow and Stansted. Aircraft are given a QC classification depending on the noise they produce during take-off and landing which is determined from their certificated noise levels measured in EPNdB [**Table 2-4**]. The QC classification is designed to measure noise in relative terms, for example, a QC 2 aircraft is deemed to have twice the impact of a QC 1 aircraft and a QC 4 aircraft has four times the impact [**36**]. In the Night Noise Quota Scheme, aircraft score these QC value against a maximum quota for each season (5,610 for summer and 4,140 for winter) between 23:30 and 06:00.

There is also an annual limit of aircraft movements for each season (3,200 for summer and 2,550 for winter) during this period regardless of the QC ratings [**37**]. Every departure, or arrival, during this period counts as 1 against the movement quota. In addition, Heathrow bans the movements of all aircrafts with a QC rating of 8 or above between 23:00 and 07:00. Heathrow also uses the QC system in formulating its landing charges scheme. The recently proposed Civil Aviation Bill further restricts any increase in the number of night flights for the next six years [**38**]. The QC system is so effective that airframe manufacturers now started to use the QC system as benchmark when developing the latest aircraft. The QC 2 limit has become a key design parameter for Boeing and Airbus in their development of long haul aircraft. The forthcoming Boeing B787 and *Dreamliner* for example, are guaranteed to achieve QC1 noise limit on arrival and QC2 on departure [**39**]. Back in 2000, the Airbus A380 design has been reworked to increase its target noise performance from QC4 to QC2 standard [**40**]. For the civil aviation sector, the QC 2 limit has become the worldwide noise standard as it is more stringent than the Chapter 4 standard agreed by the ICAO.

ICAO Certification noise levels (EPNLs) are used for determining the QC category; Departures = [EPNL(Takeoff) + EPNL (Sideline)]/2 for Chapter 3 aircraft or; = [EPNL(Takeoff) + EPNL (Sideline)]/2+1.75 for Chapter 2 aircraft Arrivals = EPNL(Approach) – 9	
Certificated Noise Level (EPNdB)	Quota Count
More than 101.9	QC 16
99-101.9	QC 8
96-98.9	QC 4
93-95.9	QC 2
90-92.9	QC 1
Less than 90	QC 0.5

Table 2-4, Quota Count noise metric used at Heathrow airport [41]

2.6 The Valuation of Aircraft Noise

The development of noise abatement technologies for aircrafts has increased immensely in recent years. It is very important to be able to justify the cost of these development projects in a business context. To do that one must be able to quantify the cost of aircraft noise in monetary terms so that project appraisals can be properly assessed. However, noise is a difficult issue to valuate, as it is highly subjective. Further, it is almost impossible to quantify some of the impact of aircraft noise such as the negative effects on education and child development. Governments use a range of techniques for valuing the social costs of aviation noise for appraising policy

options such as airport expansion and setting levels of environmental taxation. Although economic techniques and underlying science are constantly improving, valuation remains prone to uncertainties.

Unlike other modes of transport such as motor vehicles where noise is a problem everywhere, the effects of aircraft noise are limited only to the vicinity of airports and under flight paths. The costs of these impacts are regularly assessed in detail by the local aviation authorities. Two types of noise valuation methods are commonly used: the stated preference (SP) and the revealed preference (RP) method [**42**]. The majority of studies on the valuation of noise use the RP approach of Hedonic Price (HP). This method determines the price of noise in the affected area. While there is no real market for noise, noise levels have a direct affect on prices of the property market. The HP method uses the concept of Noise Depreciation Index (NDI), which measures the percentage house price decrease per unit per decibel [**43**]. NDI studies have been mainly carried out in the UK, Canada and US and showed a 0.4-2.3% depreciation in house prices per 1 dB(A) increase in noise level, assuming depreciation starts at 55 dB, the noise level at which most people start to feel annoyed [**44**]. Using this technique, the UK government has valued the aviation damage at around £1.6 billion for the year 2000 (rising to nearly £5 billion by 2030) [**45**]. The strength of this method is that it relies on the actual behavior in the housing market where the level of 'willingness to pay' (WTP) can be observed. However, this approach relies heavily on the value of noise being reflected in the pricing of the property market, which may not always be the case, especially when the market is distorted by factors such as rent control or increase in taxes [**46**]. SP methods such as the Contingent Valuation Method (CVM) have recently become popular. This type of

valuation methods commission surveys to investigate how much people are willing to pay to reduce their noise exposure by a given amount. Differing from the HP approach, CVM takes into account people who are not willing to be exposed to a particular noise level at any price, the so-called 'zero-valuation' [**47**]. CVM surveys are difficult to construct and can lead to biased results, which is the main reason for its low up-take.

When developing noise abatement technologies, cost-benefit-analysis (CBA) would normally be carried out to assess whether the cost of the development project offsets the benefit they could bring to the business. One of the primary inputs in CBA for these projects is the cost of aircraft noise. However, the concept of cost of noise to the airframe and engine manufacturers is rather different to that of the local authorities. The costs of compensating the population and installing insulation to the properties affected by aviation noise are already absorbed by the airport authorities, which in turn, passed onto the airline operators through a number of airport fees and penalties. Thus the aforementioned valuation methods are inappropriate in providing information for CBA in development projects. A more meaningful way to value noise in CBA for development projects is to base the valuation on the costs that directly affect the sales of aero-engines and aircraft. When developing noise technologies, developers are mainly concerned with whether the saving in noise related fees and penalties that the end-users would benefit from the developing technology offset the cost of acquiring, operating and maintaining such technology.

2.7 Noise Abatement Technologies

Technically speaking, any technology that improves the efficiency of aircraft would also reduce the aircraft noise as the aircraft can maintain the same level of performance with a lower power setting and fan speed. The ever-growing demand by airlines for higher efficiency engines saw the by-pass ratio of the engine soar and, as a by-product of these improvements, vast reductions in engine noise has been achieved. However, as the pressure to reduce the environmental impact caused by aircraft builds up, it became apparent that further noise reduction can no longer be achieved solely by increasing the by-pass ratio of the engine. A number of programs have therefore been set up to develop both short- and long-term solutions to aircraft noise. For long-term solutions, projects such as the Silent Aircraft Initiative (SAI) have been set up in an attempt to revolutionise the industry to produce a truly "silent" aircraft, one that is imperceptible to the people living in the urban environment around airports. Such aircraft design requires a totally different design ethos and an effective integration of technologies developed for airframe, engine and mode of operations. These silent aircraft require a long time to develop and validate and would not be in our sky for at least 20 years. Short- to medium-term development such as the *Quiet Technology Demonstrator (QTD)* and the *Silence(R)* project, on the other hand, focus on the evolutionary improvements that involve mainly improvements of existing components or the addition of acoustic treatments to noisy components. Many of the technologies developed in these projects are designed to relieve the noise problem in the near future and could be available to next-generation aero-engines in 5-10 years time.

2.7.1 Long Term Development Projects

2.7.1.1 Silent Aircraft Initiative (SAI)

Launched in November 2003, the SAI is a programme that aimed to develop silent aircraft technologies from a new perspective [**48**]. The SAI was set up with a bold goal to develop technologies that would enable aircraft to operate at a noise level that would be imperceptible to the people living in the urban environment around airports. The SAI recognised that to achieve such a challenging goal requires highly integrated airframe and engine design together with the modes of operation all optimised for low noise emission. It attempts to revolutionise the civil aerospace industry by taking noise as the prime criterion at the conceptual design stage. Instead of reducing the noise generated by aircraft, engineers and designers would develop aircraft that would produce less noise in the first place. The SAI is divided into five main areas. Airframe and engine technology being the obvious focal points, with their effective integration – the third area where it is believed that the biggest advance could be achieved. Aircraft Operation attempts to reduce aircraft noise by changing the take-off and approach procedures. Finally, the economical researchers are looking into both the regulatory scenarios under which the aircraft would meet airline's business case, and possible benefits to the U.K. economy, both nationally and regionally. Such a radical change in the way research and development is conducted in this industry requires time to implement and it is unlikely such an ambitious programme would come to fruition in the near future. In fact, the most optimistic prediction predicts that the silent aircraft will be flying in 2025.

2.7.1.2 Cambridge-MIT Institute (CMI)

The CMI is a government-supported joint venture between Cambridge University in the UK and the Massachusetts Institute of Technology (MIT) in USA. It is also one of the SAI's 'knowledge integration communities' designed to utilise the strong ties that the two academic institutions have with the major airframe and engine manufacturers as well as other research institutes in the field of "silent aircraft" and to look for ways in which academia and industry can work together to synergise the technology advancement in aerospace. Bringing academia and all the associated industries together would ensure that any technologies developed in the programme would not be wasted and issues with incompatibility and accessibility can be minimised [**49**].

The CMI have come up with the Blended Wing Body (BWB) aircraft concept, shown in **Figure 2-6**, to achieve the goals set by the SAI. The BWB concept aims to blend the wings seamlessly into the body. Such configuration has many performance and aerodynamic benefits over the current airframe designs including significant improvement in aerodynamic efficiency. With this configuration, the engine design also needs to change in order to take full advantage of the BWB design. Mounting engines on top of the wing instead of the traditional underslung mounting methods would allow the wing surface to act as a noise absorber and deflect the noise upward thus minimising the noise absorbed at ground level.

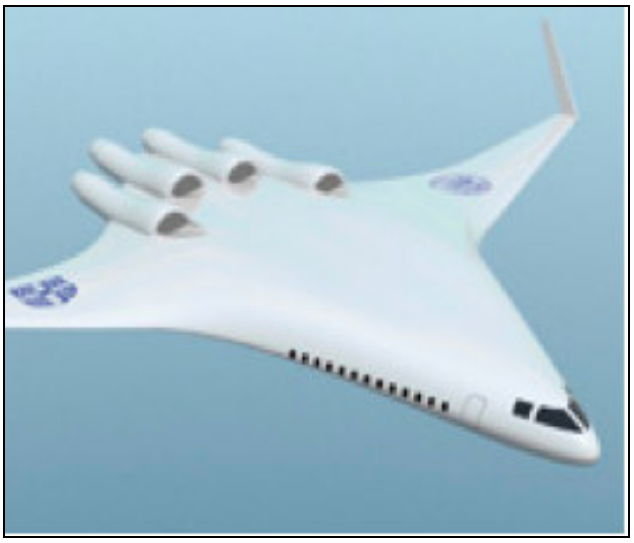

Figure 2-5, Blended Wing Body concept developed by the CMI [50]

2.7.1.3 Fuel Cell Technology

Fell cell technology is one of the most promising forms of sustainable energy, although the technology has not yet reached commercialisation. It has made major advances in recent years, especially in the automotive industry where the commercialisation of fuel cell road vehicles is imminent. However, in the civil aviation industry, fuel cell technology is still a concept. The power output produced by current fuel cell engines are considerably lower than the level required to power aircraft. Moreover, the storage capacity of current fuel cells is inadequate to supply the energy requirement for aircraft to cover the necessary distances [**51**].

2.7.2 Short to Medium Term Development Projects

2.7.2.1 Quiet Technology Demonstrator (QTD)

QTD is a major collaboration between Rolls Royce and Boeing to develop noise abatement technologies. The project focused on three most significant sources of noise, namely the fan, jet and airframe noise [**1**] and utilised the previous experience that both participants have in low noise nacelle inlet and nozzle technologies to address the noise problems in these areas. This has led to the development of the A_{Max} (Area Maximisation) acoustic inlet liner and the serrated nozzle as well as a detailed mapping of noise generated throughout the airframe and engine during operation.

The A_{Max} acoustic inlet liner is designed to reduce the noise created at the front of the engine by increasing the acoustically treated area relative to the conventional Datum design. A comparison between the improved acoustically liner design and the Datum design is illustrated in **Figure 2-7a and b.** The treated area of different acoustic liner designs is shown in white. The improved A_{max} design extend the acoustic lining area by 30% to cover the mechanical joint and other features, preventing sound waves reflecting at these areas. In-flight as well as static tests have been carried out to quantify the full extent of the newly developed technologies, which saw the A_{max} liner produce a noise reduction at the front of the engine by as much as 13 dB.

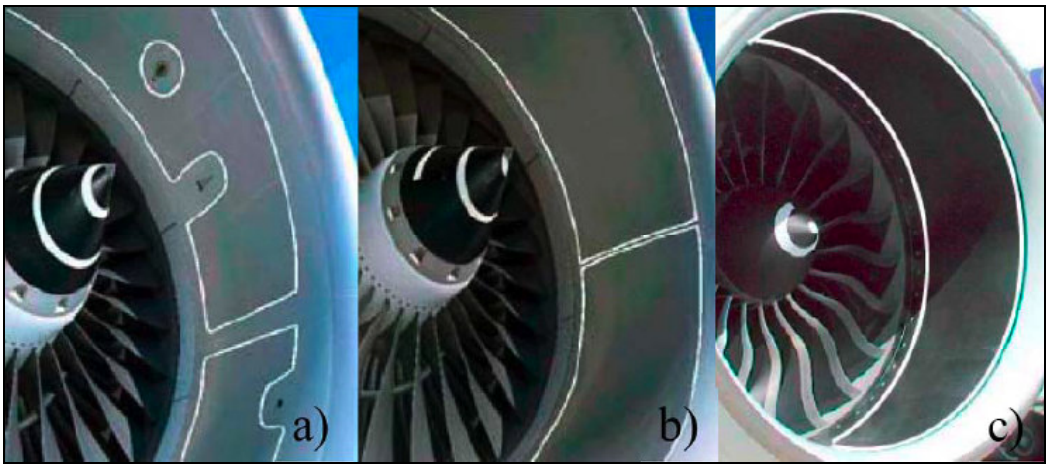

Figure 2-6, Schematics of a) Datum, b) A_{max} and c) Seamless acoustic inlet liner.

The subsequent QTD2 programme, an all American collaboration between Boeing, NASA, General Electric and Goodrich Corporation have taken the liner technology further and developed the *seamless acoustic liner* [**Figure 2-7c**]. The seamless design has further increased the acoustically treated area by a massive 78% compare to the Datum design. At a flight test carried out in August 2005 at Boeing's flight facility in Glasgow, Montana the seamless inlet liner successfully produced a reduction in fan noise at the front of the engine by up to 15dB [**52**].

The Serrated Nozzle is designed to reduce the noise produced by the shearing between the jet stream and the surrounding ambient at the nozzle exit. Serrations strategically placed at the cold and hot nozzle exit produce turbulence and force enhanced mixing between the two air streams. Both Boeing and Rolls Royce have been developing such technologies prior to the QTD programme. Boeing has been testing the *chevron*, their version of the serration, at the Boeing Low Speed

Aeroacoustic Facility (LSAF) whilst Rolls Royce has been undertaking development projects at the QinetiQ Noise Test Facility (NTF). The serrations have achieved 4 dB of noise reduction at the nozzle exit during both in-flight and static tests on the QTD programme [**53**].

However, a by-product of the turbulence at the nozzle exit is an increase in drag, which in turn reduces the overall performance of the engine. In the subsequent QTD2 programme, the Variable Geometry Chevrons (VGC) has been developed to address such a problem. The VGC consist of 3 strips of NiTi shape memory alloy actuators running along a composite backing plate. Wires running alongside the NiTi strips provide resistance heating to deploy the actuation. A photo of the prototype VGC is shown in **Figure 2-8**. When actuated, the VGCs protrude into the exhaust airflow which cause turbulence and provide the noise reduction effect. The VGCs have been successfully tested in a flight test in the QTD2 programme, during which the VGC recorded a reduction in jet exhaust noise of 2 dB and a reduction of *shock cell* noise. In addition, the interior noise cause by the vibration of the nacelle has been reduced by up to 4-6 dB.

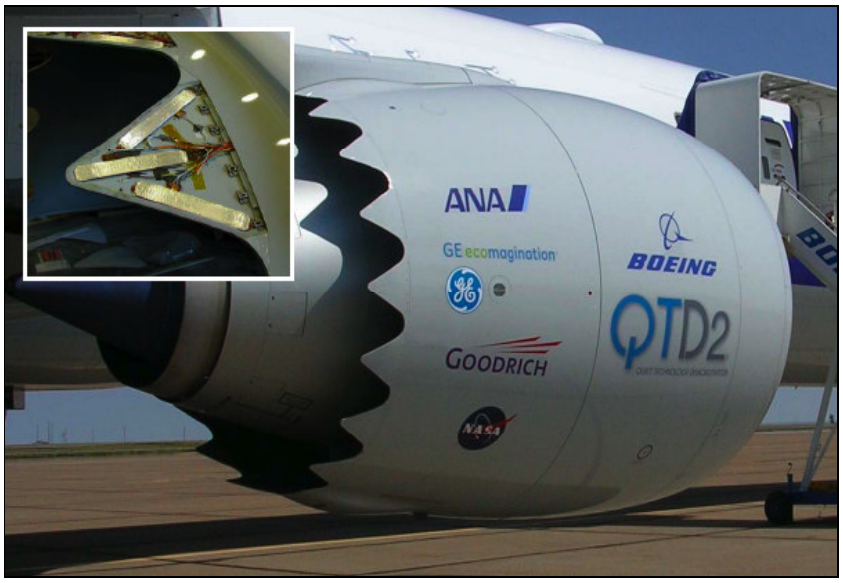

Figure 2-7, VGC demonstrated at the QTD2 flight test [1]

The QTD2 also attempted to address the third area – airframe noise that was not covered in the original QTD program. With engine noise continuing to reduce, the aerodynamic noise of the airframe becomes more and more apparent, especially during landing approach. **Figure 2-9** shows a breakdown of noise component of a typical aircraft at approach and take-off condition. Note that the proportion of airframe noise to total aircraft noise at approach condition is significantly higher than that at the take-off condition. This is because the engines are operating at full power during take-off as oppose to approximatly 30% power during approach [**62**].

The main contributors to the generation of airframe noise, especially during landing configuration are the high lift components such as flaps and landing gear. **Figure 2-10** shows a breakdown of the noise generated by each component. Landing gear has complex and non-streamlined geometry. Upon deployment, it generates highly turbulent wakes and it is the vortices generated from one component impinging onto

the other that generates noise. Low noise landing gear designs such as those shown in **Figure 2-11** cover up the components that generate these wakes with acoustic liner, thus improve the aerodynamic efficiency and reduce the noise generated by the landing gear.

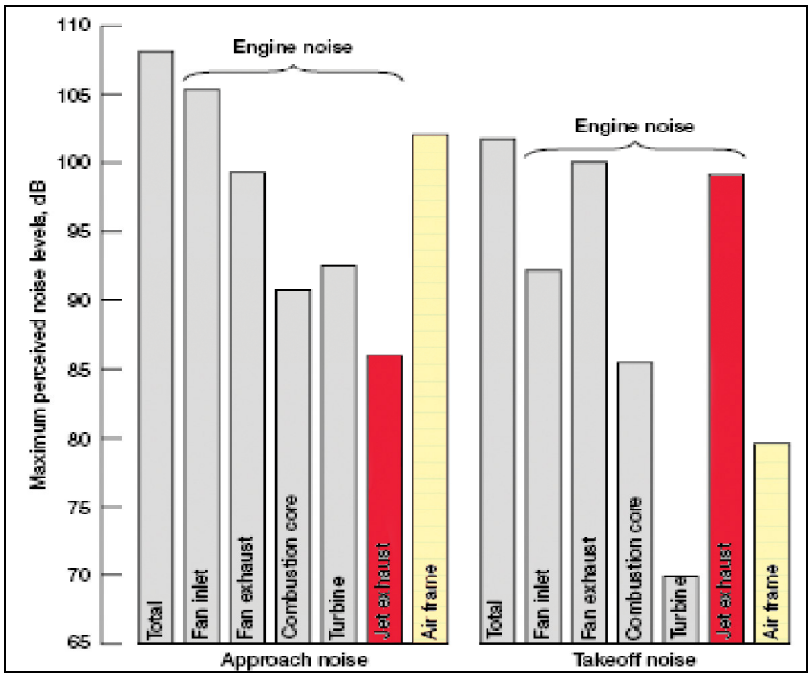

Figure 2-9, Engine and airframe noise during takeoff and approach [64]

****Data based on 1992 technology level***

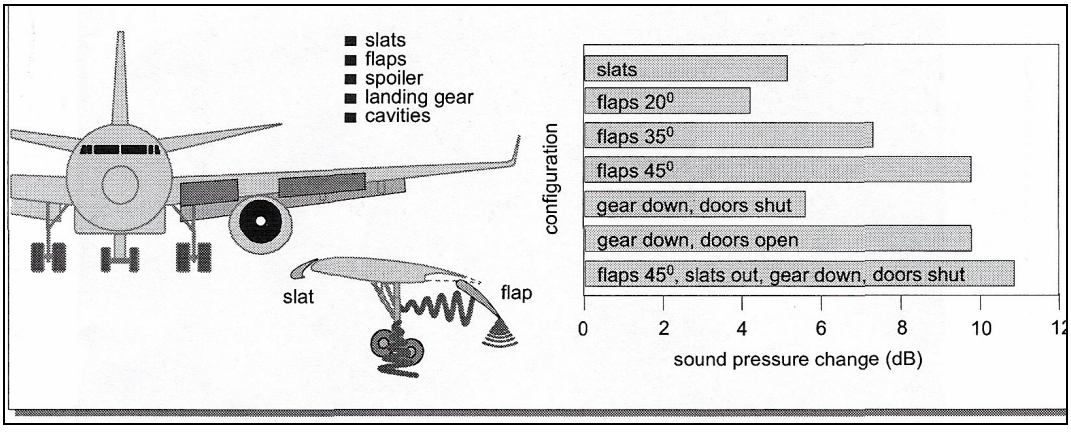

Figure 2-10, Noise generated by high lift components [53]

Figure 2-81, Low noise landing gear operating at the QTD2 flight test [1]

2.7.2.2 Silence(R) Aircraft Project

SILENCE(R), which stands for **SI**gnificantly **L**ower aircraft **E**nvironmental **N**oise **C**ommunity **E**xposu**R**e is a major European collaborative effort, involving airframe and engine manufactures such as Rolls Royce, MTU, SNECMA, Airbus and many academic outlets to investigate new technologies that may lead to the reduction of aircraft noise. The program started in 2001 and aimed to incorporate new applications of liner material, new low-noise fans, a circumferential 'splitter' in the fan outlet guide vane and a negatively-scarfed intake that directs fan-generated noise upwards rather than towards the ground. A test vehicle incorporating some of these innovations has been tested at Rolls Royce's noise testing facility at Hucknall, UK [**Figure 2-12**].

Figure 2-9, Rolls Royce's special noise test facility at Hucknall, UK [54]

2.7.2.3 Adaptive Serrated Nozzle (ASN)

The principle of the Adaptive Serrated Nozzle (ASN), developed by Rolls Royce is similar to the VGC described in the previous chapter. Both concepts are based on the principle of the serrated nozzle jointly developed by Rolls-Royce and Boeing in the QTD programme. Essentially in both concepts, NiTi shape memory actuators are used to deploy the serrations or chevrons, which create protrusions into the jet stream during takeoff to reduce the exhaust noise during take-off. The serrations or chevrons are designed to retract back by the shape memory actuators at altitude where noise is less of an issue, thereby eliminating the performance penalty at cruise. However, instead of Boeing's triangular chevron design, Rolls Royce went for a much simpler rectangular design, with a single NiTi SMA strip the same size of the serration, working against a pre-stressed titanium backing plate to produce the actuation. Such designs are not only simpler; but also produce a larger deflection. This is probably

one of the reasons why the ASN achieves a noise reduction of up to 4 dB (relative to the base line configuration) during flight test, 2 dB more than Boeing's design [**55**]. Both the VGC and the adaptive serrated nozzle are targeted to be used in next generation aero-engines due to come into service in 5-10 years time.

3 Adaptive Serrated Nozzle

The serrated nozzle is one of the most promising short-term noise abatement technologies. As described in **Chapter 2.7.2.3**, the use of an adaptive system could provide significant fuel savings, particularly to trans-oceanic aircrafts that spend the majority of their in-flight time at cruise condition compare to the fixed serration design. Unique to Rolls-Royce's adaptive design is the use of large shape memory actuators. The use of shape memory alloys in such a large structure and in such a demanding operating condition is believed to be unprecedented.

3.1 Design Philosophy

The adaptive serrated nozzle concept is designed to fully integrate SMA actuators into the structural design of the serration such that its shape changes between two pre-determined positions at either side of the transition temperature [**4**]. A schematic representation of the serration design is shown in **Figure 1-3** and **3-1**. A preliminary design study has been carried out at Rolls-Royce and the operating conditions and mechanical requirements for the component have been established and shown in **Table 3-1 [56]**.

Operating Conditions	
Temperature range	47 – 157 °C
Transition Temperature	~110°C
Hysteresis range	As narrow as possible
Gas Loading	3 psi = 21 kPa
Fatigue resistance	10^6 cycles at up to 2% strain

Table 3-1, detailed design specification [57]

The dimensions of an individual serration fitted to the Boeing test flight are shown in **Figure 3-5**. The serrations are fitted along the circumference of the nacelle at the nozzle exit and the number as well as the exact dimension of the serration fitted to each engine will depend on the individual engine types and sizes.

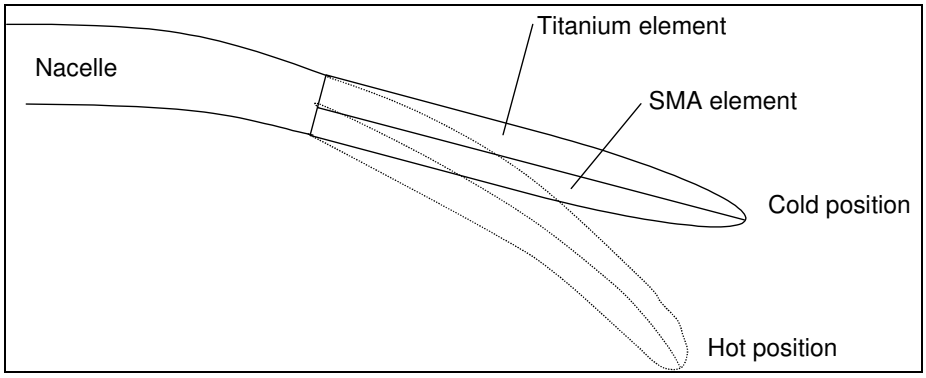

Figure 3-1 Schematics of the adaptive serrated nozzle system [4]

Each serration consists of two sub-components [**Figure 3-2a**], a parent structure made from aerospace grade Ti-6Al-4V alloy and a thin sheet of SMA attached to the bottom surface of the structure. The parent structure's pedestal construction is designed to

provide maximum tip deflection. During operation, the pre-stressed parent structure act as a bias spring, inducing a constant upward force on the serration. When the operating temperature rises during take-off and climb conditions, the SMA undergoes a phase transformation causing its elastic modulus to rise, thus pulling the component downwards towards position Ra shown in **Figure 3-3** thereby creating the protrusion. The design study showed that the temperature rise across the engine at take-off and climb conditions was estimated to be sufficient to deploy the serrations [**4**]. As the aircraft cruises at altitude the temperature drop will cause the structure to return to its original position. However, environment and engine conditions vary widely with global position and altitude and so an extensive study on the conditions at major airports around the world has been carried out at Rolls-Royce. The conditions within 180 miles of a representative selection of 37 international airports have been studied [**4**]. Results showed that 99% of conditions lie within the operating range of SMA actuators, which ensures the applicability of the concept. An alternative control system using electrical resistance heating or hot air from the by-pass duct of the engine have also been considered to ensure the deployment of serrations in all conditions.

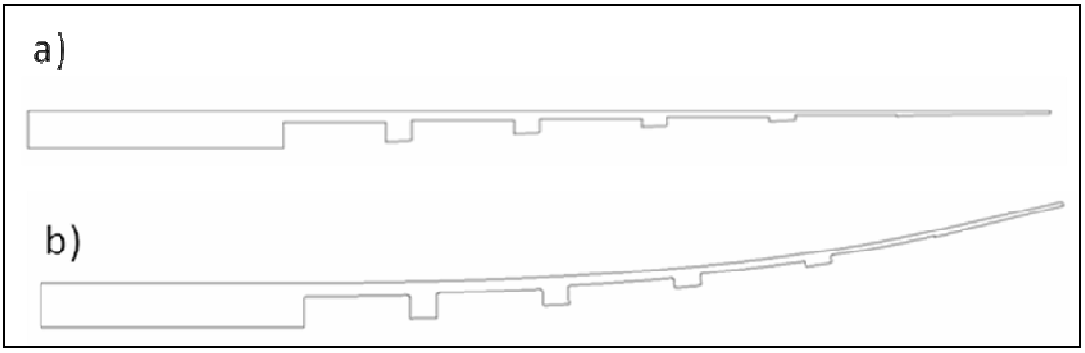

Figure 3-2 a, Machined titanium parent structure; b, processed titanium parent structure [56]

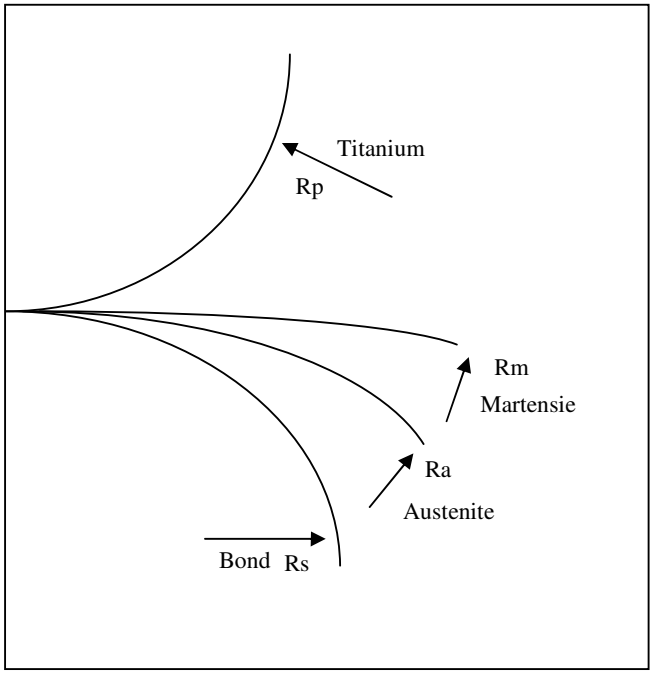

Figure 3-3, schematic representation of the manufacturing process of a serration [57]

The manufacturing process of the component compromises several stages: first the titanium structure is machined to the shape shown in **Figure 3-2a**; it is then be forced upward to the position shown in **Figure 3-2b** and subjected to a heat treatment at 600ºC for 1 hour to relieve stresses built up during the process. The parent structure is then elastically bent downward to position Rs shown in **Figure 3-3** and held in a jig while a strip of SMA is joined to the bottom surface of the pedestals. When joining is completed, the assembled structure is released from the jig. The pre-stressed titanium part will attempt to return to its original shape, but is restrained by the SMA actuator, which goes into tension. Providing the geometry of the parts has been correctly designed, the equilibrium position for the assembled serration should be horizontal (position R_m in **Figure 3-3**). **Figure 3-3** shows a schematic of the manufacturing

process of the component. A scaled-down prototype has already been produced by Rolls Royce. **Figure 3-4** shows a picture of the prototype being assembled in a jig **[4]**.

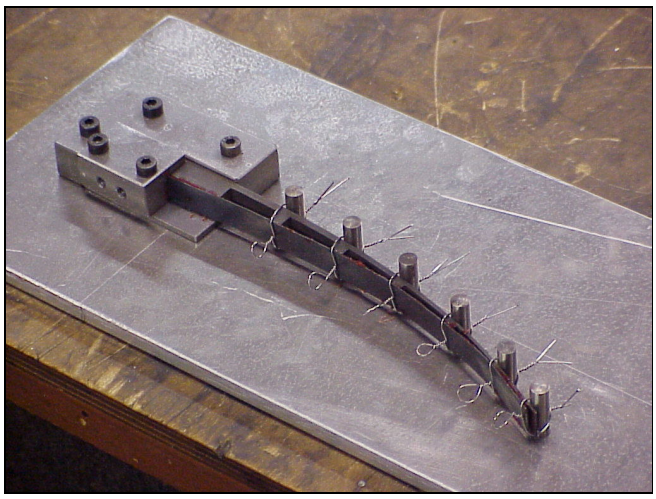

Figure 3-4, demonstration prototype [4]

The manufacturability of the adaptive serrated nozzle is hindered by the problems with identifying a viable joining technique to join NiTi SMA to the titanium parent metal. This is the reason why the prototype shown in **Figure 3-4** was held in a jig by fasteners. Joining of NiTi SMAs either to itself or to other dissimilar metals has been well documented to be very difficult if not impossible [**58, 59**]. An internal risk assessment by Rolls Royce reveals that joining methods have been identified as the task that carries the most significant risk in the development programme [**60**]. This is also likely to be one of the most expensive tasks to mitigate. An initial stress analysis carried out based on simple bending theory showed that the shear stresses at the joint interface are estimated to be around 340 MPa [**61**]. However, attempts have been carried out to join NiTi SMAs to the titanium parent materials using low temperature

soldering and chemical adhesive which failed to delivery ultimate shear strength at joint interface over 50 MPa [**4**].

The shape memory alloys currently commercially available can only preserve their SME at temperatures up to 150ºC which is adequate to use in the cold nozzle [**Figure 3-5**]. Several high temperature SMAs have been under extensive research and development, but these materials are still in their development stage. Until further advances in high temperature SMAs have been achieved, the operating temperature at the hot nozzle is too high for the SMAs currently available. Therefore, this project will focus primary on the adaptive serrated cold nozzle, but with the view that any development work being carried out here can potentially be carried forward to other high temperature applications when high temperature SMAs become commercially available.

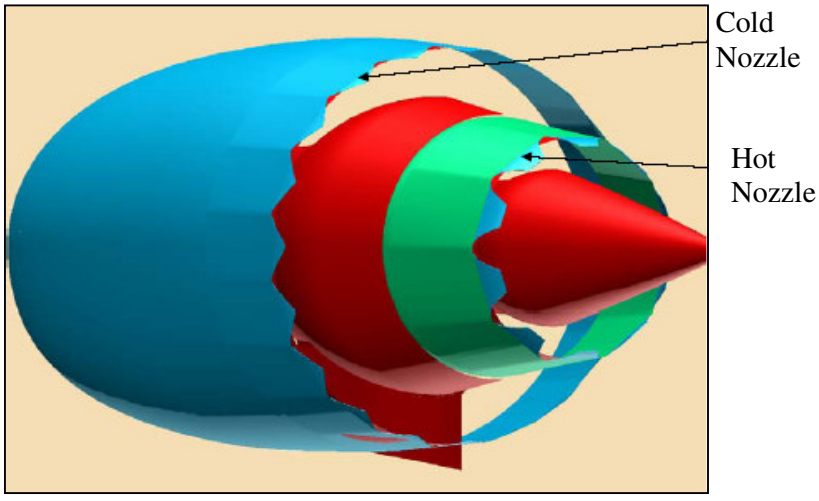

Figure 3-5, Adaptive serrations installed in the hot and cold nozzle [61]

3.2 Stakeholder Analysis of Adapted Serrated Nozzle

Stakeholder management is critical to the success of every project. Stakeholders are groups of people who have influence or power over the outcome of a project, or have an interest in its successful or unsuccessful conclusion [**62**]. There are many benefits to identify and manage the stakeholder of a project before it commences. For example, by identifying and powerful stakeholders, one may win more support and resources to make the success of the project more likely; also by identifying different groups of stakeholders, one can better anticipate their reactions to the project thus develop strategies to ensure the successful implementation of the project.

Stakeholder management can broadly divide into three steps [**62**]: *Stakeholder Analysis* where sets of people with influences, interests or power over the project are identified through intensive brainstorming; *Stakeholders Prioritisation* where groups of stakeholders are sorted in terms of the level of power and interest they have over the project; and *Stakeholder Management* where plans are devised to engage and communicate to different groups of stakeholders in the best way possible in order to ensure the success of the project.

3.2.1 Stakeholder analysis

Stakeholder analysis is the technique used to identify these key sets of people. Groups of people who have influence, interests or power over the outcome of the

project are identified through brainstorming. For the current project, six groups of stakeholders have been identified.

- Internal investors – these include principal engineer, managers and financial officers within Rolls Royce who either holds the resources or have the power to halt or advance the current project.)
- Aircraft manufacturers (e.g. Airbus and Boeing)
- Airline operators
- Governing bodies – such as airport authorities who set local, national and international aircraft noise regulations
- Environmental groups
- General Public (passengers)

3.2.2 Prioritising Stakeholders

Amongst the list of stakeholders, some may have the power to block or accelerate the progress of the project, some may have significant influence over the direction of the project and some may only have an active interest over the outcome of the project. One must then prioritise the groups of stakeholders in terms of the level of power and interests they have over the project in question so that they can be better managed. A *power/interest chart* can be used to help the prioritisation process [**63**]. The groups of stakeholders identified in the last step were systematically placed in the power/interest chart shown in **Table 3-2,** based on the level of power and interest they possess over the current project. For example, internal investors hold all the resources needed for

the project and have the power to control the progress of the project, they have the highest power and interest over the current project; the general public in contrast have no control over either the outcome or the direction and the progress of the project. They have however an active interest over the overall outcome of the project as the level of aircraft noise affects the quality of their lives. Thus they are placed in the bottom right corner in the power/interest chart [**Table 3-2**].

3.2.3 Stakeholder Management

Once the list of stakeholders is sorted in terms of the level of power and interest that each group has over the current project. Strategies can be developed to effectively manage the influence of each stakeholder. Those who possess low power and interest requires the least effort to manage. Only governing bodies fall into this category, the only interest they have over the current project is the effect it has to the overall noise performance of aircraft when it is introduced to aero engines. However, they do not have any power over the current project. This group of stakeholders requires the least effort to manage, they only require to monitor regularly, in case of any changes in noise regulation which could result in the need to modify the design of the ASN.

Stakeholders with low power but high level of interest require more effort to manage. As their opinions may influence the opinions of other stakeholders, they need to be kept informed regularly so that their reaction towards the outcome of the project can be better anticipated and managed.

Stakeholders with high power and relatively low level of interest need to keep satisfied for the entire duration of the project. For the current project, there is only one group of stakeholder falls into this category – the airline operator. The ASN is designed to install at the nozzle exit and is visible from outside. Airline operators may not approve a change in the shape of the nozzle as a result of the introduction of the ASN. The design of ASN may need to be modified throughout the project in order to meet the airline operators' requirement. One must therefore communicate with the airline operators throughout the project to ensure they approve the new nozzle.

For stakeholders such as the general public and environmental groups who do not have any power but with a high level of interest over the current project. The opinion of these groups of stakeholders can put pressure on the governing bodies to tighten noise regulation which in turn alter the opinion of the airline operators towards the current project. Thus they have an indirect influence over the progress of the current project. This group of stakeholders must be kept informed regularly in order to better anticipate and manage their reaction towards the progress of the current project.

Stakeholders with high level of power and interest have the power to advance or halt the progress of the current project. This group of stakeholders must manage closely so that they fully support the direction of this project. The effective management of this group of stakeholder has many advantages, such as the maximisation of resource and the elimination of key obstacles to the project. This group of stakeholder requires the most effort to manage effectively.

By identifying and understanding the motive of the key stakeholders early in the project, potential obstacles to implementation and results can be avoided. When used in conjunction with other tools such as qualitative economic analyses and social impact assessments, Stakeholder Analysis can help project manager to devise strategies to overcome opposition and channel information and resources to promote and sustain proposed project.

		Interest	
		Low	High
Power	Low	**Latents** • Airline Operators	**Promoters** • Internal Investors • Aircraft Manufacturers
	High	**Apathetic** • Governing bodies	**Defenders** • Environmental Groups • General Public

Table 3-2, Power/Interest Grid for Stakeholder analysis

3.3 The Economic Impact of Adaptive Serrated Nozzle

There is no doubt that the market demands noise reduction technologies such as the ASN. However, it is important to ensure that these new technologies could help to increase the levels of economic and social prosperity of the developer. Therefore an extensive study has been conducted in this project to investigate both the social and economical value of the ASN to its stakeholders. To quantify the benefit of ASN in a business context, the benefit that the ASN could create to the business of the users

must first be identified. These benefits can then be converted into economic and social values.

The ASN is essentially a noise abatement device that provides up to 4 dB of noise reduction to the jet noise, the noise reduction have been proven on a Rolls-Royce Trent 800 engine in both in-flight and static tests [**52**]. Decibel is measured on a logarithmic scale, so the total noise reduction equates to approximately 10 dB for a quad-engine aircraft and approximately 7 dB for a two-engine aircraft fitted with similar engines [**Table 3-2**].

Quad-Engine Aircraft	Two-Engine Aircraft
$L_{wt} = 10\log_{10}[\sum_{i=1}^{n}\log^{-1}(\frac{L_{pi}}{10})$ $= 10\log_{10}(\log^{-1}(\frac{4}{10})\times 4)$ $= 10.02 decibels$	$L_{wt} = 10\log_{10}[\sum_{i=1}^{n}\log^{-1}(\frac{L_{pi}}{10})$ $= 10\log_{10}(\log^{-1}(\frac{4}{10})\times 2)$ $= 7.01 decibels$
*where L_{wt} = total Sound pressure level (SPL) and L_{pi} = single event SPL	

Table 3-2, Effect of ASN on a dual and quad-engine aircraft

The noise reduction recorded at in-flight and static tests are measured at the nozzle exit and as illustrated in **Figure 3-7**, this only account for a fraction of the total engine noise. However, it is impossible to determine the effect of ASN to the reduction of total engine noise for current engine models since engine noise data is highly commercially-sensitive and is therefore not obtainable. Furthermore, the noise performance is specific to individual aircraft's make, model, engine, configuration

and weight. With no accurate noise data available, the effect of ASN in reducing the level of total aircraft noise has been estimated using the proportion shown in **Figure 2-9**. The figure shows a breakdown of the noise component of a typical aircraft with 1992 technology level during take-off and approach. The data is obviously out-dated, hence the current study uses it for demonstration purposes. Using these proportions, a 7 and 10 dB drop in jet noise is estimated to produce approximately 1.46 and 1.56 dB reduction in the total engine noise respectively. For simplicity, a noise reduction of 1.5 dB will be used throughout the current study irrespective of aircraft model and configuration.

The ASN benefits its user in two ways: 1) it helps to improve the social responsibility of airlines through a reduction in aircraft noise and; 2) it reduces the cost base of the aircraft operator through a reduction in noise-related charges. The potential saving in these two areas can run into millions of pounds. A case study has been used to illustrate the level of saving that a typical airline can achieve by fitting the ASN in its existing fleet. Virgin Atlantic has been chosen for the current case study as it is Britain's second largest international air travel service provider and its fleet consists of only large trans-oceanic aircrafts, which is the main target market segment for the ASN. For simplicity, the current case study focused on flights operating to and from Heathrow airport. Heathrow airport is the busiest airport in the world, with a plane landing or taking-off every 55 seconds at peak periods [**65**] and is renowned for its stringent environmental restrictions (Heathrow's environmental policy for managing aircraft noise is described in **Chapter 2.5.3**).

3.3.1 Social Costs

As discussed in the previous section, the social costs of aviation noise have been extensively evaluated by governments and airport authorities. However, the valuation methods that these bodies used are not appropriate for evaluating the cost of noise for appraising novel noise abatement technologies such as the ASN. In the current study, the social benefit of the ASN has been determined by: 1) the reduction in noise damage to the affected community and 2) the potential saving for airport authorities in reducing the required provision of home relocation assistance to the affected households.

3.3.1.1 Reduction in Noise Damage

One way to determine the social cost of aviation noise for a single event is to determine the cost of noise to the affected households around an airport. A workshop run by the European Commission on noise valuation in 2002 has taken representative values from each European country and determined that the average value for the benefit of outdoor noise reduction is €25.8 per household per decibel per year and the median value is €23.5 per household per decibel per year [**66**]. The workshop recommended its member state to use a value of €25 per household per decibel per year as the value of the perceived benefit of noise reduction, assuming that the money value is constant across the range of noise levels. The validity of this interim value is between 55 L_{den} and 75 L_{den}. The social cost of aviation noise per decibel per year can therefore be determined by multiplying the recommended cost of noise per

households per decibel per year by the number of affected households around the airport. The latest figures published from Heathrow shows that there is 168.1 km^2 affected by the noise generated by the airport with over 180 thousand households residing in such an area [**Table 3-3**]. Assuming all the aircraft operating to and from Heathrow is fitted with ASN producing an over all noise reduction of 1.5 dB at take off, this would equate to a reduction of over €7 million worth in social damage caused by aviation noise per year.

Leq_A (dBA)	Area (km^2)	Population (´000s)	Households (´000s)	Effect of ASN (1.5 dB reduction in total noise) per Year (€´000s)*
>54	168.1	436.9	188.4	7,065.00
>57	95.8	195.5	81.9	3,071.25
>60	54.5	88.2	35.2	1,320.00
>63	33.7	41.0	16.2	607.50
>66	19.9	15.4	6.0	225.00
>69	9.8	3.3	1.3	48.75
>72	5.0	0.2	0.1	3.75

**Assuming cost of noise is €25 per decibel per household per year*

Table 3-3, Noise Exposure Contour at Heathrow Airports [67]

Note that the valuation is based on the average depreciation of the properties around airports that are affected by noise. Airport authorities will no doubt save money in terms of the buildings and residential houses that require noise insulation, but the amount of the money saved is likely to be substantially less than the figures shown in **Table 3-3**.

3.3.1.2 Prevention Costs

Another method to determine the economic benefit of fitting ASN to aircrafts is to determine the reduction in the costs of compensating the population around the airport that is affected by aviation noise. A recent NASA study has shown that a 5, 10 and 20 dB reduction in aviation noise can produce a reduction in the area of the noise contour around an airport by 40, 68 and 90% respectively [**Figure 3-8**]. The level of reduction in noise contour area for 1.5 dB noise reductions that the ASN provide can be determined by extrapolating the data from **Figure 3-8** as shown in **Figure 3-9**.

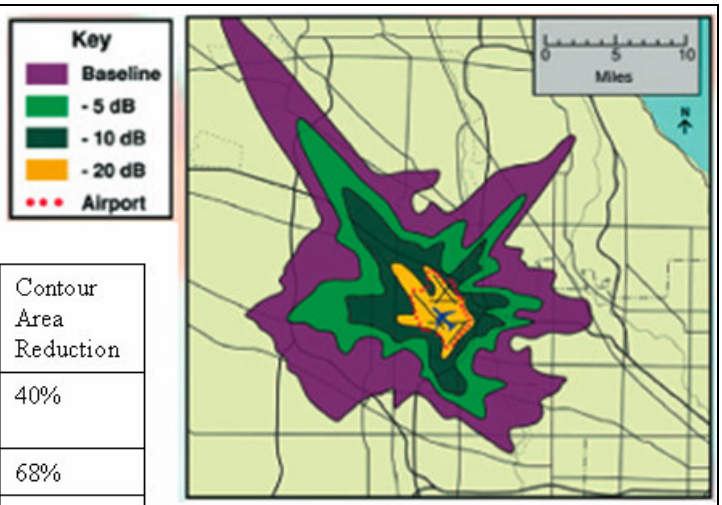

Level Reduction	Perception	Contour Area Reduction
5dB	Significantly quieter	40%
10dB	Half as loud	68%
20 dB	One fourth as loud	90%

Figure 3-6, Graphical representation of the effect of noise reduction on the size of noise footprint [68]

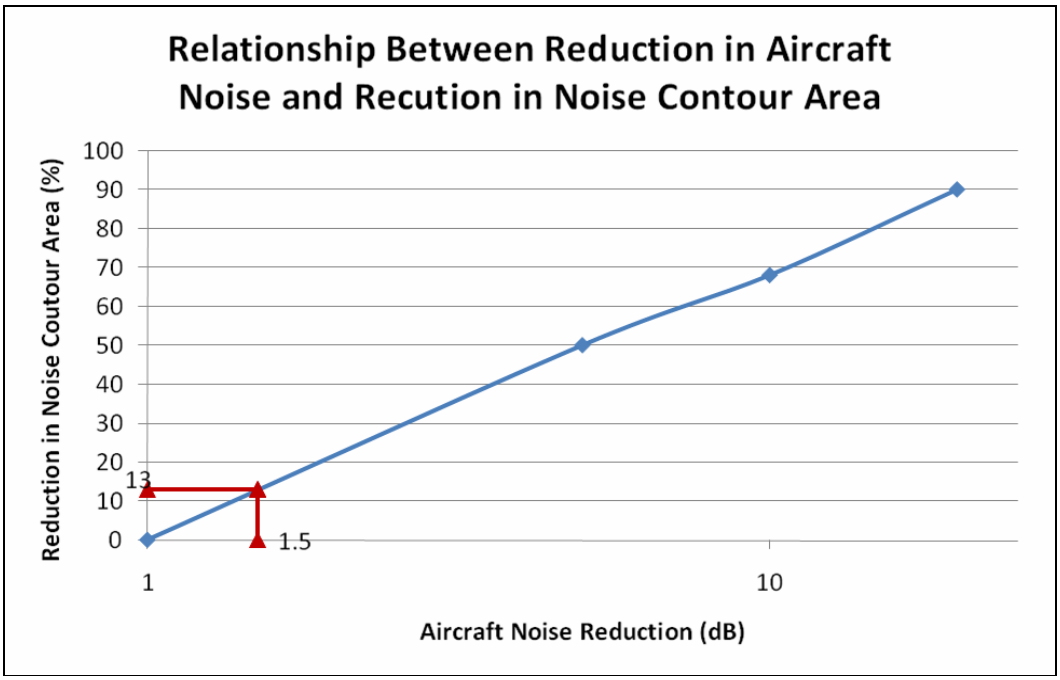

Figure 3-7, Relationship between aircraft noise reduction and reduction in noise contour area around an airport

From the extrapolation, the level of reduction in the noise contour area at Heathrow airport for a 1.5 dB reduction in aircraft noise is approximately 13%. Applying this figure to the noise contour data in **Table 3-3** gives rise to a reduction of up to: 21.85 km^2 of affected area or; 56,800 of affected population; or 24,490 of affected households [**Table 3-4**].

Leq_A (dBA)	Area (km^2)			Population ('000s)			Households ('000s)		
	Current Level	ASN fitted to aircrafts	Reduction (-13%)	Current Level	ASN fitted to aircrafts	Reduction (-13%)	Current Level	ASN fitted to aircrafts	Reduction (-13%)
>54	168.1	146.25	21.85	436.9	380.1	56.8	188.4	163.91	24.49
>57	95.8	83.35	12.45	195.5	170.09	25.42	81.9	71.25	10.65
>60	54.5	47.42	7.09	88.2	76.73	11.47	35.2	30.62	4.58
>63	33.7	29.32	4.38	41	35.67	5.33	16.2	14.09	2.11
>66	19.9	17.31	2.59	15.4	13.4	2	6	5.22	0.78
>69	9.8	8.53	1.27	3.3	2.87	0.43	1.3	1.13	0.17
>72	5	4.35	0.65	0.2	0.17	0.03	0.1	0.09	0.01

Table 3-4, Effect of fitting ASN to aircrafts on the noise contour area at Heathrow

Heathrow airport launched the 'Home Relocation Assistance Scheme' in October 2005 to address airport noise for the communities close to the airport [**69**]. This offers help with the cost of relocation for people living in the area with the highest levels of noise and wishing to move away from those areas. Following guidelines on the White Paper on the Future of Air Transport, this noise level is set at 69 decibels or more, averaged over a daytime of 16 hours, (i.e. >69 dB(A) Leq_{16h}). The relocation assistance scheme provide eligible home owners with a relocation package consisting of a payment of 1.5% of the completion sale price of the property plus a lump sum payment of £5000 towards the cost of moving with a cap of £12,500 on each package. According to the data on **Table 3-4**, a total of 1300 households reside in the 'highest noise level' areas around Heathrow. This equates to a reduction of around 170 households if aircrafts are fitted with ASN. The latest property report published by Land Registry showed that the average price at Hillingdon, the Borough where Heathrow airport is situated, during the period of January to March 2006, was £247,715 [**70**]. The potential cost of the home relocation assistance scheme could therefore reach over 11.3 million pounds, if all the eligible households wish to move immediately [**Table 3-5**]. However, if aircrafts arriving and departing from Heathrow

are fitted with the ASN nozzle, this figure reduces to just over 9.8 million pounds, making a potential saving of nearly 1.5 million pounds.

Average Cost per Property	£247,715.00	
Relocation Assistance Payment (1.5% of Property Sale Price)		£3,715.73
Lump Sum Payment		£5,000.00
Total Payment Per Eligible Household		£8,715.73

	Number of Eligible Household	Total Cost of Scheme (£)
Current Noise Level	1300	£11,330,442.50
With ASN Fitted to Aircrafts (-1.5 dB)	1130	£9,848,769.25
Potential Saving	170	£1,481,673.25

Table 3-5, Total costs of the home relocation assistance scheme to Heathrow airport and the potential saving by fitting ASN to aircraft

3.3.2 Economic Costs

To quantify the benefit of the ASN from the end-users i.e. airline point of view, one must first determine the cost of noise to airliners. The only noise related cost to airlines is the landing charges and penalties imposed by airports. Virgin Atlantic currently has 22 flights departing from Heathrow airport per day. All of which are

international, long-haul trans-oceanic flights that the ASN is designed to operate on. **Table 3-6** shows the aircraft model and the noise performance of Virgin Atlantic's current fleet, all of which are certified under the latest ICAO Chapter 4 noise standard and qualified for the Chapter 3 base rate when landing at Heathrow.

Aircraft Types	**Number of Aircrafts**	**Margin below the noise limits of ICAO Chapter 4 (ENPdB)**	**Heathrow Quota Count (QC)**	
			Departure	**Arrival**
Boeing 747-400	13	-2.7	4	2
Airbus A340-300	9	-11.1	0.5	2
Airbus A340-600	10	-4.3	1	2

Table 3-6, Noise Performance of Virgin Atlantic Fleet [71]

The level of noise reduction provided by the ASN is insufficient to reduce the landing charge. However, the ASN is just one out of the many noise reduction technologies being developed by engine and airframe manufacturers. It is unlikely that the ASN will be marketed as an individual noise abatement device. Instead, it will be included amongst a range of other novel noise reduction technologies which aims to provide next generation engines with substantial improvement to their noise performance. Currently Rolls-Royce is aiming to reduce the noise level of its product by 10 dB relatively to the 1998 level [**Figure 3-10**].

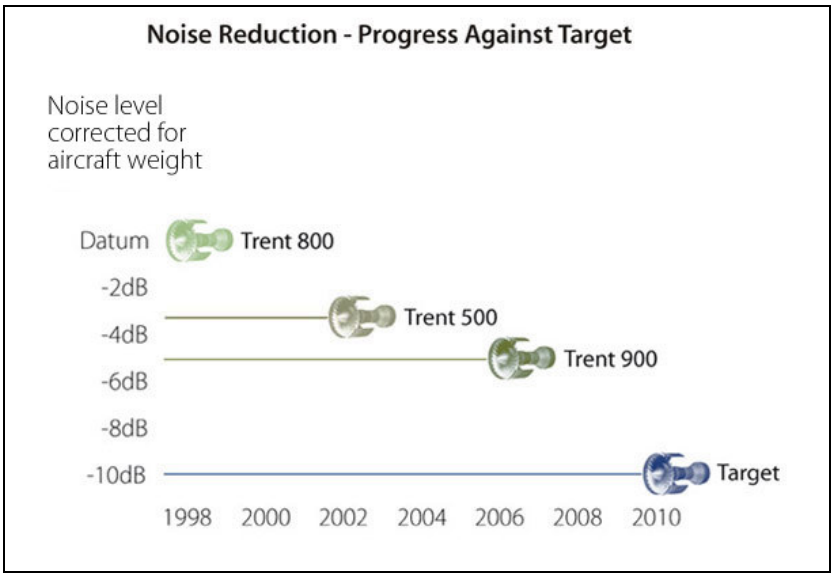

Figure 3-8, Rolls-Royce's Noise Target [72]

Assuming that Rolls-Royce reaches the 10 dB noise target with its latest engines and that the landing charge scheme at Heathrow remains the same, and if all of Virgin Atlantic aircrafts were fitted with the latest engine model, the enhanced noise performance could mean that all of Virgin Atlantic aircrafts arriving at Heathrow would qualify for the Chapter 3 minus landing rate, a full 10% off the Chapter 3 base rate. This will save the company over £400,000 a year in landing fees alone [**Table 3-7**]. This saving is likely to be significantly higher than currently estimated, as the landing fees imposed by airports is likely to increase when environmental regulations and noise standards become more and more stringent.

	Chapter 3 base rate	Number of flight landing at Heathrow per week [7373]	Total landing charge per week	Total landing charge per year (52 Weeks)
Peak	£609.00	69	£42021.00	£2,185,092.00
Shoulder	£590.00	14	£8,260.00	£429,520.00
Off-Peak	£438.00	71	£31,098.00	£1,617,096.00
		Total		£4,231,708.00
		10% saving by moving to Chapter 3 Minus Rate		£423,170.80

Table 3-7, Total Landing Charge Incurred by Virgin Atlantic

4 Shape Memory Alloys

Shape memory alloys (SMAs) are a group of metallic materials that possess two very unique properties, the shape memory effect (SME) and the superelastic effect (SE). The SME is the ability of a material to '*remember*' a pre-defined shape and deformation can be restored to its pre-determined shape upon heating. The other effect is SE, also known as the *Pseudo-elastic Effect*, is the ability of a material to exhibit extraordinary elasticity. Just like other metal alloys, the SMA change shapes during deformation and returns to the original shape after unloading if no plastic deformation has been induced. The difference is that SMAs can accommodate up to 10 times the normal amount of strains compared to other conventional metal alloys before undergoing true plastic deformation. These properties occur due to a temperature and/or stress dependent shift in the materials' crystalline structure between two phases. SME occurs at the lower transformation temperature where the martensitic phase exists; conversely, the SE occurs at the higher transformation temperature where the austenite phase exists [**74**].

SMA was first discovered in an Au- 47.5 at% Cd alloy in 1951 by Chang and Read. They noticed the reversibility of the transformation in the alloy by metallographic observation and changes in electrical resistivity [**75**]. Within ten years of the discovery, SMAs had been used in commercial applications. Since then, at least fifteen different binary and ternary alloy types have been discovered that exhibit SME. Some of these alloy types are shown in **Table 4-1**. However, only those that are able to recover substantial amount of strain and those that generate substantial

forces upon changing shapes generated real commercial interests. Due to their unique shape memory ability, SMA has lent itself to many innovative applications ranging from medical science to space deployment systems and only recently have they are being considered for adaptive control systems.

Gold-Cadmium	Titanium-Palladium-Nickel
Hafnium-Titanium-Nickel	Uranium-Niobium
Titanium-Niobium-Aluminium	Nickel-Titanium-Copper
Iron-Manganese-Silicon	Nickel-Titanium
Copper-Aluminium-Iron	Zirconium-Copper-Zinc

Table 4-1, Alloy that exhibit shape memory effect

4.1 SMA Characteristics

4.1.1 Shape Memory Effect

The SME occurs when a SMA is in its martensitic state where the alloy can be easily deformed. Unlike conventional metal alloys, the deformed alloy is completely plastic in this state. However, when the alloy is heated above the austenite finish temperature, the alloy undergoes a phase transformation. The alloy transforms to the austenite phase and restores to its original shape, also known as the *parent phase.*

Once the shape is recovered, the SMA can be cooled below the martensitic finish temperature and the alloy becomes ductile again.

The underlying mechanism of SME is a diffusionless, solid-state phase transformation between a lower temperature martensitic phase with a body centre cubic crystal structure, often known as B2 structure; and a higher temperature austenitic phase with a monoclinic crustal structure, known as the B19′ phase. The transformation process is better known as *thermoelastic martensitic transformation*. This phase transformation is crystallographically reversible, hence the strains are fully recoverable when subjected to the specific thermal procedure. The transformation does not take place at one unique temperature, instead the transformation process is characterised by a pronounced hysteresis. **Figure 4-1** shows a plot of volume fraction of martensite in a typical SMA as a function of temperature [**79**]. The curve shows a clear hysteresis loop typical of SMAs. The graph also provides the following temperatures that are unique to individual types of SMAs: austenite start temperature (A_s), austenite finish temperature (A_f), martensite start temperature (M_s) and martensite finish temperature (M_f). The hysteresis is an important characteristic of SMAs. The transformation temperature as well as the shape of the hysteresis loop can be altered depending on the type of the alloys used and its processing history. For NiTi SMA for example, the width of the hysteresis can be reduced by the addition of copper; while the transformation temperature has been lowered by the addition of iron for cryogenic applications. Hysteresis loops of 20 – 40 °C are typical for NiTi SMA systems. For most applications, the temperature at which martensite fully transforms to austenite (A_f) is the most important transformation temperature as it dictates the transition between shape memory and superelastic properties. Similar to the

hysteresis loop, the A_f temperature can be adjusted through thermo-mechanical treatments in order to optimise performance [**76 – 78**].

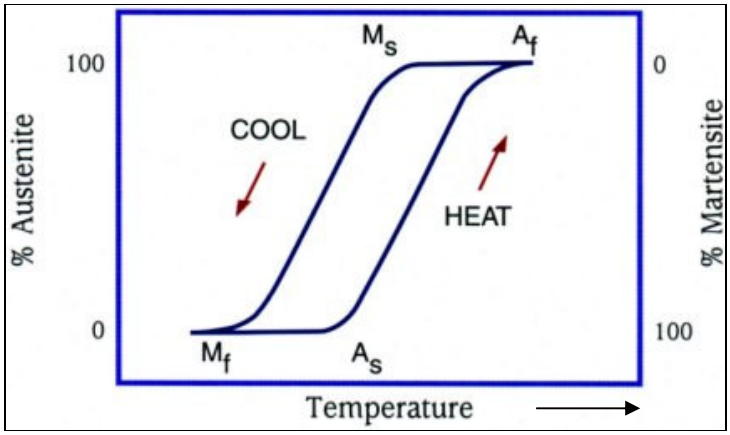

Figure 4-1, schematic representation of the hysteresis loop [79]

Below its martensitic finish temperature (M_f), SMA is completely martensitic. Unlike the martensitic microstructure usually seen in steel, this microstructure of SMAs is soft and characterised by *self-accommodating twinning* as shown in **Figure 4-2**.

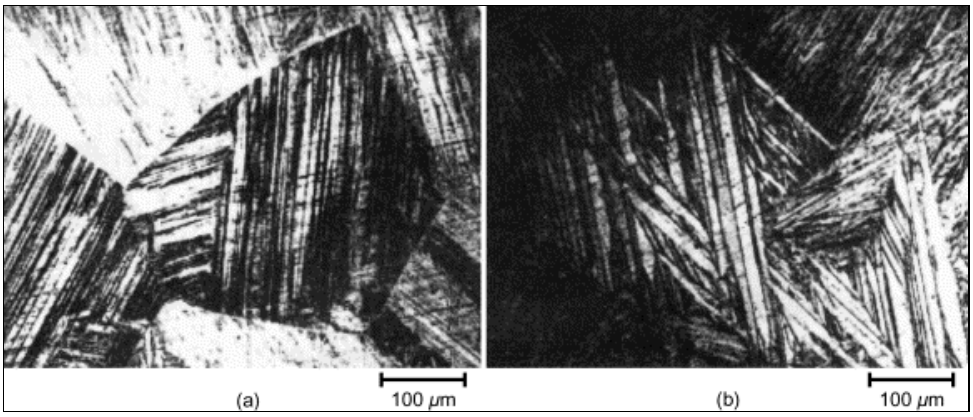

Figure 4-2, Optical micrographs of typical martensite structures and self-accommodation morphology [80]

Martensitic transformation is a first order, diffusionless, solid-to-solid phase transformation. This process generates a large strain around the newly formed martensite and the parent phase. The strain must then be relieved in order for the nucleation and growth to be continued. This can be done either by introducing 1) slip or 2) twins into the system [**Figure 4-3**]. Twinning is the lattice invariant shear mechanism found in SMAs [**77**].

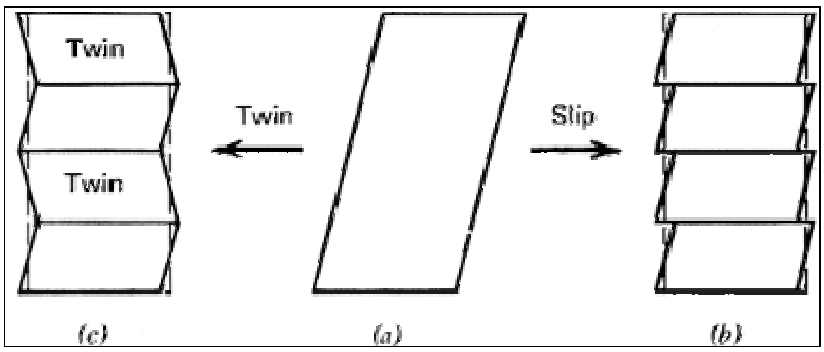

Figure 4-3, Lattice invariant shear, a) shape change upon martensitic transformation; the invariant strain accommodated by: b) dislocation slip; c) twining

While the strain generated by the transformation has been relieved, there is still the problem of the shear generated. This is alleviated by self-accommodation of martensite twins. The self-accommodation mechanism requires two or more variants to orient in such away that the variant strain in each twin variant cancels out each other, as shown in **Figure 4-4.** Thus there is no net change in the shape or volume of the alloy.

The twin variant boundaries in SMAs can be easily moved, thus enabling the SMA to be deformed via a de-twinning rather than the conventional dislocation slip mechanism. This de-twinning process aligns the variants along the direction of the

applied force enabling relatively large deformations to be accommodated without altering the crystal structure of the alloy. It is this de-twinning process that makes the restoration of the original shape possible upon heating [**81**]. Upon heating, the phase transformation process converts heat energy into motion through self-rearrangement of atoms in the alloy and restores to its original shape.

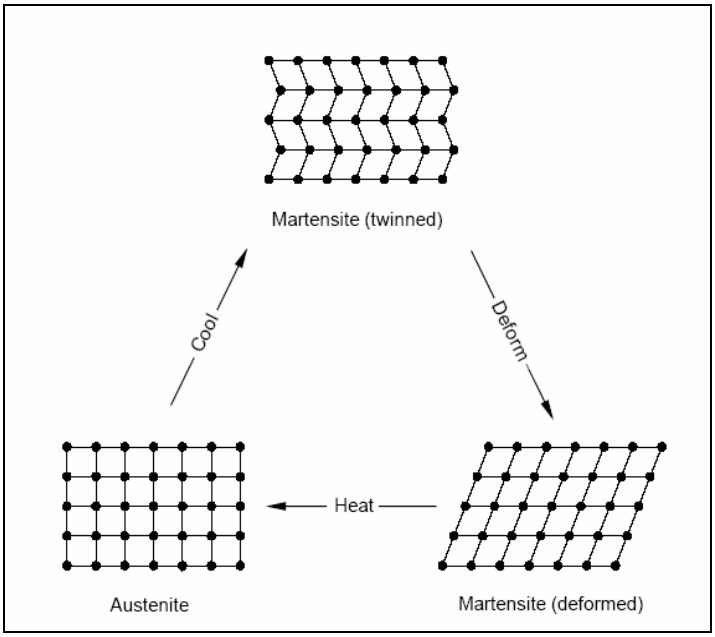

Figure 4-4, Self accommodation and de-twinning of martensite [82]

SMAs that exhibit SME only when heated are said to have a *one-way* shape memory; some SMAs also possess the same effect on subsequent cooling, these alloys are said to have a *two-way* shape memory effect. To produce one-way shape memory, specific thermal treatment is required, better known as a ***shape setting*** process; to produce two-way shape memory behaviour, a combination of specific thermal and mechanical treatments is required known as a *training* process [**83**].

4.1.2 Superelasticity (SE)

When stress is applied to a SMA in the austenitic state, a martensite transformation can be stress-induced upon loading beyond a certain stress level. Note that austenite is still the thermodynamically stable phase and stress free at this temperature. Thus upon unloading, the martensite becomes unstable, resulting in a transformation back to the austenite, restoring it to its original, undeformed shape. Strains of up to 8% can be accommodated and fully restored by this process [**85**]. This unique elastic property is known as pseudoelasticity or superelasticity. The adaptive serrated nozzle developing in this project utilises only the SME of the material thus it is beyond the scope of this project to discuss the SE of the alloy in detail.

4.2 Types of Commercial Shape Memory Alloys

Although there are a number of metal alloys that exhibit shape memory properties, only two shape memory alloy systems have achieved any level of commercial exploitation; the NiTi alloys, commonly known as Nitinol and the copper-based alloys. In addition, a group of iron-based alloys have also showed promising properties to be used in engineering applications, but these alloys have suffered from major corrosion problems and are still under extensive development.

The properties of these two commercial SMA systems are very different **[Table 4-2]**. NiTi SMAs tend to have greater shape memory strain, more corrosion resistance, more thermal stability and have much higher ductility. Copper-based SMAs on the

other hand, are much cheaper, have much higher workability and are available in a wider range of transformation temperatures. The two alloy systems thus have unique advantages and disadvantages that must be considered in specific applications.

Material Properties	**NiTi SMA**	**Cu Based SMA**
Density (cc^{-1})	6.4 – 6.5	7.1 – 8.0
Melting Point (ºC)	1250	950 – 1050
Thermal Conductivity ($WmºC^{-1}$)		
Martensite	8.6 – 10.0	
Austenite	18.0	75 – 120
Electrical Resistivity		
Martensite	0.5 – 0.6	0.14
Austenite	0.82 – 1.1	0.7
Coefficient of Thermal Expansion ($ºC^{-1}$)		
Martensite	6.6	16.0 – 18.0
Austenite	10.0 – 11.0	
Specific Heat Capacity ($JKgºC^{-1}$)	470 – 620	390 – 400
Enthalpy of Transformation (JKg^{-1})	19.0 – 28.0	7.0 – 9.0
Transformation Temperature Range (ºC)	-200 – 120	-200 – +200
Corrosion Resistance	Excellent	Excellent
Bio-Compatibility	Excellent	Assumed Poor
Young's Modulus (GPa)		
Martensite	28 – 41	70
Austenite	70 – 97	70 – 100

Yield Strength (MPa) Martensite Austenite	 70 – 140 195 – 690	 80 – 300 150 – 350
Ultimate Tensile Strength (MPa) Fully Annealed Work Hardened	 895 1900	 400 1000
Elongation at Failure (%) Fully Annealed Work Hardened	 25 – 50 5- 10	 8 – 15 8 – 15
Hot Workability	Poor – Fair	Very Good
Cold Workability	Poor	Good
Machinability	Poor	Very Good
Poisson Ratio	0.33	
Wear Resistance	Good	

Table 4-2, Summary of typical materials properties of binary NiTi and Copper-Based Shape Memory Alloys [86]

4.2.1 Copper Based Shape Memory Alloys

After it was reported in 1964 that Cu-Al-Ni alloy also showed SME, widespread studies on copper based SMAs focusing primarily on Cu-Al-Ni and Cu-Zn-A1 alloys were carried out to replace NiTi alloys. Copper based SMAs are considerably cheaper than NiTi alloys, can be melted in air with ease, and have a shape-memory strain of up to 5 % [**86**]. However, it is very difficult to use copper based SMAs in

the polycrystalline state although they have excellent properties as single crystals. Early copper based SMA suffered from intergranular failure due to their intrinsic coarse grain structure. The recent development in fine grain copper alloys has improved mechanical properties significantly [**87**]. Copper based SMAs were first applied to engineering applications for temperature switches in the late 1960s. Since then Cu-Au and Cu-Zn based ternary alloys have also been developed for practical usage. Copper based SMAs can be up to 10 times cheaper than NiTi based SMAs, which makes them very attractive alternatives to NiTi SMAs, especially in large volume uses.

4.2.2 Nickel-Titanium Shape Memory Alloys

NiTi SMA was first discovered in 1962 by the U.S. Naval Ordnance Laboratory, part of the US Department of Defense. This type of SMA is commonly referred to as Nitinol, derived from **NI**ckel, **TI**tanium, and **N**aval **O**rdnance **L**aboratory. The discovery was later patented by Buehler and Wiley [**88**]. The scientists were originally seeking a non-magnetic, high hardness, non-corrosive material for naval applications. After melting 55% nickel and 45% titanium, an alloy was created with extraordinary shape memory characteristics. NiTi SMAs have the best SME of all SMAs. Even in the polycrystalline state, 8% shape recovery is possible, 8% superelastic strain is completely reversible above A_f, and the recovery stress is of the order of 800 MPa.

1. The basis of the NiTi SMA is a binary, equiatomic intermetallic compound of nickel and titanium. The SME and SE properties for this family of alloys are limited to near equiatomic compositions, i.e., nickel content from approximately 48 to 52 at% Ni. The transformation temperatures of the alloy, and furthermore the actual presence of SME or SE is dependent on certain characteristics of the alloy such as the manufacturing methods, environmental conditions during formation, the processing conditions, the heat treatments, and the balance of Ti-Ni content.

2. The basic concept of processing NiTi SMAs is that the martensitic and austenite phases have to be strengthened to avoid plastic deformation during shape memory or superelastic loading. This occurs by a combination of strain hardening and during cold deformation, solution hardening, and precipitation hardening. The manufacturing methods, process conditions, heat treatments as well as environmental conditions during formation do not concern this research, as the alloys experimented upon will be purchased with these characteristics already established.

3. NiTi SMA has an extremely narrow composition range below the 630ºC eutectoid where the SME exists. This is shown in the equilibrium binary phase diagram in **Figure 4-5**. As a result, slight deviations in composition will greatly affect the transformation temperatures. A 0.1 at% shift of nickel content in the alloy has been proven to alter the transformation temperature of the alloy by over 10 ºC [**Figure 4-6**]. Comparing to commercial steel for example, a slight segregation will not produce any noticeable effects in the

material's behaviour. This heavy compositional dependence calls for a tightly-controlled manufacturing process. Excess nickel content is known to strongly depress the transformation temperature and increases the yield strength of the austenitic phase.

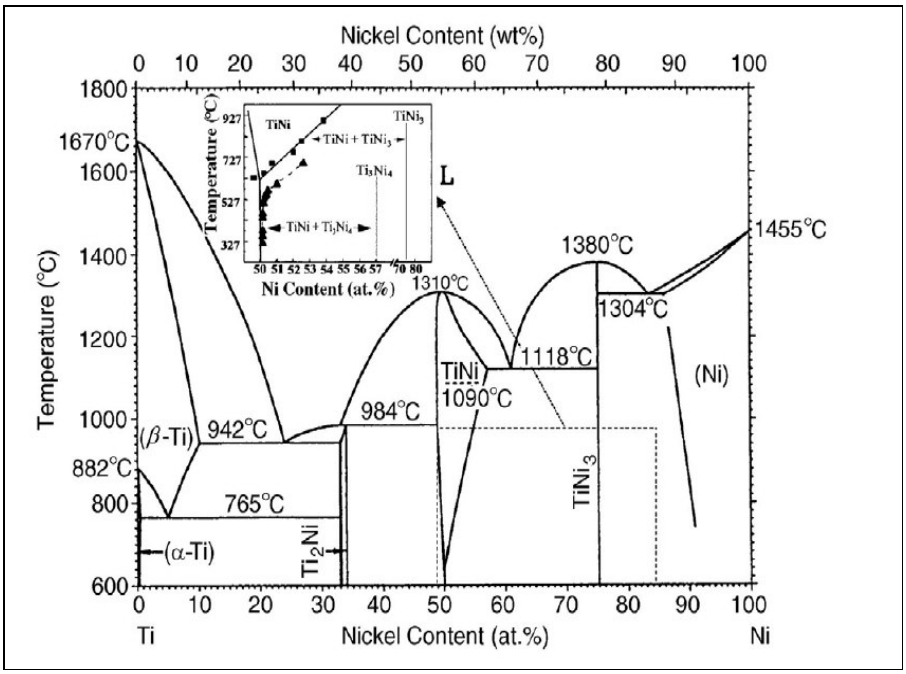

Note: please refer to Appendix A. Equilibrium binary Phase Diagram of NiTi for a detailed version of the phase diagram

Figure 4-5, NiTi binary phase diagram [89]

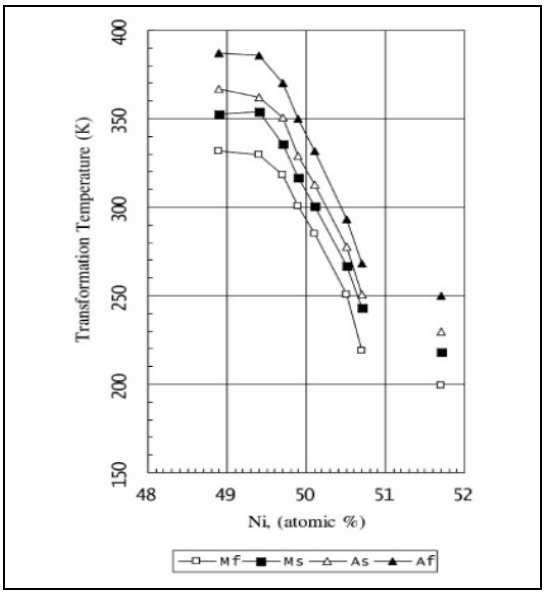

Figure 4-6, Effect of Ni content in NiTi SMA on the transformation temperature of the alloy [74]

Many researchers have attempted to take advantage of this unique sensitivity to alloy content and manipulated the alloy properties by alloy additions with mixed results [**90-98**]. Alloying with a third element not only influences the transformation temperature of the alloy but also affects hysteresis, strength, ductility and shape-memory characteristics. There are four main purposes to add a third alloying element to NiTi SMA [**99**]:

i. to decrease (Cu) or increase (Nb) hysteresis,
ii. to lower transformation temperatures (Fe, Cr, Co, Al),
iii. to increase transformation temperatures (Hf, Zr, Pd, Pt, Au), and
iv. to strengthen the matrix (Mo, W, O, C).

Various ternary SMAs are being developed and, amongst these, TiNiCu, TiNiNb and TiNiHf have received the most interest. The addition of copper is widely known to reduce the hysteresis and lower the deformation stress of the martensite phase [**100**]. When SMAs are used for actuator applications, narrow hysteresis is very useful to achieve rapid actuation. A disadvantage of most TiNiCu alloys is that the transformation temperatures do not decrease below room temperature. For applications such as pipe coupling, a wider hysteresis is more desirable so that the coupling can be stored in the martensitic state at room temperature. The addition of niobium has been shown to widen the hysteresis as a result of the precipitation of deformable niobium-rich precipitates [**101**].

Common contaminants such as nitrogen can also shift the transformation temperature and degrade the mechanical properties. Thus contamination in the production of NiTi SMAs is strictly controlled [**59**]. The necessary composition control in the melting and forging processes is of the order of between 0.1 and 0.01 at %. By comparison, the typical the variation in chromium content of 18/8 stainless steel is about 2 at% [**82**].

Because of its superior ductility at low temperature, high degree of shape-recovery capability, large superelastic hysteresis, high corrosion and fatigue resistance, biomedical compatibility, and relatively high electrical resistance, NiTi SMA is the most widely used SMA for engineering applications. When used as actuators, they can provide actuation between two stable positions with a repeated strain of up to 2%. At this strain level, actuations of up to 10^6 cycles can be achieved without failure. The repeatable strain can be increased at the expense of reduced cycles before failure

[Table 4-3]. The transition temperature of NiTi SMA can be set between -20ºC and +120ºC [**102**]. Availability of NiTi SMA has largely been driven by demands for medical and electronic applications where the majority of SMA applications exist. These applications are generally small in size thus the current world production of NiTi SMAs is small (about 100 tonnes per annum [**79**]) compared to other commercial metal alloys. Owing to the stringent process control required in the melting and forging processes, the cost of the material remains relatively high. However, as world production increases, the prices should start to drop. Wires, strip, rod, bar and sheet are all readily available and alloy foams, sintering powders and sputtering targets of high purity are also beginning to being produced.

Require Cycles	Maximum strain	Maximum stress
1	8%	500MPa
100	4%	275MPa
100000	2%	140MPa
1000000+	1%	80MPa

Table 4-3, Maximum stress and strain level permitted for the require SMA cyclic life [103]

4.3 Applications of NiTi SMAs

NiTi SMAs are the best explored system of all shape-memory alloys and occupies almost the whole SMA market. In fact, more than 10,000 patents have been proposed in the past on the applications of the alloy, but only a few have been successfully

introduced into the market. The use of SMAs has been limited by several factors. Owing to difficulties in the production process the cost of the material remains relatively high. In the UK the price of NiTi SMA wire was between £0.20-£1.00 per gram in 1999 [**104**]. The post processing, machining and thermal treatments required meant that this further adds to the cost of the alloy. Furthermore, the lack of established knowledge on the thermal and mechanical properties of SMAs meant that developers were unable to utilise SMAs to their full potential. The first successful SMA application was the *Cryofit* tube couplings developed by Raychem Corp. in the 1970s for the F-14 fighter aircrafts [**105**]. The couplings were more reliable than other conventional fasteners and the cost was less of an issue for a military application. However, due to their high costs, they have only found limited uses in the commercial market. Corrosion resistant iron-based SMA couplings have been developed as a cheaper alternative [**105**]. The *Frangibolt*™ utilises the same principle which has been used on numerous space missions for a range of deployment system including solar panels, antennae, cover doors, and various experimental payloads. The *Frangibolt*™ is a separation system that consists of an electrical heater placed around a TiNi SMA cylinder. A specially-notched design bolt was placed securely in the SMA cylinder to secure a payload to launch. To release the payload, the electric heater heats the NiTi cylinder, causing it to expand and fracture the notched-bolt which releases the *Frangibolt*™ [**106**].

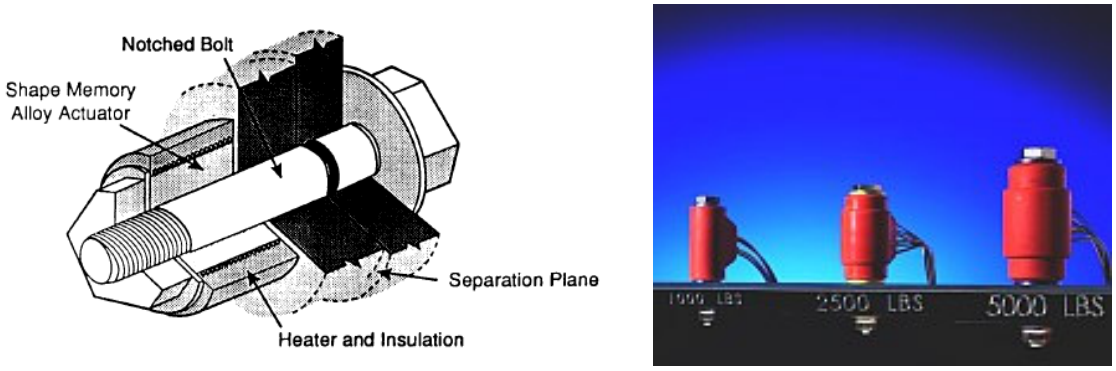

Figure 4-7, schematics of the Frangibolt™ design (left) and a range of commercial Frangibolts (right) [107]

The following is a brief review of a selection of more well-known SMA applications, it is not in the interest of this research to provide a comprehensive review of the current SMA applications. For those who wish to know more about SMA applications, please refer to references **108-111**.

4.4 Medical SMA Applications

By far the most success achieved in commercial SMA applications are those in the biomedical industry. The majority of the current medical applications require only small amounts of material thus cost is less of an issue. Owing to NiTi SMAs' inherent biocompatibility, their unique pesudoelastic property has been exploited in the development of numerous medical tools and devices for minimal invasive medical procedures. For example, NiTi SMA stents are used in the cardiovascular system following a balloon angioplasty to prevent the restenosis of blood vessel **[112]**. The stent is inserted into a catheter in the martensitic state and introduced into a body cavity. Once in place and released from the constraining catheter, the device is

triggered by the body temperature and expands to its austenitic state where it will provide a constant force against the vessel wall to prevent the re-stenosis of the diseased vessel [**Figure 4-8a**]. Stents are also used as support grafts for repairing of damaged blood vessels [**112**]. These injuries were traditionally difficult to repair by surgery but were made possible by the use of stent-grafts which anchored onto the healthy part of the artery at the proximity of the injured vessel as shown in **Figure 4-8b [113**].

Stents were traditionally manufactured with 316L stainless steel. They are expanded by the plastic deformation caused by the inflation of a balloon placed inside the vessel wall. On contrary, the NiTi SMA superelastic stents are self expanding thus the use of a balloon is not required. Other superelastic medical devices made with NiTi SMA include kink resistance guide wires which makes keyhole surgery possible, filters, orthodontic archwires and thermally activated surgical endoscopic instruments **Figure 4-9**.

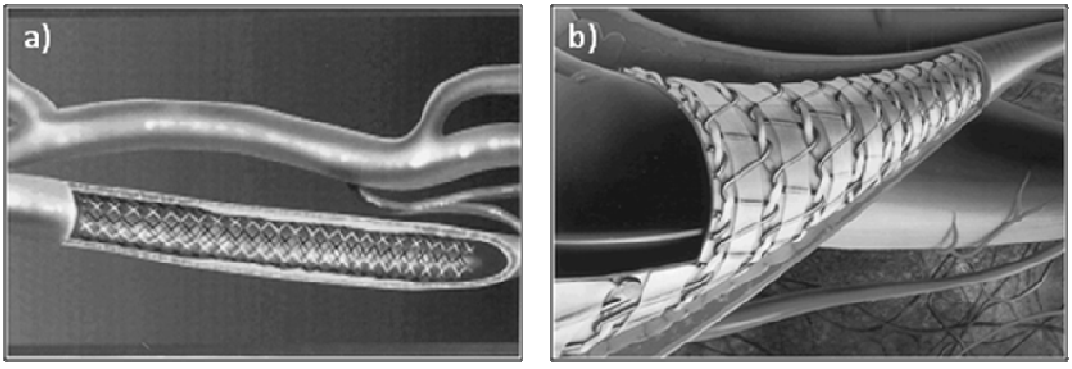

Figure 4-8, a) cross-section of a SMA stent inserted into a vessel to maintain vessel potency and blood flow; b) stent-grafts made with SMA wires incorporated into PTFE sheet to provide an artificial replacement for injured vessel [112]

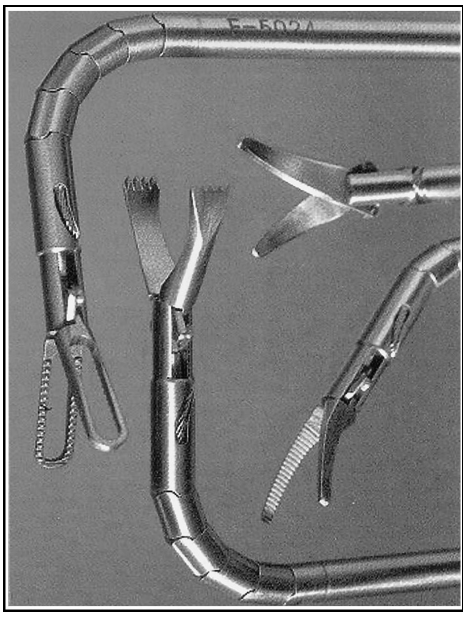

Figure 4-9, A selection of surgical endoscopic instruments activated by the NiTi SMA rods [112]

4.5 Engineering SMA Applications

Since the discovery of NiTi SMA, studies on the alloy have provided a better understanding of the behaviour of SMAs and illustrated their potential applications. Cost of the alloy has fallen drastically as a result of the advancement in processing technology and SMA is no longer considered to be prohibitively expensive. With improved understanding and gradual cost reduction, SMA applications have rapidly increased over the last few years. Most attention has been placed on SMA medical devices, probably due to the value of the business; the stents and stent-based structures represents a worldwide end-user market of approximately $2.5 billion in 2005 [**108**]. Usage of SMAs in other commercial applications by volume far exceeds

the usage in medical industry and the number of commercial SMA applications is rapidly growing [**82**].

Similar to the medical industry, most commercial engineering SMA applications exploit the superelastic properties of the alloy. Usually superelastic SMA devices require a simpler design than ones that utilise the shape memory properties of the alloy. Flexible eyeglass frames, cellular phone antennas and brassiere underwires are typical example in this category [**110**].

SMA actuators have by far the highest work and power-to-weight ratios of all available actuators. Consequently, they have lent themselves to applications such as the ASN. In many engineering applications, conventional actuators can be replaced by a single SMA element without auxiliary parts, resulting in simple compact and reliable devices. A wide range of SMA actuators have already been used in domestic applications, examples are the air-conditioning air vents developed by Matsuhi Electric, which direct air to different directions depending on temperature [**111**]; thermostatic valves in electrical applications and temperature control in showers [**Figure 4-10**]. The majority of the SMA actuators consist of a temperature sensitive actuator working against a temperature insensitive bias spring. The modulus of the SMA actuator changes with temperature thus creating either a resultant force and/or motion on the control system. The temperature is controlled linearly by utilising the *Clausius-Clapeyron* relationship between stress σ and transformation temperature T in thermodynamics [**105**].

$$\frac{d\sigma}{dT} = \frac{\rho \Delta H}{T_0 \Delta e} = \frac{1}{C}$$

Where:

P= density, ΔH = latent heat; T_0 = transformation temperatures under no stress and Δe = strain due to phase transformation

The main drawback of SMA actuators is that the actuation is activated by a change in the alloy temperature. Often, the extraction of heat from SMA can be slow during cooling, creating a large thermal lag to the actuation which limits the use of SMA actuators to relatively low frequency applications.

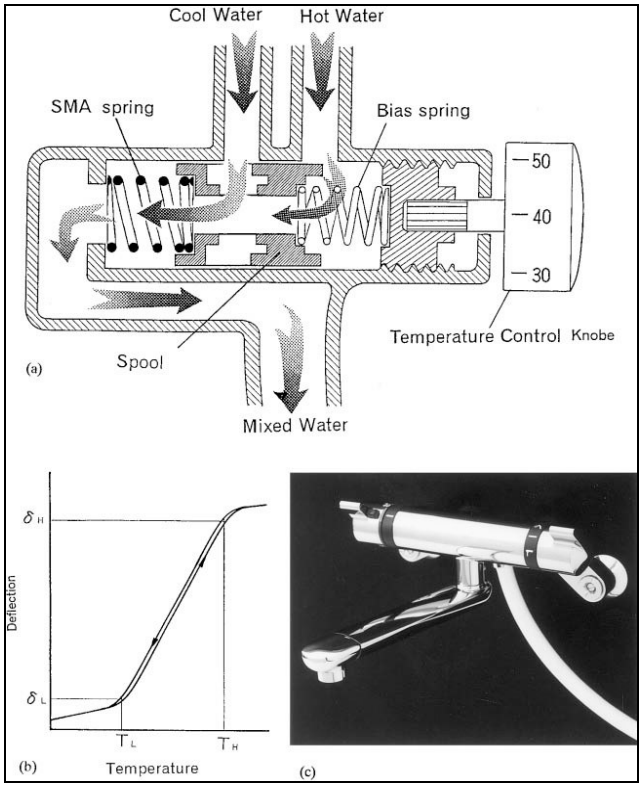

Figure 4-10, SMA thermostatic valves used in shower heads [112]

In civil engineering, SMAs have been used for seismic rehabilitation applications due to their high energy dissipation capabilities, large elastic strain capacity and good corrosion resistant. The bell tower in S. Giorgio Church in Italy has been fitted with SMA devices which increase the flexural resistance of the structure [**109**].

Composite material such as CFRPs (carbon-fibre- reinforced-plastics) prevent the problem of debonding and transverse cracking between the fibre and the matrix by embedding NiTi wires into the matrix. These wires put the composite into compression by introducing a constant compressive force onto the material. NiTi SMA wires were also used in CFRPs as vibration control purposes as the elastic constant of the wires can constantly change through the transformation temperature range [**111**].

4.6 Review of NiTi SMA Market

Since the introduction of SMA in 1960, engineers have been struggling to find genuine engineering applications for the alloy. Although several niche commercial applications have been found, such as surgical stents and guide wires in the medical industry and pipe coupling in aerospace, the use of SMAs has yet to find any main stream, mass-produced applications. Thus, the world usage of SMAs remains relatively small compared to other commercial alloys. The lack of demand for high volume SMAs has limited the level of interest and investments in the areas of alloy development and process technologies. As discussed in **Chapter 3.1**, the pace of development in high temperature SMAs has already hindered the development of the

adaptive serrated nozzle concept for the hotter core nozzle. The transformation temperature required to actuate the hot nozzle serration far exceeds the limit of current shape memory alloy commercially available. Furthermore, current alloy processing technologies are having difficulties in manufacturing NiTi SMA in the sizes and quantities required for this project. This has made it extremely difficult sourcing the NiTi SMAs for the project. The problem of sourcing SMAs has been made worse by the fact that all SMA suppliers use a number of different manufacturing routes to obtain SMAs with the required transformation temperatures. Batch-to-batch consistency in the material properties and alloy composition of the alloy is virtually non-existent. This may be acceptable for applications in the medical and electronic industry as the material requirement in these applications is considerably lower than the limits of the SMA. However, for aerospace applications, these materials will be subjected to one of the most demanding operating environments and are expected to operate very close to their limits. Therefore, a supply of SMAs that are consistent in every way would be crucial in order for SMA engineers to develop applications that would utilise the SMA to its fullest potential. In addition, major reliability, safety and certification issues associated with gas turbine engines mean that if SMAs are to be used in gas turbine engines, their mechanical properties and, more importantly, how these properties change with time in operation must be properly quantified and batch-to-batch consistency assured.

The development of the adaptive serrated nozzle concept can potentially be very beneficial for the SMA industry. When the concept eventually goes into production, the estimated usage of NiTi SMA actuators would be around four tonnes per year per engine line [**114**]. Such large demand in SMA is unheard of in this market and will

undoubtedly spark interest and investments in alloy development and processing technologies to satisfy such large demand. However, for such a large material demand, Rolls-Royce would not proceed with the development of the adaptive serrated nozzle to the production stage before securing material supply. The comments from SMA manufacturers have indicated that although the industry has the experience and know-how to develop the required processing technology, the lack of demand for large size and quantity SMAs meant that there was no incentive for them to actually develop these technologies. On the other hand, SMA designers and engineers are reluctant to develop concepts that require materials that are not available in the current commercial market. The situation becomes a vicious circle where both the demand and supply side are reluctant to make a first move, causing the growth of the shape memory technologies to grind to a halt. **Figure 4-11** shows a graphical representation of the current situation: without large scale engineering applications in place, the SMA industry has little incentive in investing in alloy development and processing technologies; on the other hand, companies would not develop SMA applications without securing the supply of material for the application.

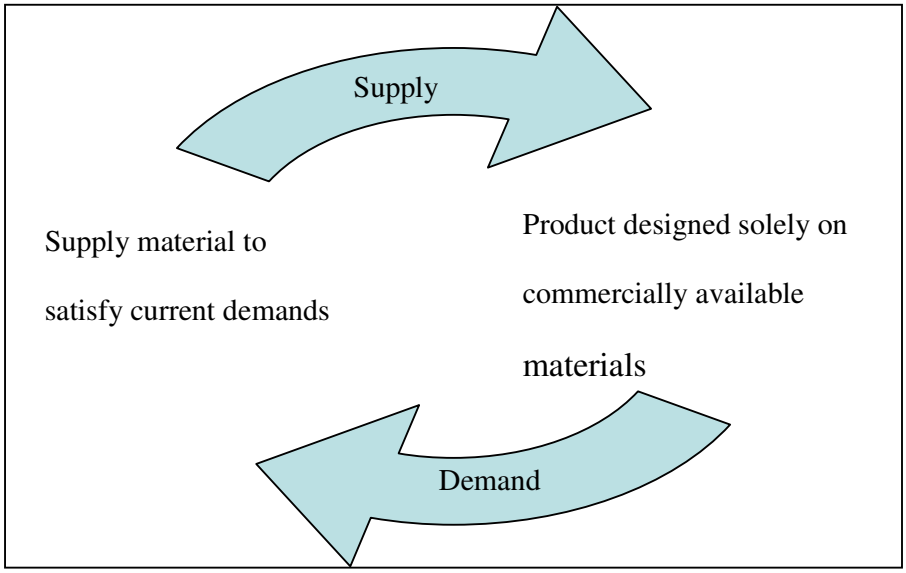

Figure 4-11, dilemma in the current SMA market

This situation can be analysed by ***Game Theory***. Game Theory is a tool used in economics to study situations where two or more decision makers (players) choose different actions in an attempt to maximise their returns (pay-off) [**115**]. It was developed by John von Neumann from the optimisation approach in neoclassical economics and provides a logical approach to social modelling in which decision makers interact with other minds [**116**]. **Figure 4-12** shows a pay-off matrix of the supply-demand relationship in the SMA market. A pay-off matrix is a table showing a firm's returns (pay-offs) for various combinations of its and other party's strategies [**117**]. The pay-off matrix shows that both the SMA suppliers and developers have the option to develop the technology required to stimulate demand and supply respectively. It was clear that the top-left cell where both suppliers and developers decide to invest resources to develop new alloys and applications could generate the most economic values. However, without knowing the other players' strategies, both sides are reluctant to take the first move, worrying about the risk of losses in

investment if the other party decides not to develop the accompanied technologies. Both suppliers and developers thus take the least risky option and stay in the bottom-right cell and do nothing. This has caused a halt in the expansion the SMA market into large engineering applications.

	Supplier (e.g. Memry Corp, Special Metals)		
Developers (e.g. Rolls-Royce)		Develop	Wait
	Develop	New market created, both buyers and suppliers gain first mover advantages. Business thrives	Suppliers suffer losses due to lack of demand for new materials
	Wait	Developers suffer losses due to lack of materials for the new applications	No business but relatively safe

Figure 4-12, Pay-off matrix of the Supply-Demand situation in SMA market

Such a problem can easily be solved by cooperative moves such as partnership and joint ventures where the suppliers and users enter into an agreement to develop the technology required for the development of new applications. However, cooperative moves usually involve the sharing of technology and information. Since the aerospace industry operates heavily on proprietary technologies, a set up involving the sharing of technologies would not be appropriate. Alternatively, SMA developers such as Rolls Royce can stimulate suppliers to develop the required material through the notion of ***signalling***.

Signalling is often used in contract theory in economics and was derived from the idea of asymmetric information. Asymmetric information arises where there are inequalities of access to information between parties which result in a disruption to the market for the exchange of contracts. Spence proposed that signalling can be used to solve such problems [**118**]. One party could send a ***signal*** to another party, revealing some information that would otherwise be unobtainable by the other party and that party will then interpret the signal and adjust its behaviour accordingly. Spence illustrated this using the job-market signalling model, where employees signal the level of their skills to employers by acquiring a certain degree of education. Equally, for the development of ASN, Rolls-Royce can send signals to the SMA manufacturers (for example in conferences and trade shows) convincing them of Rolls-Royce's commitment in developing large scale, high temperature SMA applications in gas turbine engines. This would surely spark interest and hopefully investment in the development of the required materials. In fact, the publication that the author published in this project in the International Conference on Martensitic Transformation [**119**] has already generated a lot of interest both in the commercial and the academic arena.

4.7 Procurement of NiTi SMA

For actuation applications, a NiTiCu ternary SMA was supposed to be the best NiTi SMA available, as the addition of copper reduces the width of the hystersis. However, current SMA technology can achieve similar effects by using a combination of thermal and mechanical treatments. After extensive research on the SMAs

commercially available, the author has opted for a binary NiTi SMA, as the ternary NiTi systems commercially available have very similar properties to the binary system but are considerably more expensive.

Currently, only wires and thin foils of NiTi SMA are commercially available, and after contacting all major shape memory alloy suppliers, only three showed interest in supplying materials in the specification and quantity required. All three suppliers have indicated that currently, they do not have the capability to produce the require SMAs, although the work needed to develop the capability for producing the required materials is relatively small and once an order has been placed, they should be able to produce the required material relatively quickly. Quotes from these suppliers for the SMA required for the current project vary widely from £10,000 to £20,000. However, none of the suppliers are willing to guarantee any batch-to-batch consistency. Thus the only way to eliminate this problem was to purchase the materials needed for the entire project in one batch.

Rolls-Royce is constantly exploring potential channels to source materials. One promising supplier of SMAs is the Institution of Metal Research (IMR) at the Chinese Academy of Science in China. Not only does it have the ability to manufacture the SMAs required for the project, it has been producing similar material on a regular basis with very high batch-to-batch consistency. IMR was chosen as the SMA supplier for this project. However, since IMR is a research institution rather than a commercial supplier, they are incapable of supplying the large volume of materials required for the mass production of ASN. Thus a reliable supply of SMAs must be secured before the manufacturing of ASN could proceed.

5 Joining of Shape Memory Alloys

Joining of SMA either to itself or to dissimilar alloys has traditionally been regarded to be extremely difficult, if not impossible. Recently, joining of SMA to itself has been successfully achieved by carefully controlling the alloy impurity level and welding parameters using a number of solid state as well as fusion welding techniques [**58, 120-135**]. Joining SMA to itself has now become a routine process. And apart from the traditional methods of soldering and mechanical fastening, a variety of welding processes such as TIG arc welding, resistance welding, laser welding and friction welding have been tested with very promising results [**6**]. However, as there are no standards for the manufacturing of SMAs, the types of SMA used in these studies vary widely, which has led to many confusing and conflicting results. Each researcher uses SMAs that are slightly different in either alloy composition and/or processing history making very difficult to compare the results of these studies.

Although joining NiTi SMA to itself has now becomes a routine process, the joining of NiTi SMA to dissimilar metals remains a challenge to SMA engineers. This is probably the reason behind the relatively little research on the dissimilar joining of SMAs found in the public domain. Recently, there has been a significant increase in the level of research activities in this area due to the increasing number of engineering applications, especially in the medical industry that requires welding SMA either to itself or to dissimilar metals.

5.1 Tungsten Inert Gas Welding

In tungsten inert gas (TIG) welding, an electric arc is formed between a tungsten electrode and the workpiece being welded. The arc generates intense heat which melts the weld metal and any filler metal. Gas shielding is usually used and applied through the welding torch to shield the electrode and molten weld pool from contamination. TIG welding of SMA has been tested by a number of researchers as this welding method is both inexpensive and versatile.

The feasibility of TIG welding SMA wires and sheets has been studied by Ikai et al. [**121**]. The TIG welds produced on SMA wires and sheets have a peak tensile strength of 756 MPa and 612MPa respectively. Furthermore, the level of SE in these welds was comparable to that in the parent metal. However, the SE in the weld metal deteriorated gradually with loading cycles due to the accumulation of dislocations at the martensite–parent phase interface during phase transformation. For the welded SMA sheets, Ikai et al. found that the material behaviour in the weld metal and the HAZ were very different to that of the parent metals [**Figure 5-1**] Due to the longer welding time needed to weld SMA sheets, the heat applied to the weld was higher compared to that in welding SMA wire. The increase in heat input in the weld and HAZ removed any cold work present in the alloy, giving rise to an increase in deformation and a reduction in the plateau stress. The elimination of cold work also removes the intermediate R-phase transformation present in the parent metal (characterised by the step change in the stress-strain curve).

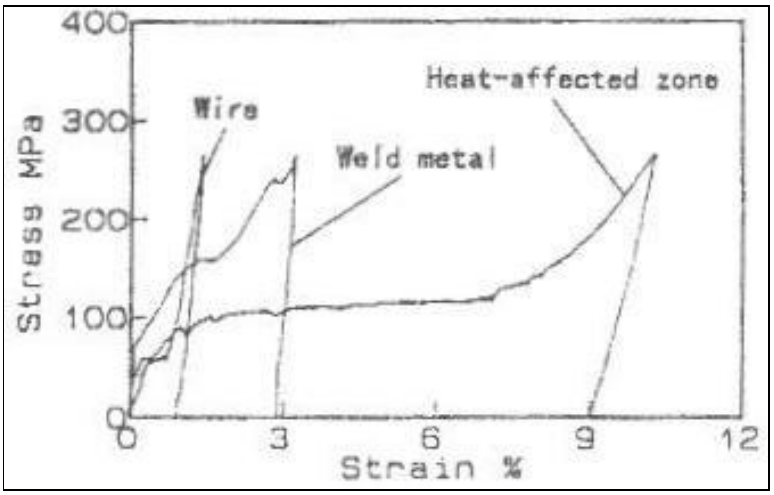

Figure 5-1, Stress-Strain graph of each component in a SMA weld [121]

The effect of welding environment on the weldability of TiNi SMA by TIG welding has been studied by Sato et al. [**120, 136**] who found that both the presence of oxygen and nitrogen in the welding environment caused the formation of brittle intermetallics. Precipitates in the form of Ti_4Ni_2O for oxygen containing weld metal and approximately TiN for the nitrogen containing weld metal were observed. The formation of these oxides and nitrides drastically reduced the transformation temperature as well as the joint strength and ductility of the weld. Thus shielding gas is necessary to avoid oxygen and nitrogen contamination during welding. This same contamination problem should apply to other fusion welding methods but to a different extent due to the difference in heat input.

This finding is in contradictions with Hall's study on welding of SMA wires. Hall found that the presence of a shielding gas, (argon gas was used in his work) minimised the oxidation on the weld metal surface but the oxidation had little effect

on the weld metallurgy [**137**]. One reasons of this discrepancy could be a result of different grades of SMAs used.

To demonstrate the effect of alloy composition, Hall also investigated the welding characteristics of Ni-rich (Ni 50.5 at%, Ti balance) and Ti-rich (Ti 51.5 at%, Ni balance) SMA wires and found that Ti-rich SMAs were susceptible to solidification cracking and the formation of brittle titanium rich intermetallics (Ti_2Ni) whereas no cracking or intermetallics have been observed on the same weld produced on Ni-rich SMAs. As a result, the Ti-rich SMA welds containing only 2% more titanium were over 30% weaker than the Ni-rich SMA welds.

5.2 Laser Welding

In order to obtain successful welded part from SMAs, it is necessary to make the HAZ as narrow as possible since the shape memory properties in the HAZ are most likely to have deteriorated. Laser welding is well known for producing narrow HAZs due to its high energy density and small heat input. Thus the majority of the early research on the joining of SMAs focuses on laser welding [**122-135**].

Hirose et al. have carried out initial investigations on the weldability of NiTi SMA sheets using a CW CO_2 (continuous wavelength carbon dioxide) lasers in the early 1990s and produced laser welds with both SME and SE that were almost identical to the parent metal [**122, 123**]. The laser welds showed formation of columnar grains at the weld metal, extending into the fusion zone. A dendritic structure has also been

observed, with the presence of a secondary phase in the inter-dendritic regions in the weld metal. The second phases have been identified to be TiN and Ti_4Ni_2O. The formation of Ti_4Ni_2O phase was found to be a result of the oxygen content present in the base metal. And the formation of the second phases at the weld metal did not have any adverse effect on the SME and SE of the welds. In addition, with proper gas shielding, no oxygen or nitrogen contamination occurred during the welding process.

Later, many of the studies were focused on the development of the Nd:YAG laser technique. The Nd:YAG laser produces more intense laser beams and can be focused down to approximately 25 μm in diameter, allowing a narrow weld (down to 0.6 mm) and greater welding depth to be achieved. In addition, operating in pulse mode produces higher cooling rates which produce finer grain size thus improving the mechanical properties of the welds.

Katayama et al. investigated the effect of Ni content on the laser weldability of NiTi SMA [**124**]. Their work mainly concentrated on investigating the microstructure characteristics of SMAs under a pulsed Nd:YAG laser welding process. Three types of commercial and 6 types of experimental SMAs with composition ranging from Ti 48 to 56 at% Ni have been investigated and it was found that the microstructure characteristics of the weld metal vary widely depending on the initial chemical composition of the alloy. Further, a reduction in Ni content in the weld metal has been observed, due to the evaporation of Ni during the welding process. Consequently, the transformation temperature at the weld increases. The reduction in Ni content at the weld has caused the segregation of Ti along the cell and grain boundaries, forming $Ti_4Ni_2O_X$ and/or Ti_2Ni phases. Solidification cracks were

formed at the fusion zone. This phenomenon was especially prominent in multiple spot welds. However, despite the formation of these brittle phases, the tensile strength of approximately 75% of that of the base metal had been achieved. The retained SME and SE properties, along with high weld strength, showed that NiTi laser welded joints were suitable for SMA applications, although more research is required to optimise the welding process.

In the late 1990s, Schloβmacher et al. carried out a number of studies to investigate the feasibility of using a modern pulsed Nd:YAG laser technique to join SMAs [**125-128**]. Two types of SMAs have been tested: a martensitic NiTi SMA (Ni 50.6 at %, Ti Bal.); and a superelastic NiTi alloy (Ni 51.5 at %, Ti Bal.). **Table 5-1** shows a summary of their findings.

SMA	Sample Thickness (μm)	Condition	Ultimate Tensile Strength (MPa)	Elongation at Rupture (%)
$Ni_{49}Ti$ Superelastic	170	Base Material	1124	
		Welded	632 ± 48	
	500	Base Material	1213	28
		Welded	604 ± 22	8.4 ± 0.6
$Ni_{51}Ti$ Martensitic	170	Base Material	1062	
		Welded	779 ± 91	
	500	Base Material	1051	29
		Welded	823 ± 53	7.0 ± 0.3

Table 5-1, Room Temperature tensile test data [128]

Tensile strengths of up to 80% of the ultimate strength of the base alloy have been achieved. This figure is very similar to that achieved by Katayama et al. [**124**]. The percentage elongation to rupture at the weld joints was substantially lower in the martensitic type SMAs. This was thought to be caused by the formation of brittle Ti_2Ni precipitates along grain boundaries in the weld metal. On the other hand, the welds produced in the superelastic SMA were completely free of precipitates and exhibited higher elongation to rupture. This shows that the formation of brittle intermetallic is heavily dependent upon the alloy composition and more research is needed to understand the underlying theory in the formation of these intermetallics during the welding process.

Recently, Falvo et al. [**130**] carried out similar weldability investigations on Ni 51at% SMA and produced some conflicting results. The tensile strength of the laser welded joints was less than half of that in the base metal and a marked reduction in the level of elongation to rupture. The SME has been retained at the weld only at low strain levels. Similar results have been reported by Tuissi et al. on the laser welding of Ni 49.6 at% SMA [**129**]. The difference in results could be a result of different grades of SMA and products used in each study. Thus more research is needed to understand the effect of alloy composition, heat-treatment and cold work on the laser weldability of NiTi SMA.

The corrosion resistance of NiTi SMA is very important in bio-medical applications thus the corrosion resistance of laser welds must be quantified prior to applying it in medical applications. The corrosion resistance of laser welded NiTi SMA has been investigated in a number of investigations [**131-135**] and it was found that the

corrosion resistance of Nd:YAG laser welded SMAs was higher than that of the base metals. The improvement in corrosion resistance is ascribed to the formation of a defect- and carbide-free weld surface as a result of melting and solidification during welding. The evaporation of Ni during welding produced welds with slightly higher Ti content which also helped to improve the corrosion resistance of the weld. However, Hsu has reported a significant increase in corrosion rates of CO_2 laser welded SMA due to the inhomogeneous nature in the weld metal. The reduction in corrosion resistance of the weld could be ascribed to the different laser sources and process settings used which resulted in the production of inhomogeneous welds.

5.3 Electrical Resistance Welding

Electrical resistance welding is a welding process which produces joining of metals with heat energy obtained from the electrical resistance of the workpiece to the applied electric current in the circuit. A forging force is often applied during welding to ensure flashing takes place during welding. Flashing is the expulsion of soften metal from the abutting joint surface. During welding, resistance heating brought the abutting surface of the work pieces to their melting point and expelled through the abutting area. Flashing ensures that the mating surfaces are free from contamination. The forging force is often held for a period after welding to prevent the formation of solidification cracking during cooling.

Studies from both Zhou and Zhao et al. **[138, 139]** have shown that the use gas shielding produced little improvement, if any, on the weld performance. Welding time in resistance welding is relatively short and that the melting zone is sealed between the electrodes which prevent gas entering into the weld pool, even in the absence of shielding gas **[138, 139]**. However, if insufficient weld current and/or forging force is applied, plastic deformation and disruption of the joint was incomplete, which could cause gas intrusion into the mating surface and lead to weld contaminations. The contaminants formed in the weld are mainly TiO_2 and TiO as a result of oxygen intrusion. The types of oxides formed were different to the Ti_4Ni_2O reported in Sato's research **[120]**. Again, this could be a result of the different types of SMA used in each study. Joint strength of up to 60% of that of the parent metal

can be achieved by resistance welding. Zhou **[138]** has also found that the strength of the resistance welds produced increases with increase in weld current to a critical point where further increase in welding current caused oxygen intrusion and grain growth thus reducing the tensile strength of the weld metal.

Results from both studies suggested that environmental protection is not essential in resistance welding of NiTi SMAs as the disruption of the joint during welding provides adequate protection from contaminations. Furthermore, the joint strength is heavily dependent upon the process parameters as they ensure the complete disruption of the joint **[138, 139]**. By optimising the process parameters, considerable improvements in joint strength can be achieved. However, both studies have been carried out solely on NiTi SMA wires. The effect of forging force on joining of thin sheets of NiTi SMA is unclear thus more research is needed.

5.4 Friction Welding

To eliminate the formation of intermetallics, a solid-state joining process such as friction welding has been considered. Friction welding is a solid state welding process in which joining is achieved through frictional heat energy. Friction welding involves holding two components in axial alignment, and then rotating them under pressure, causing the interface to heat up. This heat energy is generated by the controlled rubbing of two components until material reaches its plastic state, at which time the plasticised material begins to form layers that intertwine with one another

[**140**]. The weld is completed by the application of a forge force during or after the cessation of relative motion.

Friction welding of SMAs is a logical approach for joining SMAs as it is a solid-state process which minimises the problems of contamination and any changes in alloy composition as a result of diffusion. Further, the application of a forging force during the process prevents the formation of "hot cracking". Shinoda et al. [**141-144**] has successfully friction welded Ti 50.7 at % Ni SMA rods with 6mm in diameter to itself with no signs of brittle intermetallics forming at the joint interface. Furthermore, the process was carried out in air with no evidence of contamination. The transformation temperatures of the welds were slightly lower than that of the parent alloy but were restored to a similar level by a post heat treatment of 600°C for 30 minutes. Joint properties after heat treatment were found to be similar to that of the parent alloy. A forging force of at least 127.8 MPa was thought to be necessary in order to completely eject the surface oxide film during the welding to expose fresh metal and form a sound joint. Joints with similar or higher mechanical properties to that of the parent metal have been produced. The increase in the mechanical properties at the welds was a result of grain refinement during welding. Welding with forging force less than 127.8 MPa caused the inclusion of the oxide film in the weld which deteriorated the joint performance. Forging force above 127.8 MPa is a prerequisite criterion in the successful friction welding of NiTi SMAs [**111**].

5.4.1 Friction Stir Welding

Friction welding requires rotating the workpiece to create the frictional heating required to facilitate the joining process. Thus this process is limited to welding two components of similar size and shape. To increase the versatility of the process, friction stir welding of NiTi SMA has been experimented with [**145, 146**]. Friction stir welding uses a rotating tool piece to generate the frictional heat instead of rotating the workpiece itself. The heating is created by the frictional force between the workpiece and the rotating tool. This process setup enables flat metal sheets to be welded [**Figure 5-2**]. The choice of the tool piece is crucial in this process as an unsuitable tool piece would react with the plasticised metal during welding and contaminate the weld.

Friction stir welding of NiTi SMA have been patented by London et al., although no friction stir welds have been produced [**146**]. Instead, the friction stir weld tool was plunged into a 6.35mm thick NiTi SMA plate. This process was thought to be similar to a butt weld. The process has been experimented with a polycrystalline cubic boron nitride (PCBN) and a tungsten-rhenium tool. Welds produced by both tool pieces appear to be identical, with no contamination from the tool pieces. Both the SME and other properties of the weld are comparable to that in the parent metal. A slight increase in the tensile strength and reduction in A_f temperature have been reported in the weld, as a result of grain size refinement during welding. Friction stir welding appeared to be a promising welding process in joining NiTi SMAs. However, more research is required to fully quantify its feasibility.

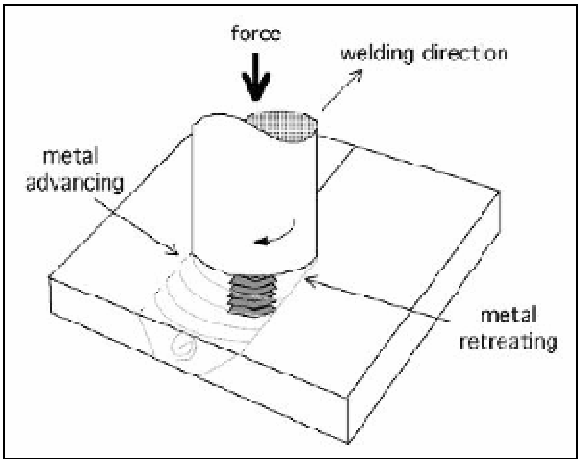

Figure 5-2, Schematic of friction stir welding process [147]

5.4.2 Brazing

Brazing is a group of joining processes in which joining is achieved through the use of suitable heating and filler metals. Brazing is essentially a solid state joining process as the filler metals used typically have a liquidus temperature of above 800K (527ºC) but lower than the solidus of the base materials. Thus the parent remains in the solid state throughout the process [**148**]. The filler metals are usually distributed between the closely fitting joint surfaces by capillary action. Metallurgical bonds are formed between the filler and the base materials. With the appropriate filler materials, a wide range of dissimilar metals can be joined. The choice of filler metals is crucial in brazing. The wettability of the braze alloy, the mechanical properties of the braze joints and the formation of brittle intermetallics must all be taken into consideration when selecting the interlayer. Inappropriate selection of filler metals could cause problems with proper wetting of the joint surface. Poor wetting can

cause the formation of voids which could lead to cracking at the joint interface. Brazing offers many significant advantages over welding and is often used in applications where parent metals are difficult to join by other joining methods. Brazing is performed at relatively low temperatures, which reduces the possibility of warping, overheating or melting the metals being joined. Heating is usually applied evenly to the base metals by various means such as furnace, induction and electrical resistance heating and thus thermal distortions are minimised. Where heating to the parent metals is undesirable, localised heating can be applied by induction, laser and microwave. However, during brazing, substantial diffusion of elements in the filler into the base material usually occurs. This is especially problematic for brazing of reactive metals such as titanium as it may result in the formation of brittle intermetallics.

Conventional furnace brazing is not suitable for brazing NiTi SMA as the parent metals would be exposed to elevated temperatures for a prolonged length of time which would drastically affect the SME as well as other material properties of the alloy. Consequently, research on brazing NiTi SMA is very limited. To the author's best knowledge, there was no research on brazing NiTi SMA when this research commenced in 2004. In the past few years, research on the subject started to appear in the public domain [**149-151**] as advance in technology have made localised heating by methods such as infrared and microwave possible. Shiue and Wu [**149**] investigated the feasibility of brazing NiTi SMA with three interlayers. Infrared heating has been used to minimise heating in the base metals. In this research [**149**] three copper containing braze alloys have been selected for investigation:

1) Pure copper foil;

2) $Ti_{70}Cu_{15}Ni_{15}$ foil;

3) Cusil ABA with the composition 63at% Ag, 35.25 at% Cu and 1.75 at% Ti; and

4) Ticusil 68.8 Ag, 26.7 at% Cu, and 4.5 at% Ti.

Copper has a high solubility in NiTi SMA and is an established alloying element widely used to manipulate the width of hysterisis of NiTi SMA. It is reported that up to 30 wt% of nickel content in the NiTi SMA can be substituted by copper atoms and still exhibit SME [**100**]. Thus copper-based braze alloys have been selected for initial investigation. The microstructures of the brazed joints were very different with the four braze alloys. Three copper-containing phases were present in the brazed joints produced by pure copper foil; a copper rich phase containing over 90 at% Cu, CuNiTi (Δ) and Ti(Ni,Cu) phase. The use of CuNiTi alloy was reported to deteriorate the SME of the alloy while the presence of the Ti(Ni,Cu) did not appear to have any effect on the SME of the alloy. The amount of CuNiTi phase present in the joint decreases with increase in brazing time due to the depletion of copper by the SMA. Thus the SME of the joint increased with brazing time [**150**].

For braze joints produced using the TiCuNi alloy as an interlayer, brittle Ti_2(Ni,Cu) intermetallics were formed at the joint interface. The SME of the alloy could not be tested due to the inherent brittleness of the intermetallics and unlike the CuNiTi phase, the amount of intermetallics present at the joint are not affected by brazing time. The presence of titanium in the Cusil-ABA substantially improved the wettability of the braze alloy. However, a CuNiTi phase formed at the braze joint

which deteriorated the SME of the joint. Brazing NiTi SMA with Ticusil caused $TiCu_2$ to form and, while this phase is less detrimental to the SEM of the joint, both Cusil and Ticusil brazed welds were reported to have significantly less SME than the parent metals [**150**].

Recently, refractory metals such as niobium and tantalum have been experimented with as a braze alloy to join NiTi SMA. Grummon [**151**] discovered that the inter-diffusion between NiTi SMA and niobium produces a reactive eutectic liquid which readily wets the parent metals and forms metallurgical bonds. A cellular honeycomb structure has been produced by brazing NiTi SMA tubes and corrugated sheets using pure niobium as interlayer. Although no testing was carried out to investigate the level of SME and SE retained at the joint, incremental compression tests have been performed with no failure of braze joints observed under repeat compression, which showed a significant SE was retained at the joint.

The above studies have shown the potential of producing high strength brazed joints while retaining a significant level of SE and SME. However, the selection of braze alloy is critical in achieving an integral braze joint. Although brazed joints have been successfully produced in a number of NiTi SMA systems, more research is needed to determine the effect of braze alloy on the material properties at and around the joint.

5.5 Joining of NiTi SMAs to Dissimilar Metals

Since NiTi SMAs are comparatively expensive with respect to most conventional engineering metal alloys, engineers often design concepts that only use NiTi SMAs in the most critical areas where unique properties of NiTi SMAs are critical to the functioning of the concept. Conventional metal alloys are often used in other parts of the design to minimise both manufacturing and material costs. Joining NiTi SMA to dissimilar metals is therefore of great importance to SMA designers.

As mentioned in **Chapter 5.4**, the joining of NiTi SMAs to dissimilar metals has always been regarded as extremely difficult. It is not surprising to see relatively little research carried out in this area. There are several problems concerning dissimilar joints. Firstly, there is the issue of metallurgical incompatibility. If two materials are metallurgically incompatible, it may lead to cracking or the formation of undesirable intermetallic phases. The titanium and nickel in NiTi SMA form a low melting point eutectic (see equilibrium binary phase diagram in **Figure 4-5**). This eutectic system often causes solidification cracking during cooling. In addition, NiTi SMA forms a number of titanium-rich intermetallics during welding. These intermetallics are extremely brittle and weaken the join so drastically that welds often fail during welding [**152**]. Secondly, both titanium and nickel have extremely low solubility for impurities. This increases impurity segregation at grain boundaries and increases the problem of solidification cracking. Thirdly, there will be a fusion zone where a steep composition gradient occurs. This fusion zone usually contains microstructures with lower mechanical properties relative to both the parent and weld metals. And lastly,

'unmixed zones', or 'partially mixed zones' consisting of fused parent material, which has not mixed fully with the bulk weld metal, e.g. due to differences in melting point, may also form adjacent to the fusion boundary. These may, similarly, be undesirable.

Low temperature joining methods such as soldering, adhesive bonding, as well as a range of mechanical fastening methods, are currently the preferred joining methods for joining NiTi SMA to dissimilar metals [**153, 154**]. These joining processes operate at temperatures where no melting and no diffusion between the parent metals occur. Thus the aforementioned problems are avoided. However, joints produced from these processes are usually relatively weak and have low operating temperature limits. A patented soldering process for joining NiTi SMAs to dissimilar metals, for example, consists of a halogen containing flux and a tin-silver based solder [**143**]. The flux removes the surface oxide on the SMA. The solder is then applied to the tinned surface to displace the activated flux while another workpiece is applied to the molten solder to form a joint. There is no claim that the SME is retained at the joint interface for these joints. And since the tin-containing solder has a low melting point, the joints produced by this process also have a low operating temperature limit.

To the author's best knowledge, the current research on the subject focuses solely on welding NiTi SMA to stainless steel, primarily for two purposes; medical applications and cavitation erosion-resistance cladding for hydraulic systems. Some of the results from these studies were again conflicting. This makes it difficult to compare between studies and draw any meaningful conclusions from them. The following is an overview of the studies carried out on the subject.

Cavitation erosion-resistance claddings utilise neither the SME nor SE of SMAs. They are simply applied onto stainless steel surface to prolong the service life of hydraulic systems. Thin sheet NiTi SMAs have been clad onto stainless steel in a number of studies. These include explosive welding, laser welding, TIG welding and microwave brazing [**155-158**]. Although the main focus on these studies is retaining the cavitation erosion-resistance in the NiTi SMA, no significant defects have been reported at the joint interface, which was a promising sign that sound joints were being produced. Microwave brazed joints achieved peak tensile strengths of up to 150 MPa using a copper-rich brazing alloy (Cu 50%, Zn 35%. Ag 9%, Cd 8%) while the explosive welds have managed a peak shear strength of 387 MPa (56.2 ksi). Failures of the explosive welds were observed either in the NiTi SMA or in the steel parent metals and not in the weld. Hence the weld strength exceeded that of the parent metals [**159, 160**].

For medical applications such as orthodontic wires, the unique superelastic property of NiTi SMA provides a constant force over long treatment time and much larger displacements can be achieved. However, the relatively low stiffness of NiTi SMA wires can result in the loss of anchorage. On the contrary, stainless steel wires provide adequate anchorage but the low elasticity can induce excessive orthodontic force and prevent teeth from moving. By combining NiTi SMA and stainless steel wires in orthodontic treatment, utilising the superelasticity of NiTi SMA for treatment and the stiffness of stainless steel for anchorage, orthodontic treatment time can be greatly reduced [**161**]. Recently, there has been a surge in the investment for research and development in welding technologies, especially for NiTi SMAs to stainless steel to take advantage of this unique combination of properties. The earliest research on this

subject was carried out by the EWI (Edison Welding Institute) [**152**]. Researchers at EWI have found that the joining of NiTi SMAs to stainless steel extremely difficult. As with many other alloying elements, titanium forms intermetallic compounds with iron during welding such as TiFe and $TiFe_2$. All of these intermetallics are extremely brittle at room temperature and can cause cold cracking at the joint interfaces. EWI have recently patented a method to overcome the formation of intermetallics by the use of an interlayer [**161, 163**]. Following Chularis's study [**164**] on the selection of refractory metals as an interlayer to join metal alloys together, EWI experimented with tantalum as an interlayer in joining NiTi SMA to dissimilar metal. Selection criteria were represented graphically, from which the value of desirability, d for each refectory metal was determined [**Table 5-2**]. Tantalum is the second most desirable refractory metal in Chularis's study after niobium. In addition, the effect of tantalum on the SME of NiTi SMA has been investigated and although the transformation temperature of the alloy was reduced as a result of the Ta addition, a significant level of SMA and SE was retained [**165, 166**]. This lent confidence to the suitability of selecting Ta for joining NiTi SMAs. The use of the tantalum interlayer successfully slowed down the diffusion of titanium into stainless steel during welding and thus minimised the formation of the intermetallics. It appears that while interfacial melting that occurs during the process is undesirable in achieving a sound joint, as long as the molten layer remains relatively thin, good quality joints can be produced by this method.

Metal	Value of Desirability
Vanadium	0.147
Niobium	0.300
Tantalum	0.278
Chromium	0.137
Molybdenum	0.228

Table 5-2, Desirability of refractory metals as interlayers for joining metal alloys [164]

The use of a tantalum interlayer has been successfully demonstrated on laser butt-welding NiTi SMA to stainless steel wires and achieved a joint strength approaching 90 ksi (620 MPa). This is in contrast to a virtually zero joint strength for joints made without an interlayer and about approximately 116 ksi (1100MPa) for a similar NiTi SMA-to-NiTi SMA weld [**152**]. Theoretically, the use of this interlayer can be applied to the majority of the conventional fusion welding methods. However, this process does have its shortcomings. The use of interlayers adds to the cost of the process. Furthermore, the complexity of the process will increase significantly as one is now dealing with two joints instead of one.

Other studies include plasma welding [**167**] and laser micro welding [**168**]. Plasma welding of NiTi SMA to stainless steel melted a much larger amount of NiTi SMA than stainless steel, which resulted in the diffusion of elements from stainless steel into NiTi SMA. Cracking has been observed at the fusion zone next to the weld. These cracks were caused by the difference in thermal expansion coefficient between

the intermetallics formed at the fusion zones and the parent metals. The thermal stresses generated initiated cracking in the brittle intermetallics at the fusion zone. Ni-rich fillers were also experimented within the same studies **[167, 168]** and it was found that the use of the Ni filler wire has little effect in preventing the diffusion of elements especially into NiTi SMA. This is contrary to the results reported by EWI [**152**]. Furthermore, in the laser micro welding study, butt-welding of NiTi SMA and stainless steel wires produced tensile strengths of up to 660MPa autogeneously[1] compared to 2300 MPa in the parent metal. This is also contrary to the result reported by Hall, which reported that autogeneous welding of NiTi SMA to stainless steel produces welds with no joint strength [**163**]. The discrepancy is probably due to the different grades of SMAs used in the research.

Where two materials are metallurgically incompatible or the formation of intermetallics is weakening the joints, it may still be possible to produce satisfactory joints by the introduction of a filler metal. Li et al. have successfully laser brazed NiTi SMA to stainless steel with a range of silver-based interlayers [**162, 169, 171**]. The interlayers contain silver, copper, zinc and tin in various compositions. Joints with over 90% of the SE of the parent SMA and a maximum tensile strength of 340 MPa were achieved at room temperature but the SE reduced to approximately 62% at 100 °C. The joint strength increases with increase in the zinc and tin content in the interlayer. The increase in the zinc and tin content lowers the melting temperature of the interlayer and improves the wetting of the parent metals. However, small amounts of brittle intermetallics (Ag_3Sn and $Cu_{41}Sn_{11}$) have been observed at the braze joints

[1] ***Autogeneous welding*** *is a term given to a type of welding in which the metals are usually united without the use of flux or filler material*

with interlayers containing 22% Cu, 18%Zn, 8% Sn, Bal. Ag which suggested that further increases in zinc and tin content in the interlayer would inevitably result in the reduction of joint performance.

6 Selection of Joining Methods

The successful joining of NiTi shape memory alloy (SMA) to dissimilar alloy is critical to the development of the adaptive serrated nozzle. The selection program assessed the suitability of using conventional joining processes for joining the NiTi SMA to Ti-6Al-4V. This is essentially a three-stage process consisting of an assessment stage, a selection stage and a ranking stage. The aim of the process is to identify joining methods that are most likely to succeed in joining NiTi SMA to Ti-6Al-4V.

6.1 Assessment

The assessment process was designed to identify the conventional joining methods that are capable of producing welds in the size and configuration required for the ASN design. To do this, the characteristics of conventional joining methods used for joining metal alloys have been extensively evaluated and compared with the joint specification of the ASN set out in **Chapter 3**. Joining methods that are incapable of joining titanium alloys were immediately discarded from further consideration. Furthermore, methods developed specifically for large structures such as submerged arc and stud arc welding and those developed for small structures such as soldering were also discarded. In addition, cold pressure welding produces extensive deformation to the parent metal and percussion welding requires substantial alteration to the geometry of the workpieces, both of which were inappropriate for the ASN

design and thus were excluded from further consideration. In all, eighteen joining methods have been studied and ten of these have been selected for further evaluation [**Table 6-1**].

Category	**Conventional Joining Methods Studied**	**Short-Listed Joining Methods**
High Energy Beam Welding	Electron Beam Welding Laser Welding	Electron Beam Welding Laser Welding
Arc Welding	Metal Arc Welding Tungsten Arc Welding* Carbon Arc Welding Stud Arc Welding Submerge Arc Welding	Metal Arc Welding Tungsten Arc Welding
Resistance Welding	Electrical Resistance Welding Percussion Welding	Electrical Resistance Welding
High Energy Impact Welding	Explosive Welding Magnetic-pluse welding	
Low Temperature Welding	Brazing Soldering	Brazing
Mechanical Joining	Riveting Climping Swaging	Riveting Climping Swaging
Chemical Joining	Chemical Adhesive Bonding	Chemical Adhesive Bonding

Table 6-1, Conventional joining methods under consideration

[*] ***Plasma arc welding was regarded as an advanced version of tungsten arc welding and was grouped under the same category***

6.2 Short Listing

For any joining methods to be successfully adapted in the production of ASN, they have to be strategically aligned with Rolls-Royce's manufacturing capability. The selection process evaluates the technology readiness level (TRL) of the short-listed joining technologies. The TRL is an indicator of how well these joining methods strategically fit into Rolls Royce's manufacturing capability. Resistance welding for example is strategically incompatible with Rolls Royce. There was no resistance welding capability available in house and accruing a resistance welder specifically for the manufacturing of the ASN would not be economically viable. The same applies to magnetic pulse and explosive welding as these are relatively now and highly specialised welding methods, many aspects of these processes are still under research and development. Due to the specialist knowledge required for these methods, they would be very costly to be carried out externally by specialists or to acquire these technologies in-house. Rolls-Royce has a policy of avoiding using mechanical joining methods if at all possible. Mechanical fasteners are regarded as "dead-weights" in the gas turbine engine as they provide no addition function to the performance of the engine other than holding components together. The addition of fasteners reduces the thrust to weight ratio of the engine and is highly undesirable. Although there are adhesives available for joining metallic materials suitable to use in the current project, Rolls-Royce are keen to apply the joining technology developed in this project in future SMA applications. These applications are intended to be used in much more demanding environments with operation temperatures of up to 750ºC. These environments would certainly exceed the operational tolerance of current

chemical adhesive technology. It would be more efficient to develop joining technology in this project that could be carried forward to be used in future SMA applications and chemical adhesives are clearly inappropriate in this respect. For the above reasons, six of the selected joining methods have been discarded from further consideration.

6.3 Balanced Scorecard

A balanced scorecard has been drawn up to rank the short-listed joining methods in order of suitability and potential to succeed in joining NiTi SMA to Ti-6Al-4V. In order to do this, a list of success criteria has been established. The list was drawn up after extensive discussion with welding experts at Rolls Royce and contained process characteristics that are perceived to Rolls-Royce as vital to the production of the ASN. A set of scoring criteria was then derived from the success criteria to quantify the suitability of each joining method against these success criteria [**Table 6-2**]. Welding specialists and machine operators from Rolls Royce and Cranfield University for each joining method were consulted during the scoring process to ensure the scores reflect the true suitability of the joining method. The five joining methods with the lowest score were selected for extensive experimental investigation. For comparison purposes, all of the joining methods in the down-selection stage have been scored and ranked [**Table 6-3**].

Note that the scores were given solely on their suitability as a process. Scoring should take into consideration factors such as current and envisage spare machine capability

and whether any of the operating costs can be shared with other processes and operations to reflect the true applicability of individual joining method from Rolls Royce point of view. However since the necessary data were not available at the time of the project, it was unable to carry out such an analysis.

Success Criteria	Scoring Criteria	Description
Process capability	Process capability	Capability of joining the desired geometry and product form
Structural integrity Joint stiffness Microstructural stability Size of Heat affected zone (HAZ) Resistance to fatigue Final stress state SMA amnesia Process environment	Applied Pressure Damage Consumables required Solid/Molten State Process Heat Input Temperature Resistant Process environment	Level of deformation to the parent metal Change to properties at the joint interface including SME Likelihood of contamination
Skill level	Tooling complexity Set-up	
Process cost	Capital cost Labour cost Processing Time	

Table 6-2, Success and scoring criteria for the down-selection process

Joining Method	Cost		Tooling complexity (9=high)	Setup (9 = complex)	Heat Inupt (1=low 9=high)	Applied Pressure (9 = high)	Processing Time (1=fast)	Penetrating Depth 1=High,	Damages (metal deformation)	Temperature Resistant Joint	Process Environment	Solid-State/Fusion Process	Consumables	Total Score
	Captial (9 = high)	labour (9 = high)												
Vacuum Brazing	7	5	2	1	7	0	3	1	3	5	vacuum/gas	Solid State	Interlayer	34
Electrical Resistance Welding	4	3	3	3	4	0	4	4	5	5	varies	Fusion	no	35
TIG Welding	4	4	4	5	6	0	5	1	3	3	gas shielding	Fusion	with/without fillers	35
Mechanical Fastening	1	6	2	8	0	0	5	1	8	5	ambient	Solid State	Fasteners	36
Soldering	2	4	2	1	2	0	3	9	4	9	ambient	Fusion	solder	36
Laser Welding	9	8	8	8	1	0	1	1	1	1	vacuum/gas	Fusion	no	38
Electron Beam Welding	9	9	9	9	1	0	1	1	1	1	vacuum	Fusion	no	41
Ultrasonic Welding	3	4	4	5	6	0	3	9	7	4	ambient	Fusion	no	45
Friction Welding	8	9	8	6	5	7	4	1	1	1	ambient	Solid State	no	50
Cold Pressure Welding	7	5	5	7	0	9	4	3	9	3	ambient	Solid State	no	52
Diffusion Bonding	8	5	7	8	9	6	3	3	4	1	vacuum/gas	Fusion	interlayer	54
Explosive Welding	7	7	9	9	5	9	1	3	8	1	ambient	Solid State	explosive	59

Table 6-3, Balanced scorecard rank the suitability of selected joining method

6.4 Summary

The selection process has narrowed the choice of conventional joining methods from twenty-three to five listed in **Table 6-4,** a brief description of the selected joining methods can be found in **Appendix B**. Although methods such as electrical resistance welding has a lower overall score than other chosen methods, thus by definition they have a high potential to succeed, these methods were excluded for strategic reasons. It is impossible to fully assess the feasibility of any technique discussed here without experimentation. This selection process was merely a tool to allow further development work to be concentrated on the most favourable candidates. The selected joining methods were subject to extensive experimental investigation detailed in the subsequent chapters.

Category	Joining Methods
High Energy Beam Welding	Electron Beam Welding Laser Welding
Arc Welding	TIG Welding
Solid State Joining	Friction Welding Brazing

Table 6-4, Final selected joining methods

7 Materials Characterisation

Before welding experiments could commence, the properties of the material available for testing needed to be verified. The Ti-6Al-4V alloy was supplied by Rolls Royce Plc and accompanied with comprehensive material properties that had been independently verified for certification purposes.

7.1 NiTi Shape Memory Alloy

The NiTi SMA was acquired from the ***Institute of Metal Research*** (IMR) in China, and unlike alloys purchased from commercial suppliers that come with extensive, independently verified material data, only limited material properties were provided. According to the information provided by IMR, the entire batch of NiTi SMA was manufactured from four 10kg ingots which were manufactured by vacuum induction melting. The manufacturing route of the alloy is as follows:

1. 10kg NiTi SMA ingots were manufactured by vacuum induction melting, the average diameter of each ingot is approximately 90mm;
2. The ingots were forged at 820°C to produce thick plates with a cross-section measuring 50 x 20mm;

3. Thick plates were then hot rolled at 850°C to the final strip with cross-sections of approximately 63 x 3mm;

4. Hot rolling produced curved strips. To straighten the curved SMA strips, they were annealed at 860°C for 40 minutes then air cooled to room temperature.

IMR noted that the strips had an A_f of approximately 80 °C before annealing process, and the transformation temperature of the alloy usually increased slightly after annealing. This data is insufficient to be used in the current research as other vital material data are needed to fully determine the chemical and metallurgical characteristic of the alloy. A full material characterisation programme was therefore conducted to obtain the material data required for testing, analysis and process development. The material characterisation programme consisted of the measurement of transformation temperatures, composition, microstructure analysis and determination of mechanical properties.

7.1.1 Transformation Temperature Analysis

Differential Scanning Calorimetry (DSC) was used to determine the transformation temperatures of the NiTi SMA received. DSC measures the difference in temperature between the sample metal alloy and a reference material as a function of temperature or time while they are subjected to a controlled thermal cycle. Phase transformation is either

endothermic or exothermic, therefore when SMA undergoes a phase transformation, the heat flow will change accordingly. DSC measures the change in heat flow in the sample during a phase transformation against that of the reference material.

The SMA strips were sectioned into 3x3 mm cubes weighing approximately 20mg and ultrasonically cleaned in isopropanol. The samples were then placed into an aluminium crucible in the DSC cell and subjected to a thermal programme of cooling from 140°C to 0 °C at 10°C per minute followed by heating from 0°C to 140 °C at the same rate. **Table 7-1** lists the phase transformation temperatures determined by DSC for all 13 strips of the as-received NiTi SMA. Typical DSC curves are shown in **Appendix C**. The results showed that the difference in the transformation temperatures between each strip was extremely small. Given that it only takes a compositional shift of 0.1 at% to generate a shift in transformation temperature up to 10 ºC [**74**], the compositional constituency between strips was extremely high.

Sample	Cooling Cycle (°C)			Heating Cycle (°C)		
	M_s	M_f	Peak	A_s	A_f	Peak
SMP 3-1-1	75.6	50.4	61.8	86.4	110.6	101.0
SMP 3-2-1	79.7	52.3	64.6	87.9	116.1	105.3
SMP 3-3-1	77.5	52.5	64.7	87.4	114.5	103.1
SMP 3-4-1	78.8	52.5	64.7	86.9	115.0	104.7
SMP 3-5-1	80.1	51.0	64.1	86.9	115.7	105.7
SMP 3-6-1	74.6	48.3	61.9	84.9	112.4	101.9
SMP 3-7-1	74.1	47.7	62.3	85.8	112.4	102.0
SMP 3-8-1	75.0	48.7	62.3	91.4	116.5	106.0
SMP 3-9-1	75.9	47.4	62.3	85.6	113.9	102.7
SMP 3-10-1	76.9	50.5	64.0	91.2	116.2	105.7
SMP 3-11-1	77.3	51.4	63.8	87.1	114.8	104.1

Table 7-1, Transformation temperatures of as-received NiTi SMA

7.1.2 Microstructural Analysis

Strips of NiTi SMA and Ti-6Al-4V were cross-sectioned into approximately 10 mm thick sections using a high precision, low-speed circular saw with tungsten carbide cutting blade for metallographic examinations. The sectioned specimens were then prepared using different techniques. For NiTi SMA, samples were prepared using a conventional

metallographic preparation technique for metallic materials. The sectioned samples were first hot compression mounted in phenolic resin, then grounded using increasingly finer silicon carbide (SiC) papers, from grit size 120 down to 1200, on an automatic polisher. The samples were then polished using standard polishing clothes and polycrystalline diamond paste of reducing diamond particle sizes from 9µm to 3 µm, followed by a final polishing stage with colloidal silica.

For the titanium alloy, the preparation was more complex. Titanium is a relatively ductile metal and is prone to mechanical deformation. This makes it very difficult to cut, grind and polish. Special cutting wheels specifically designed to cut ductile metals were used to section the titanium strips into approximately 10 mm thick sections. The sectioned samples were then hot compression mounted in phenolic resin. Contrary to the usual polishing procedure where diamond is used as the polishing medium, diamond polishing introduces continuous mechanical deformation, which creates scratches and smears on the sample surface. Once introduced, this layer of deformation is extremely difficult to remove. Diamond polishing was therefore avoided; instead titanium samples were ground using increasingly finer SiC papers, from grit size 120 down to 4000 on an automatic polisher. The ground samples were then polished on a hard polishing cloth (MD-Plan, manufactured by Struers) with a chemical-mechanical polishing agent consisting of a mixture of colloidal silica and a solution containing 50% hydrogen peroxide and 50% ammonia.

The microstructures of the polished samples were revealed by chemical etching process. The NiTi SMA is a relatively new alloy and there are no established metallographic

etchants. Two immersion etchants were explored [**Table 7-2**]. Both produced satisfactory surfaces for metallographic analysis but the addition of the glacial acetic acid in etchant A produced a surface with more contrast in the micro structure and was chosen as the better metallographic etchant for this work. This etchant was also tested on Ti-6Al-4V with satisfactory results.

Immersion Etchant A	Immersion Etchant B
2 vol. % ml HF 5 vol. % HNO_3 30 vol. % COH_3COOH (Glacial Acetic Acid) Immersion for 20-30s	3.2 vol. % HF 14.1 vol. % HNO_3 82.7 vol. % H_2O Immerse for 10-15s with gentle agitation

Table 7-2, Metallographic etchants for NiTi SMA

The metallographically prepared samples were examined on an optical phase contrast microscope (Nikon Optishot) and by scanning electron microscopy (SEM) (Philips XL-30) with energy-dispersive X-ray microanalysis (EDX). **Figure 7-1** shows an optical micrograph of the NiTi SMA. The alloy consisted of coarse grains size up to 39.5 µm at the centre of the alloy. The grain size gradually reduced towards the surface with an average grain size measuring approximately 16.8 µm at the surface of the alloy. The variation in grain size is probably as a result of the thermal gradient built up during the manufacturing process which resulted in non-uniform cooling.

*Figure 7-2***Figure 7-2** is an SEM micrograph showing the microstructure of the NiTi SMA at room temperature at a higher magnification. The microstructure is typical of martensitic alloys with martensite plate size measuring approximately 2µm wide and less than 1µm thick. The HF based etchant created pores on the sample surface [**Figure 7-2**].

Figure 7-1, Optical micrograph showing NiTi SMA microstructure showing grain refinement towards the surface of the alloy

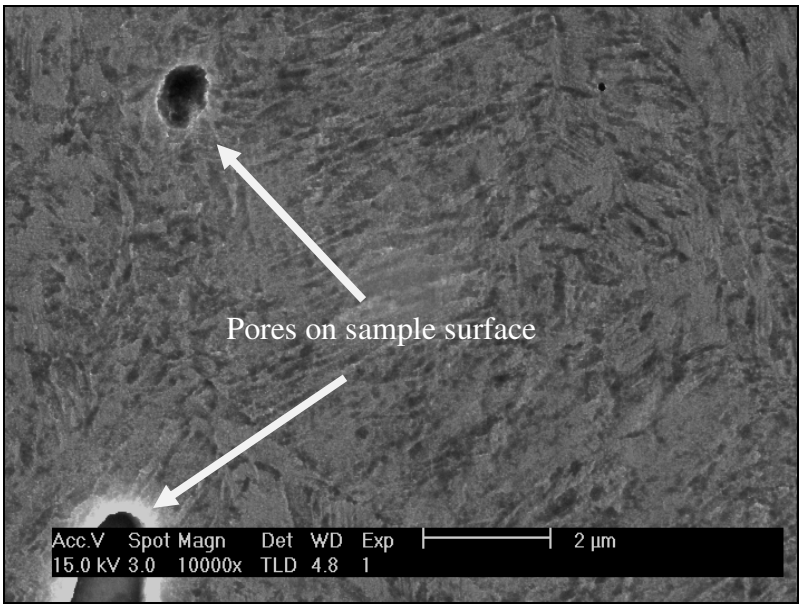

Figure 7-2, SEM micrograph showing NiTi SMA microstructure and micro pores created by the etchant

7.1.3 Compositional Analysis

EDX was used to determine the composition of the as received NiTi SMA. Results showed that the as-received SMA consisted of 51.21 at% Ti and 48.89 at% Ni. The SMA was therefore classified as a Ti-rich alloy. However, EDX only has a resolution of up to ±5% of the result, i.e. the composition of the alloy can be anywhere between 49.23 and 52.49 at% Ti. It was therefore not possible to accurately determine whether the SMA is a Ni-rich or Ti-rich alloy using this analysis technique. Induction Coupled Plasma – Optical Emission Spectrometry (ICP-OES) was subsequently chosen to analysis the composition of the SMA to a higher degree of accuracy. The ICP-OES analyses was prepared and carried out by an external independent test lab (INCOTEST). ICP-OES analyses a substantially larger

amount of material and is reported to be capable of analysing the chemical composition of metal alloys down to a resolution of ±0.1at %. Results from the ICP-OES accurately identified the as-received alloy as a titanium-rich alloy with less than 0.15 at% of impurities [**Table 7-3**].

Elements	Mn	Al	Co	Cr	Cu	Fe	Mo	Nb
at%	0.0097	0.039	0.0090	0.010	0.0084	0.038	0.0055	0.0057

Elements	V	W	Zr	Ti	Ni	Total
at%	0.010	0.014	0.00058	50.59	49.26	100

Table 7-3, ICP-OES chemical compositional analysis

7.1.4 Hardness Testing

The micro-hardness of the raw materials was tested by a Vickers hardness testing method where a pyramid diamond is forced into a polished sample surface at a pre-defined load and duration, producing an indentation. The Vickers hardness is defined as the quotient of test load and area of the indentation and has a unit of Hv.

The micro-hardness profile of cross-sectioned NiTi SMA samples was obtained with a micro-hardness tester manufactured by Matsuzawa Seiki Co. Ltd (Model no. MHT–1) at a load of 200g and dwell time of 15s. Hardness measurements were taken from the top to

bottom surface of a polished sample at 50-micron intervals. The SMA hardness profile in **Figure 7-3** which shows that the hardness of the SMA was slightly higher towards the surface of the specimen. This may be due to grain refinement towards the surface, which is in agreement with the microstructural examination.

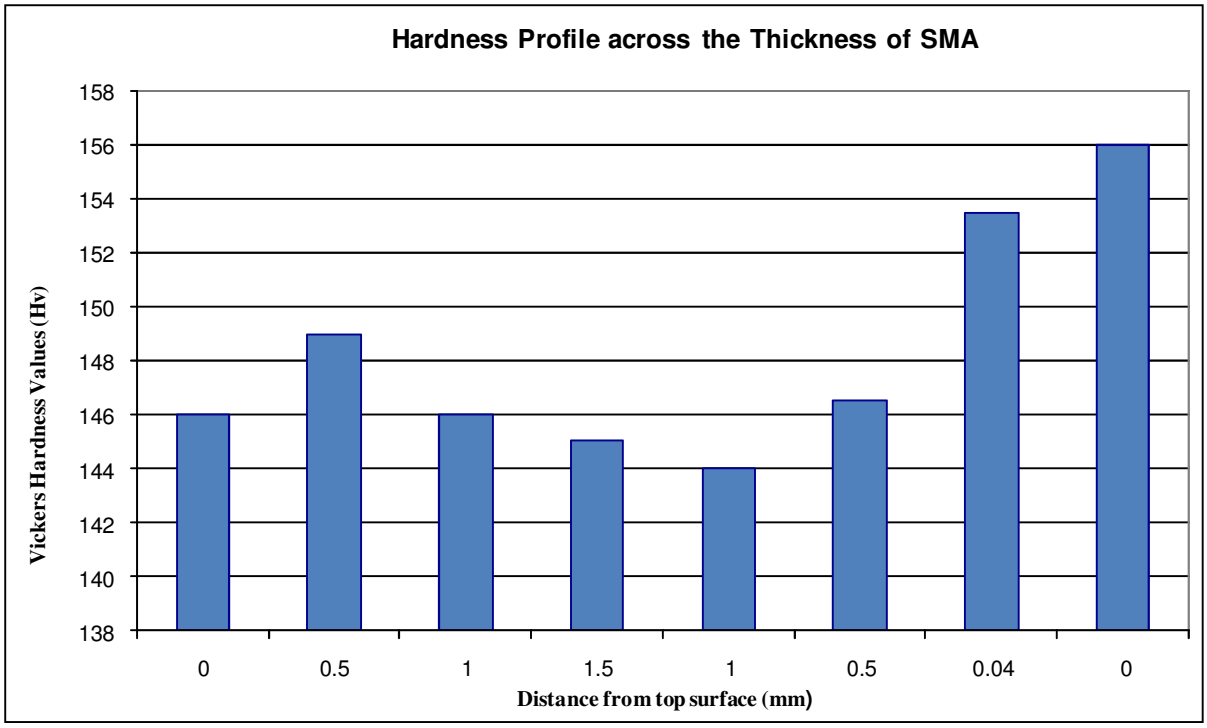

Figure 7-3, NiTi SMA Hardness Profile

7.1.5 Mechanical Testing

Mechanical testing was carried out to fully characterise the mechanical properties of the NiTi SMA. NiTi strips were machined to the conventional 'dog-bone' tensile specimen

shape for tensile testing using a wire electrical discharged machine (WEDM). A schematic of the specimen is shown in **Figure 7-4**.

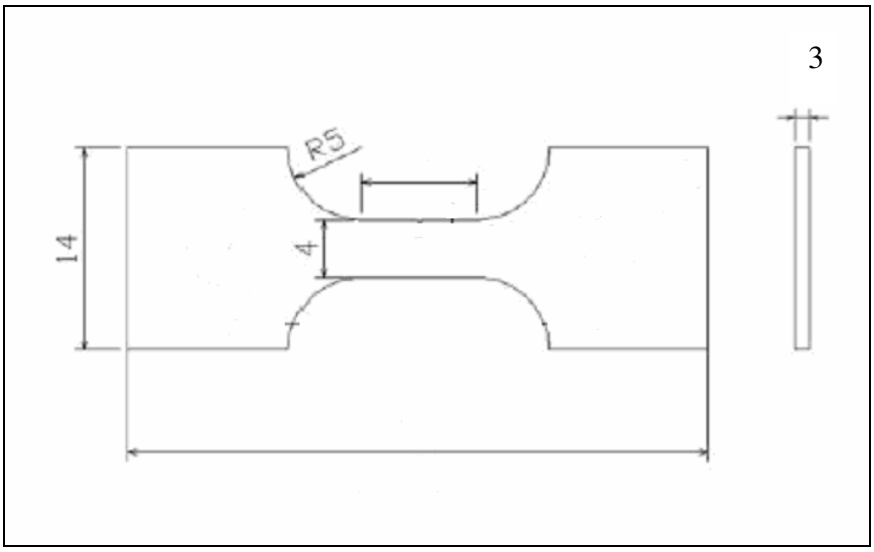

Figure 7-4, schematic of tensile test samples (dimension in mm)

The tensile tests were carried out using a twin-screw tensile testing machine (Instron 5500R). Samples were fixed by clamps and extended at a cross-head speed of 0.1 mm per minute at room temperature until failure. The load and extension were recorded by a computerised acquisition system. During initial testing, samples slipped from the clamps, causing samples to bend in the lateral direction instead of extending longitudally as intended. Slip marks were clearly visible on the deformed samples [**Figure 7-5**]. Discussion with IMR suggested the problem may be a lack of material for the clamp to properly grip and exert a uniform load onto the samples. A modified version of the fixture was recommended so that the same size specimen could be used to preserve material. The improved fixture design is shown in **Figure 7-6a**. Such a fixture holds samples by the 'neck' area, which eliminates the problem with gripping at both ends. However, as shown

in **Figure 7-6b**, the recommended fixture design has square 'necks', which could be potential areas of stress concentration, and could lead to premature failure through crack propagation at these areas. A filleted neck design was used to prevent this from occurring [**Figure 7-7**].

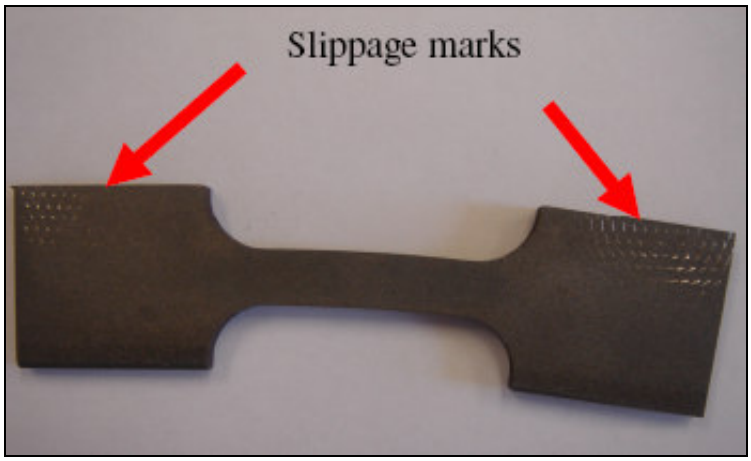

Figure 7-5, Tensile testing specimen failure by slipping

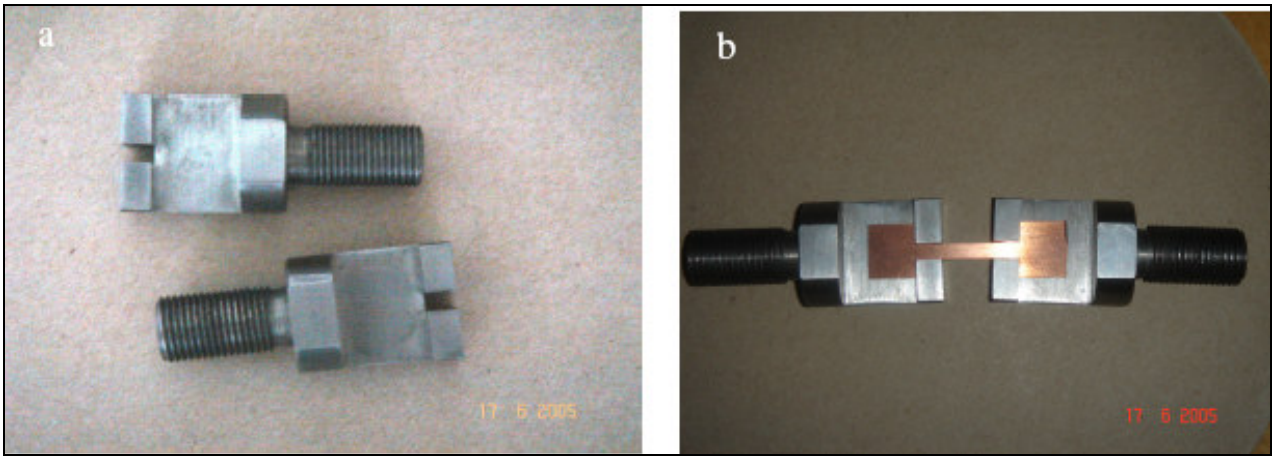

Figure 7-6, a) Tensile testing fixture recommended by IMR; b) Fixture holding a tensile testing specimen

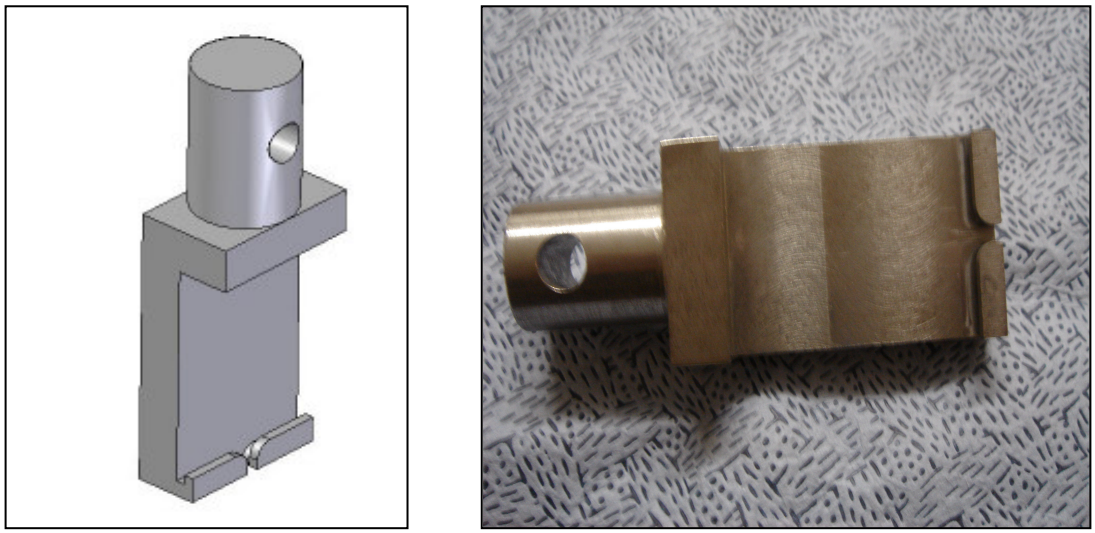

Figure 7-7, schematic of the improved specimen fixture for tensile testing: CAD design (left); final product (right)

Tensile testing showed that the NiTi SMA has an ultimate tensile strength (UTS) of approximately 783 MPa and approximately 20% of elongation to rupture. A typical stress-strain curve of the as-received NiTi SMA in **Figure 7-8** shows a distinct plateau area where martensitic deformation occurs. Martensitic deformation accounted for approximately 7% of strain before the *true* plastic deformation occurred which eventually led to failure. The mechanical properties of the as-received SMA were slightly lower than the typical alloy properties listed in **Table 4-2**. This may be due to the difference in alloy composition and the annealing heat treatment applied at the end of the manufacturing process, which removes some of the cold work stored in the alloy.

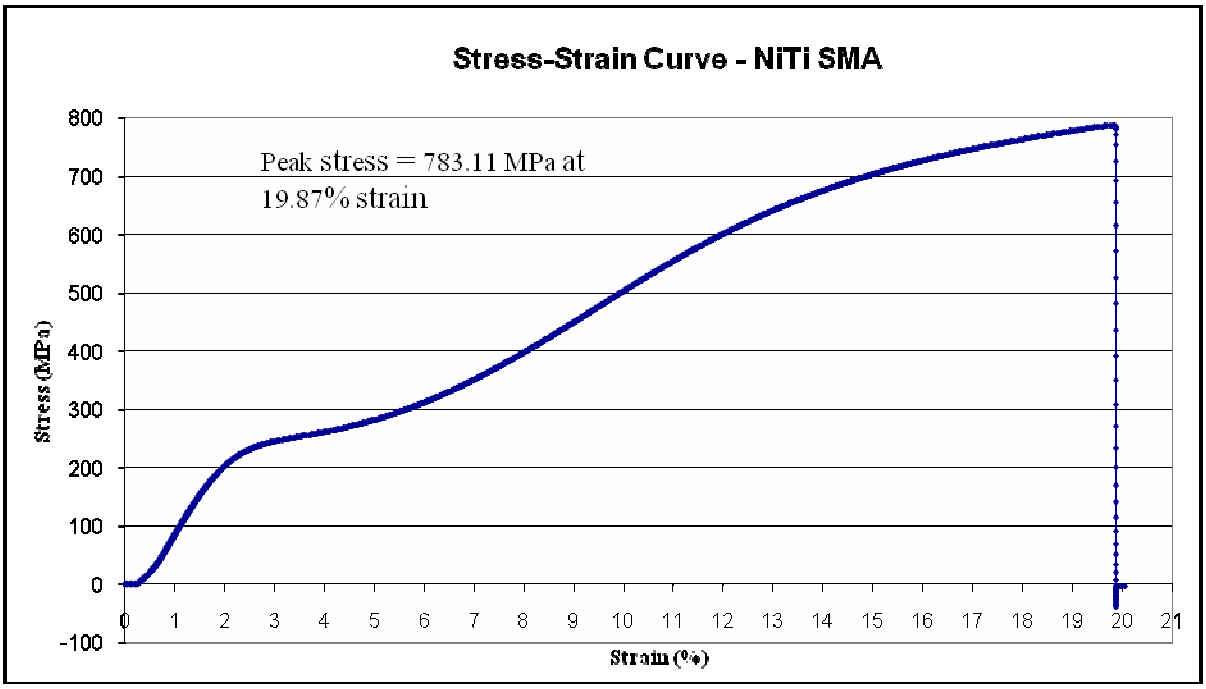

Figure 7-8, Typical Tensile testing of NiTi SMA (typical result)

7.1.6 Thermo-Mechanical Analysis

The shape memory performance of the SMA was characterised by thermo-mechanical testing. The strain recovery of the SMA at elevated temperatures was measured by strain gauges (Type QFLA-3, Tokyo Sokki Kenkyujo Co. Ltd) mounted on tensile specimens with 40mm gauge length using polyester adhesive (Type P-2, Tokyo Sokki Kenkyujo Co. Ltd). A K-Type thermocouple was attached to the specimen for real-time temperature measurement. Load, temperature and deformation output were acquired against time by means of a data acquisition system consisting of a personal computer equipped with an acquisition card (DAQ PCI0MIO16-E-1, National Instruments) controlled by the Labview (Labview 7.0©) software package.

Tensile specimens were placed in a tensile tester (Instron 5500R) with an integrated furnace where a 3% plastic strain was introduced via the cross-head strain of the equipment. The bottom fixture was then removed to allow movement in the longitudinal direction. The extended sample was subsequently heated up from room temperature to 130ºC at a rate of approximately 5ºC per minute in the integrated furnace while the strain recovery was monitored against time and temperature via the acquisition system.

Figure 7-9 showed the strain recovery as a function of temperature (typical results). The SMA exhibited strain recovery which started at approximately 92ºC with full complete recovery occurring at approximately 116.2ºC. These were similar to the A_s and A_f temperatures detected by DSC [**Table 7-1**]. The small discrepancy between the two may be due to the positioning and the sensitivity of the thermal couple, which may not be reading precisely the actual metal temperature. Notice that the graph shown in **Figure 7-9** has a moving base line. This was caused by the thermal effects on the strain gauge, cross-head and the load cell in the tensile tester. This phenomenon has been observed in other thermo-mechanical testing but to a lesser extent [**170**].

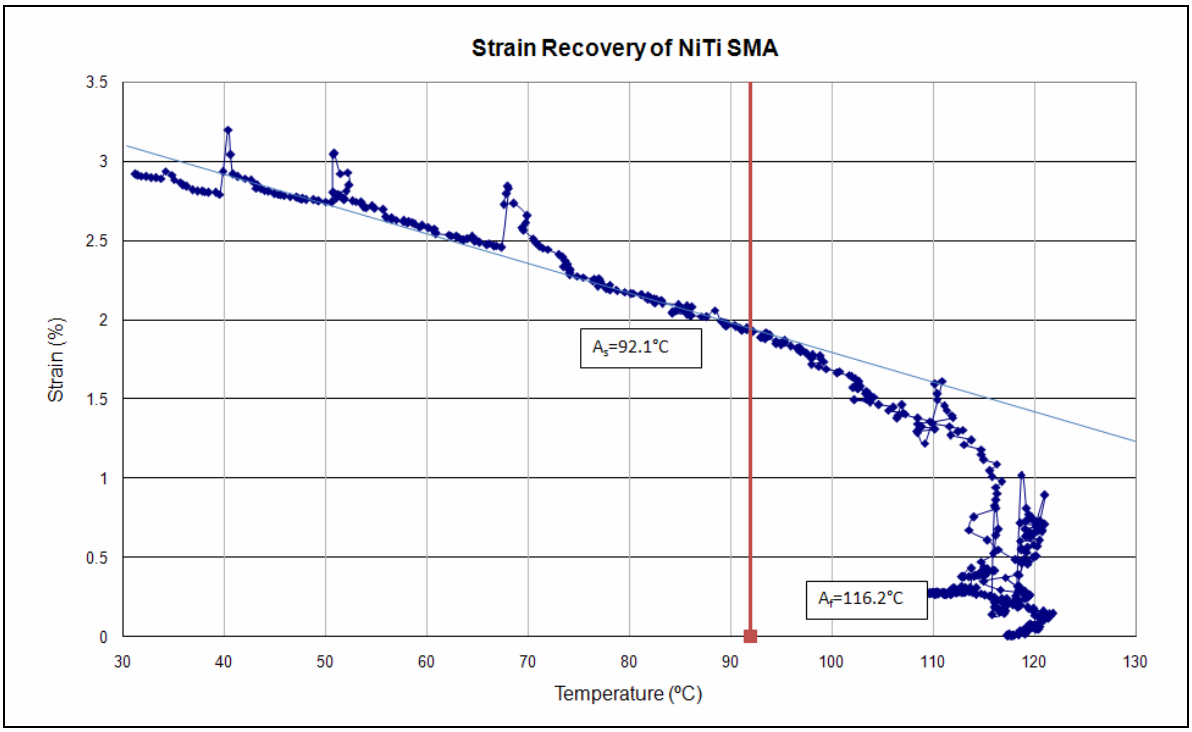

Figure 7-9, Thermo-mechanical testing of NiTi SMA (typical result)

8 Welding Programme

Once the material properties of the received alloys were established and verified, the welding feasibility experiments commenced. Tungsten Inert Gas welding (TIG) was the first welding method used as it was the most accessible and inexpensive.

8.1 Tungsten Inert Gas (TIG) Welding

TIG experiments were carried out at the Cranfield Welding Research Centre. Work had been originally planned to carry it out on a TIG welder mounted on a CNC table. However due to a problem with the CNC table, the experiments were eventually carried out manually by an experienced TIG welder using a manual TIG torch (Invertor LDH 1600, Migatronic) with an electrode diameter of 2.5mm.

The Ti-6Al-4V and NiTi strips were sectioned into 60x30x3mm coupons. The abutting surfaces of the coupons were ground flat to ensure close contact between the parent metals. The coupons surfaces were cleaned using a wire brush to remove the surface oxide and then with isopropanol to remove any organic products prior to welding. Coupons of Ti-6Al-4V were butt-welded to NiTi SMA under argon gas shielding. Argon shielding was applied 10 seconds prior to welding and remained at a constant flow rate of 40 litres per minute throughout the welding process and 10 seconds after welding was complete to minimise contamination. Spot tag-welds were initially produced at either end of the seam to ensure

close fit-up between the workpieces. TIG butt-welds were produced using the process parameters employed for welding commercial titanium alloys of similar thickness. The quality of the welds were assessed visually by the appearance and the shape of the weld bead contours post joining. The welding parameters were then adjusted until the optimum process parameters were achieved. The details of this welding programme are listed in **Table 8-1**. When the optimum process parameters had been obtained, welding experiments were performed to investigate whether a gap between the workpiece had any effects on joint performance. In addition, investigations of the effects of metallic fillers on the performance of the joint were also conducted under the optimum process parameters. Filler wires were manually fed into the weld metal during welding. Inconel 625 filler wire with 1.6 mm diameter was the only filler wire available at the time of testing and was used throughout the experiments. The nominal composition of Inconel 625 is listed in **Table 8-2**. The TIG welds were examined by optical and scanning microscopy and analysed by micro-hardness and for composition.

Sample No.	Welding current (A)	Gap	Interlayer
TIG W1	55	No	None
TIG W2	62	No	None
TIG W3	66	No	None
TIG W4	68	No	None
TIG W6	68	No	Inconel 625
TIG W7	70	No	None
TIG W8	70	No	Inconel 625
TIG W9	72	No	None
TIG W10	72	No	Inconel 625
TIG W11	70	1mm	Inconel 625

Table 8-1, TIG welding parameters

Elements	Ni	Cr	Mo	Nb	Co	Fe	C	Si	Mn	Ti	Al
Composition (at %)	Bal	20.00-23.00	8.00-10.00	3.15-4.15	1.00	5.00	0.10	0.50	0.50	0.40	0.40

Table 8-2, Nominal composition of Inconel 625

8.1.1 Joint Characterisation

The metallurgy of welded samples was analysed extensively by metallographic and mechanical examinations. The metallographic preparation of the welded samples was more difficult than that of the parent metals. Welding dissimilar metals together produces welds that consist of zones with different microstructures and hardnesses. During grinding and polishing, these areas deform and wear at different rates, creating uneven surfaces. An electrolytic polishing process was explored to provide a preparation process that was free from any mechanical contact with the sample surface. The process electro-polished samples in an electrolyte consisting of 20% H_2SO_4 and 80% methanol at 28v for 5 minutes. However, not only did the process fail to produce flat, polished surfaces, it also caused excessive pitting. Mechanical preparation techniques were therefore used for the metallographic preparation of welded samples.

All welded samples were initially sectioned into approximately 10 mm thick sections using a high precision, low speed tungsten carbide cutting wheel. Butt-welded samples were prepared following the same technique used for preparing NiTi SMA for metallographic examination. The butt-welded samples did not appear to suffer from deformation problems during the diamond polishing stages. Etching of welded samples used the same chemical etch employed for the parent metals. However, the microstructure at the weld was significantly different to that of the parent metals and it etched at a different rate. To avoid over etching, the welded samples were subjected to an iterative etching process of immersion etching for 15 seconds with the sample examined under the optical microscope

between each stage until the microstructure of the sample was revealed. The welds etched significantly faster than the parent metals, thus the microstructure of the parent metals were only partially etched and not clearly visible.

The cross-sections of selected samples were subjected to micro-hardness testing using a micro-hardness tester (Matsuzawa Seiki co. Ltd. Model: MHT-1). This provided information on the changes in material properties across the weld. The micro-hardness testing was carried out following the Vickers hardness testing method using the same set up described in **Chapter 7.1.4**. Hardness measurements were taken from the parent metal perpendicular to the sample surface at 50-micron intervals across the weld.

The microstructural changes at the welds were examined using optical and scanning electron microscopy. Different phase constituents of the weld microstructure were identified by EDX. Although the resolution of the EDX precludes accurate measurement of phase composition, the measurements were adequate to identify phases in this alloy system as the intermetallic compounds occur at widely different compositions [**Figure 4-5**]. The examination procedures for subsequent welding techniques followed the same procedure as described above unless stated otherwise.

8.1.2 Microstructural Analysis

All the autogeneous TIG welds failed on cooling as a result of hot cracking. Visual examination showed that the weld did not penetrate fully through the parent metal. **Figure 8-1** clearly shows the absence of a bottom bead.

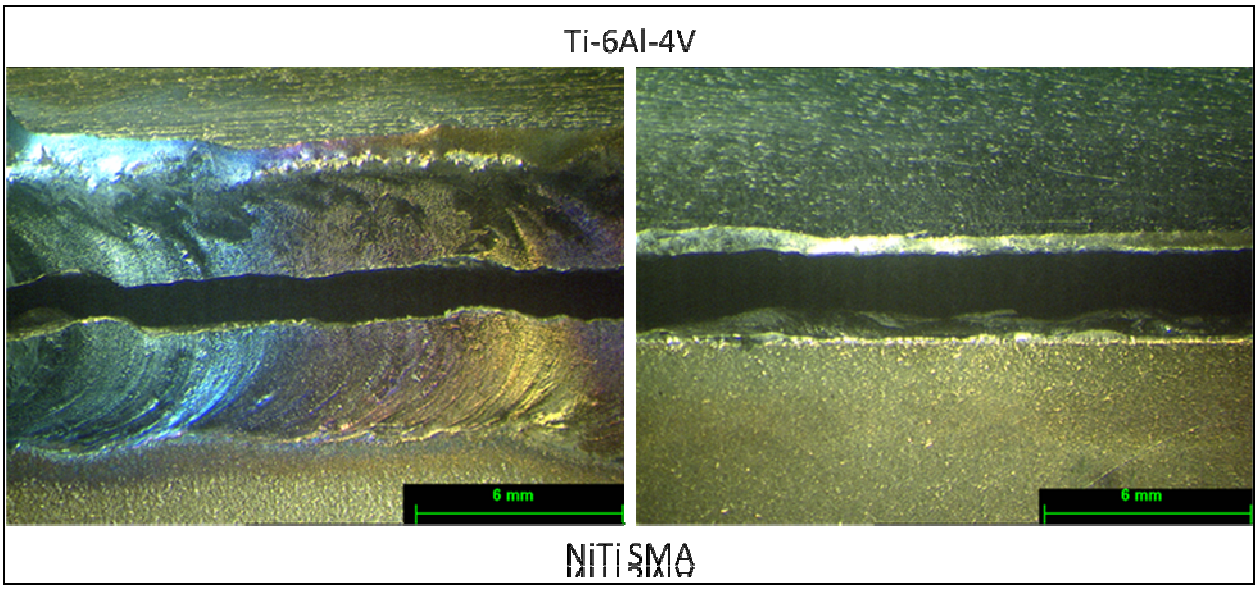

Figure 8-1, Photographs of TIG weld that failed on cooling (TIG W7): a) Top view and; b) bottom view

For welds produced with the addition of filler wire, visual examination revealed that the surfaces of these welds were free from any defects. Similar to the autogeneous welds, these also suffered from some surface oxidation due to the combination of inadequate gas shielding and inconsistent welding speed. However, the thickness of the weld meant that surface oxidation should not have had significant effect on the overall properties of the

weld. Furthermore, the surface layer of the weld could be machined off after welding should surface oxidation become an issue.

Figure 8-2 shows macrographs of the optimised TIG weld produced with and without a gap between the parent metal. The average width of the top bead was approximately 6mm, with a heated affect zone on the Ti-6Al-4V side of up to 2.5mm wide. Re-crystallisation of the base metal occurred at the HAZ and as a result of the relatively slow cooling, large equiaxed grains formed. Grain size at the HAZ could be up to 300µm in diameter. No obvious microstructural change was observed on the NiTi SMA side.

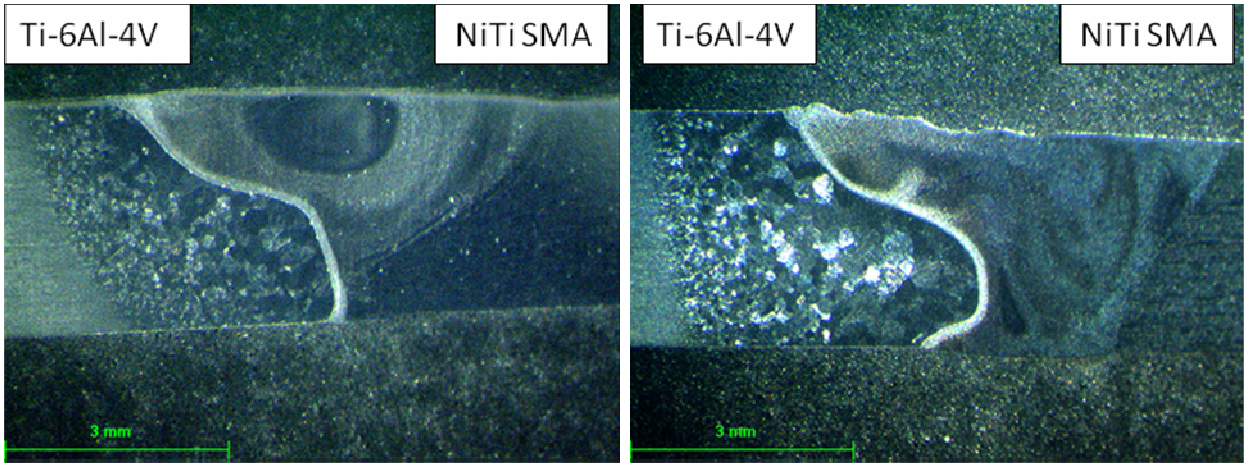

Figure 8-2, macrographs of optimised TIG welds: without 1mm gap (left) and with 1mm gap (right)

The presence of a 1mm gap between the base metal plates enabled welding heat to channel to the bottom of the weld, thus creating a thicker and deeper weld. Without the gap, the transportation of welding heat relied solely on conduction of parent metal and as a result, full penetration was not achieved for the same welding current. The microstructures of the

two welds were virtually identical. Apart from the boundary of fine columnar dendrites towards the Ti-6Al-4V fusion interface, the weld microstructure was very consistent [**Figure 8-3**]. The microstructure was characterised by two distinct phases. Compositional analyses using EDX indicated that the main constituents were Ni and Ti [**Table 8-3**]. Referring back to the binary equilibrium phase diagram showed in **Appendix A**, the microstructures of these two phases were a $NiTi_2$ matrix and a NiTi second phase.

The dendrites at the fusion boundary were identified as $NiTi_2$. There were no cracks observed through the cross-section of the weld, which is a marked improvement compared to the autogeneous welds. However due to the large amount of alloying elements present in the filler wire, it was not possible to identify the effect of each element in the evolution of the weld microstructure during the solidification process.

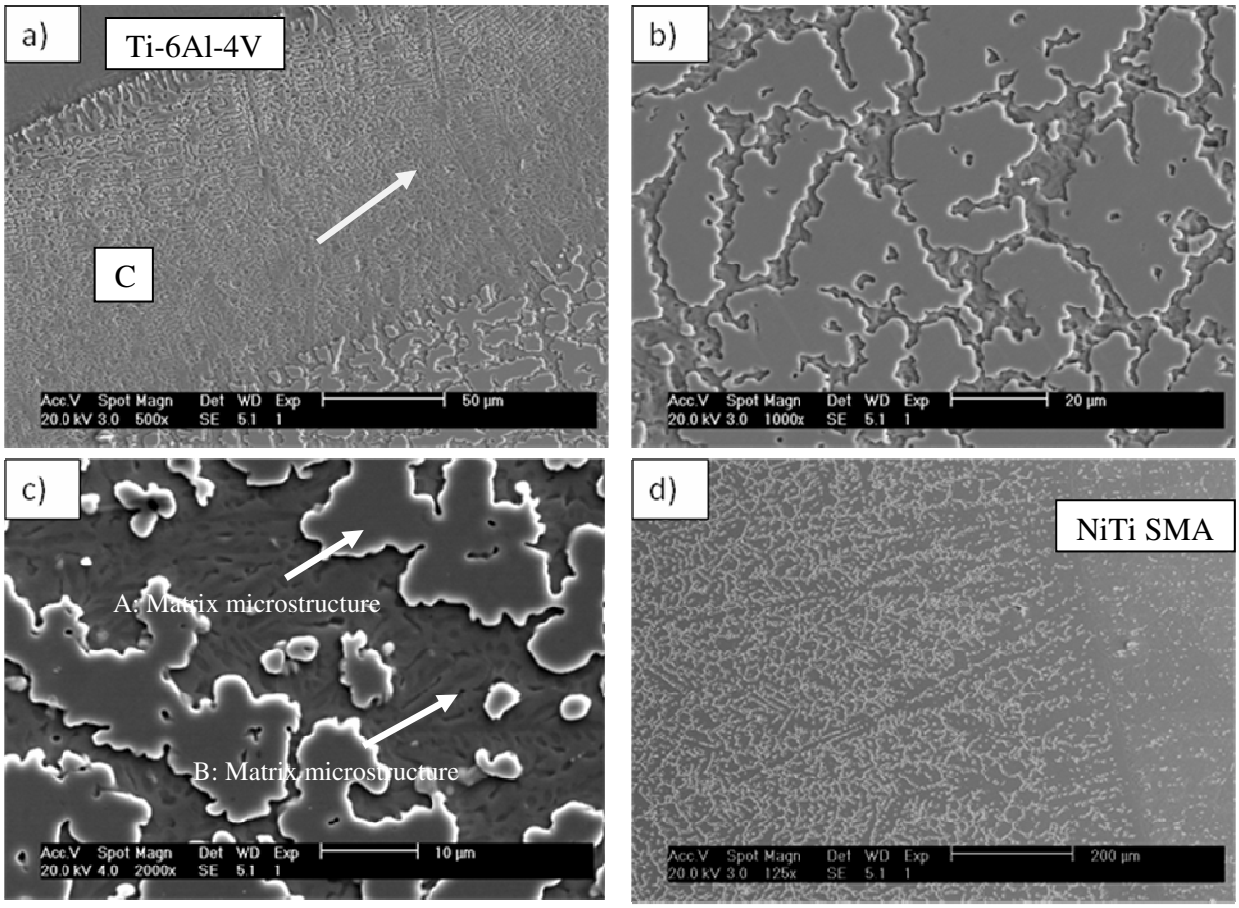

Figure 8-3, SEM micrographs of TIG weld, a) at Ti-6Al-4V weld interface, b) matrix mircostructure; c) high magnification of matrix structure ; d) SMA-Weld interface

Site	Elemental composition (at%)						
	Al	Ti	V	Cr	Fe	Ni	Mo
A	2.50	48.16	0.83	4.21	0.35	42.51	1.44
B	4.17	61.17	0.99	3.09	0	30.67	0.01
C	4.98	60.70	1.63	3.44	0	29.24	0

Table 8-3, Composition analyses of TIG weld

8.1.3 Mechanical Analysis

Tensile tests were carried out to evaluate the mechanical performance of the TIG welds [**Figure 8-4, 8-5**]. The technique used here was that used in the material characterisation programme described in **Section 7**. The shape memory characteristics of the joints were not tested as it was not in the interest of the current project to monitor changes in the shape memory properties at the joint area. Both welds performed similarly in tensile tests, with welds produced with a gap between the parent metals proving marginally stronger than the welds without the gap. This is due to the welds being deeper and thicker than those without a gap. The TIG welds with gap between parent metal achieved a peak ultimate tensile strength of 108MPa and 3.7% elongation to rupture. The welds without a gap were slightly weaker, managing a peak ultimate tensile strength of only 61 MPa and 3.6% elongation to rupture. This is approximately a third of what was required for the ASN design and with simple process optimisation, the target joint performance should be achievable by this method. However, the thickness of the weld far exceeded the tolerance in the ASN design, let alone the HAZ. Furthermore the filler wire used consisted of 11 elements and it is impossible to identify the role of individual elements in the solidification of the weld. Thus TIG welding was deemed an unsuitable joining method for the ASN design.

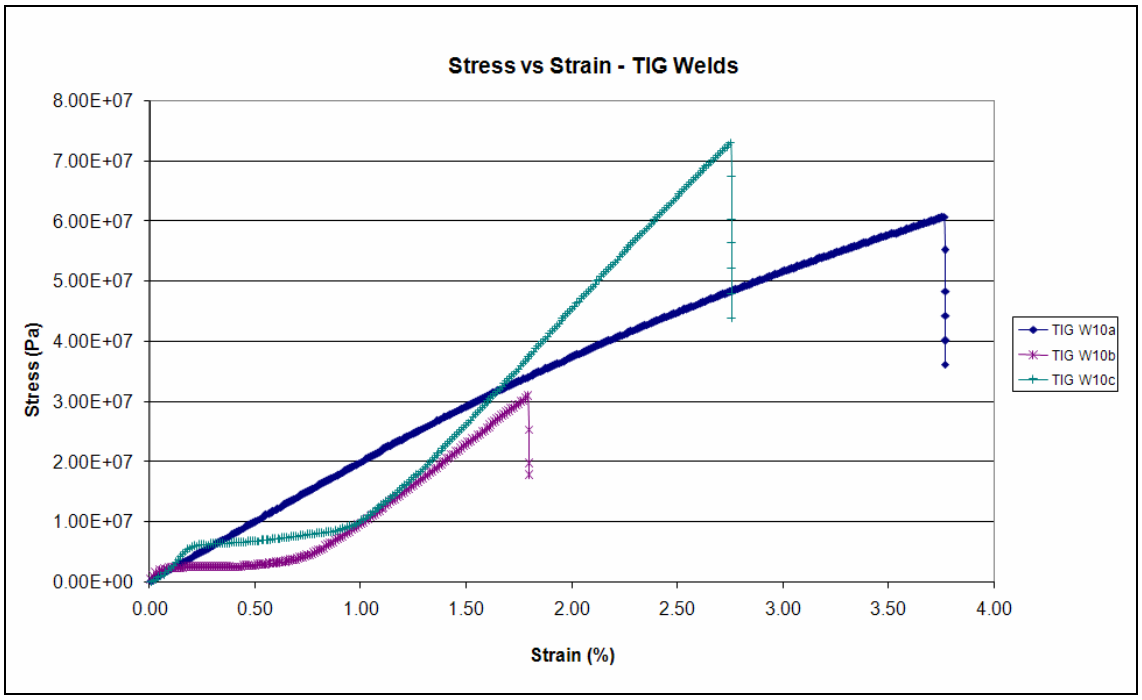

Figure 8-4, Mechanical Testing of optimised TIG weld

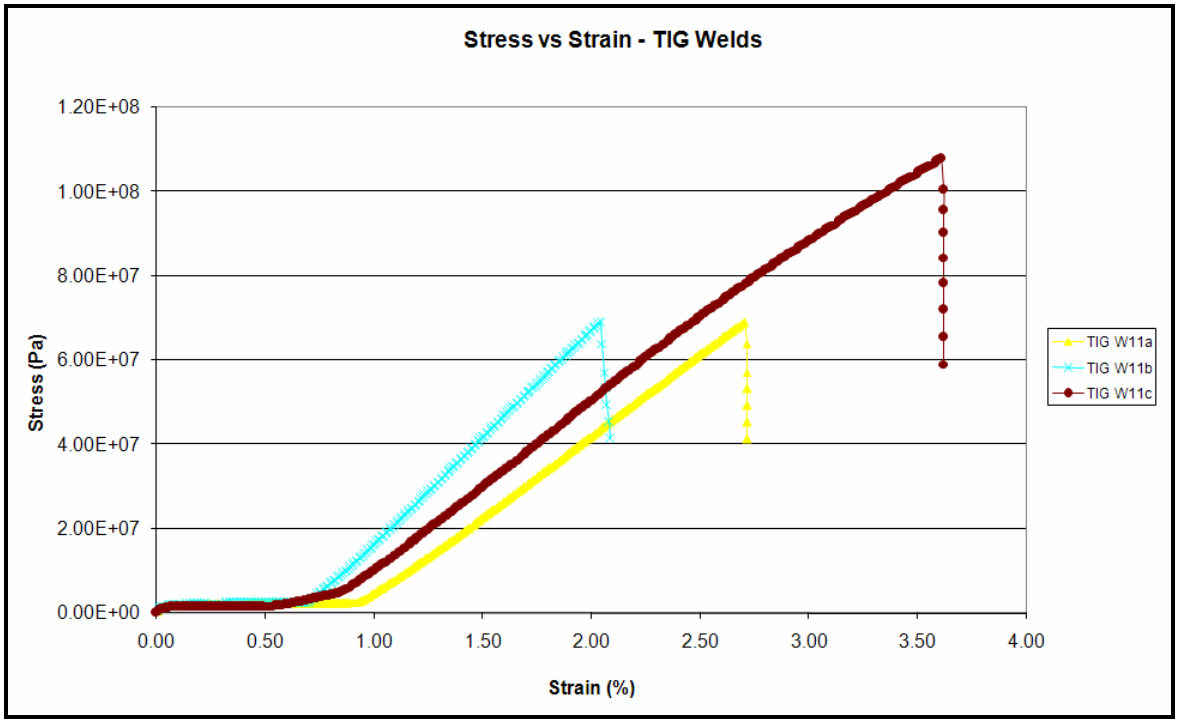

Figure 8-5, mechanical testing of optimised TIG weld with gap between parent metals

There were no apparent explanations as to the marked improvement in weld performance with the addition of the nickel-rich filler wire. One possible explanation is that matrix microstructure in the weld contained α and β-Ti phase as well as the $NiTi_2$ suggested by the binary equilibrium phase diagram. The local enrichment of nickel provided by the filler wire has suppressed the formation of $NiTi_2$. These titanium phases formed at the weld are far stronger and less brittle than the $NiTi_2$ intermetallic that would give rise to the increase in weld performance observed here. The identification of phases with reference to the binary equilibrium diagram should only apply to equilibrium conditions. The experiment conditions here were certainly not binary and far from equilibrium. The author suspects that the actual microstructure of the weld under the welding conditions should be somewhere towards the left of the equilibrium phase diagram (point A in **Appendix A**), which would explain the formation of α and β-Ti phase. Note that the volume fraction of titanium phase formed at the weld was relatively low hence the small increase in weld performance.

Results from hardness tests also support this speculation. **Figure 8-6** showed the hardness profile of TIG welds, the hardness values at the weld ranged between 350-400 Hv. Although the hardness values at the weld were still substantially higher than that of both parent metals, they were at least 80 Hv lower than the average hardness level recorded on the fractured autogeneous welds. The softer welds suggest a lower volume of the brittle intermetallics present at the weld compared to that in the autogeneous welds.

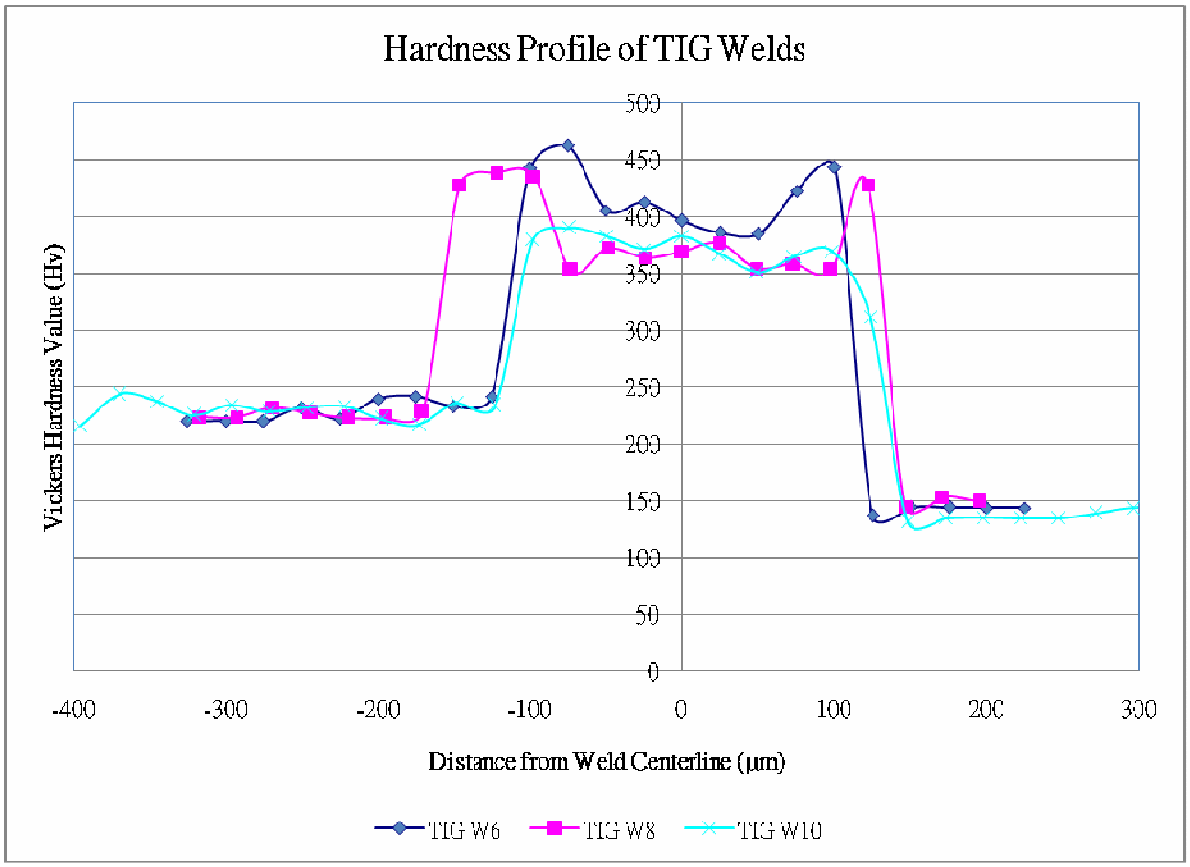

Figure 8-6, Mechanical Testing of optimised TIG weld

TIG welding provided a quick and economical method to investigate the potential problems surrounding the dissimilar joining of SMA to titanium alloys. Although most welds failed under hot cracking, experiments have clearly shown that the performance of SMA welds can be improved by the careful control of weld composition and metallurgy. The use of a filler wire looks promising but it would be simpler and more cost effective if autogeneous welding can be employed.

The problem with hot cracking could be minimised by pre-heating while the lack of penetration can be improve by employing a more concentrated heat source. However,

unless localised heating methods are employed, pre-heating will cause a detrimental effect to the SME of the entire ASN.

8.2 Electron Beam Welding

Preliminary feasibility study by TIG welding showed that autogeneous welding of NiTi SMA to Ti-6Al-4V was extremely difficult. Hot cracking and the inability to produce fully penetrated welds were the major cause of failure. Weld performance was drastically improved by the addition of a filler wire, but the filler system used was too complex to enable a full understanding of the solidification process at the weld. In an attempt to minimise the problem of hot cracking and improve weld penetration, a welding method with lower and more concentrated heat input is required. Electron beam welding offers such a possibility since of all the conventional fusion welding processes, electron beam welding possesses one of the lowest heat inputs due to the small, intense energy beam it produces. This highly concentrated heat input also helps to improve the problem with lack of penetration that observed in TIG welding

A preliminary feasibility study of electron beam welding was carried out at Rolls-Royce, Derby. The electron beam welder used was rated at 15kW and manufactured by Steigerwald. Strips of NiTi SMA and Ti-6Al-4V were sectioned into 60 x 30 x 3 mm coupons [**Figure 8-7**]. The abutting surfaces of the coupons were ground flat to ensure close fit-up between the workpieces. The coupons were cleaned using a wire brush to remove the surface oxide and then with isopropanol to remove any organic products prior to welding. During welding, a NiTi coupon was placed in close contact with Ti-6Al-4V coupon and clamped in place in a butt-welding configuration. A seam tag-weld was then produced using a beam current of 8 mA. The tag weld was essentially a shallow seam weld

running along the weld path. This ensured the alignment of the electron beam with the weld path and held the workpieces in place during welding. Once the tag welds were produced and the beam alignment verified, butt-welds were then produced using the setting shown in **Table 8-4**.

The welding parameter used for butt welding Ti-6Al-4V sheets of similar thickness was chosen as the initial testing parameter. Prior to welding, a bead-on-plate test had been conducted to ensure that the electron beam produced by the chosen parameters fully penetrate the NiTi coupon. During initial welding, thermal contraction induced in the parent metals caused fracture to occur during cooling [**Figure 8-8a**]. This was as a result of inappropriate clamping. A different clamping mechanism that restrained the lateral movement of the base metals was therefore used to prevent further thermal distortion occurring during cooling [**Figure 8-8b**]. To evaluate the performance of the welds, they were subjected to micro-hardness, microstructural and mechanical examinations.

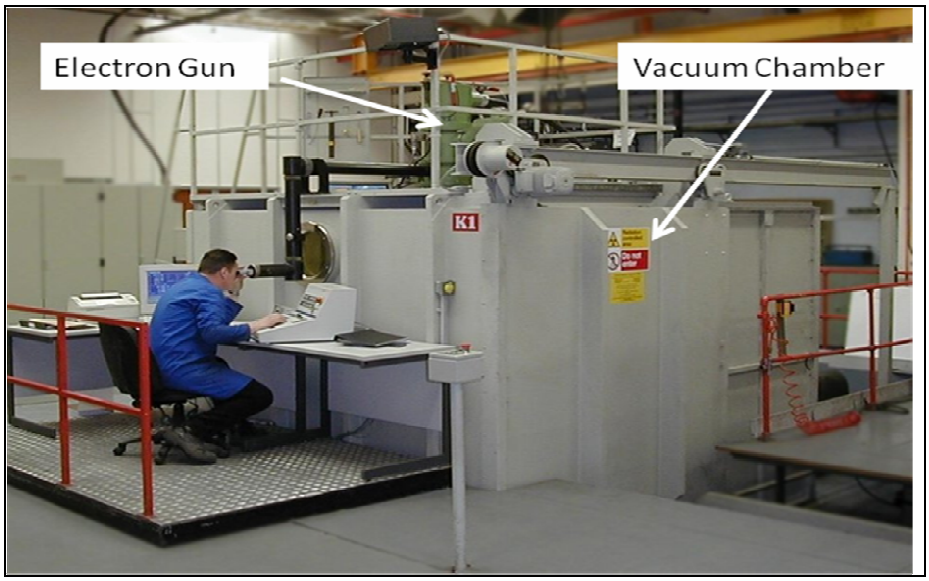

Figure 8-7, photographs of electron beam welder

Beam Power	120 KV
Beam Current	30 mA
Focus	2005 mA
Welding speed	50.8 mms-1
Work height	533 mm

Table 8-4, Welding parameters used in initial e-beam trails

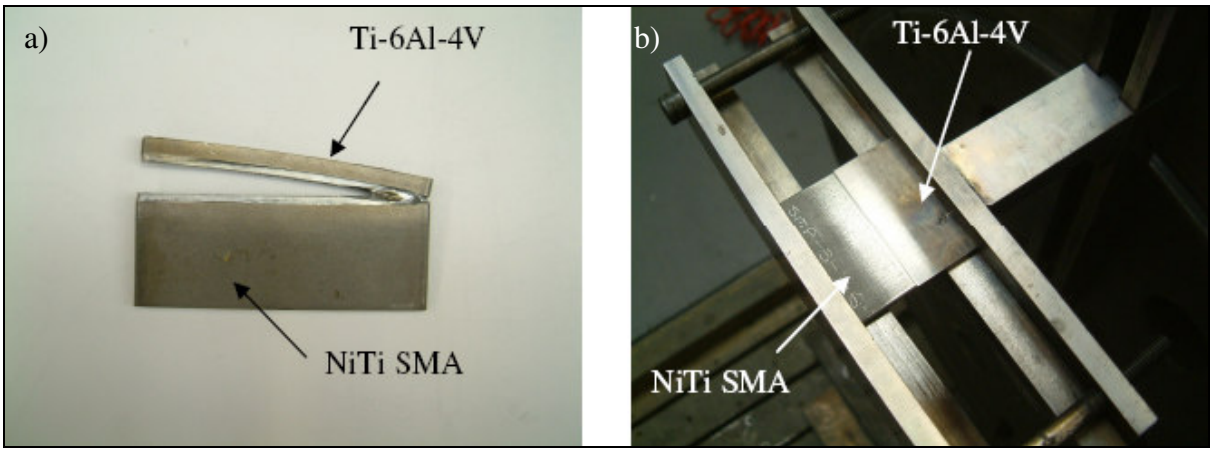

Figure 8-8, a) Photograph of a failed e-beam weld as a result of inadequate clamping, Note that a section of the Ti-6Al-4V coupon has been machined off to be reused in subsequent welding; b) photograph of improved clamping mechanism

The microstructures of the electron beam welds were very different to the microstructures of the parent metals. Different to welding similar metals together where solidification of weld pool proceeds by the growth of parent metal grains into the weld pool, the parent metal grains in the electron beam welds did not grow into the weld pool. Instead, solidification of the weld pool is characterised by very distinctive phases [**Figure 8-9**]. At the NiTi SMA side, solidification proceeds by the formation of a $NiTi_2$ matrix and columnar

NiTi dendrites [**Figure 8-10**]. The volume fraction of the NiTi dendrites gradually reduced towards the centre of the weld. At the Ti-6Al-4V side, the microstructure was dominated by $NiTi_2$ dendrites which grew from the weld zone towards the parent metal. The inter-dendritic spacing was too narrow for EDX to be carried out [**Figure 8-11**], but judging by the lamellar microstructure and referring to the binary phase diagram of the system in **Appendix A**, this inter-dendritic phase should be the Ti+$NiTi_2$ eutectic phase. It is suspected that the growth of the $NiTi_2$ dendrites towards the parent metal limits the growth of grains from the parent metal into the weld pool.

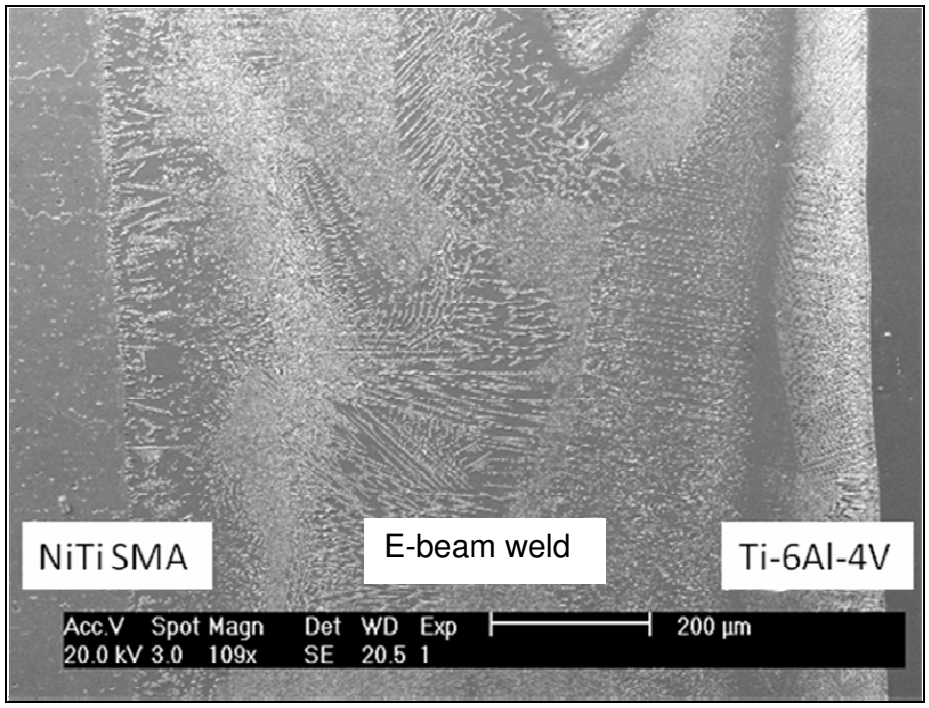

Figure 8-9, SEM micrograph of electron beam weld

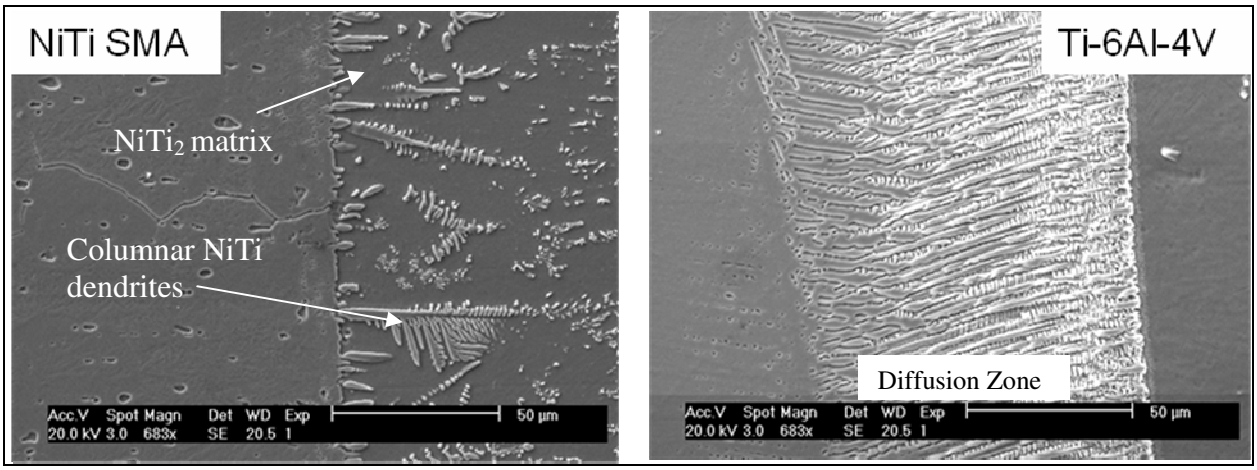

Figure 8-10, interfaces at NiTi SMA side (left) and Ti-Al-4V side (right)

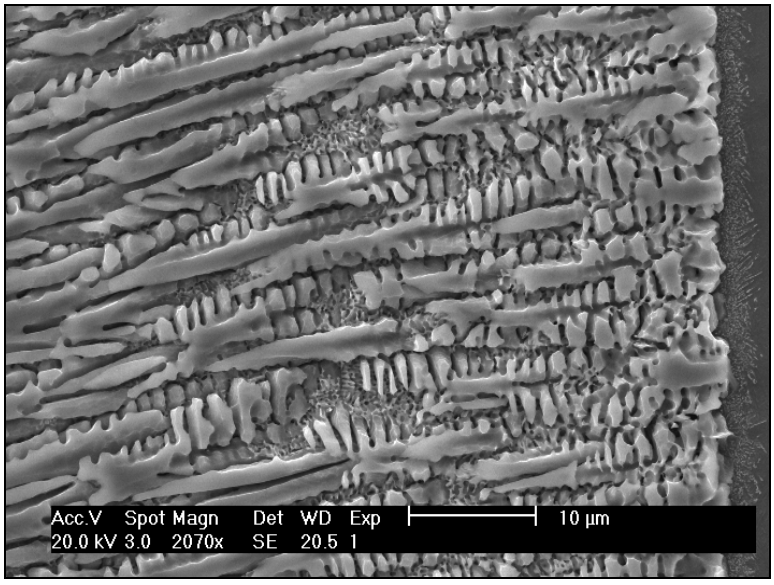

Figure 8-11, Dendritic weld microstructure at the diffusion zone towards Ti-6Al-4V

Compositional analysis showed that virtually no diffusion occurred between the weld metal and the parent metals. The high heating and cooling rate, coupled with the short welding time prevented any diffusion taking place during welding. The compositional profile in **Figure 8-12** showed that the weld zone was less than 1mm thick, well within the tolerance of the ASN design. Since the NiTi SMA has a slightly lower melting temperature, a higher

volume fraction of this alloy was melted and fused into the weld pool during welding. Average titanium content of approximately 62 at% was detected in the weld zone, this means that the weld zone was made up of approximately 70% of NiTi SMA and 30% of Ti-6Al-4V. The relatively constant compositional profile in the weld zone suggests that complete mixing was achieved. This weld composition falls in the $NiTi_2$ + NiTi two phase region of the phase diagram [**Figure 4-5**]. The nickel content in the weld zone fell gradually from 49 at% at the weld interface on the NiTi SMA side to approximately 37 at% at the Ti-6Al-4V side. This reduction in Ni content promoted the formation of Ti-rich Ti_2Ni intermetallics. The volume fraction of Ti_2Ni reduced across the weld towards the Ti-6Al-4V side to compensate for the fall in Ni content across the weld. This is in agreement with the microstructural observations.

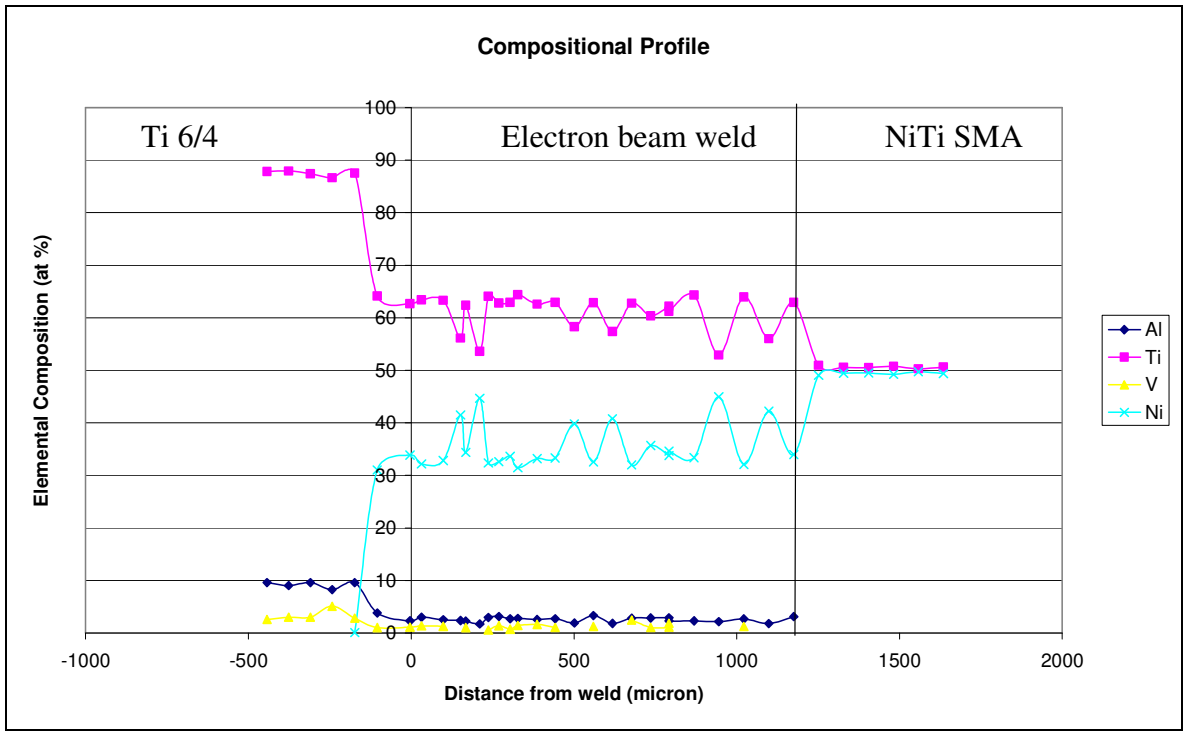

Figure 8-12, Chemical compositional profile of an electron beam weld

The hardness profile produced across electron beam welds showed a sharp increase in hardness due to the presence of the $NiTi_2$ intermetallic [**Figure 8-13**]. Consistent with the microstructural observations, no change in hardness was observed at either side of the weld, indicating the absence of the HAZ. The weld metal consisted of predominately $NiTi_2$ intermetallic, with a hardness value of almost 2.5 times that of the NiTi SMA.

Tensile testing of electron beam butt welds confirmed the poor mechanical properties of these welds. Most of the tensile specimens fractured whilst being set up for tensile testing. Only one specimen remained intact for tensile testing. The ultimate tensile strength of electron beam welds was just over 70 MPa with 1.5% of elongation to rupture [**Figure 8-14**]. This is less than 10% of that of typical NiTi SMA and less than half of what was required for the ASN.

The fracture surface of the tensile specimen was investigated using a scanning electron microscope. SEM micrographs [**Figure 8-15**] revealed that the fracture surfaces were typical of brittle fracture with intra-granular cracks propagating at the centre of the weld.

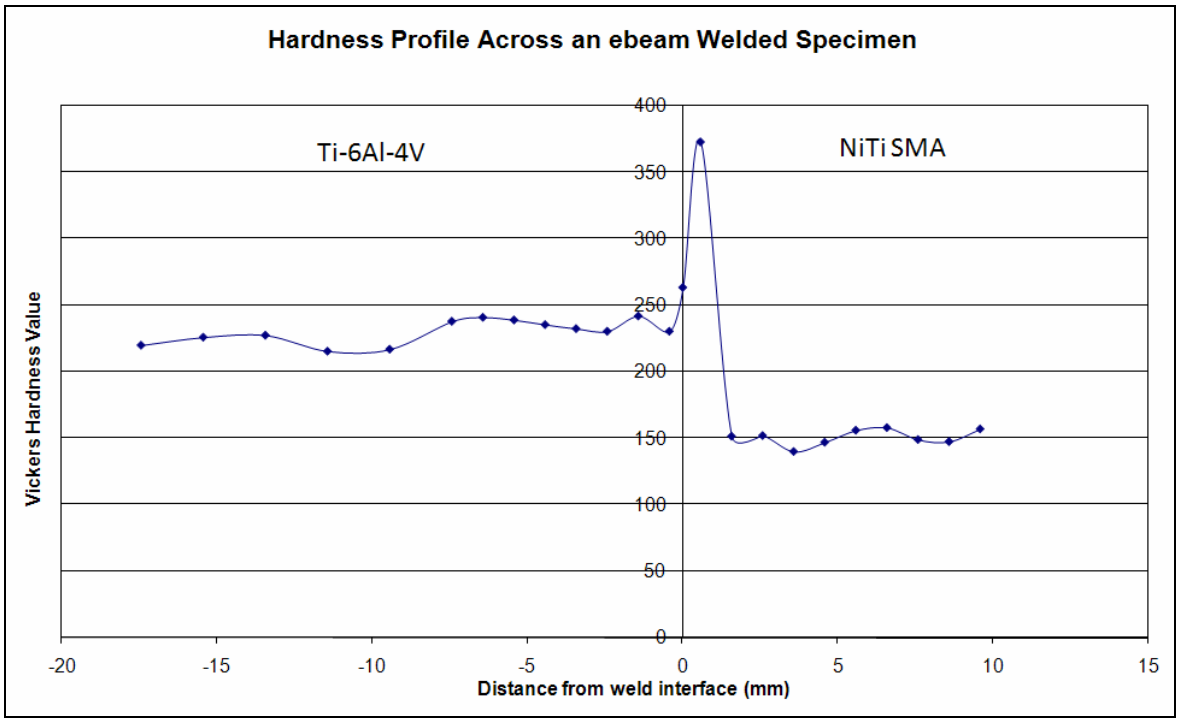

Figure 8-13, hardness profile across an electron beam weld

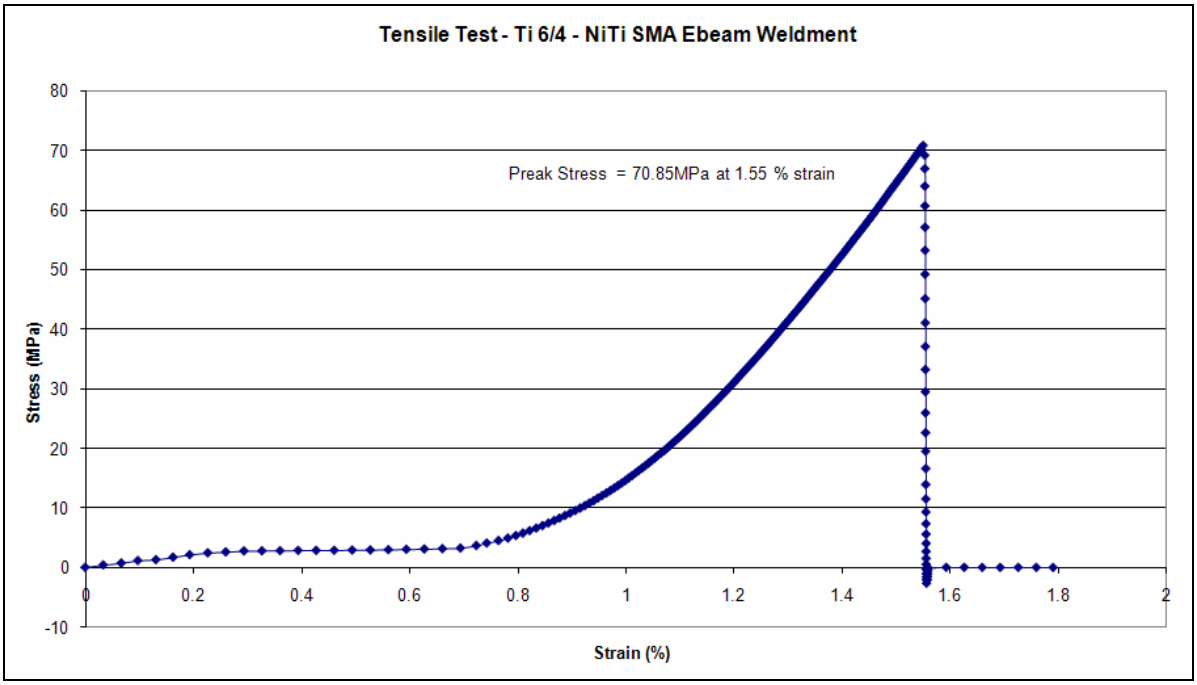

Figure 8-14, Mechanical tensile testing of NiTi electron beam butt-welds (typical result)

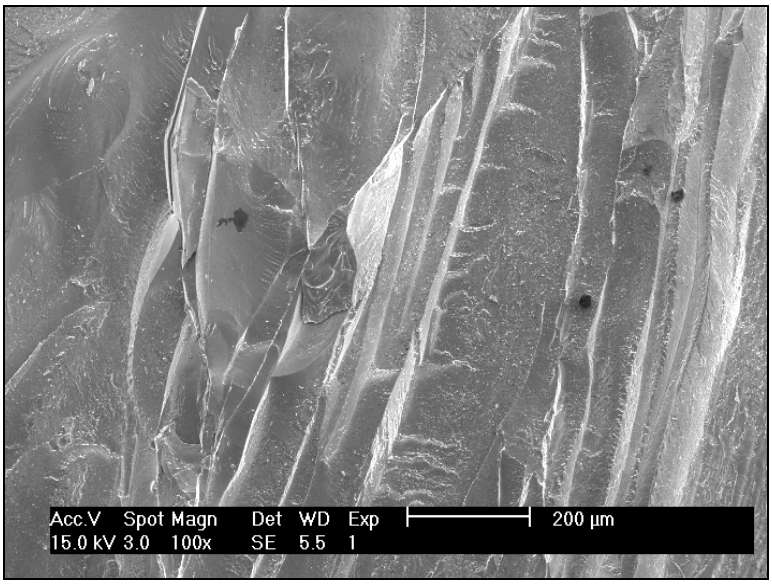

Figure 8-15, Micrograph of facture surfaces of electron beam weld

8.2.1 Weld Composition Manipulation

It is clear that autogeneous fusion welding of NiTi SMA to Ti-6Al-4V, even with the lowest heat input produced poor welds. Joint performance was severely deteriorated by the formation of brittle Ti_2Ni intermetallic phase. The formation of this brittle phase was trigged by a reduction in the Ni content with the weld and this cannot be prevented by either reducing the heat input or the interaction time. However, it has been observed that the volume fraction of $NiTi_2$ changes with the Ni content at the weld and it may be possible to improve the properties of the weld by varying the weld composition. A study of the effect of joint composition on the weld performance was therefore carried out. The manipulation of joint composition should ideally be carried out in a butt configuration where the joint composition can be varied readily by altering the position of the heat source thereby varying the volume of each parent metal which is fused into the weld pool. However, this requires a

precision positioning system to control the position of the heat source throughout the process and is too complex and time consuming at this stage of the development process. Instead this investigation carried out welding in a lap configuration where the composition of the welds was varied by varying the depth of the weld. This is a much simpler process but due to the thickness of the parent plate, there could be a problem of the molten metal not being properly mixed, especially in the deepest welds.

For weld composition analysis, strips of NiTi and Ti-6Al-4V were electron beam welded in lap configuration as shown in **Figure 8-16**. To minimise set-up time, long strips were used instead of coupons to allow multiple welds to be produced on the same strip. The penetration depth of the electron beam welds were altered by varying the beam current to produce welds varying in composition. The effect of welding speed was also investigated. Two high speed welds varying in penetration depth were also produced, the welding parameters used for high speed welding being extrapolated from a regression analysis of all the welding parameters used for welding titanium alloys held in Rolls-Royce's database. In addition, the effect of commercially pure tantalum foil as an interlayer was investigated. 50 μm thick commercially pure tantalum foil was sandwiched between parent metals and fully penetrated lap welds were produced in both orientations. In all 16 weld depths and configurations were tested. The details of these tests are listed in **Table 8-5**. The welds were then examined through a series of metallurgical analyses. The welds were examined using the same metallurgical, micro-hardness and mechanical analysis techniques used for examining the earlier electron beam butt welds.

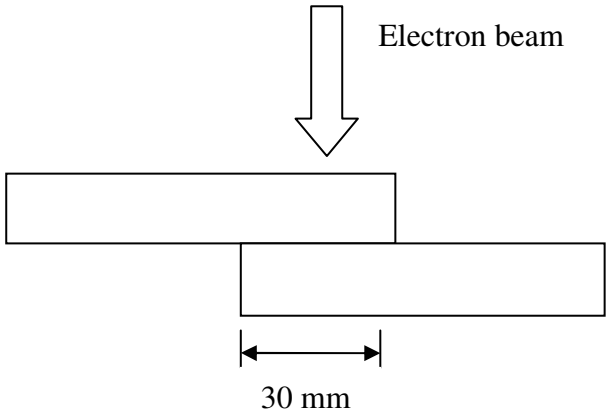

Figure 8-16, Lap weld geometry used during electron beam welding trial. The order of the top and bottom sheets was varied during the trials (see Table 8-5 for details of weld parameters)

	Beam Power (kV)	Beam Current (mA)	Focus (mA)	Welding speed (mms-1)	Work height (mm)	Orientation	Interlayer
EBLS-S1	120	8	1960	6.3	454	NiTi SMA on top	None
EBLS-S2	120	9	1960	6.3	454	NiTi SMA on top	None
EBLS-S3	120	10	1960	6.3	454	NiTi SMA on top	None
EBLS-S4	120	10.2	1960	6.3	454	NiTi SMA on top	None
EBLS-S5	120	10.5	1960	6.3	454	NiTi SMA on top	None
EBLS-Ta	120	10.5	1960	6.3	454	NiTi SMA on top	Commercially pure tantalum
EBLS-F1	120	46	2180	42.3	454	NiTi SMA on top	None
EBLS-F2	120	46	2162	42.3	454	NiTi SMA on top	None
EBLT-S1	120	8	1960	6.3	454	Ti-6Al-4V on top	None
EBLT-S2	120	9	1960	6.3	454	Ti-6Al-4V on top	None
EBLT-S3	120	10	1960	6.3	454	Ti-6Al-4V on top	None
EBLT-S4	120	11	1960	6.3	454	Ti-6Al-4V on top	None
EBLT-S5	120	12.1	1960	6.3	454	Ti-6Al-4V on top	None
EBLT-Ta	120	12.1	1960	6.3	454	Ti-6Al-4V on top	Commercially pure tantalum
EBLT-F1	120	46	2180	42.3	454	Ti-6Al-4V on top	None
EBLT-F2	120	46	2162	42.3	454	Ti-6Al-4V on top	None

Table 8-5, Electron beam welding settings for weld composition analysis

For preparing lap-welds for metallographic analysis, samples were initially cross-sectioned with a low-speed, precision cutter similar to the one used in previous preparation processes. Samples were then cleaned ultrasonically in isopropanol for 30 minutes to remove any debris trapped between the parent metals. The cleaned samples were hot compression

mounted in phenolic resin, ground, polished and etched for metallographic examination. These lap-welds suffered from extensive smearing and deformation when prepared using the multi-stage diamond polishing technique. The diamond-less preparation method used for metallographic preparation of Ti-6Al-4V was therefore employed for preparing these lap-welded samples. Furthermore, the phenolic resin failed to fill the narrow gap between the parent metals next to the weld. As a result, during the grinding stage, silicon carbide particles often became trapped in the gap and later deposited on to the grinding medium on subsequent stages creating deep scratches. To avoid this, samples were ultrasonically cleaned in water and detergent for 20 minutes between each preparation stage.

Although a range of welding speeds and beam current were used, the generic features of microstructural evolution were similar. **Figure 8-17, 8-18** and **8-23** show micrographs of the electron beam welds varying in weld depth with both configurations. Porosity was a problem in the lap welds in both orientations, this is due to unstable plasma gas collapsing during welding. A slower welding speed would allow metal vapour to escape thereby reducing the level of porosity in the weld.

For the electron beam welds produced with the NiTi SMA plate placed on top [**Figure 8-17**], the weld microstructures bore a resemblance to that of the butt welds. The microstructure consisted of cellular NiTi phase in a $NiTi_2$ matrix. Although the titanium content at the weld increased with increasing weld depth, the global alloy composition did not change. Instead, the weld microstructure compensated for the loss of Ni at the weld by forming a higher volume fraction of $NiTi_2$ matrix. **Figure 8-19** shows SEM micrographs of

the microstructure for the shallowest and deepest welds produced. Notice how much more compact the NiTi cells were at the shallower weld. Since the same phase is formed irrespective of weld depth, the local weld composition remained the same **[Table 8-6**]. Columnar dendrites of $NiTi_2$ were formed at the fusion interface and characterised by a dark band that outlined the interface of the bottom plate. The formation of this band of $NiTi_2$ dendrites was caused by the combination of the high thermal and compositional gradients ahead of the interface. This was also the region where cracking was observed [**Figure 8-20 a, b**]. Cracking became more severe with increasing weld depth. For shallow welds, cracks initiated and propagated within the dendritic region at the fusion interface [**Figure 8-20c];** for the deep welds (EBLS-S5), large cracks initiated at the dendritic region and propagated into the weld zone [**Figure 8-20d].** This showed that the joint properties deteriorated with increasing weld depths, this is due to the increasing $NiTi_2$ content in the weld zone as weld depth increases.

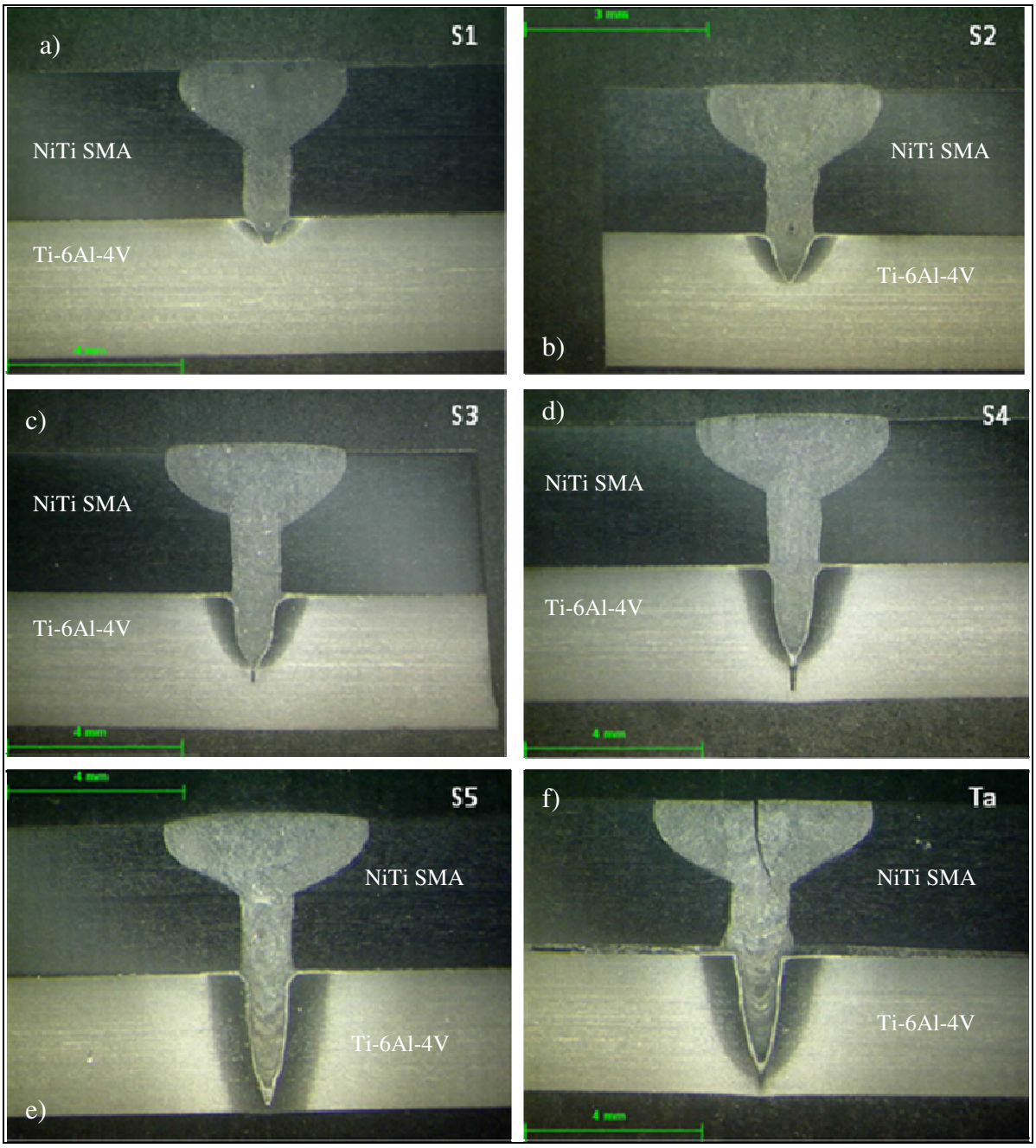

Figure 8-17 a-f, macrographs of electron beam lap welds with NiTi SMA plate on top (EBLS) shown in order of penetration depth

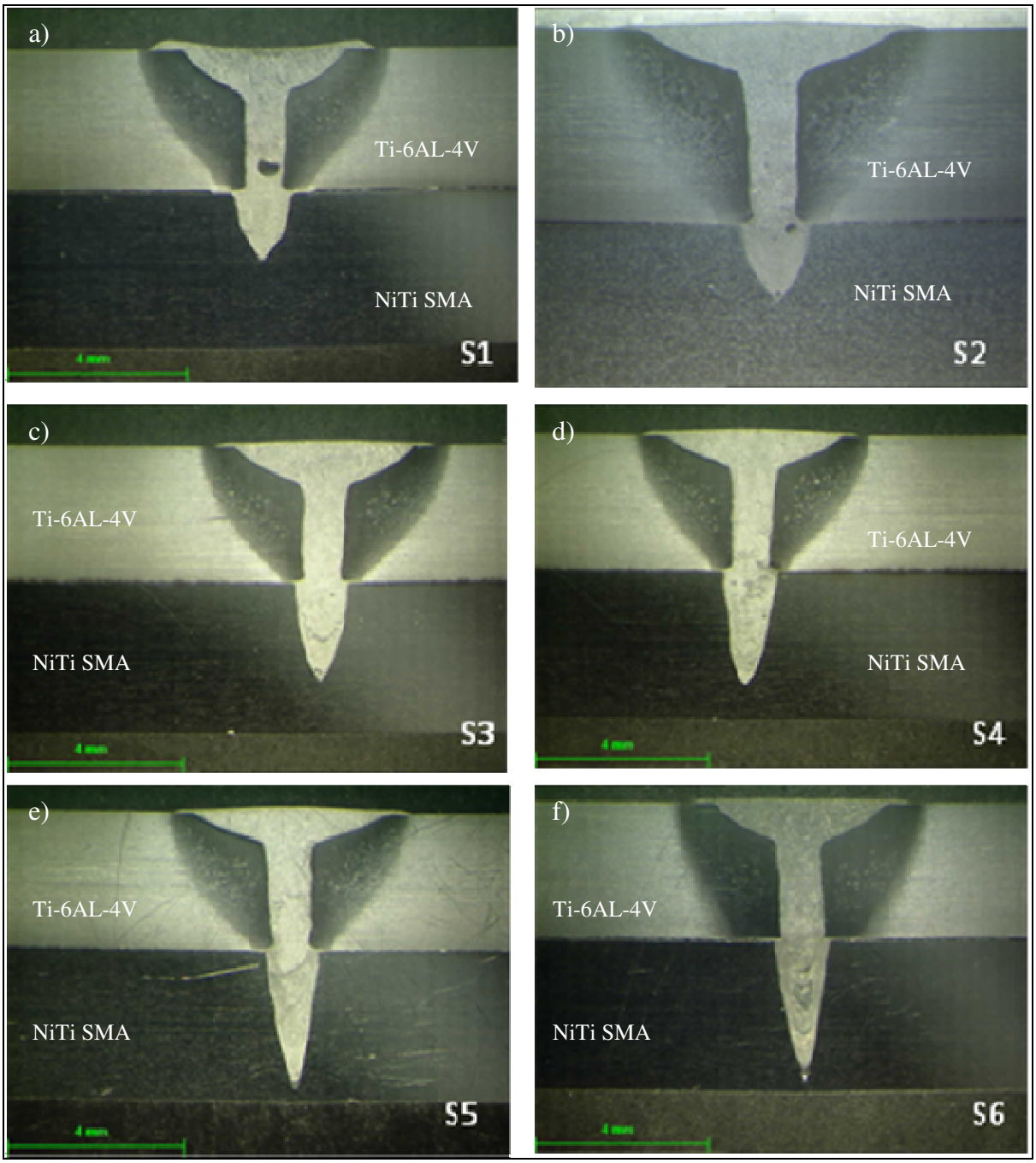

Figure 8-18 a-f, macrographs of electron beam lap welds with Ti-6Al-4V on top (EBLT) shown in order of penetration depth

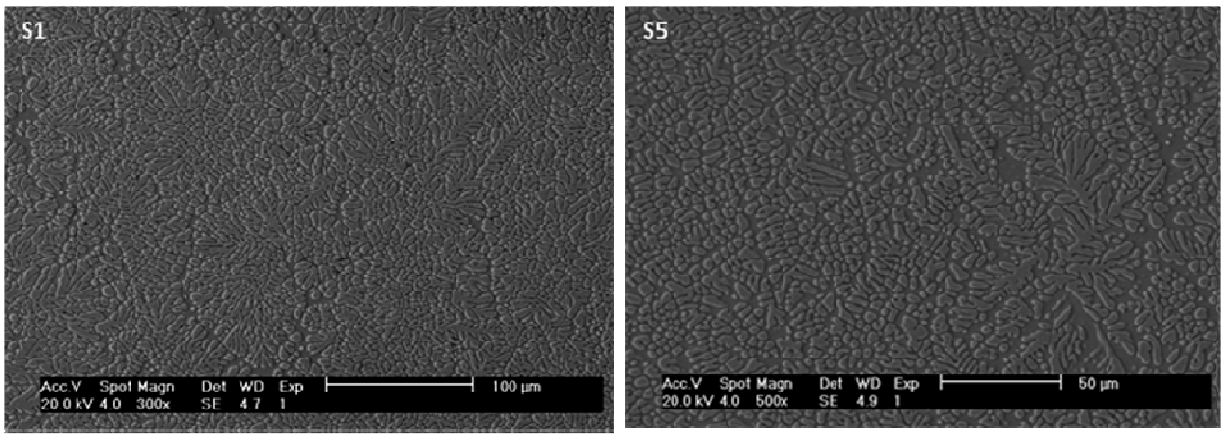

Figure 8-19, microstructures of electron beam lap welds showing the density of second phase increase with penetration depth

	EBLS		EBLT	
	Weld depth (mm)	Nickel content (at%)	Weld depth (mm)	Nickel content (at%)
S1	4.24	54.64	4.84	16.64
S2	4.71	55.29	4.9	18.90
S3	5.56	55.44	5.37	23.31
S4	5.87	55.26	5.78	24.74
S5	6.76	55.39	6.52	24.34

Table 8-6, weld depth and average nickel content in electron beam lap welds

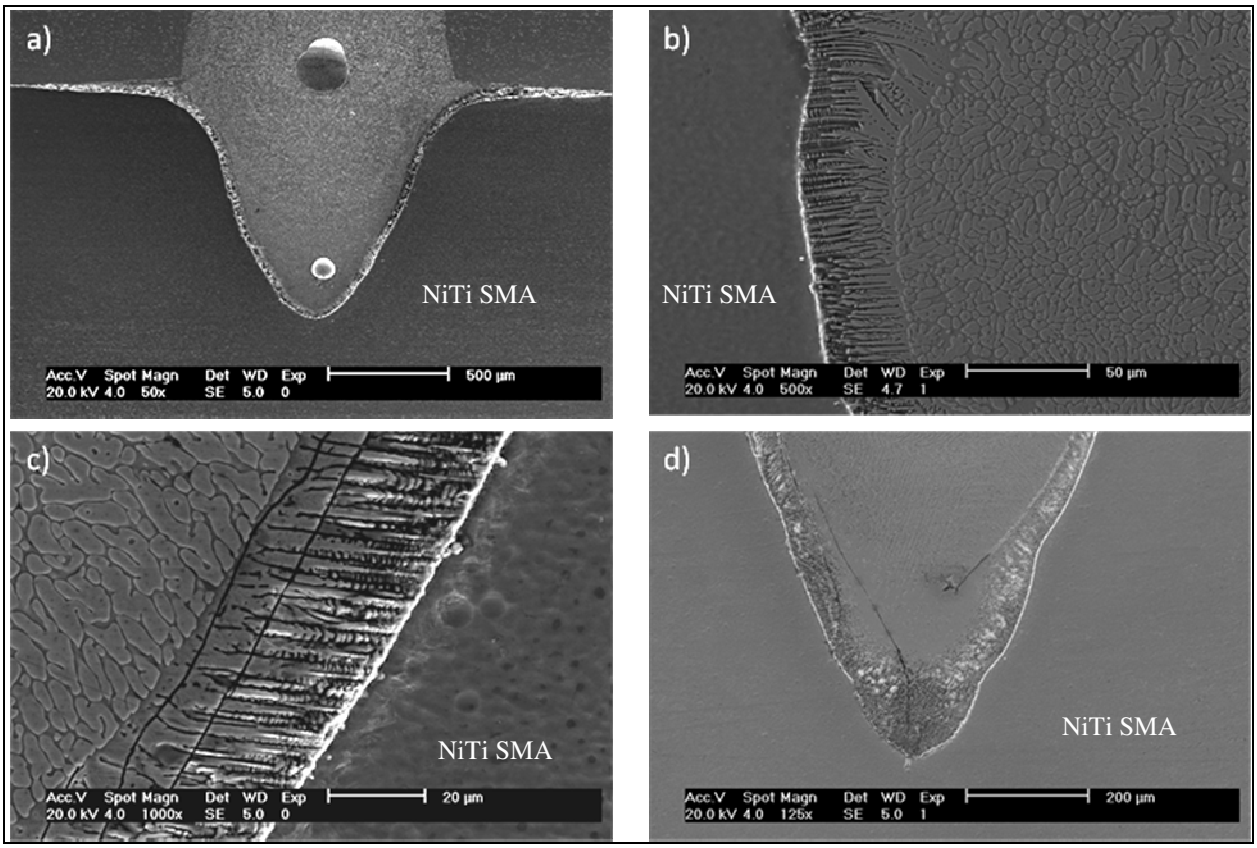

Figure 8-20, micrographs showing: a) columnar dendrites formed at weld interface (EBLS-S3); b) high magnification micrographs of the dendrites (EBLS-S3); c) cracking initiated at weld interface and (EBLS-S3); d) severe cracking in high penetrated weld (EBLS-S5)

Macrographs of electron beam lap welds produced with the Ti-6Al-4V plate on top are shown in **Figure 8-18**. These welds were considerably narrower than those with TiNi SMA on top, due to Ti-6Al-4V's higher melting temperature. Porosity remained problematic in both configurations but such problems could be eliminated by further optimisation of the process.

The electron beam welds produced had very different microstructures to other electron beam welds. There were two distinct microstructures present in the welds. Towards the top

portion of the weld, the microstructure was characterised by a titanium-rich dendritic structure as shown in **Figure 8-20a, b**. Compositional analyses identified this titanium-rich phase as a meta-stable β-Ti phase as a result of the high undercooling. The inter-dendritic phase has a eutectic structure and was identified as the $NiTi_2$ phase. The volume fraction of this phase decreases with increases in weld depth and hence Ni content of the weld. Close to the interface where the two parent metals meet, the microstructure of the weld changed to one that was dominated by very fine $NiTi_2$ dendrites [**Figure 8-21d**]. This change was sharp rather than gradual, and the increase in Ni content towards the bottom of the weld suggested that the inter-dendritic phase corresponded to $NiTi_2$+NiTi eutectic on the binary phase diagram [**Figure 4-5**].

Surprisingly, no cracks were observed on welds produced with the Ti-6Al-4V plate on top except for the fully penetrated weld, where cracks were initiated at the base metal interface and propagated across the weld [**Figure 8-22d**]. It is proposed that there may be a critical weld composition where the global weld microstructure becomes so brittle that hot cracking starts to initiate. According to the results from weld depth analyse [**Table 8-6**], this critical weld composition appears to be around 25 at% Ni.

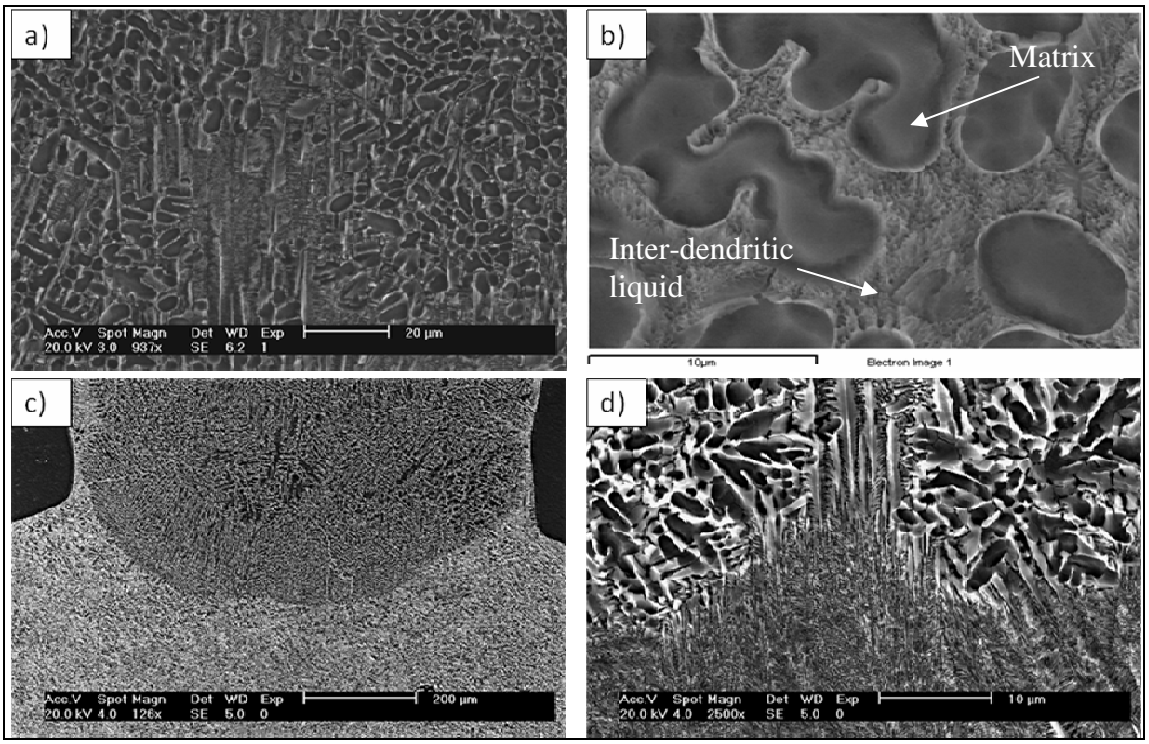

Figure 8-21, SEM micrographs of electron beam lap welds

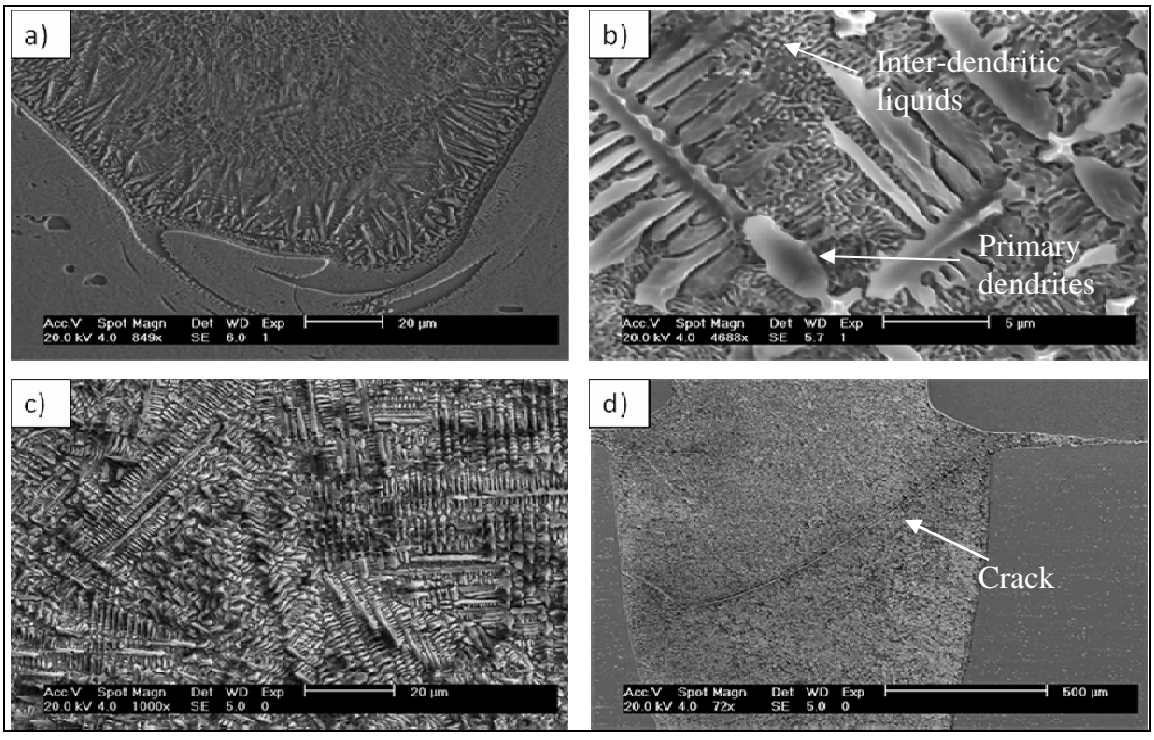

Figure 8-22, SEM micrographs of electron beam lap welds

Partially mixed and unmixed areas were clearly visible on high speed welds in both configurations [**Figure 8-23**]. The combination of high heating and cooling rate and short interaction time limited the level of mixing which occurred during welding. The widths of these high speed welds were also considerably wider due to the higher beam current used to achieve the same weld depth. No cracks were observed at the weld zone. Pockets of the partially mixed and unmixed zones must have consumed most of the Ni at the weld and thereby prevented the $NiTi_2$ phase from forming, and thus strengthened the weld. However, the uncontrollable nature of the unmixed and partially mixed zone meant that the properties of the weld were also uncontrollable and inconsistent. It is beyond the nature of this research to discuss the effect of welding speed on the weld performance in great detail. However, from a weld performance point of view, the presence of unmixed and partially mixed zone renders these high speed welds useless in engineering applications.

The weld microstructure of the welds with tantalum foil sandwiched between the parent metals were identical to that of the autogenous lap welds in both orientation except that cracking was more severe in the EBLS Ta weld [**Figure 8-17 and 8-18**]. Compositional analysis revealed that tantalum was fully saturated in the weld zone. Less than 1 at% of tantalum was detected throughout the entire weld zone. The level of tantalum was very constant throughout the weld zone indicated that tantalum mixed completely in the weld. Contrary to the work conducted by EWI, the effect of tantalum was still detrimental to the EBLS welds, even at such a low Ta level. However, the effect of tantalum in the EBLT weld was less prominent. The level of tantalum in the weld was too low to have any real effect on the joint performance.

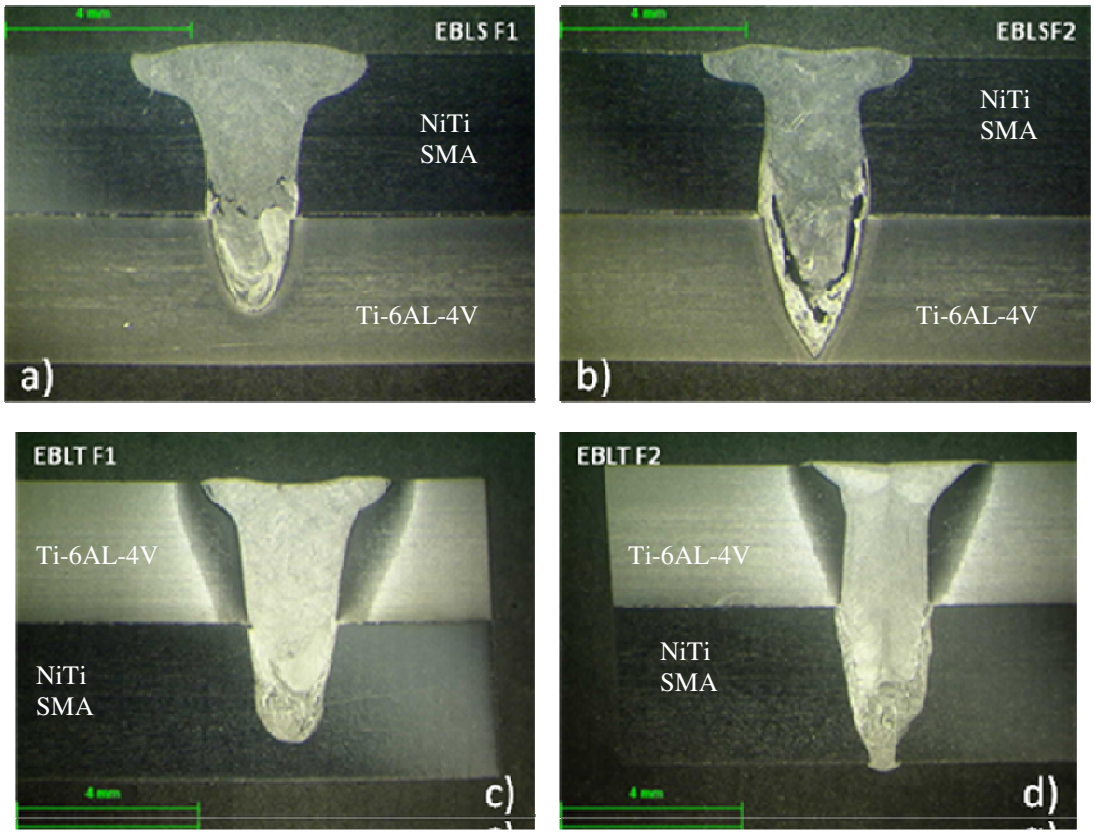

Figure 8-23, Macrographs of high speed electron beam lap welds varying in welding speed

From the above observations, one could conclude that unless the formation of the $NiTi_2$ phase can be completely prevented, poor weld performance in an autogeneous fusion weld is inevitable due to the inherent brittleness of the $NiTi_2$. Where NiTi SMA is the predominant component in the weld, the weld microstructure consists of cellular NiTi phase in a $NiTi_2$ matrix. This microstructure causes hot cracking irrespective of weld composition. However, where Ti-6Al-4V is the dominant component of the weld microstructure, several forms of $NiTi_2$ dendrites were formed. Such microstructures appeared resistant to hot cracking, provided that the local Ni composition does not exceed 25 at %.

8.3 Laser Welding

Microstructural observation in electron beam lap welds revealed that crack-free lap welds can be produced between Ti-6Al-4V and NiTi SMA provided that the global weld composition does not exceed 25 at% Ni. Unfortunately, the electron beam welder was unavailable to produce samples for mechanical investigation. Laser welding was subsequently made available and was used to replicate the lap weld specimens for mechanical investigation.

The facilities used for this work were situated at Cranfield University. The laser welder used is a high power continuous-wave (CW) ytterbium fibre laser manufactured by IPG Photonics. This high power Class IV laser was rated 8kW and mounted on a fully anthropomorphic robot capable of transportation and orientation in up to six axes [**Figure 8-24**].

Long strips of NiTi SMA and Ti-6Al-4V measuring 700 mm long were used for this welding trial. The process preparation and configuration were the same as those used for electron beam welding trials. Only welding with Ti-6Al-4V on top has been investigated as the electron beam welding trials showed that cracking was inevitable in welds with NiTi SMA plate on top irrespective of welding depths. The welding parameter used for welding Ti-6Al-4V sheets of the same thickness was chosen as the initial welding parameter for this study and the weld depths were varied by varying the welding speed. The setting used to determine weld depth was listed in Table **8-7 and 8-8**.

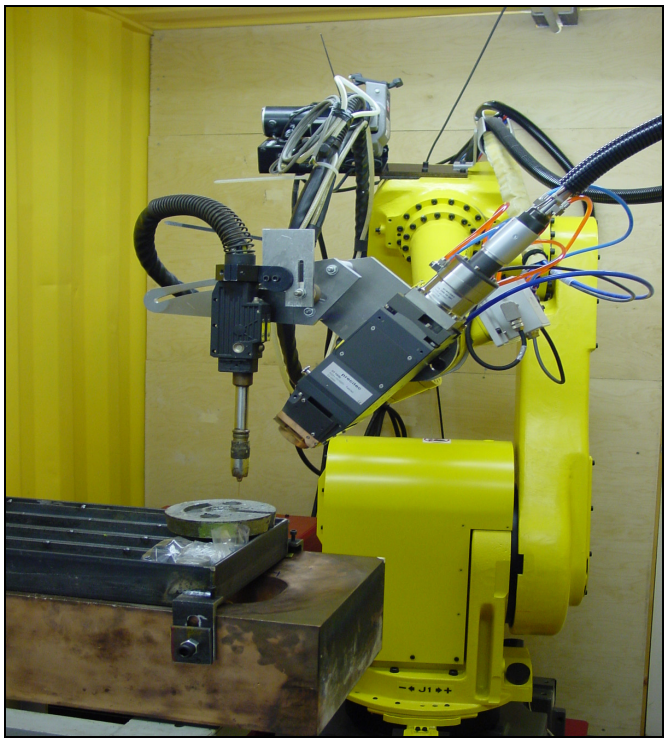

Figure 8-24, CW ytterbium fibre laser welder

Beam Power	4kW
Work Height	236.7mm (in focus)
Argon Shielding	46 litre per minute
Spot size	0.5 mm (diameter)

Table 8-7, Laser welding programme

Sample Number	Welding Speed ($mmin^{-1}$)
LT-W1	7.0
LT-W2	5.75
LT-W3	4.5
LT-W4	3.25
LT-W5	2.0
LT-W6	1.5
LT-W7	1.0

Table 8-8, Weld depth investigation

8.3.1 Joint Characterisation

Optical micrographs in **Figure 8-25** showed that the weld depth increases with reducing welding speed. Porosity that as observed in electron beam lap welds also occurred here. Mixing was clearly a problem, especially in the shallower welds resulting in macro-segregation. As observed in high speed electron beam lap welds, the relatively high welding speed prevented complete mixing of weld metal to take place before solidification. **Figure 8-26** clearly showed macro-segregation towards the top of the weld. Compositional analysis revealed that the two phases corresponding to the top and bottom microstructure were β-Ti and $NiTi_2$ respectively. Welding speed was subsequently reduced to increase weld depth. This also reduced the cooling rate thus allowing more time for the weld metal to mix, hence the macro-segregation reduced with welding speed. Compositional analysis has been conducted to determine the nickel content in each weld.

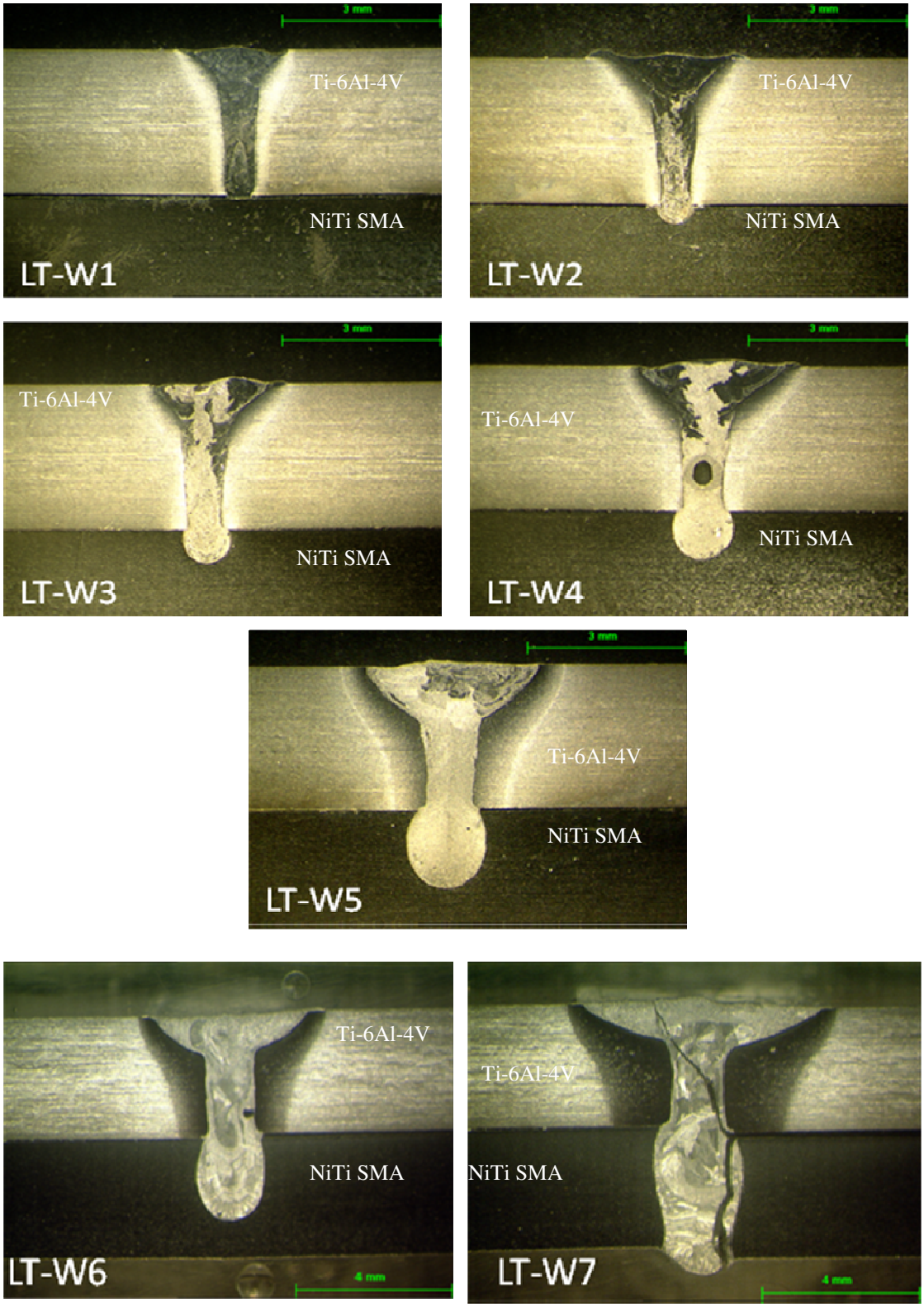

Figure 8-25, Laser lap weld for weld depth investigation

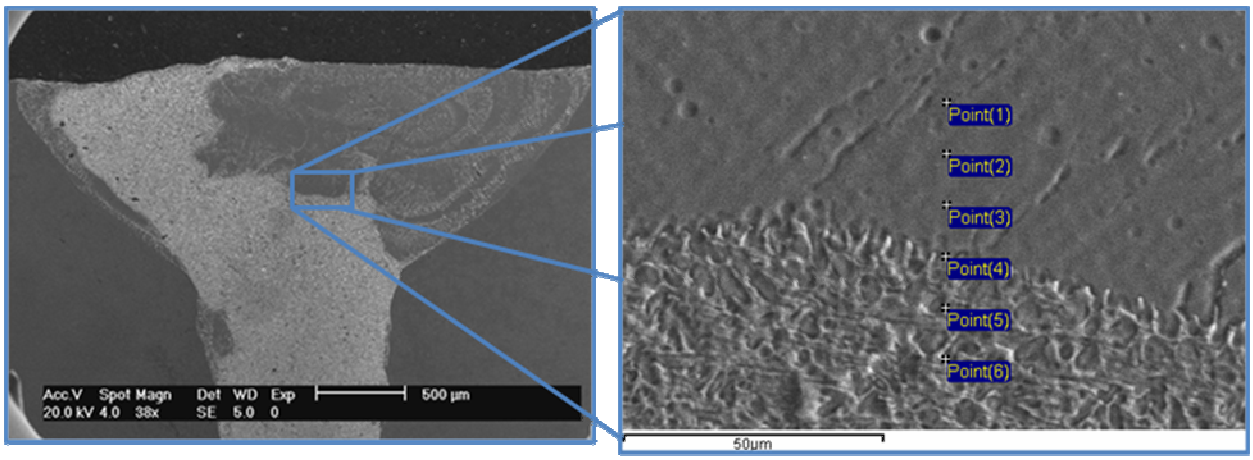

Spectrum	Elemental Composition (at %)			
	Al	Ti	V	Ni
Point(1)	4.87	80.75	3.34	11.04
Point(2)	4.91	80.61	3.31	11.17
Point(3)	5.08	80.85	3.50	10.56
Point(4)	5.48	79.20	3.25	12.07
Point(5)	1.97	65.16	1.73	31.14
Point(6)	4.61	72.61	2.37	20.41

Figure 8-26, microstructure of LT-W5 (Left); macro-segregation of weld metal (right) with EDX compositional analysis results (bottom right)

Table 8-9 clearly showed that the nickel content in weld LT-W5, W6 and W7 exceeded the critical nickel content required for cracking to initiate. Fine cracks have been observed in LT-W5 [**Figure 8-27**] and large cracks have propagated though the centreline of the entire weld in W7 [**Figure 8-25**]. This is in agreement with the results observed in electron beam lap welds. For some unknown reasons, no cracks can be observed in sample LT-W6 even though the Ni content at the weld exceeds that of the critical limit for cracks to occur. This could well be a result of the inhomogeneous nature of the weld.

Shear testing have been conducted to investigate the mechanical properties of the welds. Only LT-W5 specimens were tested, the combination of weld depth and crack-free weld structure should provide the maximum joint strength achievable by fusion joining methods.

Sample no.	Weld Depth (mm)	Average Nickel Content (at%)
LT-W1	3.17	0
LT-W2	3.52	11.20
LT-W3	3.80	16.94
LT-W4	4.25	20.18
LT-W5	4.77	26.23
LT-W6	5.25	28.82
LT-W7	7.11	n/a

Table 8-9, Average nickel content in laser lap welds

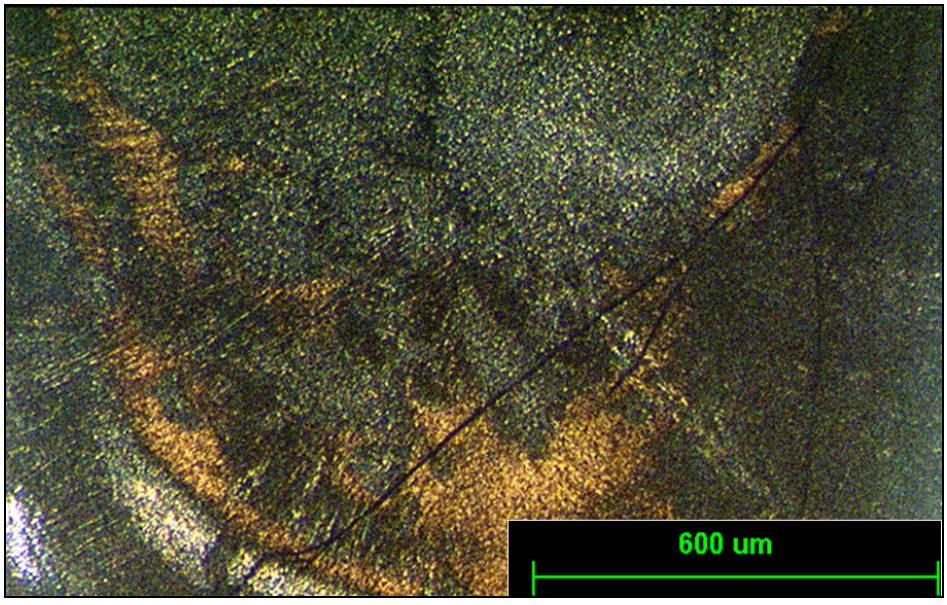

Figure 8-27, cracking at the bottom of laser lap weld (LT-W5)

A peak shear strength of 28.4 MPa has been achieved [**Figure 8-28**]. Note that the loading condition during the ASN would experience during operation are far more complex than those used in the mechanical testing in this project. Thus the results of these tests can only be used for comparison between similar tests, and should not be used as indicators of actual joint performance during operation. Furthermore, as shown in **Figure 8-28** the mechanical properties of the lap welds were not consistent. This is most likely due to the inhomogeneous weld microstructure. Thus it is unlikely that any autogeneous fusion welds could meet the joint specification for the ASN.

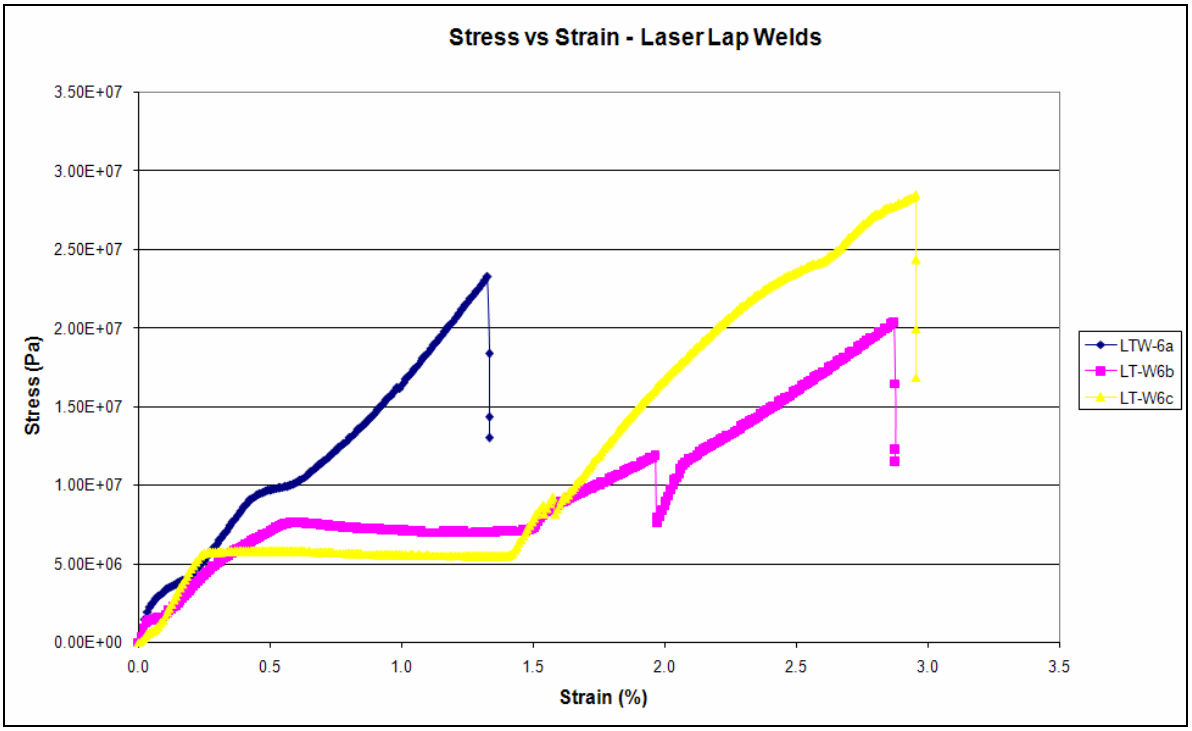

Figure 8-28, Stress-Strain graph of optimised laser lap welds

8.4 Friction Stir Welding

The formation of brittle NiTi2 intermetallic at joint interfaces was identified as the major contributor to the poor joint performance of fusion welds. Preliminary studies in previous chapters show that the formation of this brittle phase is inevitable in fusion welding. Solid-state joining methods were therefore explored to investigate whether the formation of $NiTi_2$ can be eliminated by joining the parent metals in their solid-state. Friction stir welding (FSW) was the first of the solid-state joining methods explored. The facilities used in FSW were situated at TWI's regional facility in South Yorkshire. The friction stir welder is a CNC, high precision welder manufactured by Transformation Technologies Inc. with a concentric spindle specifically designed for welding high temperature materials **[Figure 8-29]**.

Figure 8-29, Friction stir welder

Friction Stir Spot Weld (FSSW) was selected for an initial feasibility study as it generates less deformation to the parent metal compared to that of friction stir seam welding. The selection of tool materials for this project was based on TWI's recommendations. Silicon Nitride (Si_3N_4) was originally chosen due to its availability and low cost. The silicon nitride toolpiece used is manufactured from a gas pressure sintered bar with 15mm diameter shoulder and a 3.75mm pin. The toolpiece has features specifically designed to aid the mixing of the softened metals during the process [**Figure 8-30**]. The Si_3N_4 tool suffered from a high tool wear rate during the first set of tests and was subsequently replaced with a tungsten rhenium (W-Re) toolpiece. The W-Re tool piece is powder sintered with approximately 25 wt% tungsten and the toolpiece design was identical to that of the Si_3N_4 tool (see the drawing for the tool in **Appendix D**). The W-Re tool is featureless due to the difficulties in machining rhenium, but the high temperature properties of the rhenium help reduce tool wear rate and contamination of the work pieces.

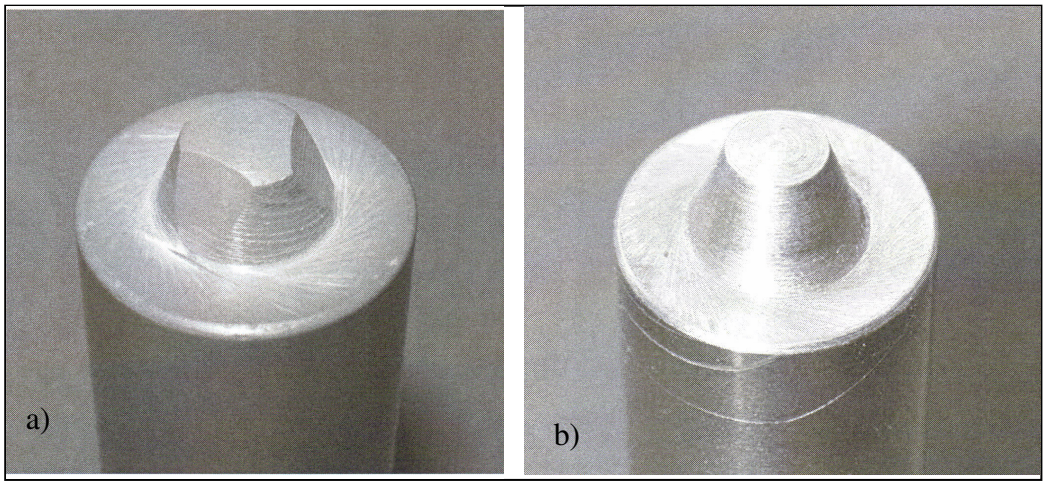

Figure 8-30, a) faceted Si_3N_4 tool [tool A1]; b) re-machined Si_3N_4 tool [tool A2]

The surfaces of NiTi and Ti-6Al-4V strips were cleaned using a wire brush to remove the surface oxide and then with isopropanol to remove any organic products prior to welding. Friction stir spot welds were produced on strips of NiTi and Ti-6Al-4V in a lap configuration.

During initial welding, large metal sheets were used so that consecutive spot welds could be produced on the same sheet to minimise set-up time. However, the welds failed pre-maturely when machining individual spot-welds into coupons. As a result, the fixture was modified to produce spots-welds individually on coupons measuring approximately 30 x 63 x 3 mm as shown in **Figure 8-31**. This eliminated the need for machining, but test set-up times were considerably prolonged.

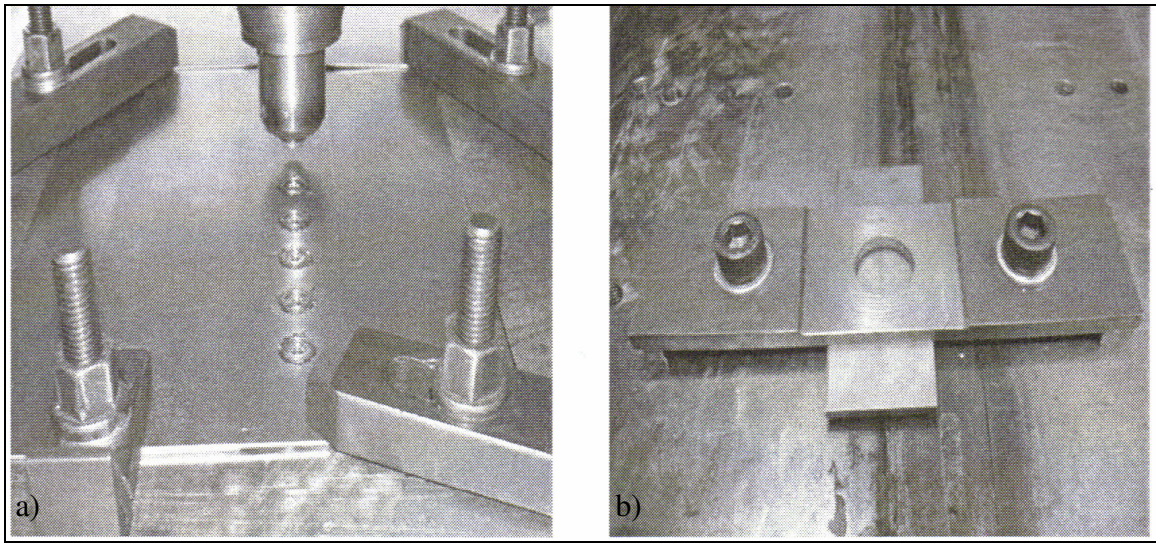

Figure 8-31, a) fixtures holding large metal sheets in place for multiple FSSWs; b) customised fixture for welding individual coupons

Following TWI's recommendations, friction stir spot welds (FSSW) were produced using the process parameters used to weld Ti-6Al-4V sheet to itself. The welds were then subjected to on-site restrained bend tests. The on-site restrained bend test forces the two parent metal sheets apart by fixing the titanium plate in a clamp and manually pulling the SMA plate away from the weld until the workpieces separate. The forces required to break the welds were compared. This testing method is by no means scientific, nor does it provide any quantitative results, but it serves well as an on-site indicator of joint performance, which is crucial to determine the optimum process parameters. A schematic of the test set-up is shown in **Figure 8-32**. The process parameters were adjusted according to the result of each restrained bend test and the process was repeated until maximum joint strength was reached. In all 15 tests parameters and configurations were evaluated before the optimum parameters were reached. The details of the tests are listed in **Table 8-10**. Welds produced using the optimum process parameters were then examined through a series of metallurgical, micro-hardness and mechanical analyses.

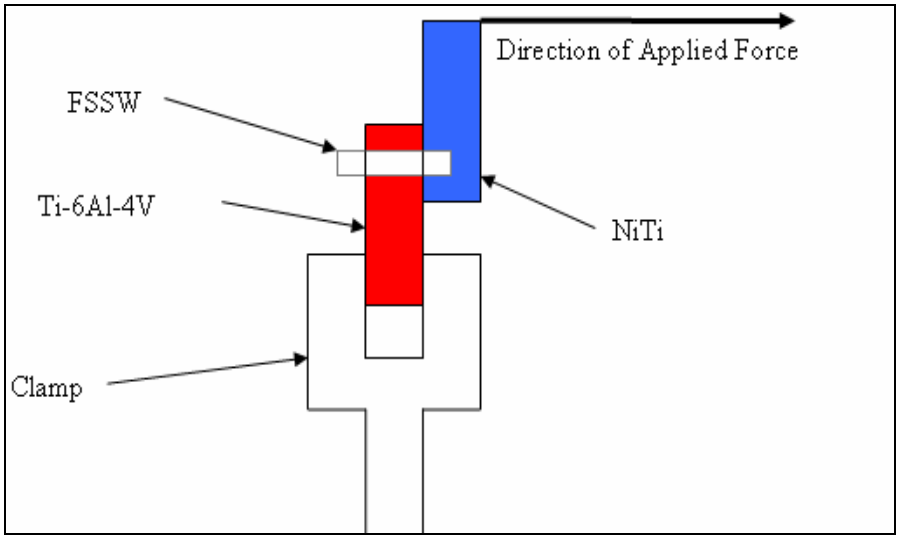

Figure 8-32, Schematic of on-site shear testing

Trial Number	Tool Material	Tool No.	Configuration (Top Sheet)	Rotation Speed (RPM)	Z-axis Plunge Rate (mm/min)	Dewll Time (s)	Plunge Depth Below Upper Surface (mm)	Fail at
W1	Si_3N_4	A001	NiTi	1500	12.5	0	-0.05	Sectioning
W2	Si_3N_4	A001	NiTi	1500	25	0	-0.05	Sectioning
W3	Si_3N_4	A002	NiTi	1500	12.5	0	-0.05	Sectioning
W4	W-Re	A003	NiTi	1500	15	0	-0.05	Did not fail
W5	W-Re	A003	NiTi	1500	30	0	-0.05	Did not fail
W6	W-Re	A003	NiTi	1500	50	0	-0.05	Sectioning
W7	W-Re	A003	NiTi	1500	50	0	+0.4	Sectioning
W8	W-Re	A003	NiTi	2000	50	0	-0.05	Sectioning
W9	W-Re	A003	NiTi	1000	50	0	-0.05	Sectioning
W10*	W-Re	A004	T1-6Al-4V	500	15	0	-0.05	N/A
W11*	W-Re	A004	T1-6Al-4V	750	15	0	-0.05	N/A
W12*	W-Re	A004	T1-6Al-4V	1000	15	0	-0.05	N/A
W13*	W-Re	A004	T1-6Al-4V	1000	15	3	-0.05	N/A
W14	W-Re	A004	T1-6Al-4V	1000	15	1	-0.05	Did not fail
W15	W-Re	A004	NiTi SMA	1000	15	1	-0.05	Did not fail

*Constrained bend test results for sample W10-W13 indicated that their joint performances were too poor for further testing to be worthwhile.

Table 8-10, FSSW Test Programme

8.4.1 Tool Wear

Tool wear was a major problem throughout this work. Toolpieces made from Si_3N_4 were originally selected following TWI's recommendation due to their cost advantage and accessibility. However, these toolpiece suffered from extensive wear during the first day of testing to such an extent that they required re-machining before they could be used in subsequent tests. Due to time constraints, the features that were originally designed to enhance mixing were not re-machined on to the Si_3N_4 tool, a picture of the re-machined Si_3N_4 is shown on **Figure 8-33**. During the second day of testing, the Si_3N_4 tool suffered from an even higher wear rate due to the more demanding process requirements. Tool wear was so severe that they had to be replaced by a W-Re tool piece. The W-Re tool used was a feature-less tool piece that was specially designed to weld high temperature materials, the high temperature properties of Re ensuring that tool wear and workpiece contamination were kept at minimal during welding. The wear rate of the W-Re tool was considerably lower than that of the Si_3N_4 tool. However, in contrast to results reported by London et al. [**146**], the wear rate was still unacceptable from a mass production point of view. **Figure 8-35** shows the W-Re tool after weld 10 and weld 15. The shoulder of the tool piece was almost completely worn out and virtually unusable after some 16 spot welds. A thin metal layer had been deposited on the surface of both tool pieces after each process [**Figure 8-34**]. The composition of this metal layer was analysed by EDX and confirmed to be titanium oxides.

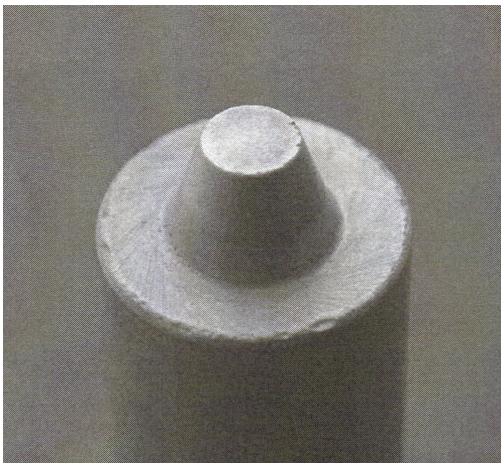

Figure 8-33, Silicon nitride toolpiece re-machined for further testing.

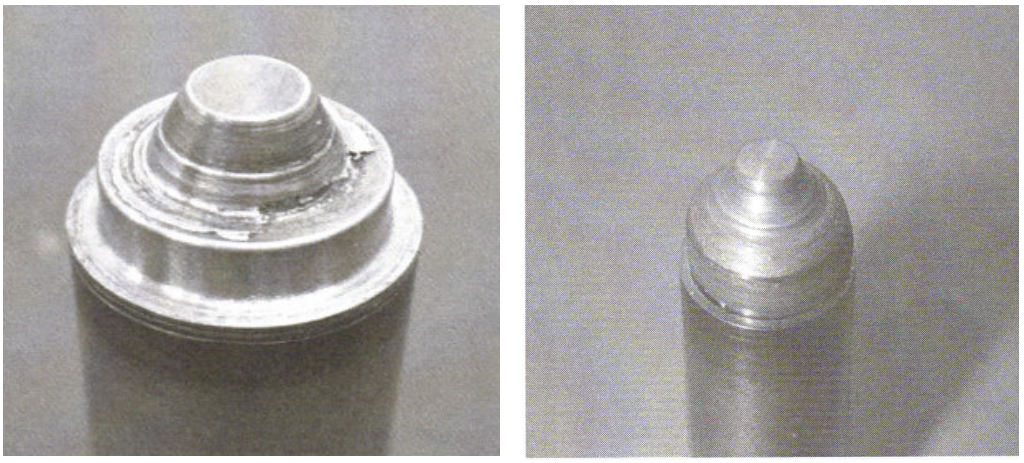

Figure 8-34, Re-W tool piece after weld 10 (left) and after weld 15 (right)

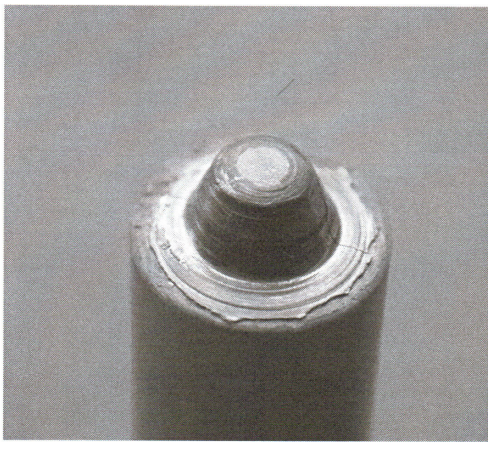

Figure 8-35, Thin layer of metal deposited onto the surface of Re-W tool

8.4.2 Joint Characterisation

The FSSW specimens for metallurgical analysis were prepared following the procedures for preparing weldments for metallographic examination. However, a number of sample failures during sectioning meant microstructural examination could only be performed on the samples that remained intact after the preparation process. The microstructure of the spot welds were analysed using a combination of optical and scanning electron microscopy (SEM). The SEM used was a Philips XL-30 SEM with integrated energy dispersive x-ray (EDX) analysis capability. Elemental analyses were carried using EDX within the SEM. The mechanical properties of FSS welds were analysed by a simple shear test using an Instron tensile tester (Instron 5500R). The welded samples were simply pulled apart at a rate of 0.1 mm per minute until failure.

Optical images of the FSSW specimens are shown in **Figure 8-36**. Large gap were clearly visible between the workpieces, which indicated the absence of any metallurgical bonding at the joint interface. With no metallurgical bond forming at the interface, the metal sheets were held together solely by the mechanical interlocking provided by the deformed metal around the spot weld, resulting in the low joint performance. This is in agreement with the results from the constrained bend tests.

As expected from a solid-state joining process, the level of oxidation on the surface of the weld was low even with the absence of gas shielding. The friction stir spot welds produced were circular in appearance with an average spot size of 7 mm in diameter. The different process parameters used did not have much effect on the size of the welds. For weld W10-W14 where Ti-6Al-4V sheets were placed on top, substantial flashes were produced as a

result of the Ti-6Al-4V super-plastically deforming during welding. The amount of flash produced increased with the rotational speed of the tool piece [**Figure 8-37**]. Typically, Ti-6Al-4V deforms superplastically at temperatures above 925ºC, unless substantial refinement treatments have been carried out which lower the superplastic temperature to approximately 800ºC [**172**]. This is a good indication of the temperature at the weld during welding.

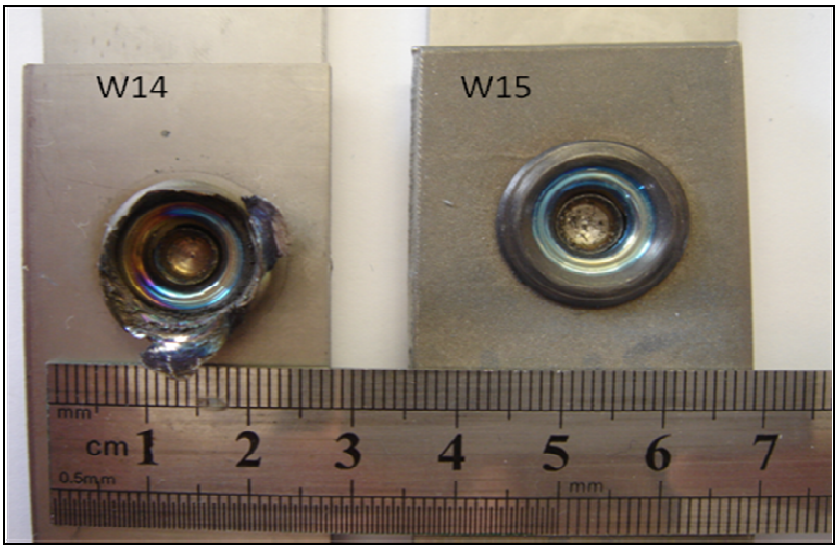

Figure 8-36, Photograph of W10 (left) and W12 (right)

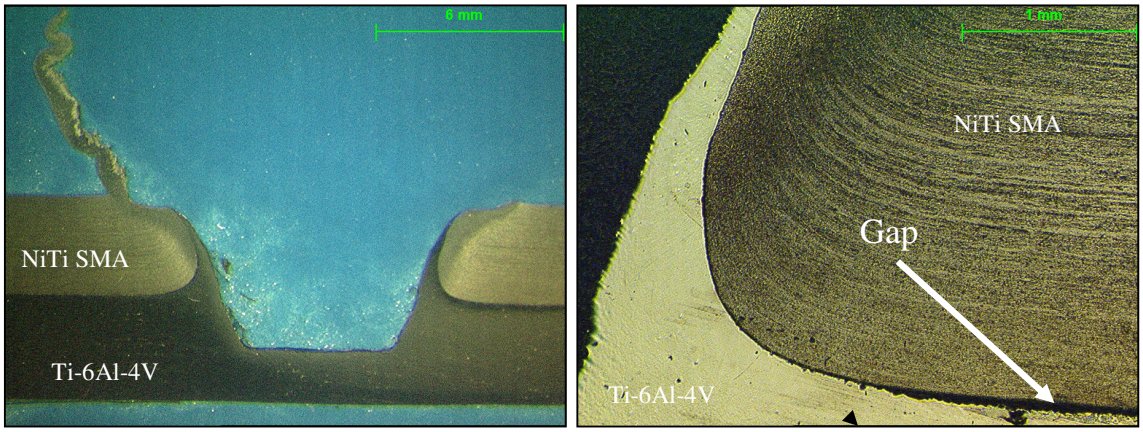

Figure 8-37, optical micrographs of friction stir spot welds (FSSW W14)

At the crown of the weld, there were regions where metallurgical reactions occurred between the workpieces [**Figure 8-38**]. EDX analysis revealed that there was some diffusion between the workpiece in these regions. However, the amount of diffusion was so small that it would not have had any apparent effects on joint performance.

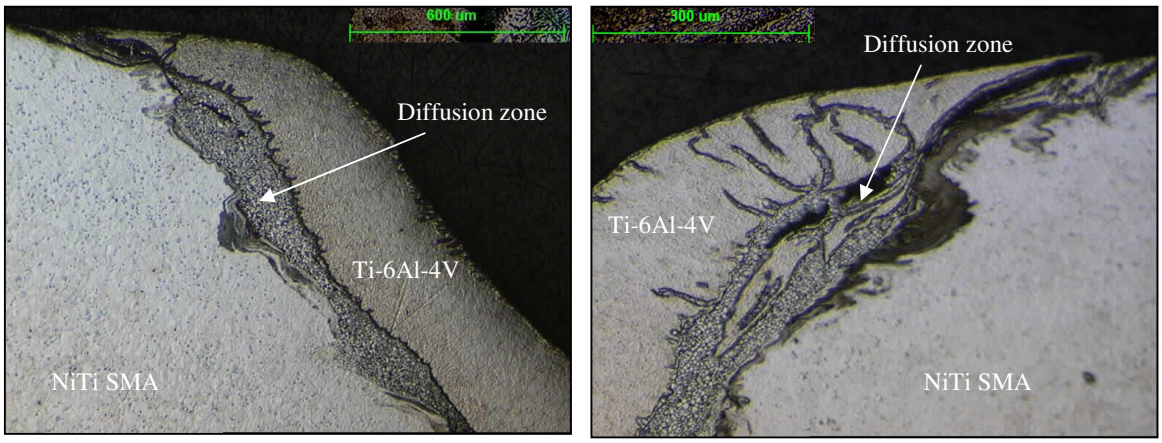

Figure 8-38, SEM micrographs of friction spot weld (FSSW W14) showing diffusion at the crown area

8.4.3 Mechanical Testing

Constrained bend testing showed that the joint strength of these welds was substantially weaker than that of other titanium or NiTi welds. Close examination of the failed specimens revealed that no mixing of molten metals or metallurgical bonds had been formed between the workpieces, even when process parameters had been optimised. Instead the workpieces were held together by the mechanical interlocking formed as a result of the deformation of the softened metal during the process. This was very unusual given that over 7 tonnes of plunge-force was applied to the workpiece during welding. It was first thought that this was due to the low thermal conductivity of the NiTi SMA, which prevented the bottom Ti-6Al-4V plate being heated to the required temperature. However, tests conducted with Ti-6Al-4V

plate placed on top exhibited similar results indicating that such a phenomenon was independent of the difference in thermal conductivity between the parent metals.

Only samples from test W14 were subjected to shear testing using the same procedures as those used for shear testing of laser lap welds. Shear strengths of up to 6.2kN were achieved [**Figure 8-39**]. This is significantly higher than those reported by TWI [**173**]. Furthermore, complete failures were not observed at maximum load. Instead, the load reduced with further increases in extension, accompanied by a series of further cracking at irregular intervals until catastrophic failure. Close examination of the failed samples revealed typical brittle failure. Failure occurred at different sites around the circumference of the spot welds. Cracking was first initiated in the shear specimens at peak shear load. However, the specimens did not fail immediately. Instead, the specimens went through a series of subsequent 'stable' cracking events before final rupture occurred. Multiple cracking was as a result of the relatively low strain rate.

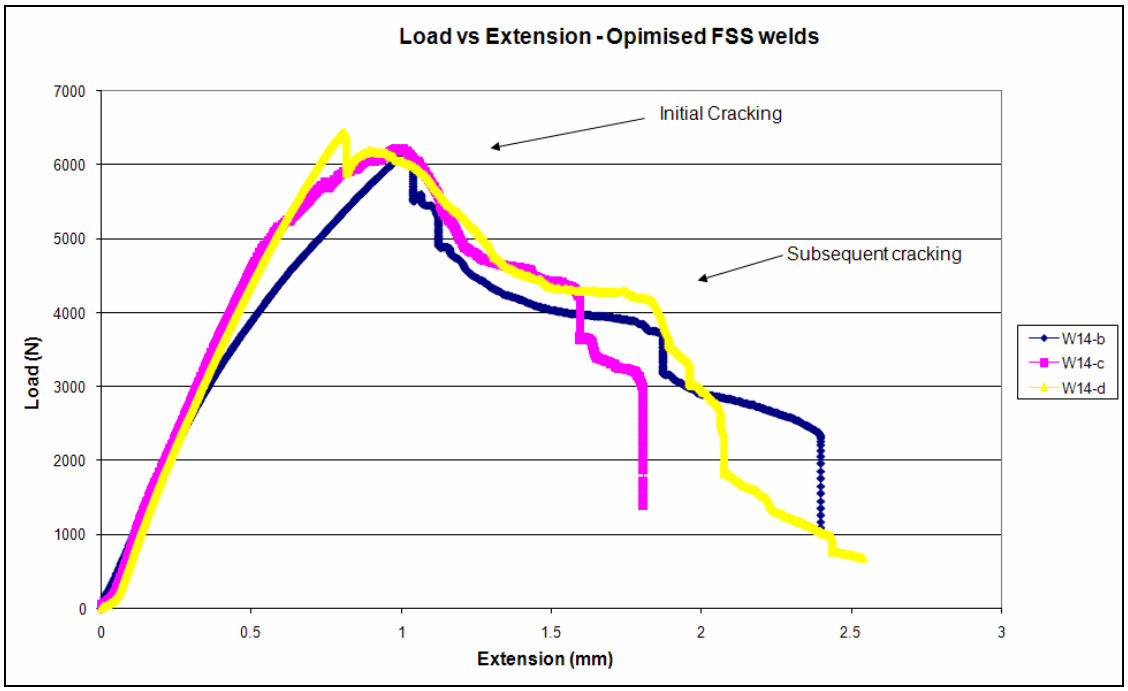

Figure 8-39, Mechanical testing of friction stir spot welds

This initial feasibility study revealed that the inability of the parent metals to amalgamate at temperature as high as 925ºC was unusual. To solve this problem, the thermodynamics occurring between the parent metals during welding must first be understood. However, it is not within the scope of this research to carry out such a study. From a business point of view, it would be more productive to explore other types of joining methods.

8.5 Brazing

As all autogeneous joining methods failed to produce joints that match the joint specification for the ASN, the focus was shifted towards the feasibility of joining the parent metals with the aid of an interlayer. As discussed previously, the feasibility of joining NiTi SMA to dissimilar metals using a range of interlayers has already been explored by a number of researchers [**149-151, 174**]. However, research has only been carried out on wires and thin foils where the joint composition can be altered using relatively small volumes of filler materials, even in fusion welds. For joining thick sections of SMA such as those used in this project, the manipulation of joint composition requires more consideration. Fusion welding of thick SMA sections in lap configuration melts relatively large volumes of parent metals. As a result the molten parent metals consume most of the interlayer and prevent bonding at the joint interfaces. This has been observed in electron beam welding trials in **Chapter 8.2** where the tantalum interlayer diffused away from the joint interface into the parent metals and failed to improve the performance of the electron beam weld. Solid-state joining was considered to avoid the interlayer diffusing into the parent metals during the process. Vacuum brazing was selected for this study. For the production of ASN, vacuum brazing would not be appropriate as this joining process heat the entire assembly to the brazing temperature in a vacuum furnace. This will not only destroy the SME in the NiTi SMA, it will also stress relax the pre-stresses introduced in the Ti-6Al-4V parent component thereby rendering the actuator useless. Alternative localised heating methods such as microwave, induction or laser heating should therefore be employed for the production of ASN in order to retain the adaptive function in the nozzle. However, vacuum brazing is the optimum joining method for an initial feasibility study as the microstructural development at the joint interface

is the same irrespective of the joining methods but vacuum brazing is simpler, less expensive and widely available.

Three braze alloys were selected for this feasibility study, two TiCuNi alloys, which are laminates consisting of a NiCu alloy sandwiched between two pure titanium foils in the corresponding compositions. TiCuNi is commercially used in the brazing of Ti-6Al-4V alloy in many engineering applications and has recently been tested for joining NiTi SMA to itself [**149**]; and a TiNi 67 alloy which is a developmental braze alloy intended to be used to join conventional titanium alloys. Samples of each alloy were manufactured by Westco Metals and supplied by Vacuum Brazing Group (VBC). The specification of the alloys is listed in **Table 8-12**.

Interlayer	**Composition (wt %)**		**Solidus Temperature (ºC)**	**Liquidus Temperature (ºC)**
	wt %	at %		
TiCuNi 60	Ti 60; Ni 15; Cu 25	Ti 53.78; Ni 16.48; Cu 29.73	890	940
TiCuNi 70	Ti 70; Ni 15; Cu 15	Ti 64.66; Ni 16.96; Cu 18.38;	910	950
TiNi 67	Ti 67; Ni 33	Ti 62.36; Ni 37.64	942	980

Table 8-11, Interlayer for vacuum brazing

Vacuum brazing experiments were initially carried out at Birmingham University. The vacuum furnace used was built in-house and consisted of a glass tube connected to a single

stage vacuum pump and a conventional tubular furnace. Ti-6Al-4V and NiTi strips were sectioned into 60 x 30 x 3 mm coupons. The surfaces of NiTi and Ti-6Al-4V coupons were cleaned using a wire brush to remove the surface oxide and then with isopropanol to remove any organic products prior to welding. The metallic interlayer was cleaned with isopropanol and sandwiched between NiTi and Ti-6Al-4V coupons. The assembly was then placed on an alumina boat and inserted into the glass tube. The glass tube was sealed and inserted into the tubular furnace with the sample positioned in the hot zone of the furnace. The vacuum pump was turned on 2 hours prior to testing to ensure a vacuum was produced within the glass tube before the furnace heated the samples up to the target temperature at a rate of approximately 10ºC per minute. An intermediate dwelling stage was introduced where the specimens were initially heated and held at 450ºC for 10 minutes to ensure the entire assembly had reached thermodynamic equilibrium before heating up to the liquidus temperature of the interlayer and held for a further 10 minutes and subsequently cooled in the furnace. Details of the brazing program are listed in **Table 8-13**.

Sample	**Interlayer**	**Dwell Time and Temperature**	**Brazing Time and Temperature**
W1	TiNi 67	450ºC for 600s	980ºC for 600s
W2	TiCuNi 60	450ºC for 600s	960ºC for 600s
W3	TiCuNi70	450ºC for 600s	960ºC for 600s

Table 8-12, Vacuum brazing program carried out at Birmingham University

Initial visual examination indicated that brazed joints had been successfully produced with both TiCuNi systems, with no obvious cracking. TiNi67 alloy on the other hand, failed to melt and form a bond with the parent metals. SEM examination has confirmed the presence

of metallurgical bonds in both specimens [**Figure 8-40]**. Both TiCuNi 60 and TiCuNi 70 interlayer produced braze joints with average thicknesses of 259.2 and 226.3 µm respectively. Both joints interfaces were slightly wavy in nature and the joints profile produced with TiCuNi 70 were slightly wavier than with TiCuNi 60. This could be due to the interlayer crinkled under heating before melting and metallurgical bonds can be formed. The wavy interface did not appear to have any adverse effects on the joint properties and could be eliminated by increasing the heating rate. However, the vacuum furnace used in this work was not capable of rapid heating thus this was not investigated in this project.

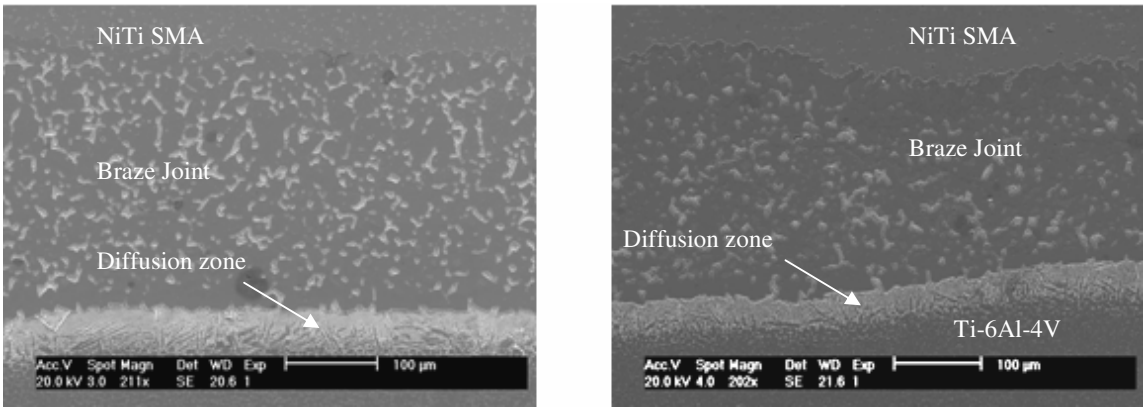

Figure 8-40, SEM micrograph of NiTi brazed joint: a) with TiCuNi 60 (BW2); b) with TiCuNi 70 (BW3)

Compositional profiles for both braze joints were virtually identical, except that the presence of slightly higher titanium content in TiCuNi 70 alloy produced a slightly more gradual change in titanium content at the interface [**Figure 8-41, 8-42**]. This is not unexpected, given that the only difference between the two alloys was the 10 wt% copper content.

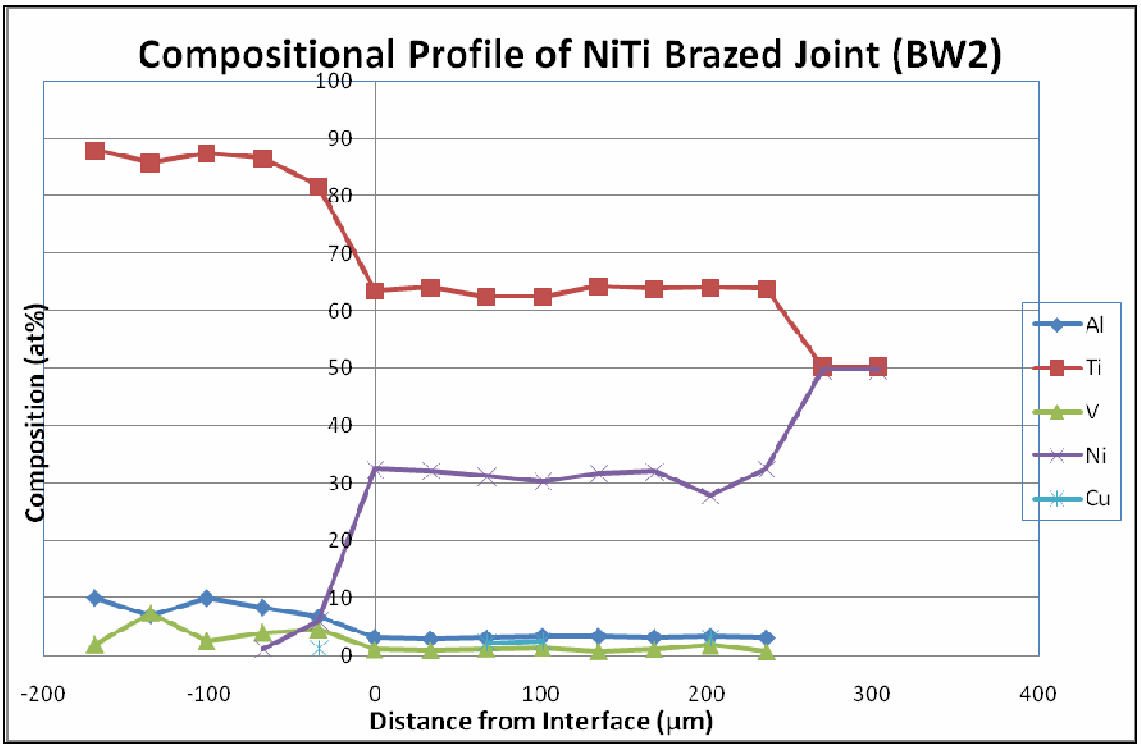

Figure 8-41, compositional profile of NiTi brazed joint (BW2)

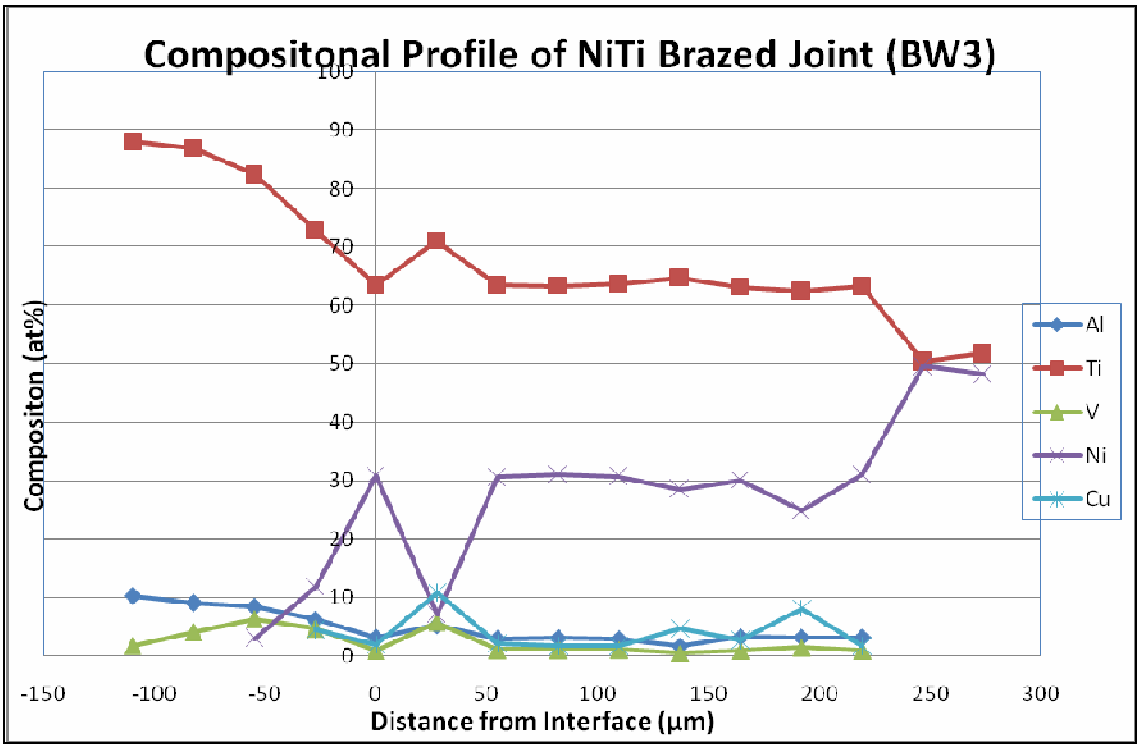

Figure 8-42, compositional profile of NiTi brazed joint (BW2)

The microstructure of the brazed joints was very different to those reported by Shiue et al. [**149, 151**]. They were characterised by a two-phase structure consisting of a lighter and a darker phase. Compositional analysis identified these phases as titanium-rich $CuTi_2$ and the $NiTi_2$ intermetallics respectively using a ternary equilibrium phase diagram [**Figure 8-43]**. The volume of $CuTi_2$ present in the TiCuNi 60 braze joint was slightly higher than that in TiCuN 70 braze joint as a result of the higher copper content. Since both parent metals were in the solid state throughout the process, the amount of inter-diffusion was minimal, no diffusion effect being detected more than 50 µm away from the joint interface. At the interface between the brazed joint and Ti-6Al-4V, very fine $NiTi_2$ dendrites were formed. This is due to the diffusion of nickel into the Ti-6Al-4V matrix. On the NiTi SMA side, no changes to the microstructure were observed. Both of the intermetallics present at the braze joint have been reported in a previous study to be extremely brittle and severely deteriorate the joint performance [**149**]. Unfortunately, the vacuum furnace had been contaminated by another user during the project thus mechanical evaluation of these initial brazed joints was not possible. Attempts have been carried out in replicating the braze joints using another vacuum furnace available at Cranfield University. The vacuum furnace was similar to that at Birmingham University except that the single-stage vacuum pump was connected directly to a sealed tubular furnace where the samples were heated. The vacuum pressure within the furnace was in the order of 10^{-2} bar [**175**]. In all, 13 tests have been carried out using this low vacuum furnace with the process parameters shown in **Table 8-13.**

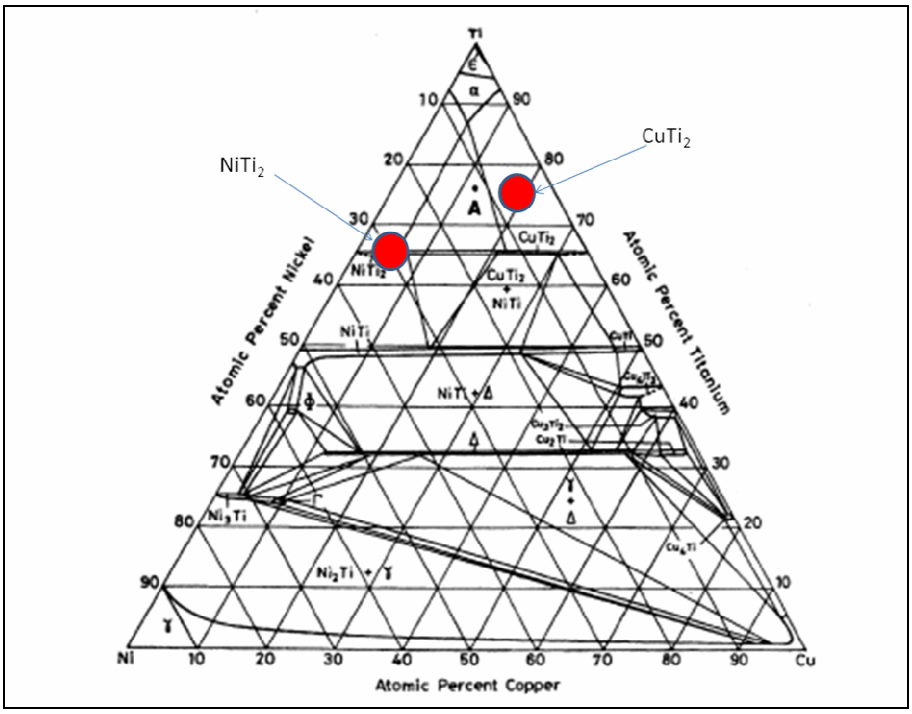

Figure 8-43, Cu-Ni-Ti ternary equilibrium phase diagram at 800ºC [176]

Sample	Interlayer	Dwell Time and Temperature	Brazing Time and Temperature
W4	TiNi 67	450ºC for 600s	980ºC for 600s
W5	TiCuNi 60	450ºC for 600s	940ºC for 600s
W6	TiCuNi 70	450ºC for 600s	940ºC for 600s
W7	TiCuNi 60	450ºC for 600s	940ºC for 600s
W8	TiCuNi 60	450ºC for 600s	960ºC for 600s
W9	TiCuNi 60	450ºC for 600s	980ºC for 600s
W10	TiCuNi 70	450ºC for 600s	980ºC for 600s
W11	TiCuNi 60	450ºC for 600s	960ºC for 600s
W12	TiCuNi 60	450ºC for 900s	940ºC for 600s
W13	TiCuNi 60	450ºC for 600s	900ºC for 600s
W14	TiCuNi 60	450ºC for 600s	880ºC for 600s
W15	TiCuNi 60	450ºC for 600s	1000ºC for 1200s
W16	TiCuNi 60	450ºC for 600s	1000ºC for 600s

Table 8-13, Vacuum brazing program carried out at Cranfield University

Melting of the interlayers has never been achieved using this low vacuum furnace. Tests varying brazing temperatures and time have proven that the problem was not related to the process settings. It was later discovered that the oxides formed on the surface of the interlayer during braze was to protect the bulk of the braze alloy from melting. To minimise the oxidation from occurring, the furnace was purged with argon prior to vacuum. However, the additional purging stage, the environment at the furnace was still inadequate to prevent oxidation from occurring. A high vacuum furnace was subsequently used for further testing. This high vacuum furnace is capable of producing a vacuum pressure of 10^{-5} bar and melting of the interlayer and metallurgical bonding has eventually been achieved. Brazing experiments carried out in the high vacuum brazing furnace followed the same procedures as those carried out in the other furnace brazing. Visual inspection of the initial brazed joint revealed that the brazed alloy has successfully melted with no apparent oxidation on the sample surface. However, the viscosity of the molten braze alloy was so low that it spilled over to the bottom of the parent metal and bonded with the alumina disc supporting the sample [**Figure 8-44**]. The brazing temperature was reduced by 10 ºC in subsequent brazing to prevent this from happening. In all, 8 tests have been carried out using the high vacuum furnace and the test parameters are listed in **Table 8-15**.

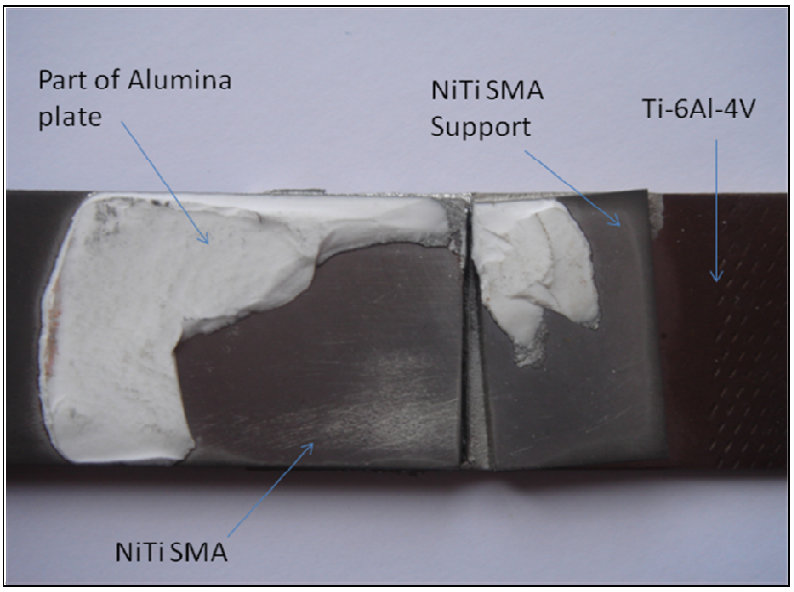

Figure 8-44, photograph of braze specimen showing braze alloy bonded to the alumina plate underneath the sample

Sample	Interlayer	Dwell Time and Temperature	Brazing Time and Temperature
W17	TiCuNi	450ºC for 600s	1000ºC for 60s
W18	TiCuNi	450ºC for 600s	960ºC for 60s
W19	TiCuNi	450ºC for 600s	960ºC for 1200s
W20	TiCuNi	450ºC for 600s	960ºC for 600s
W21	TiCuNi 60	450ºC for 900s	950ºC for 60s
W21	TiCuNi 60	450ºC for 600s	950ºC for 600s
W22	TiCuNi 60	450ºC for 600s	950ºC for 600s
W23	No interlayer	450ºC for 600s	950ºC for 600s

Table 8-14, High vacuum brazing program

The microstructure and the compositional profile of the brazed joints produced were almost identical to those produced previously [**Figure 8-45, 8-46**] except that the braze joints produced were almost twice as thick as those produced using the low vacuum furnace. This may be due to a combination of different heating and cooling rate and vacuum pressure.

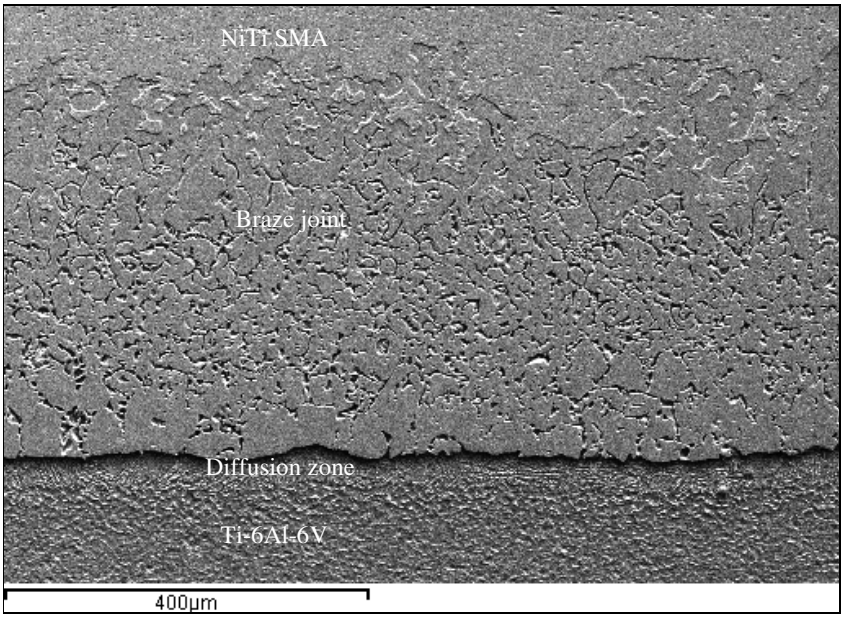

Figure 8-45, SEM micrographs of high vacuum brazed joints: a) with TiCuNi 60 (BW 21)

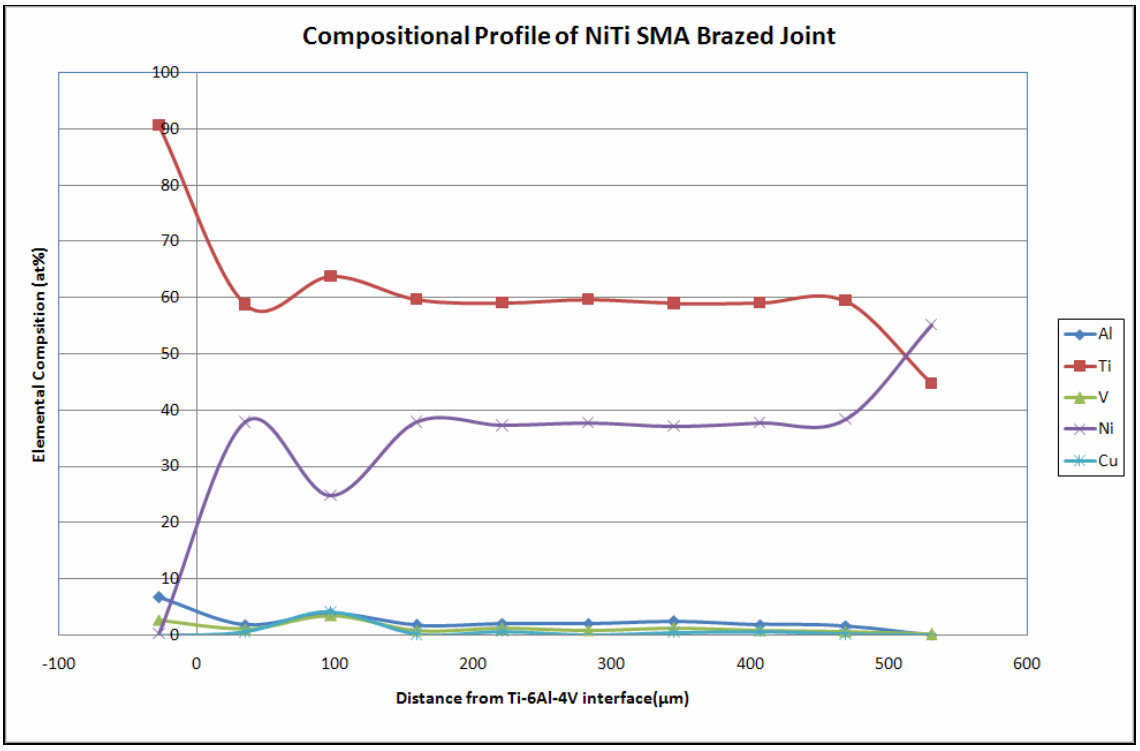

Figure 8-46, Compositional profile of NiTi braze joint

Since the current facility available was only adequate to produce braze lap joints, shear testing has been chosen to evaluate the mechanical performance of the brazed joints. The Instron tensile tester (Instron 5500R) was used for the shear testing where the brazed samples were simply pulled apart at a rate of 0.1 mm per minute until failure. **Figure 8-47** showed the stress-strain curve for the shear testing of the brazed joints. The samples exhibited a small amount of plateau stress, this plateau area was probably due to the martensitic deformation of the parent metal in the gauge. Hence the plateau strain is substantially lower than that in the base alloy since the proportion of NiTi SMA at the gauge length is relatively small. The brazed samples then undergo true plastic deformation which led to failure. Ultimate shear strength of just over 30MPa has been recorded with elongation to rupture of nearly 6%. The loading condition is different in the ASN than the tests here thus the suitability of applying the brazed joints to the ASN cannot be directly determined by the shear strength of the joint alone. However, this is an improvement over the autogeneous laser lap welds. The braze joints can be further improved by further optimisation of the process parameters and the application of a forge pressure that was not available at the time of testing.

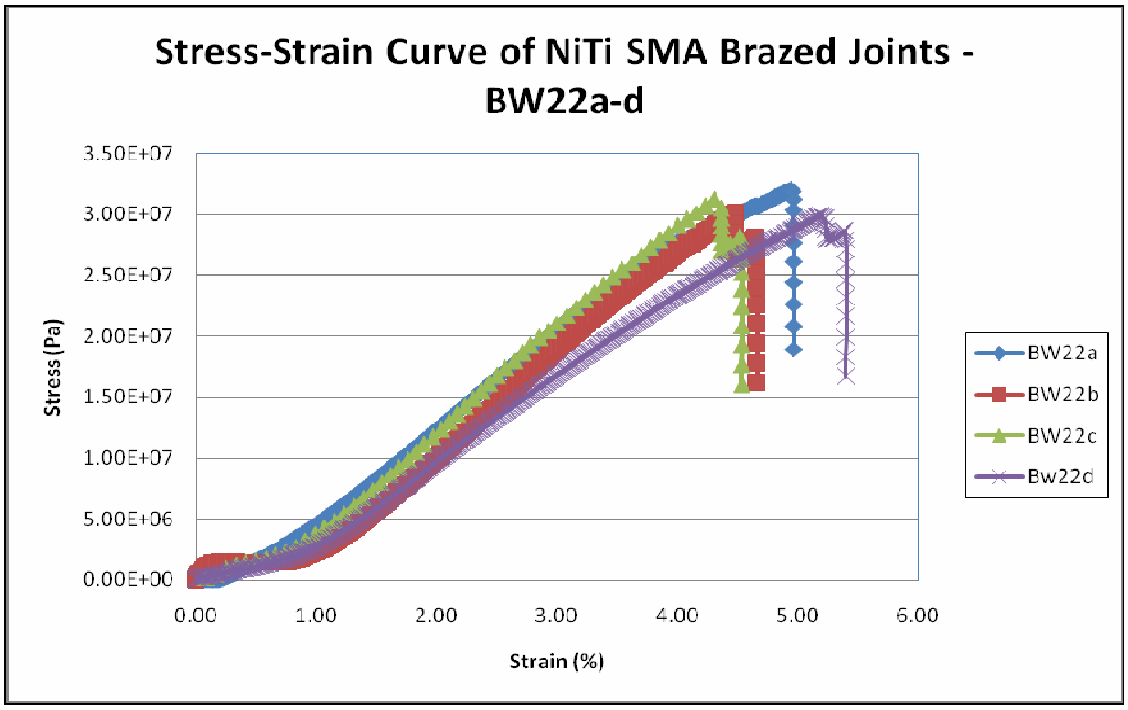

Figure 8-47, mechanical testing of NiTi brazed joints (BW22 a-d)

9 Implication of Joining Results

The joining of NiTi SMA to dissimilar metals posed immense difficulties. Autogeneous fusion welding failed to produce welds that match the requirements of ASN. Solidification cracking has been identified as the main contributor to the poor joint performance, similar to that identified by Hall in his work welding Ti-rich SMA to stainless steel [**137**]. Improvements in weld performance can be achieved by the local enrichment of either nickel or titanium. Effectively change the weld compositions to one where intermetallics are not the primary phase on the binary equilibrium phase diagram [**Figure 9-1**]. This is contrary to EWI's patent on welding NiTi SMA to ferrous metals where the inventors claimed that at least 50 at% of nickel content at the joint is necessary in order to produce integral SMA joints [**163**]. In this study, the presence of nickel above a critical level of 25 at% has been shown to have detrimental effect on the joint performance. A maximum shear strength of 28.4 MPa was achieved with a nickel level just below 25 at% at the weld. However, this was still less than 10% of that required for the ASN. Thus fusion welding is unlikely to be viable without the addition of metallic fillers.

Autogeneous solid-state joining produced some unexpected results. During friction stir welding, the softened parent metals failed to mix together and form metallurgical bonds. Conclusions as to the cause of such a phenomenon cannot be drawn until a full understanding in the thermodynamics of the process can be understood. However, it is likely that localised pre-heating methods, such as electrical induction heating, should help to further soften the parents metal thus improve the possibility of them mixing together to form strong integral joints.

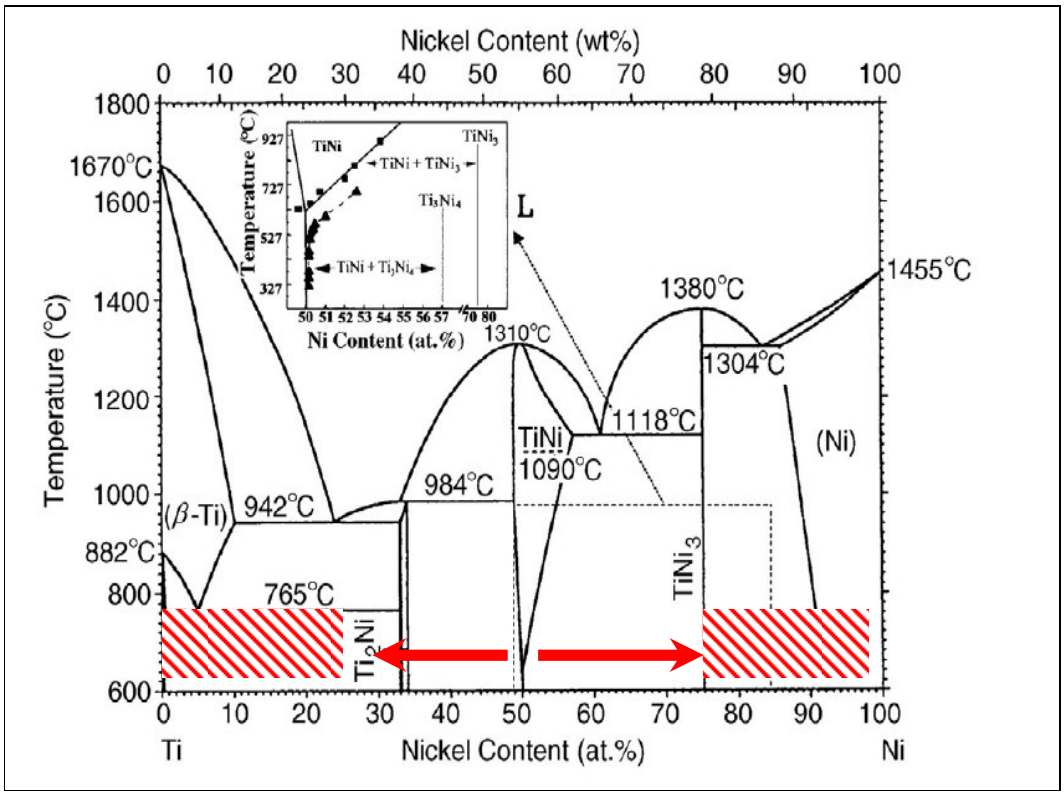

Figure 9-1, Binary equilibrium phase diagram showing areas of possible joint composition where joint performance can be maximise

Joining with interlays produced some positive results in providing a viable joining method for the manufacturing of ASN. Fusion welding with a nickel-rich filler wire in a butt configuration produced the strongest welds in this research. However, the complexity of the interlayer used meant that the effect of individual constituents to the joint performance could not be identified. It was suspected that the addition of nickel beyond a critical level has similar effect as keeping the nickel contents at the weld composition level a critical level down to minimise the formation of intermetallics. Referring to the binary equilibrium phase diagram on **Figure 9-1**, the nickel content at the weld should be maintained within the range of 25 at% > Ni > 67 at% in order to produce an integral joint.

Vacuum brazing with titanium-based interlayers produced joints with improved joint properties over autogeneous fusion welds. However, they were still less than 10% of what was required for the ASN.

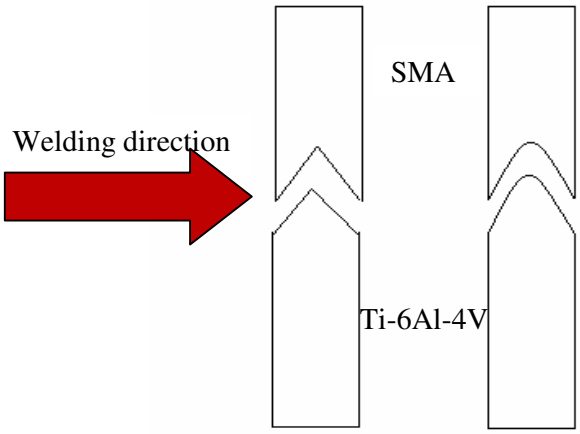

Figure 9-2, Possible weld design that enable the precise control of weld composition

According to the theory developed in this study, joint performance is strongly affected by the volume of intermetallics present at the joint. To minimise or to avoid the formation of intermetallics, the joint composition must be in the shaded area on the binary equilibrium phase diagram on **Figure 9-1.** This equates to a joint composition of 25 at% > Ni > 67 at%. More research is required to fully understand the variation in weld performance of a SMA-Ti-6Al-4V joint as a function of weld composition. Also whether any alloying elements have the effect of suppressing the formation of intermetallics would certainly help to identify the most effective interlayer for the system. Once an optimum weld composition and interlayer are identified, weld composition can be better controlled by using alternative weld design such as a grooved or a cup-and-cone design shown in **Figure 9-2**.

10 Conclusions

- Aircraft noise is considered to be one of the main factors obstructing the continual development of the aerospace industry. Noise abatement technologies are therefore crucial in order to sustain the constant expansion in the aerospace market. The economic evaluation conducted in this thesis highlights the costs of aircraft noise and justified the development of noise abatement technologies.

- NiTi SMA provides a unique solution for the control system in the adaptive serrated nozzle. However the ASN used SMAs in the size and volume that are difficult to obtain in the current commercial market. SMA suppliers could be incentivised to accelerate the development of SMA and process technologies by employing the notion of ***signalling***.

- Autogeneous fusion welding methods including TIG, laser and electron beam welding produced welds with poor joint properties. The formation of $NiTi_2$ brittle intermetallic phase at the weld caused solidification cracking to occur. The formation of brittle $NiTi_2$ intermetallics is inevitable in autogeneous fusion welds. If an autogeneous fusion welding method is a prerequisite requirement, then it should be carried out in such a way the resultant weld microstructure is composed of predominately Ti-6Al-4V and that the local Ni content at the weld must be maintained within the range of 25 at% > Ni > 67 at%.

- Fusion welding with the addition of an interlayer showed mixed results. In a lap configuration, the thick parent metals consume most of the metallic interlayer and eliminate the intended effect. However, integral joints have been achieved in a butt configuration with joint properties closer to that specified in the ASN design.

- FSSW failed to mix the soften metals together to produce integral joints. The developmental effort required to fully understand the thermodynamics during the process in order to derive a solution for the problem is too great at this stage.

- Brazing proves to be the most promising joining methods out of those studied in this research. Vacuum brazing produced by far the narrowest and defect free joints. However, the use of vacuum furnaces is inappropriate for the production of ASN, thus a localised heating method must be used instead.

- Brazed joints produced in this work were still relatively weak compared to that is required for the ASN. Further development is required to further optimise the process and improve the joint properties.

11 Future Work

1. Crack initiation in autogeneous fusion welding of NiTi SMA to Ti-6Al-4V has been shown to depend strongly on the nickel content in the weld. A study of the change in weld microstructure as a function of nickel content would provide a better understanding into the cause of crack initiation.

2. The use of interlayers in vacuum brazing has been shown to improve the properties of brazed joints. However, the joint properties were still substantially lower than required for the ASN. Further process optimisation and studies into the effect of alloying elements and brazing systems would enable braze joints to be further improved.

3. While this research made significant strides in the development of viable joining methods for the ASN, how these joints would perform under the actual operating loading conditions is still unknown. A simulated test would enable the joint performance to be better tailored to the intended application.

12 References

1. Barnett, P., Humphreys, N., Phillipson, P., Lan, J., Nesbitt, E. and Premo, J., 'The Joint Rolls-Royce/Boeing Quiet Technology Demonstrator Programme', The 10th AIAA/CEAS Aeroacoustic Conference, Manchester, UK, May 10-12, 2004, AIAA 2004-2869

2. Webster, J., Friend,C., and Cartmell, M., 'High Integrity Adaptive Shape Memory Systems (HIASMS) - Development of design and manufacturing methods to enable large scale structural integration of Shape Memory Alloys (SMAs) in metallic components', Rolls Royce Internal Report, Document number DNS 90936, March 2002 (unpublished Report)

3. Howse, M., 'Environmental Technologies' Presentation Presented at the Paris Air Show, Paris: Rolls Royce; 2001.

4. Current, M., "Initial Joining Methods for the Shape Memory Alloy Serrated Nozzle Sub-Element Demonstrator", Rolls Royce Internal Report, Document number DNS 94257, Jan 2003 (unpublished Report)

5. Webster, J. R., and Beardsley, P.; 'Risk Management of the Adaptive Serrated Nozzle Concept. Rolls Royce Internal Report.' Document number DNS 83119, Jun 2001 (unpublished Report)

6. Potluri, N. B., "Joining of Shape Memory Alloys", Welding Journal, March 1999, p.39-42

7. Webster, J. R., 'Selective Risk Mitigation of the Shape Memory Alloy (SMA) Adaptive Serrated Nozzle.' Rolls Royce Internal Report, Document Number: DNS 84701, Feb 2002. (unpublished Report)
8. 'Other International Development – Air Transport and Policy of Sustainability', Environmental Policy and Law, 35 (3), 2005, p. 114-121
9. 'Key Trends Highlight Enduring Success of the World Air Transport Industry', ICAO Journal, no.8, November 2004, p. 4-6, 23
10. 'Outlook for Air Transport to the Year 2015', International Civil Aviation Organization, Montreal, 2004, p. 6
11. 'The Future Development of Air Transport in the UK: a National Consultation Paper', Department of Transport, England, 2002, p.7
12. 'Air Traffic Forecasts for the United Kingdom 2000', Department of the Environment, Transport and the Regions (DETR), May 2000, p.9
13. 'UK Air Travel Forecasts up to 2030', Department of Environment, Transport and the Regions (DETR), May 2000, Annex A, p. 2
14. Reed, A., 'Britain's Aircraft Industry- What Went Right? What Went Wrong?', Dent & Sons Ltd, London, 1973, p.146
15. Ballal, D. and Zelina, J., 'Progress in Aero Engine Technology (1939-2003)', AIAA 2003-4412, The 39th AIAA/ASME/SAE/ASEE Joint Propulsion Conference and Exhibit, 20-23 July 2003, Huntsville, Alabama, US
16. 'Research to Develop New Technology Targets Aircraft Engine Emissions', ICAO Journal, no. 5, 2004, p.7-10
17. 'Stansted Heads Airport Expansion', [Web Page] Politics, BBC News, 16 December, 2003., available at http://news.bbc.co.uk/1/low/uk_politics/3322277.stm, last accessed on 06/60/2006

18. Kors, E., 'Significantly Lower Community Exposure to Aircraft – Halfway Towards Success', AIAA Acoustic Conference, Manchester, 2004
19. Morrell, S., Taylor, R. and Lyle, D., 'A Review of Health Effects of Aircraft Noise', Australian and New Zealand Journal of Public Health, 21 (2), 1997, p. 221-236
20. Findell, I. H. et al., 'Aircraft Noise and Sleep – 1999 UK Trial Methodology Study', ISVR Consultancy Services, Southampton, UK, Nov 2000
21. Griefahn, B., 'Sleep Disturbance Related to Environmental Noise', Noise and Health, 4 (12), 2002, p. 57-60.
22. 'Conventional on International Civil Aviation, Annex 16: Environmental Protection: Annex 16 to the Convention on International Aviation Vol.1, Aircraft Noise.', International Civil Aviation Organisation, Montreal, 2005, Appendix 2, APP 2-9
23. Berglund, B., Lindvall, T., and Schwela, D., 'Guidelines for Community Noise', World Health Organisation , Geneva, 1999, p.22-38
24. 'Performance Assessment for Airport Noise Charge Polices and Airline Network Adjustment Response', Transportation Research Part D, no. 10, 1995, p.281-304
25. Darling, A., 'Civil Aviation Bill', House of Commons, England, 2006
26. Bond, D., 'The Book on Noise Reaches Chapter 4', Aviation Week and Space Technology, Jan 2001, p.48-54
27. 'Noise Regulation Time Line', [Web Page]. Boeing Corporation, available at http://www.boeing.com/commercial/noise/charts_all.html, last accessed on 06/60/2006
28. 'Bothered by Aircraft Noise? We're Listening', Community Matters, BAA Heathrow, England, p.12
29. Ollerhead, J. B., Rhodes, D. P. and Monkman, 'Review of the Departure Noise Limits at Heathrow, Gatwick and Stansted Airports: Effect of Take-Off Weight and

Operating Procedure on Noise Displacement', D. J., R&D Report 9841, Environmental Research and Consultancy Department, Civil Aviation Authority, UK, 1999, p.3

30. Green, J., 'Civil Aviation and the Environmental Challenge', The Aeronautical Journal, June 2003, p. 281-299
31. 'Cease Fine in U.S./Europe Hush-Kit Battle', Business & Commercial Aviation, 91 (5), 2002, p.58
32. Edward, A. and Daniel, D., 'EU to Withdraw Plan on Noisy Aircraft', Finical Times, Oct 30 2001, p.16
33. 'The Future of Air Travel – White Paper', Depart for Transport, December 2003, [Web Page], available at http://www.dft.gov.uk/stellent/groups/dft_aviation/documents/divisionhomepage/029650.hcsp, last accessed 06/10/2006
34. 'Noise', BAA Heathrow,2006, [Web Page], available at http://www.heathrowairport.com/noise, last accessed on 21/06/2006
35. 'Condition of Use including Airport Charges from 1 April 2006', BAA Heathrow, Feb 2006, UK, pp.16
36. Ollerhead, J. B., Hopewell, H., 'Review of the Quota Count (QC) System: Re-Analysis of the Differences between Arrival and Departures', ERCD Report 0204, Department of Transport, November 2002, UK.
37. 'Aircraft Noise', BAA Heathrow, [Web Page], available at http://www.heathrowairpot.com/heathrow_noise_inforamtion.pdf, last accessed on 06 June 2006.
38. 'Night Flight Restrictions For Heathrow, Gatwick and Stansted Airports', Government News Network, Department for Transport, [Web Page], available at

http://www.gnn.gov.uk/environment/fullDetail.asp?ReleaseID=205921&NewsAreaID=2&NavigatedFromDepartment=True, last accessed on 06 June 2006.

39. Tinseth, R. J., 'The Shape of the Future', presentation given at Farnborough International Airshow, 2006, Farnborough, UK
40. Deguihem, Y., 'Hurel-Hispano – A Foursquare Solution for A380 Nacelles', Snecma Magazine, no.1, December 2002, p. 8.
41. 'London Heathrow, London Gatwick and London Stansted Airports Noise Restrictions (No 2) Notice 2006', Civil Aviation Authority, S 35/2006, August 2006, p. 2
42. Navrud, S., 'State-of-the-art on Economic Valuation of Noise', Final Report to European Commission DG Environment, Department of Economics and Social Sciences, Agricultural University of Norway, April 2002
43. Schipper, Y., 'Environmental Costs in European Aviation', Transport Policy, 2004, no.11, p. 141-154
44. Gonzalez, J. G., 'Environmental Noise-Main Focus: Aircraft noise', Europaeische Akademie, 2004, p.78
45. 'The Environmental Costs of Aviation', Postnote, Parliamentary Office of Science and Technology, No.207, Nov 2003, p. 4
46. Schipper, Y., Nijkamp, P. and Rietveld, P., 'Aircraft Noise Valuation Studies and Meta-analysis', International Journal of Environmental Technology and Management, 1(3), 2001, p. 317-320
47. Feitelson, E., Hurd, E. and Mudge, R., 'The Impact of Aircraft Noise on Willingness to Pay for Residences?', Transport Research Part D, no. 9, 1996, p. 1-4.

48. ‘Silent Planes ‘will fly in 20 years’, Jha, A., The Guardian, 19 Aug 2005, [Web Page]. Available at http://www.Guardian.co.uk/uk_news/story/0,1442100,00.html, last accessed on 06 June 2006.
49. ‘Academia Exploring Innovative Approaches to Achieving “Silent” Flight’, ICAO Journal, no.1, 2006, p.24-25, 37
50. ‘Silent Aircraft Initiative – a New Approach’, [Web Page]. Available at http://www.silentaircraft.org, last accessed on 06 June 2006.
51. Committee for the Review of NASA's Pioneering Revolutionary Technology (PRT) Program, ‘Review of NASA’s Areospace Technology Enterprise: An Assessment of NASA’s Pioneering Revolutionary Technology Program’, National Research Council of the Academes, 2003, p.30-31
52. Herkes, B., ‘The Quite Technology Demonstrator 2 Flight Test’, The Aviation Noise & Air Quality Symposium, Palm Spring, USA, March 2006, p. 11.
53. Wurzel, D., ‘Technical Development in the Field of Aircraft Noise Reduction’, in ‘Environmental Noise – Main Focus: Aircraft Noise’, Edited Gonzalez, J., Europaische Akademie, Germany, p.58-71
54. ‘Test Flight Prove Quiet Aircraft Techniques’, Professional Engineering, 18 (21), 2005, p. 47
55. Fisher, M. and Self, R., ‘Aeroacoustic Research in Europe: the CE AS-ASC Report on 2001 Highlights’, Journal of Sound and Vibration, 258 (1), 2002, p. 1-30
56. Beardsley, P. and Webster, J. R., ‘The Application of Shape Memory Alloys (SMAs) to Exhaust Nozzles to Reduce Noise During Take Off and Approach Whilst Minimising SFC Impact at Cruise.’ Rolls Royce Internal Report, Document Number: PDM 5008, Apr 2001 (unpublished report)

57. Webster, J. R.; 'Shape Memory and Superelastic Materials - Background and Significance to Rolls- Royce', Rolls Royce Internal Report, Document Number: DSN 78831, Feb 2001, (unpublished report)

58. Kim, Y. S., and Kim, J. D. 'Laser Welding of Ti-Ni Shape Memory Alloy Wire and its Fatigue Properties.' Key Engineering Materials, 183-187, 2000; p.1309-1314.

59. Sato, Y., Kokawa, H., Takahshi, H., Kuwana, Yamauchi, K and Sato, S., 'Effect of Nitrogen on Transformation Temperatures of Arc-Melted, Ti-Ni Shape Memory Alloys', Welding International 13(10), 1999, p.770-777

60. J. R. Webster, 'Selective Risk Mitigation of the Shape Memory Alloy (SMA) Adaptive Serrated Nozzle', Rolls Royce Internal Report, Document Number: DNS 84701, Feb 2002, pp.9, (unpublished report)

61. Beardsley. P and Webster, J., 'The Application of Shape Memory Alloys (SMAs) to Exhaust Nozzles to Reduce Noise During Take Off and Approach Whilst Minimising SFC Impact At Cruise', Rolls Royce Internal Report, Document Number: PDM5008, 12 Apr 2001, p. 25 (unpublished report)

62. Freeman, R., 'Strategic management: a stakeholder approach.', Pitman, Boston, USA. 1984, p. 126

63. Mitchell, R., Agle, B., and Wood, D., 'Toward a Theory of Stakeholder Identification and Salience: Defining the Principle of Who and What Really Counts', Academy of Management Review 22(4) 853-886, 1997

64. 'Making Future Commercial Aircraft Quieter', NASA fact sheet FS-1999-07-003-GRC, NASA Glenn Research Centre, July 1999,

65. Johnson, T. and Lockley, P., 'Emission Impossible', Aviation Environment Federation, Feb 2006, England, pp.4

66. Vainio, M. And Paque, G., 'Highlights of the Workshop on the "State-of-the-art in Noise Valuation"-Final Report', European Commission, July 2002, p. 4

67. 'Heathrow Airport – Interim Master Plan', BAA airports, UK, June 2005, pp.35

68. 'NASA's Quiet Aircraft Technology Program', NASA Fact Sheet FS-2002-09-73-LaRC, NASA Langley Research Centre, Virginia, USA

69. 'Home Relocation Assistance Scheme', BAA Heathrow, August 2005, pp. 6, [Web Page], available at http://www.heathrowairport.com/assets/B2CPortal/Static%20Files/LHR_HRAS_complete.pdf, last accessed, 06/10/2006

70. 'Residential Property Price Report: January – March 2006', Land Registry, [Web Page], available at http://www.landreg.gov.uk/publications, last accessed on 10/10/2006

71. 'Balance-Key Data on Sustainability at Lufthansa', Lufthansa Airline, Issue 2006, 2006, [Web Page], available on http://responsibility.Lufthansa.com, last accessed on 10/10/2006.

72. 'Powering a Better World Environmental Report 2003' [Web Page], Rolls Royce Plc, 2003; Available at http://www.rolls-royce.com/community/downloads/environment04/environment.pdf, Last accessed 09/01/2005.

73. 'Flying Facts: Schedules & Information', Virgin Atlantic, March 2006, [Web Page]. Available on http://www.virgin-atlantic.com/en/gb/flighttimes/monthlyschedules/index.jsp, last accessed on 06/10/06

74. Otsuka, O., and Wayman C. M., 'Shape Memory Materials.' UK, Cambridge University Press,., 220-222 (49-73), 1998, p.1-5

75. Srinivasan, A. V., and McFarland, D. M.; 'Smart Structures – Analysis and Design', Cambridge University Press, 2001, p. 26-33

76. Liu, Y. And McCormick, P., 'Thermodynamic Analysis of the Martensitic Transformation in NiTi-I. Effect of Heat Treatment on Transformation Behaviour', Acta metallurgica et materialia, 42 (7), 1994, p2401-2406

77. Chumlyakov, T., Kireeva, L., Litvinia, E., and Lisyuk, A., 'Superelasticity during the Elastic Twinning, Slip and Martensitic Transformations', SMST-97: Proceedings of the Second International Conference on Shape Memory and Superelastic Technologies, edited by Pelton, A., Pacific Grove, California, USA, 1997, p. 29-34.

78. Yeung, K., Chugng, C., Cheung, K., Lu, W. And Luk, K., 'Effect of Heat-Treatment on Phase Transition Temperatures of a Superelastic NiTi Alloy for Medical Use', Materials Science Forums, vols. 394-395, 2002, p.321-321

79. Anson, T.; 'Shape Memory Alloy Medical Applications.' Materials World. Dec; 7(12) 1999, p.745-747.

80. Aydogdu, Y., Aydogdu A. and Adiguzel, O., 'Self-Accommodating Martensite Plate Variants in Shape Memory CuAlNi Alloys', Journal of Materials Processing Technology, 123(3), 2002, p.489-500

81. Chumlyakov, Y. U., Kireeva, I. V., Litviniva, E. I., and Lisyuk, A. G., 'Superelastic During the Elastic Twinning, Slip and Martensitic Transformations.' SMST 97: Proceedings of the International Conference on Shape Memory and Superelastic Technology Conference; edited by Pelton, Asliomar Conference Centre, Pacific Grove, California, USA. 1997.

82. Duerig, T. W. Melton K. N. Stockel D. and Wayman C. M. 'Engineering Aspects of Shape Memory Alloys'. Butterworth-Heinemann; 1990. Pp.63

83. Thompson, S. P.; 'Enhancing the Post Buckling Response of Composite Plat/Panel Structure Utilizing Shape Memory alloy Actuators – A Smart Structural Concept', PhD Thesis, Cranfield University, 1999

84. Ariapour, A., Yakubtsov, I., and Perovic, D.; 'Shape Memory Effect and Strengthening Mechanism in a Nb and N- dope Fe-Mn-Si Based Alloy.' Materials Science and Engineering A, vol. 32, 2001; p.1621.

85. Morgan, N. B., 'The Stability of NiTi Shape Memory Alloys in Actuator Applications. EngD Thesis, College of Defence Technology, Cranfield University: 1999.

86. Morgan, N. B., and Friend, C. M., 'Shape-Memory Alloys - A 'Smart' Technology?', Internal Report prepared for Rolls Royce, Cranfield University, 1999, pp. 1-22.

87. Leu, S. S., Chen, Y. C., and Jean, R. D., 'Effect of rapid solidification on mechanical properties of Cu-Al-Ni shape memory alloys', Journal of Materials, 27(10) 2792-2798, 1992

88. Burhler, W. J., Gilfrich, J. V., and Wiley, R. C., 'Effect of Low-Temperature Phase Change on the Mechanical Properties of Alloys Near Composition Ti-Ni', Journal of Applied Physics, 34, 1963, p. 1475-1477

89. Massalski, T. B., Okamoto, H., Subramanian, P. R., and Kacprzak, L., 'Binary Alloys Phase Diagrams', 2nd Edition, vol 3. ASM International, USA, 1999, p. 2874

90. Gong, C. W., Wang, Y. N. and Yang, D. Z., 'Martensitic Transformation of $Ni_{50}Ti_{45}Ta_5$ Shape Memory Alloy', Journal of Alloys and Compounds, 419(1-2), Aug 2006, p.61-65

91. Tang, W. J., and Sandstrom, R., 'Some Aspects on TiNi SMA Properties Based on the Calculation of Ti-Ni Phase Diagram.' SMST 97: Proceedings of the International Conference on Shape Memory and Superelastic Technology Conference; Asliomar Conference Center, Pacific Grove, California, USA. 1997
92. Ma, J. L., and Wu, K. H., 'Effects of Tantalum Addition on Transformation Behaviour of $(Ni_{51}Ti_{49})_{1-x}Ta_x$ and $Ni_{5-}Ti_{50-y}Ta_y$ Shape Memory Alloys', Materials Science and Technology Vol.16, June 2000, p. 716-719
93. Hsieh, S. F., and Wu, S. K., "A study on the nickel-rich ternary Ti-Ni-Al shape memory alloys," Journal of Materials Science, 32(41), 1997 p. 989-996,
94. Kolomytsev, V. I., 'Trend Across Periodic Table in the Effect of Alloying by Transition Metal on Martensitic Transformation Temperature in Compound TiNi', In: Proceedings of the international symposium on shape memory materials (SMM'94), (eds. Chu, Y. Y. et al.). International Academic Publisher, 1994, pp.136-139
95. Matsumoto, H., 'Effects of Transformation-Induced Defects in Cobalt and $Ti_{48}Ni_{52}$', Physics B 334, 2003, 112-117
96. Feng, Z., Gao, B., Wang, J., Qian, D and Liu, Y., 'Influence of Zr Additions on Shape-Memory Effect and Mechanical Properties of Ni-Rich NiTi Alloys', Materials Science Forums, vol. 394-395, 2002, p.365-368.
97. Arenas, M. F., Acoff, V. L. And Reddy, R. G., 'Physics Properties of Selected Brazing Filler Metals', Science and Technology of Welding and Joining, 9(5), 2004, p.423-429
98. Liu, F., Ding, Z. and Xu, H., 'Phase Transformation Behaviours and Mechanical Properties of TiNiMo Shape Memory Alloys', Intermetallics 13, 2005, p. 357-360

99. Van Humbeeck, J., Keuven, K. U., and Stalmans, R., 'Encyclopedia of Smart Materials', John Wiley & Sons, 2002, p. 258

100. Tang, W., Sandström and Miyazaki, S., 'Phase Equilibria in the Pseudobinary $Ti_{0.5}Ni_{0.5}$-$Ti_{0.5}Cu_{0.5}$ System', Journal of Phase Equilibria, 21(3), 2000, p.227-234

101. Zhao, L. C., Duerig, T. W., Justi, S., Melton, K. N., Profit, J. L., Yu, W. and Wayman, C. M., 'The study of niobium-rich precipitates in a Ni-Ti-Nb shape memory alloy', Scripta Metallurgica et Materialia, 24(2), Feb 1990, p. 221-225

102. Humbeeck, J. V., and Cederstrom, J., 'The Present State of Shape Memory Materials and Barriers Still to be Overcome.' SMAT 94: Proceeding of the First International Conference on Shape Memory and Superelastic Technologies; Asliomar Conference Centre, Pacific Grove, California, USA. 1994.

103. Cederström, J., and Van Humbeeck, J., "Relationship Between Shape Memory Properties and Applications", Journal de Physique IV, Colleque C2, Supplément au Journal de Physique III, 5, Feb 1995, C2-335-340

104. Rao, C., 'Chemistry of Advanced Materials A: Chemistry for the 21st Century Monograph.', Backwell Scientific Publications, Oxford, UK, 1992; p.269

105. Otsuka, K. and Ren, X., 'Recent Development in the Research of Shape Memory Alloys', Intermetallics, 7, 1999, p.511-528

106. Busch, J. D., "The Frangibolt Files: Using Shape Memory Alloy on the Spacecraft Clementine', SMST-94: The First International Conference on Shape Memory and Superelastic Technologies; Pacific Groove, California, USA, 7-10 March 1994, p. 259-264, 1995.

107. 'Frangibolt – Non-Explosive Actuators', [web page] available on http://www.tiniaerospace/frangibolt.html, last accessed on 18 Oct 2006

108. ‘Making a Material Difference’, Memry Corp. 2005 Annual Report, Memry Corp., USA, 2005

109. Indirli, M., Castellano, M., Clemente, P., and Mrtelli, A., “Demo-Application of Shape Memory Alloy Devices: The Rehabilitation of the S. Giorgio Church Bell-Tower”, in ‘Smart Structures and Materials 2001: Smart Systems for Bridges, Structures, and Highways,’ Edited by Liu, S. C., Proceedings of SPIE 4330, 2001, p. 262-272, 2001

110. Hu, M. H., and Schetky, L. McD., “Industry Applications for Shape Memory Alloys”, Proceedings of International Conference on Shape Memory and Superelastic Technologies, Pacific Grove, California, USA, 2000, p.171-182

111. Otsuka, K., Tomoyuki, K., “Science and Technology of Shape-Memory Alloys: New Developments”, MRS Bulletin, Feb 2002, p. 91-100

112. Duerig, T., Pelton A., and Stöckel, D., ‘An overview of nitinol medical applications’, Materials Science and Engineering A, vol. 273-275, 1999, p. 149-160

113. Sachdeva, R., and Miyazaki, S., ‘Superelastic Ni-Ti Alloys in Orthodontics’, Engineering Aspects of Shape Memory Alloys, 1990, p. 452-469.

114. Private conversation with John Webster, Rolls Royce Mechanical Specialist, Derby, 12 Sept 2004

115. Nellis, J. and Parker, D., ‘Principles of Business Economics’, Prentice Hall, UK, 2002, p. 179-181

116. McKinsey, J., ‘Introduction to the Theory of Games’, McGraw-Hill Book Company Inc., New York, 1952, p.1-8

117. Maddala, G., Miller, E., ‘Microeconomics’, Dobson, S., McGraw-Hill, London, 1989, p. 223

118. Spence, M., 'Job Market Signalling', Quarterly Journal of Economics, 87,(3), 1973, p. 355-374

119. Chau, E., Friend, C., Allen, D., Hora, J., Webster, J., 'A Technical and Economic Appraisal of Shape Memory Alloys for Aerospace Applications', Materials Science and Engineering A 438-440, 2006, 589-592.

120. Sato, Y., Kokawa, H., and Kuwana, T. 'Weldability of Ti-Ni Shape Memory Alloy.' Proceeding of the 6th International Symposium of JWS; Nagaya, Japan. 1996, p.695-700.

121. Ikai, A.; 'TIG Welding and Shape Memory Effect of TiNi Shape Memory Alloy.'. Journal of Intelligent Materials Systems and Structures. No.7, 1994; p. 646-655.

122. Hirose, A, Uchihara, M., and Araki, T.; 'Laser Welding of Ti-Ni Type Shape Memory Alloy.' The 5th International Symposium of the Japan Welding Society; Tokyo, Japan. 1990, p.122

123. Hirose, A., Uchihara, M., Araki, T., Honda, K., and Kondoh, M., 'Laser Welding of Ti-Ni Type Shape Memory Alloy.' The 5th International Symposium of the Japan Welding Society; April 1990., p.63

124. Katayama, S., Matsuda, H., and Matsunawa, A.; 'Pulsed Laser Weldability and Solidification Microstructure of Ti-Ni Shape Memory Alloys.' 5th International Conference on Welding and Melting by Electron and Laser Beams; La Baule, France. 1993.

125. Schloßmacher, P., Haas, T., and Schussler, A., 'Laser-Welding of a Ni-Rich TiNi Shape Memory alloy: Mechanical Behaviour.' Journal De Physique. Colleque C5 (Supplement) 1995 pp. C5-251 - C526.

126. Schloßmacher, T., Haas, T., and Schussler, A., 'Laser Welding of Ni-Ti Shape Memory Alloys', SMAT 94: Proceeding of the First International Conference on Shape Memory and Superelastic Technologies; Asilomar Conference Centre, Pacific Grove, California, USA. 1994, pp.85-90

127. Schüßler, A., 'Micro-Machining and Joining of NiTi-Alloys using Nd:YAG Lasers: Status and Prospects', SMAT 97: Proceeding of the International Conference on Shape Memory and Superelastic Technologies; Asilomar Conference Centre, Pacific Grove, California, USA. 1997, pp. 143-148

128. Schloßmacher, P., Hass, H., and Schüßler, A., 'Laser-Welding of a Ni-Rich TiNi Shape Memory alloy: Peseudoelastic Properties', SMAT 97: Proceeding of the International Conference on Shape Memory and Superelastic Technologies; Asilomar Conference Centre, Pacific Grove, California, USA. 1997, pp.137-142

129. Tuissi, A., Besseghnin, S., Ranucci, T., Squatrita, F., and Pozzi, M., 'Effect of Nd-YAG Laser Welding on the Functional Properties of he Ni-49.6 at% Ti', Materials Science and Engineering A, A273-275, 1999, p.813-817.

130. Falvo, A., Furgiuele, F. M. and Maletta, C., 'Laser Welding of a NiTi Alloy: Mechancial and Shape Memory Behaviour', Matierlas Science and Engineering A 412, 2005, p.235-240

131. Hsu, Y. T., Wang, Y. R., Wu, S. K., and Chen, C.; 'Effect of CO_2 Laser Welding on the Shape-Memory and Corrosion Characteristics of TiNi Alloys', Metallurgical and Materials Transactions, 32A, 2001, pp. 569-576

132. Yan, X. J., Yang, D. Z. and Liu, X. P., 'Corrosion Behaviour of a Laser-Welded NiTi Shape Memory Alloy', Materials Science and Engineering A, in press, 2006

133. Yan, X. J., Yang, D. Z, and Liu, X. P., 'Electrochemcial Behaviour of YAG Laser-Welded NiTi Shape Memory Alloy', Transactions of Nonferrous Metals Society of China, 16, 2006, p. 572-576

134. Yan, X. J., Yang, D. Z, 'Corrosion Resistance of a Laser Spot-Welded Joint of NiTi Wire in Simulated Human Body Fluids', Journal of Biomedical Materials Research Part A, 77(1), 2006, p.97-102

135. Yan, X. J., Yang, D. Z. and Qi, M., 'Rotating-Bending Figure of a Laser-Welded Superelastic NiTi Alloy Wire', Materials Characterisation, 57(1), 2006, p.58-63

136. Sato, Y. and Kokawa, H., 'Effect of Nitrogen on Transformation Temperature of Arc-Melted, Ti-Ni Shape Memory Alloys', Welding International, 12(10), 1999, p.770-777

137. Hall, P. C., 'Resistance of Welding Ti-Rich Nitinol Wire', Proceeding of the International Conference on Shape Memory and Superelastic Technologies 2001 (SMST 2001), Asliomar Conference Centre, Pacific Grove, California, USA, Edited by Russell, S. and Pelton, A., p. 67-75, 2001

138. Zhou, Z.; 'Effect of Welding Technology on the Performance of Ti-Ni Shape Memory Alloy Wire.' International Academic Publishers (China), 1994 p. 200-204

139. Zhao, X. H., Hau L. J, and Zhao L.; 'Analysis on the Joint Tensile Strength and Fractography of TiNi Shape Memory Alloy Precise Pulse Resistance Butt Welding.' China Welding, 11(1), 2002; p.84-88.

140. Messler, Jr. R. W., 'Principle of Welding: Process, Physics, Chemistry, and Metallurgy.' John Wiley & Sons, Inc., USA., 1999, p.269

141. Shinoda, T.; Tsuchiya, T., and Takahashi, H. 'Functional Characteristics of Friction Welded Near-Equiatomic TiNi Shape Memory Alloy.' Transactions of the Japan Welding Society. 22(2), 1999, p.30-36.

142. Shinoda, T., Owa, T., Magula, V., and Bernasovsky, P.; 'Evaluation of Weldability and Microstructures of Friction Welded Joints in Ni-Ti Shape Memory Alloy.' Proceedings of the 20th International Welding Conference, High-Tatras - Stara Lesna., Welding Research Institute (VUZ); 1999.

143. Hall, P. C., 'Methods of Promoting Solder Wetting on Nitinol.' Proceedings of the International Conference on Shape Memory and Superelastic Technologies 1997 (SMST 97); Asliomar Conference Centre, Pacific Grove, California, USA. 1997

144. Shindo. T, Owa, T. and Magula, V., 'Microstrucutral Analysis of Friction Welded Joins in TiNi Alloy', Welding International, 13(3), 1999, p.180-185

145. London, B. D., Mahoney, M., and Pelton, A., 'The Use of Friction Stir Processing and Friction Stir Welding for Nitinol Medical Devices', European Patent EP1690627A2, 2005

146. London, B., Fino, J., Pelton, A., Fuller, C., and Mahoney, M., 'Friction Sitr Processing of Nitinol', Friction Stir Welding Processing III, Proceeding of TMS, 2005, p.67-74

147. Weman, K. 'Welding Process Handbook, CRC Press, USA, 2003, p. 88

148. Schwartz, M., 'Brazing for the Engineering technologist', Chapman& Hall, UK, 1995, p. 1-6

149. Yang, T. Y., Shiue, R. K. and Wu, S. K., 'Infrared Brazing of $Ti_{50}Ni_{50}$ Shape Memory Alloy using Pure Cu and Ti-15Cu-15Ni Foils', Intermetallics 12, 2004, p.1285-1292

150. Shiue, R. K. and Wu, S. K., 'Infrared Brazing of $Ti_{50}Ni_{50}$ Shape Memory Alloy Using Two Ag-Cu-Ti Active Braze Alloys', Intermetallics, 14, 2006, p.630-638

151. Grummon, D. S., Shaw, J. A. and Foltz, J., 'Fabrication of Cellular Shape Memory Alloy Materials by Reactive Eutectic using Niobium', Materials Science and Engineering A, 438-440, 2006, p.1113-1118

152. Wang, G.; 'Welding of Nitinol to Stainless Steel.' Edison Welding Institute, Internal Report SR9730, USA, Oct 1997 (unpublished report)

153. 'Matsunura, H., Tanoue, N., Yanagida, H., Atsuta, M., Koike, M. and Yoneyama, T., 'Adhesive Bonding of Super-Elastic Titanium-Nickel Alloy Castings with a Metal Conditioner and an Acrylic Adhesive', Journal of Oral Rehabilitation, 30, 2003, p.653-658

154. Hall, T., 'Joint, a Laminate, and a Method of Preparing a Nickel-Titanium Alloy Member Surface for Bonding to Another Layer of Metal', United State Patent, 5,242,759, September 1993.

155. Chiu, K., Cheng, F. and Man, H. 'A Preliminary Study of Cladding Steel with NiTi by Microwave-Assisted Brazing', Materials Science and Engineering, A407, 2005, p. 273-281

156. Chiu, K., Cheng, F. and Man, H., 'Cavitations Erosion Resistance of AISI 316L Stainless Steel Laser Surface-Modified with NiTi', Materials Science and Engineering A, A392, 2005, p.348-358

157. Cheng, F., Lo, K. and Man, H., 'A Preliminary Study Cladding of AISI 316 Stainless Steel using Preplaced NiTi Wire', Materials Science and Engineering A, A380, 2004, p.20-29

158. Chiu, K, Cheng, F. and Man, H., 'Corrosion Behaviour of AISI 316 Stainless Steel Surfaced-Modified with NiTi', Surface & Coating Technology, 200, 2006, p.6054-6061

159. Richman, R., Rao, A. and Kung, D., 'Cavitations Erosion of NiTi Explosively Welded to Steel', Wear, 181-183, 1995, p. 80-85

160. Zimmerly, C. and Inal, O., 'Explosive Welding of a Near-Equiatomic Nickel-Titanium Alloy to Low-Carbon Steel', Materials Science and Engineering, A188, 1994, p. 251-254

161. Hall, P.; 'Welding of Titanium and Titanium Based Alloys to Ferrous Metals (Patent Pending) Notification of Availability for Licensing.' Edison Welding Institute, Internal report SR0307, USA, July 2003 (unpublished report)

162. Li, M., Qiu, X., Sun, D. and Yin, S, 'Effects of Laser Brazing Parameters on Microstructure and Properties of TiNi Shape Memory Alloy and Stainless Steel Joint', Materials Science and Engineering, A 424, 2006, p.17-22

163. Hall, P., 'Method of Welding Titanium and Titanium Based Alloys to Ferrous Metals', United State Patent 6,875,949, April 2005

164. Chularis, A. A., 'A Calculation-Graphical Method of Evaluating the Criterion of Selecting a Refractory Metal of the Barrier Layer When Joining Active Metals to Others Metals and Alloys', Welding International, 8(3), 1994, p.236-238

165. Ma, L. J. and Wu, K. H., 'Effects of Tantalum Addition on Transformation Behaviour of $(Ni_{51}Ti_{49})_{1-x}Ta_x$ and $Ni_{50}Ti_{50-y}Ta_y$ Shape Memory Alloys', Materials Science and Technology, 16,2000, p.719-719

166. Gong, C. W., Wang, Y. N. and Yang, D. Z., 'Martensitic Transformation of $Ni_{50}Ti_{45}Ta_5$ Shape Memory Alloy', Journal of Alloys and Compounds, 419(1-2), 2006, p. 61-65

167. Van der Eijk, C., Fostervoll, H., Sallom, Z. and Akselsen, O., 'Plasma Welding of NiTi to NiTi, Stainless Steel and Hastelloy C276', ASM Materials Solutions 2003 Conference, Pittsburgh, Pennsylvania, USA, 13-15 Oct 2003

168. Uenishi, K., Seki, M., Kunimasa, T., Takatsugu, M., Kobayashi, K., Ikeda, T. and Tsuboi, A., 'YAG Laser Micro Welding of Stainless Steel and Shape Memory Alloy', Third International Symposium on Laser Precision Microfabrication, Proceeding of SPIE, vol. 4830, 2003, p.57-62

169. Li, M., Qiu, X., Sun, D. and Yin, S, 'Properties of Laser-Brazed Joint of NiTi Shape Memory Alloy and Stainless Steel Orthodontic Wires', The Orthodontic CYBER Journal, Oct 2005, [web page], available on http://www.oc-j.com/oct05/LaserbrazedNiTi.htm, last accessed on 23/03/07

170. Liu, Y., Li, T. And Ramesh, K., 'Rate Dependence of Deformation Mechanism in a Shape Memory Alloy', Philosophical Magazine A, 82(12), 2002, p.2461-2473.

171. Li, M. G., Sun, D. Q., Qiu, M. X. And Yin, S. Q., 'Effect of Tin on Melting Temperature and Microstructure of Ag-Cu-Zn-Sn Filler Metals', Materials Science and Technology, 21(11), 2006, p.1318-1322

172. Ko, Y. G., Kim, W. G., Lee, C. S. and Shin, D. H., 'Microstructural Influence on Low-Temperature Superplasticity of Ultrafine-Grained Ti-6Al-4V Alloy', Materials Science and Engineering A, 410-411(25), 2005, p. 156-159

173. Kyffin, W. J., 'Friction Stir Spot Welding of Shape Memory Alloy to Ti-6Al-4V', TWI Report no: 16318/1/05, TWI, UK, Dec 2005 (unpublished report)

174. Melton, K. and Mercire, O., 'Brazable Shape Memory Alloys', US Patent 4,274,872, June 1981

175. Private conversation with T. Pryor, Technician, High Temperature Materials Group, Cranfield University, 19 November 2006.

176. Gupta, K., 'Phase Diagrams of Ternary Nickel Alloys', Indian Institute of Metals, 1990, p.258

13 Appendices

Appendix A. Equilibrium binary Phase Diagram of NiTi

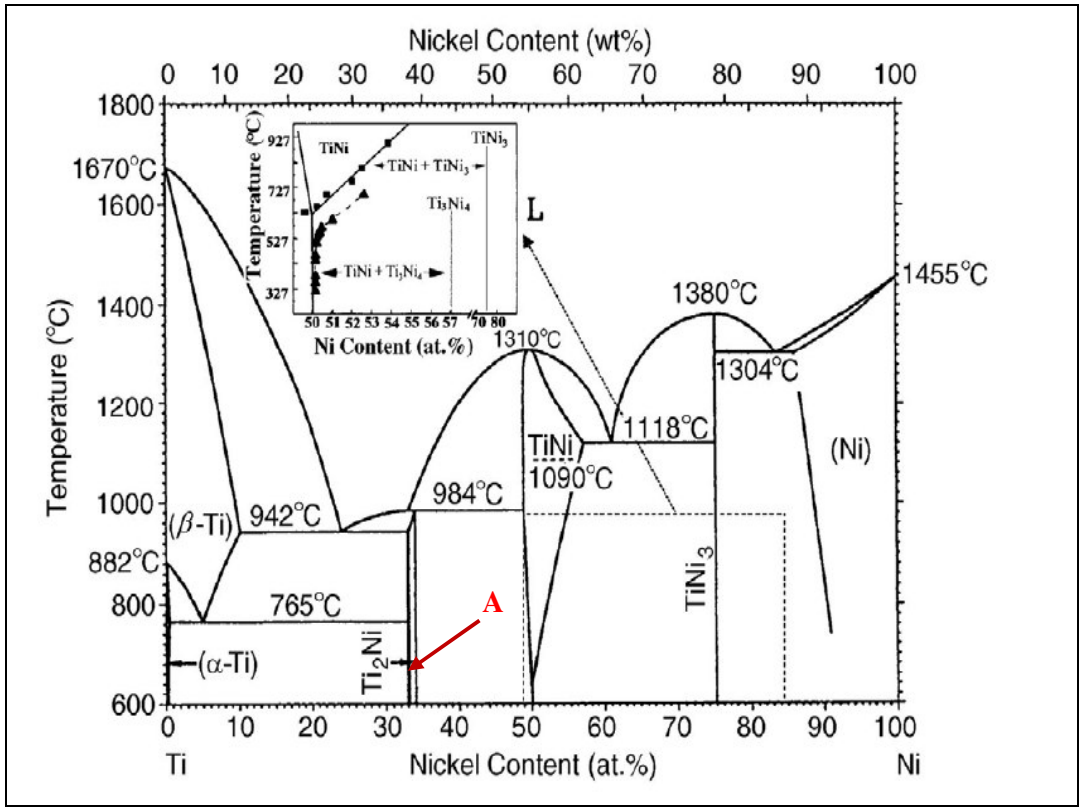

Figure 13-1, Equilibrium binary phase diagram for NiTi alloy [89]

Appendix B. Description of Selected Joining Methods

B1. Electron beam welding

Electron Beam Welding (EBW) is a welding process that employs a beam of high velocity, focused electrons to produces spot of high energy density which creates intense heat and melts the metals to produce a fusion weld. This process produces high integrity welds, with minimal thermal distortion and freedom from component oxidation. The electron beam for welding is generated in an electron gun [**Figure B1.1**] usually in a vacuum (typically $>5x10^{-5}$ mbar) where electrons are accelerated to approximately 30 – 70% of the speed of light and focused onto the workpicece by electromagnetic lenses [**1**]. The electron beam is then bombarded at the weld join. On impact, the kinetic energy of the electrons is converted into heat input to make which instantaneously melts the metal parts and forms a fusion weld.

EBW was first developed in Germany and France in the 1950's for welding of refractory metals for element encapsulations in the nuclear industry. These metals, because of their affinity for oxygen and nitrogen of the air, are very difficult to weld. However, due to its superior weld strength and retain properties, it is rapidly spread into the aerospace, automobile and electronics industries.

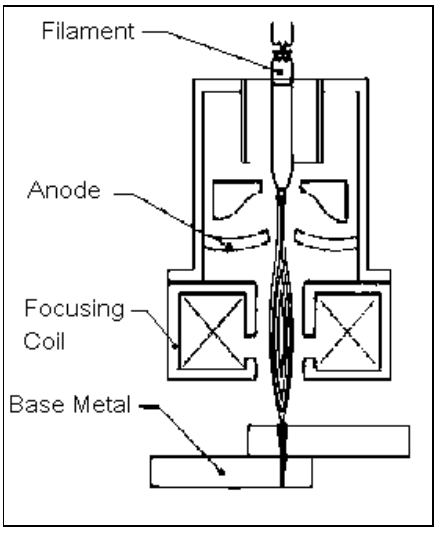

Figure C1.1, schematic representation of a conventional electron gun [1]

One of the main advantages of EBW is its tremendous penetration capability. Electrons are usually accelerated by a high potential - typically 30,000-200,000 volts, and magnetically focused into a spot with a power density of the order of 30,000 W/mm^2 [**1**]. This causes almost instantaneous local melting and vaporisation of the workpiece material. The electron beam is thus able to establish a 'keyhole' delivering heat, deep into the material being welded. Penetration of up to 50:1 depth-to-width ratio can be achieved, depending on the type of metal. This produces a characteristically narrow, near parallel, fusion zone with the least possible distortion and smaller heat affected zone (HAZ) than that of most conventional welding process. In addition, with most materials, the mechanical properties of EB welds are better than welds made with conventional fusion processes. The addition of filler and pre-heat are generally not required. However, in some cases, the addition of filler material or post weld heat treatment may be necessary to develop the desired mechanical properties. Most metals can be welded by this process.

The metals that are most often welded are the super alloys, refractory metals, reactive metals, and the stainless steels.

The main drawback of EBW is its high capital cost. The prices of the equipment is very high and since EBW must be perform in vacuum to allow the electron beam to flow to the workpiece unimpeded by collision with air molecules, it is also expensive to operate due to the constant need for vacuum pumps. However, it is very versatile and is capable of high volume production which justifies its costs. Manufacturing costs may be further reduced through the elimination of production steps and waste materials. Traditional post-welding operations, such as machining, straightening, cleaning, polishing and heat treatment can often be avoided in EBW. Another disadvantage is its set up time, process set ups in EBW are highly complex as fit up must be precise and locating the parts with respect to the beam must be perfect. In addition, EBW produces tremendous temperature differential between the molten metal and the base metal immediately adjacent to the weld. Thus heating and cooling rates are much higher than in traditional welding processes. This rapid cooling rate can create problems such as cracking in high carbon steels that would not normally occur in other traditional welding process.

B2. Laser welding

Laser welding is also a fusion joining process but instead, uses a laser beam as its energy source. Laser beam is a source of electromagnetic energy that can be projected without diverging and can be concentrated to a precise spot of less than 0.03 inches in diameter

[**2**]. The beam is coherent and of a single frequency. Laser welding uses a highly concentrated coherent laser beam impinging upon the joint surface, where light energy is converted to heat input required to melt the metal parts and produce a fusion weld. There are many types of lasers welding in used today and each produce laser light at a unique frequency. Amongst the common sources of lasers is the carbon dioxide (CO2) laser, the Nd:YAG (neodymium-yttrium aluminium garnet) laser and the diode laser [**3**]. Each type of laser has its advantages and drawbacks and is therefore used for different applications.

Laser welding is very similar to electron beam welding that they both employs a high energy beam onto the joint surface, melting and subsequently crystallise the metal parts, resulting in a bond between parts. What sets them apart is that laser beam possess much less energy than electron beam thus produces less heating (only marginal higher than that of arc welding) and penetrating capabilities. Laser welding can also be used in air and the beam is focused and directed by optical lenses and mirrors. Due to their similarity, the advantages and disadvantages for electron beam welding also applies to laser welding but to a lesser extent. Laser welding can be used to join most metals to themselves as well as to dissimilar metals. Main applications are related to welding steels, titanium, and nickel alloys.

B3. Gas Tungsten Arc Welding

The term *Arc Welding* donates to a large group of fusion welding processes that use an electric arc as the heat source to melt the base materials to produce the joint. An electric

arc is a sustained high current, low voltage electric discharge through a conducting plasma that produces sufficient thermal energy to produce to heat and melt the metal and filler rod is added as required. The electric arc is struck between the base metals and the tip of an electrode. The electrode carries the welding current and can be both consumable and non consumable.

Gas Tungsten Arc welding (GTAW) was first developed in the late 1930s as Heliarc or tungsten inert gas (TIG) welding [3]. In TIG welding, an arc is formed between a tungsten electrode and the work piece being welded [**Figure B1.2**]. The arc generates intense heat which melts the weld metal and any filler metal. Gas shielding is fed through the torch to shield the electrode and molten weld pool from contamination. If filler wire is used, it is added to the weld pool separately. Argon is common used as the shielded gas and helium is common added to increase the heat input thus increase welding speed or weld penetration. TIG welding has become a popular choice of welding processes when high quality, precision welding is required. It is controllable and clean, thermal distortion is low due to the localised heat provided by the electric arc.

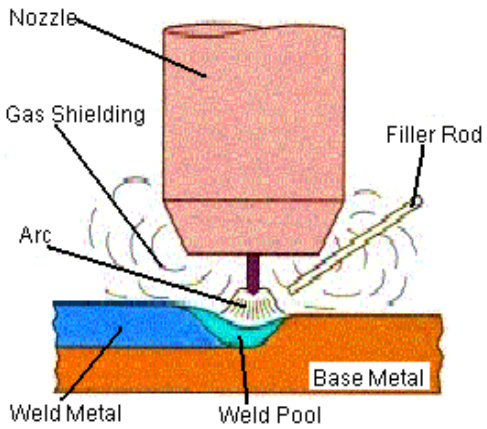

Figure B1.2, Gas Tungsten Arc Welding

B4. Friction welding

Friction welding is a solid state welding process in which joining is achieved through frictional heat energy. Friction welding involves holding two components in axial alignment, and then rotates them under pressure, causing the interface to heat up [**Figure B8.1**]. This heat energy is generated by controlled rubbing of two components until material reaches its plastic state, at which time plasticized material begins to form layers that intertwine with one another [**1**]. The weld is completed by the application of a forge force during or after the cessation of relative motion.

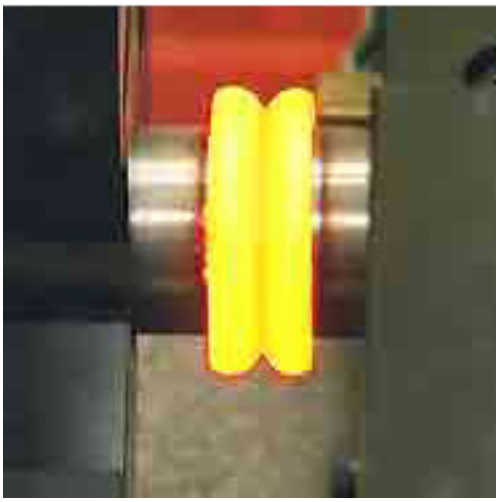

Figure B8.1, Schematics of friction welding process

B5. Brazing

Brazing is a group of joining processes in which joining is achieved through the use of suitable heating and filler metals. The filler metals typically have a liquidus temperature of above 800K (427ºC) but lower the solidus of the base materials [**2**]. The filler metals

are usually distributed between the closely fitting joint surfaces by capillary action. Brazing is essentially a solid state joining process, where heat is usually applied evenly to the base metals, thus thermal distortions are minimised. Chemical bonds are then formed between the filler and the base materials. With the appropriate filler materials, a wide range of dissimilar metals can be joined.

Brazing offers many advantages over welding. Brazed joints are ductile and able to withstand considerable shock and vibration [**1**]. They are usually easy and rapidly made, with operator skill readily acquired. Brazing is ideally suited to the joining of dissimilar metals and is essentially a one-operation process. There is seldom need for any post processing. Brazing is performed at relatively low temperatures, reducing the possibility of warping, overheating or melting the metals being joined. Brazing is relatively economical, the cost- per-joint compares quite favourably with joints made by other metal joining methods. Brazing is also highly adaptable to automated methods. However, during brazing, substantial diffusion of elements from the filler into the base materials usually occurs. This is especially problematic for brazing of reactive metals such as titanium as it may result in the formation of brittle intermetallics. There are also problems with properly wetting of the joint surface. Poor wetting can cause the formation of voids which will lead to cracking at the join interface.

B6. Reference

1. Schwartz, M. M.; 'Metal Joining Manuals' McGraw-Hill, 1979. p. 2-1

2. Degarmo, E. P., Black, J. T., and Kohser, R. A.; 'Matierals and Processing in Manufacturing' Third Edition, John Wiley & Sons, 1997

3. Askeland, D. R.; 'The Science and Engineering of Materials' Thired S.I. Edition, Chapman & Hall, 1996

4. Weman, K.; 'Welding Processes Handbook' Woodhead Publishing Ltd, 2003

Appendix C. DSC Curves of NiTi SMA

a)

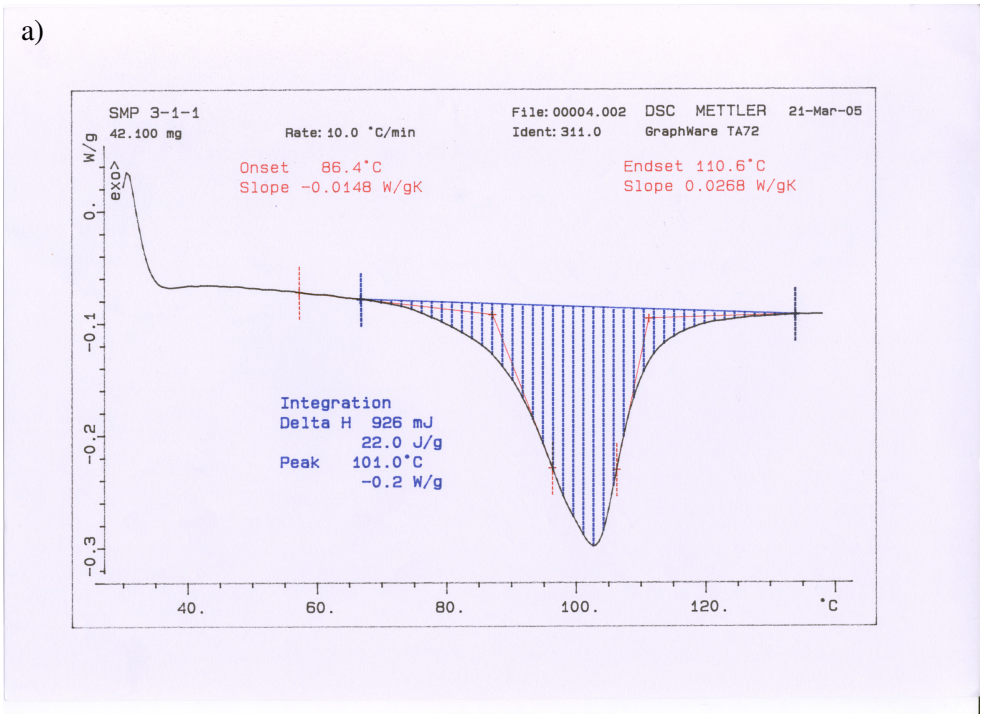

b)

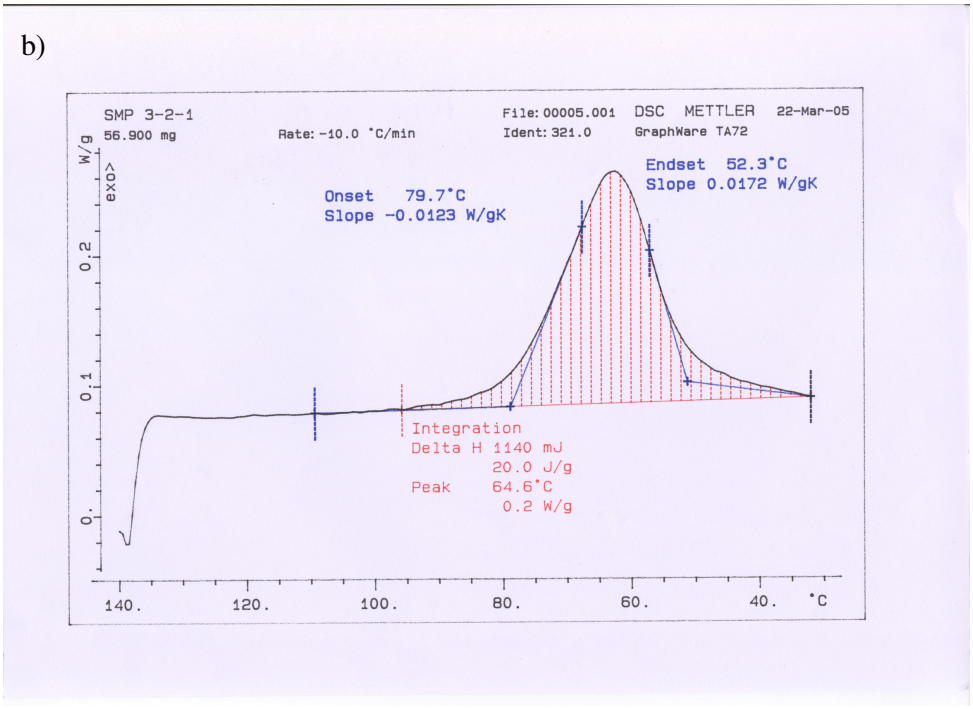

Figure B1, Typical DSC graphs for a) the heating and b) the cooling cycle

Appendix D. FSSW Tool Drawings

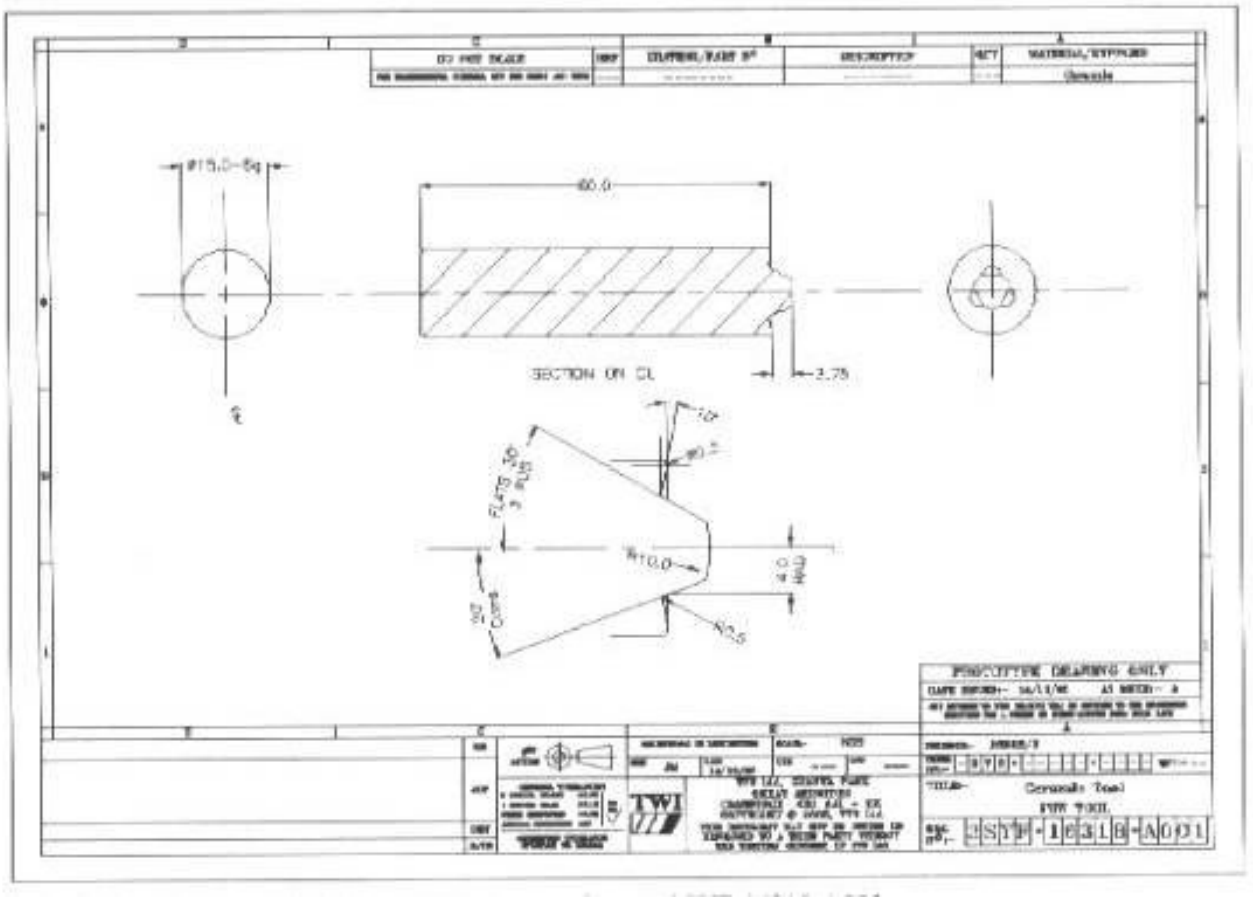

Figure C1, Drawing of Si_3Ni_4 tool A001, TWI Drawing Reference 3SYF-16318-A001

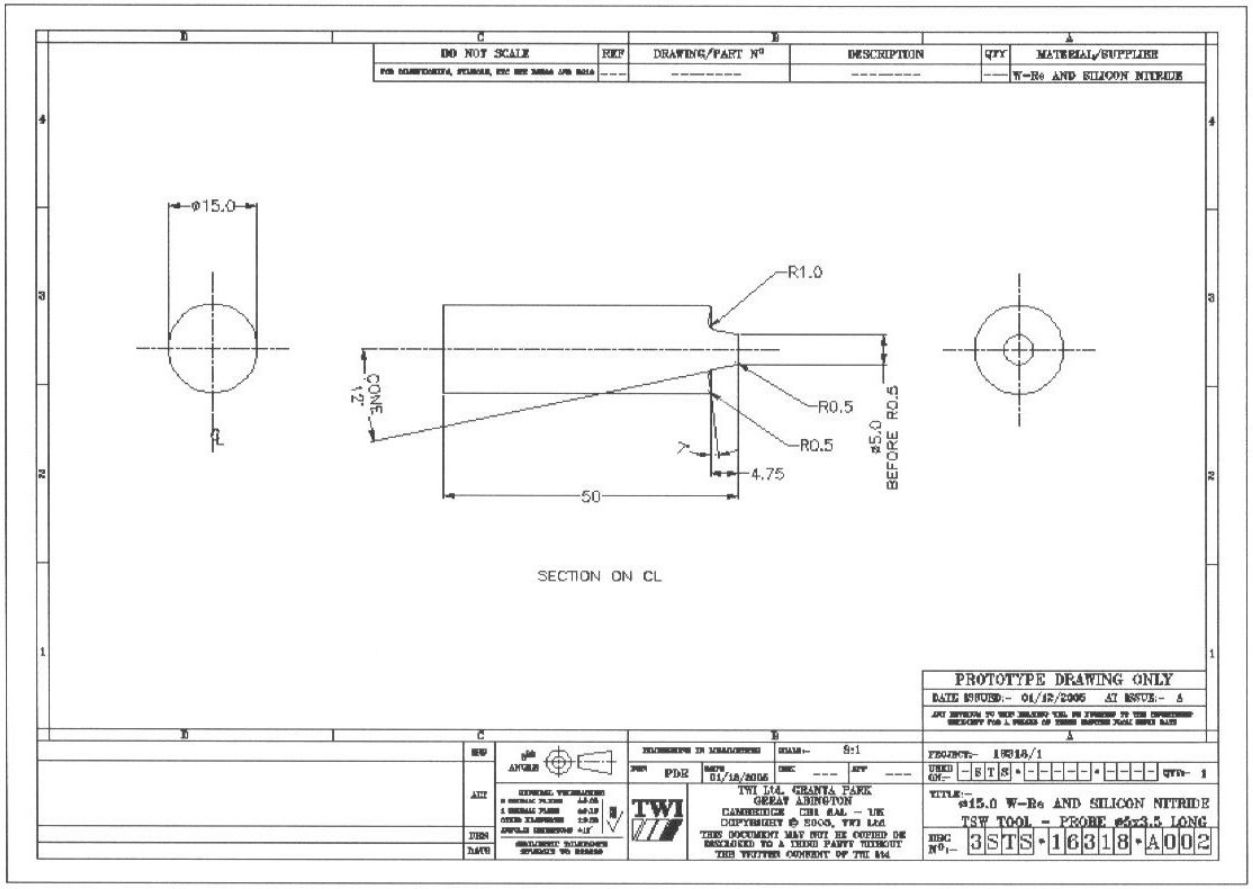

Figure C2, Drawing of Si_3Ni_4 and Re-W tools no. A002 and A003, TWI Drawing Reference 3SYF-16318-A002